Novel interfacial adsorption properties of collagenous polypeptides and their interactions with model surfactants

A thesis submitted to The University of Manchester for the degree of

Doctor of Philosophy

in the Faculty of Engineering and Physical Sciences

2012

Maria Angeles Rodriguez Rius

School of Physics and Astronomy

List of Contents

Word count: 65,279

List of Figures

1. Introduction

2. Theoretical background and relevant experimental techniques

2.1. Surface adsorption

2.2. ζ-potential

2.3. Foam studies

2.4. Neutron scattering theory

3. Methodology

4. Characterization of the 40 KDa polypeptide

5. Mixtures with ionic surfactants I: SDS/40K mixtures

6. Mixtures with ionic surfactants II: DTAB/40K mixtures

7. Mixtures with non-ionic surfactants: $C_{10}E_8$/40K mixtures

List of Tables

Abstract

Maria Angeles Rodriguez Rius
Doctor of Philosophy
The University of Manchester
2012

"Novel interfacial adsorption properties of collagenous polypeptides and their interactions with model surfactants"

The interfacial adsorption and bulk properties of a collagenous polypeptide derived from chicken eggshell membranes, the 40 KDa polypeptide, and its mixtures with common low molecular weight (LMW) surfactants, SDS, DTAB and $C_{10}E_8$, have been studied for the first time using surface tension, ζ-potential, foam observations and neutron scattering techniques.

The biopolymer has been shown to act as an effective biosurfactant by lowering the surface tension of water below the values commonly achieved with conventional LMW surfactants, i.e. $\gamma = 32 \pm 1$ mN/m. This capability is maximized at its isoelectric point, pH ~5, and addition of NaCl does not have a major impact upon adsorption.

On its own, the 40 KDa polypeptide lacks the ability to foam. When mixed with cationic and anionic surfactants, a positive synergy is observed at low concentrations of both materials that exceeds the expectations from the individual components due to the formation of polypeptide/surfactant complexes with high surface activity and high ability to foam and foam stability. At these concentrations, maximum interfacial adsorption is achieved.

The synergy is observed in spite of the type of charges present in the surfactant polar head. However, under the conditions studied, there is a difference in behaviour in regards to colloidal stability and surface film formation between the mixed solutions with the anionic SDS and the cationic DTAB. The non-existence of the synergy in the surface adsorption profile of the mixtures of the polypeptide with the non-ionic surfactant $C_{10}E_8$, as obtained via the plate method, suggests that electrostatic interactions are necessary for this strong synergy to act.

ζ-potential has been used to prove the electrostatic nature of the synergy. Specular neutron reflection and SANS measurements offered an insight into the complex size and structure.

The 40 KDa polypeptide thus offers a promising alternative to the use of high amounts of LMW surfactants in a range of products in which low surface tension and/or high and stable volumes of foams are needed, by combining small amounts of polypeptide and an ionic surfactant. This could be exploited by industries which have an interest in nanoparticle formation such as personal care or pharmaceutical companies. However, further work is needed to fully characterize these interactions.

Declaration

No portion of the work referred to in the thesis has been submitted in support of an application for another degree or qualification of this or any other university or other institute of learning.

Copyright statement

i. The author of this thesis including any appendices and/or schedules to this thesis) owns certain copyright or related rights in it (the "Copyright") and she has given The University of Manchester certain rights to use such Copyright, including for administrative purposes.

ii. Copies of this thesis, either in full or in extracts and whether in hard or electronic copy, may be made **only** in accordance with the Copyright, Designs and Patents Act 1988 (as amended) and regulations issued under it or, where appropriate, in accordance with licensing agreements which the University has from time to time. This page must form part of any such copies made.

iii. The ownership of certain Copyright, patents, designs, trade marks and other intellectual property (the "Intellectual Property") and any reproductions of copyright works in the thesis, for example graphs and tables ("Reproductions"), which may be described in this thesis, may not be owned by the author and may be owned by third parties. Such Intellectual Property and Reproductions cannot and must not be made available for use without the prior written permission of the owner(s) of the relevant Intellectual Property and/or Reproductions.

iv. Further information on the conditions under which disclosure, publication and commercialisation of this thesis, the Copyright and any Intellectual Property and/or Reproduction described in it may take place is available in the University IP Policy (see http://www.campus.manchester.ac.uk/medialibrary/policies/intellectual-property.pdf), in any relevant Thesis restriction declarations deposited in the University Library, The University Library's regulations (see http://www.library.manchester.ac.uk/aboutus/regulations/) and in The University's policy on presentation of Theses.

List of chemical name abbreviations

40K	40 KDa polypeptide
BSA	Bovine serum albumin
$C_{10}E_8$	Octaethylene glycol monodecyl ether
$C_{12}E_5$	Pentaethylene glycol monododecyl ether
C_nTAB	n-trimethylammonium bromide (with n =10 (decyl), n = 14 (tetradecyl), n = 16 (cetyl))
DPS	Dimethyldodecylammoniopropane sulfonate
DHPC	1,2-diheptanol-sn-glycero-3- phosphocholine
DTAB	Dodecyl trimethylammonium bromide
HCl	Hydrochloric acid
HFBII	Hydrophobin
NaOH	Sodium hydroxide
NaPSS	Sodium poly(styrene sulfonate)
NRW	Null reflecting water
PDMDAAC	Poly(dimethyldiallylammonium chloride)
PEI	Polyethylenimine
PEI-$(EO)_n$	Ethoxylated polyethylenimine
PEI-$(PO)_1$	Propoxylated polyethylenimine
PEO	Poly(ethylene oxide)
PMAOVE	Poly(maleic acid/octyl vinyl ether)
PNIPAM	Poly(N4sopropylacrylamide)
PSS	Poly(styrene sulfonate)
PVP	Poly(vynilpyrrolidone)
SDS	Sodium dodecyl sulfate
Triton X-100	Octyl phenol ethoxylate
UHQ Water	Ultra high quality water

Acknowledgements

I would like to express my deep gratitude to my supervisor Jian Lu for the all the help offered and for giving me the opportunity to embark in this project; and to my industrial supervisors, Ian Tucker and Jordan Petkov, for their support and for making me feel welcomed every time I visited Port Sunlight or met them in ISIS and always (or almost) making me smile.
The scientists and technicians at ISIS (Max in particular), at Unilever R&D and the people at the Biological Physics Group are also acknowledged as are the funding bodies that have supported this research (Unilever R&D and EPSRC).
Of course, I would also like to thank my family and friends for their unconditional support.

Dedication

Over the course of my life, I have encountered many people whom were destined to be part of my thoughts forever. Some I may have met only once, others have stayed by my side for longer periods.
It is their presence in my life that gave me the strength I needed whenever I suffered a temporal loss of motivation, which over the course of this project happened more often than I had wished for. These people bring inspiration to my life and that is the reason why I would like to dedicate this work to them. In the list are included Uros, Hicham and Pamela; and from within University, Phil Dawson, George King and Lars Nilse.
This is also dedicated to Patán for sharing with me a magical September night under the stars of Albacete that I have never forgotten.

Chapter 1. Introduction

Current home and personal care products are mainly formulated from ingredients derived from petroleum. With increasing oil prices and environmental concerns, it is becoming strategically important to develop ingredients that can be produced from natural and sustainable resources. Success in this vision could benefit manufacturing and formulation in a huge scale and thus have enormous social, economic and environmental benefits. In the case of non-surface active species, technological processes can be rather easily developed, leading to the accomplishment of the mission.

However, if the ingredients are surface active species, it would be non-trivial because there is yet no successful example of transforming this dream into reality in a sizable scale. Thus this global technological hurdle must be overcome if natural surface ingredients can be used to replace existing and well practiced petroleum derived ones.

In addition to the home and personal care sector, surfactants and surface active polymer blends also represent a significant proportion of materials in other formulated products including paints, agrochemicals, food, pharmaceuticals and biomedical devices. If any naturally derived materials are used to substitute petroleum derived surface active blends, they need to show equivalent physical properties, in particular, surface activity, an essential ability to adsorb on the surface of water and reduce surface tension.

Proteins and polypeptides are a group of natural products that can be derived from meats, foods, plants and bacteria. In fact, they can also be derived from waste materials, with well known examples of production of collagens or gelatines (denatured collagens) from non-food worthy meats, skins and bones and keratins from low grade wools and feathers.

A well known drawback of proteins and polypeptides is however their limited ability to lower surface tension. This means that in systems where more surface active species are present, they can be replaced from the surface or interface, resulting in the alteration of the system’s properties, e.g. collapse of food foams. Gelatines are relatively more surface active, but they can even be substituted from competitive adsorption processes.

Thus, if we are to find any application of polypeptides as surface active materials, a huge scientific challenge lies in exploring how to improve their surface activity.

This thesis is concerned with the characterisation of a polypeptide derived from egg membranes (processed from waste eggshells) with an average molecular weight of 40 KDa (the 40 KDa polypeptide). The main body of the experiments was devoted to examining how the polypeptide interacted with surfactants at the surface of water and in solution, through a set of equilibrium and dynamic surface tension measurements, neutron reflection, ζ-potential measurements and small angle neutron scattering (SANS).

The effort was then made to seek correlation between surface properties and foam stability. This thesis work thus focused on investigating the physical and surface active properties of the polypeptide and the main patterns of its interaction with surfactants. This work thus contributes to the development of a knowledge base about how to manipulate the surface activity of this polypeptide through binding with different surfactants.

The main outcome of this thesis work is that egg membrane derived polypeptide is unusually surface active. It can reach surface tensions as low as 32 mN/m, a value that cannot even be reached by most known surfactants. Because of this high surface activity, it is very tolerant to the competitive adsorption of non-ionic surfactants. In addition, it binds very favourably with anionic and cationic surfactants through forming surface active peptide-surfactant complexes. These features make this polypeptide distinctly different from known proteins and polypeptides, making it a highly promising candidate for replacing petroleum derived surfactant-polymer blends in product formulation.

In this opening Chapter, the basic background to this thesis is to be introduced including the molecular structures of surfactants and proteins and their general physical properties.

1.1. General background

Surface active agents or surfactants are an important group of chemicals, (amphiphiles), whose structure and function affect our life, as well as more menial tasks such as cleaning clothes or lubricating surfaces. Amphiphilic substances are capable of lowering the surface tension of a liquid in an energetically favourable process [1]. They possess two distinct parts: a hydrophobic tail and a hydrophilic head. When surfactants are added to a polar solvent such as water, there is an unfavourable contact between the water molecules and the hydrocarbon. To ameliorate this there is a drive for the molecules to relieve this stress, and this leads to a phenomenon known as micellisation, where self-aggregation takes place in solution.

Surfactants are classified by the headgroup moiety. Anionic surfactants, such as sodium dodecyl sulfate (SDS) have a negatively charged headgroup. The headgroup in cationic surfactants is positively charged, i.e. dodecyl trimethylammonium bromide or DTAB. Non-ionic surfactants, such as octaethylene glycol monodecyl ether ($C_{10}E_8$) rely on the hydration of ether-oxygen via dipole interactions to solvate the water-soluble headgroup to control solubility. Surfactants whose water-soluble moiety contains both negative and positive charges are classified as zwitterionic [2].

Surfactants in common use are derived from crude oil, vegetable and animal fats (see Figure 1.1.1). However there are many cases of surfactants being produced by living organisms and these so called “biosurfactants” have important biological functions. For instance, the alveoli in the lungs are covered in pulmonary surfactants to reduce the pressure needed for lung aeration [3, 4].

Hydrophobins, known as the most powerful biosurfactants, are proteins secreted from fungi which lower the surface tension to allow the hyphae to penetrate the air/water interface and protect the exposed fungi parts and the spores by coating them. These proteins also play a role in the attachment of fungi to certain surfaces.

Surfactant class	Volume	Regional share (%)
Soap	8800	
Anionic surfactants		
– alkyl benzene sulfonates	3400	
– fatty alcohol ether sulfates	1000	
– fatty alcohol sulfates	500	
Nonionic surfactants		
– alcohol ethoxylates	800	
– alkylphenol ethoxylates	700	
Cationic surfactants	810	
Amphoteric surfactants	180	
Others (incl. carbohydrate-based surfactants)	2900	

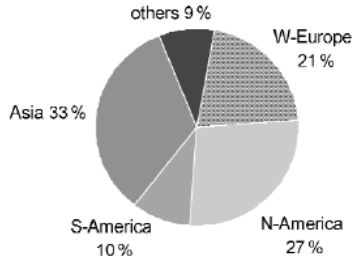

Fig. 1.1.1. Global surfactant consumption in 2000 (volumes in 1000 tons) [5].

Several synthetic surfactants are used in foaming processes to produce fire extinguisher foams amongst other products. In nature, foams derived from biosurfactants are produced, for example, to protect the eggs laid by several species of freshwater fish, frogs and other animals. These biofoams are usually the result of synergistic behaviour between specialised surfactant proteins and other proteins which result in stable foams with antimicrobial and antiparasitic properties [3].

With increasing consumer demand and a finite resource of oils and fats, there is an increased interest in the application of biosurfactants.
The broad availability of collagenous structures in nature means that they can be sourced cheaply from a variety of different sources. Bovine and swine collagens had already been successfully sourced until the emergence of bovine spongiform encephalopathy, or Creutzfeld-Jakob disease (CJD), and foot and mouth disease, caused the widespread avoidance of collagen-based products from bovine and swine origins [6-9].

Eggs are a common alternative source. Whereas the yolks and whites are directly used in the food industry, the eggshell membranes are still attached to the eggshells and they are an important source of proteins, in particular, collagen. This entails on the one hand, expensive egg waste disposal due to its attractiveness to vermin. On the other hand, it represents a source of commercially available collagen so much in demand in recent years [9]. Unfortunately, the separation of the membrane from the eggshell is not

straightforward. Many patents with different procedures to obtain this protein have been filed [10, 11].

Furthermore, the versatility of collagenous materials extracted from the eggshell membranes varies greatly with different extraction procedures. For instance, insoluble materials extracted from the egg shell membranes have been proved to be an effective biosurfactant with applications in water treatment and bioremediation of actinides related pollution [12]. However, it is the modified soluble version of these materials that has been studied as a biosurfactant for selenium and arsenic bioremediation [13].

Different procedures for the preparation of soluble eggshell membrane peptides are possible. For instance, one method consists of suspending raw pieces of the eggshell membrane in a 1.25 N solution of 3-mercaptopropionic acid with 10 % acetic acid at 90°C [14]. An alternative method uses an ME-4 bacterial strain of Pseudomonas aeruginosa to decompose the membranes. In this case, the solubilisation is caused by the protease enzyme produced when these bacteria attack the membranes [15].

In addition, surfactants applied in biomedical, pharmaceutical, cosmetic and personal care industries must be biocompatible and low in toxicity. The soluble eggshell membranes are currently a promising biomaterial for skin grafts and collagen matrix reconstruction thus proving its biocompatibility [16, 17].

Qingdao Ecole Biotech Ltd. (Qingdao, China) is one of the many companies that have attempted to separate the membranes from the egg shells. A water-soluble collagenous polypeptide (40 KDa polypeptide) derived from the membranes of the chicken eggshells by the method utilised by this company (described in Chapter 4) is the focus of this work. Its surface active properties at the air/water interface have been investigated in the absence and presence of model low molecular weight (LMW) surfactants with different polar head charges. The relation between the interfacial properties and the composition of the solution phase has also been studied.

From the successful use of this polypeptide as a collagenous biosurfactant hangs a possibility to find an important remedial solution to egg waste problems and reduce low

molecular weight (LMW) surfactant pollution. Besides, an important economic gain can result by reducing waste disposal expenses and obtaining a profit from products developed from the polypeptide.

1.2. Polymers

A polymer has a sequence of structural units or monomers. If the sequence is built by repetition of only one type of monomer, it is termed a homopolymer. If the sequence is composed of two or more monomers, it is a copolymer. Polymers can be synthetic or natural. Examples of commercial synthetic polymers are some plastics and fabrics [18] such as polystyrene, poly(vinyl chloride) and nylon. Examples of natural polymers or biopolymers are the tortoise shell and horn used for centuries as hair combs and jewellery [18]. In this work, the interest is centred around biopolymers and more specifically, around proteins. These are repeat sequences of amino acids.

1.3. Amino acids

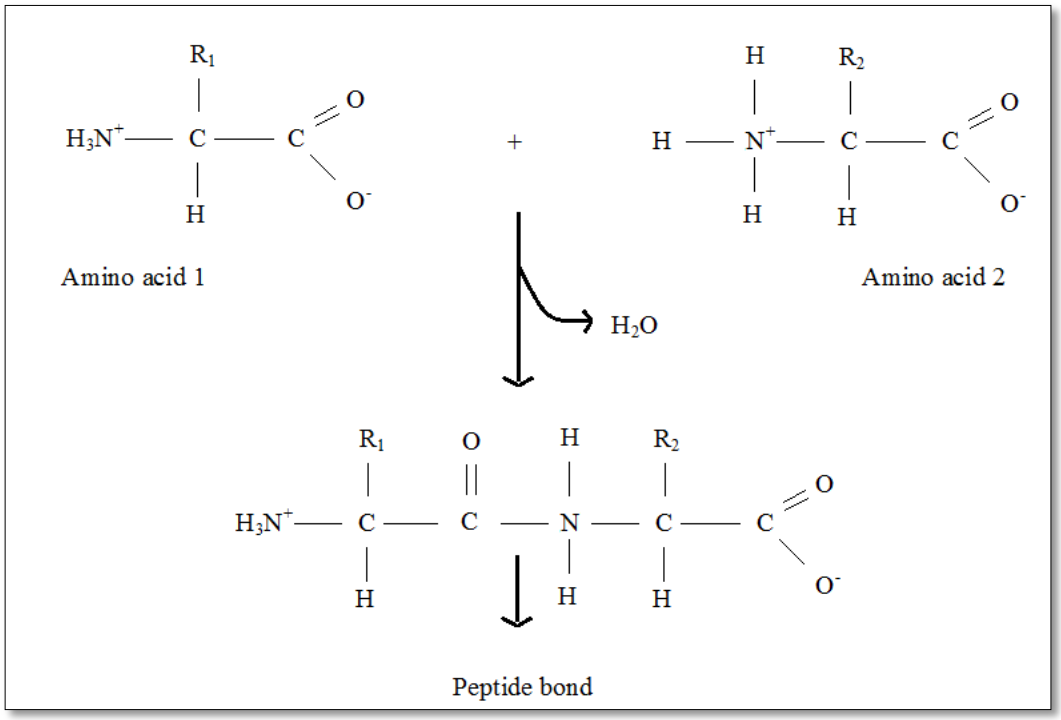

Fig. 1.3.1. The peptide bond and its formation.

At physiological pH, amino acids are organic zwitterions with a central α-carbon and four side chains; an amino group (-NH_2), a carboxylic group (-COOH), a hydrogen (-H) and a fourth side chain (-R) which determines the properties of the amino acid [1, 6]. There are twenty standard amino acids (see Figure 1.3.2) which can be linked via peptide bonds to form proteins (see Figure 1.3.1). The –R group in these amino acids can be polar, non-polar, aromatic, positively or negatively charged or uncharged.

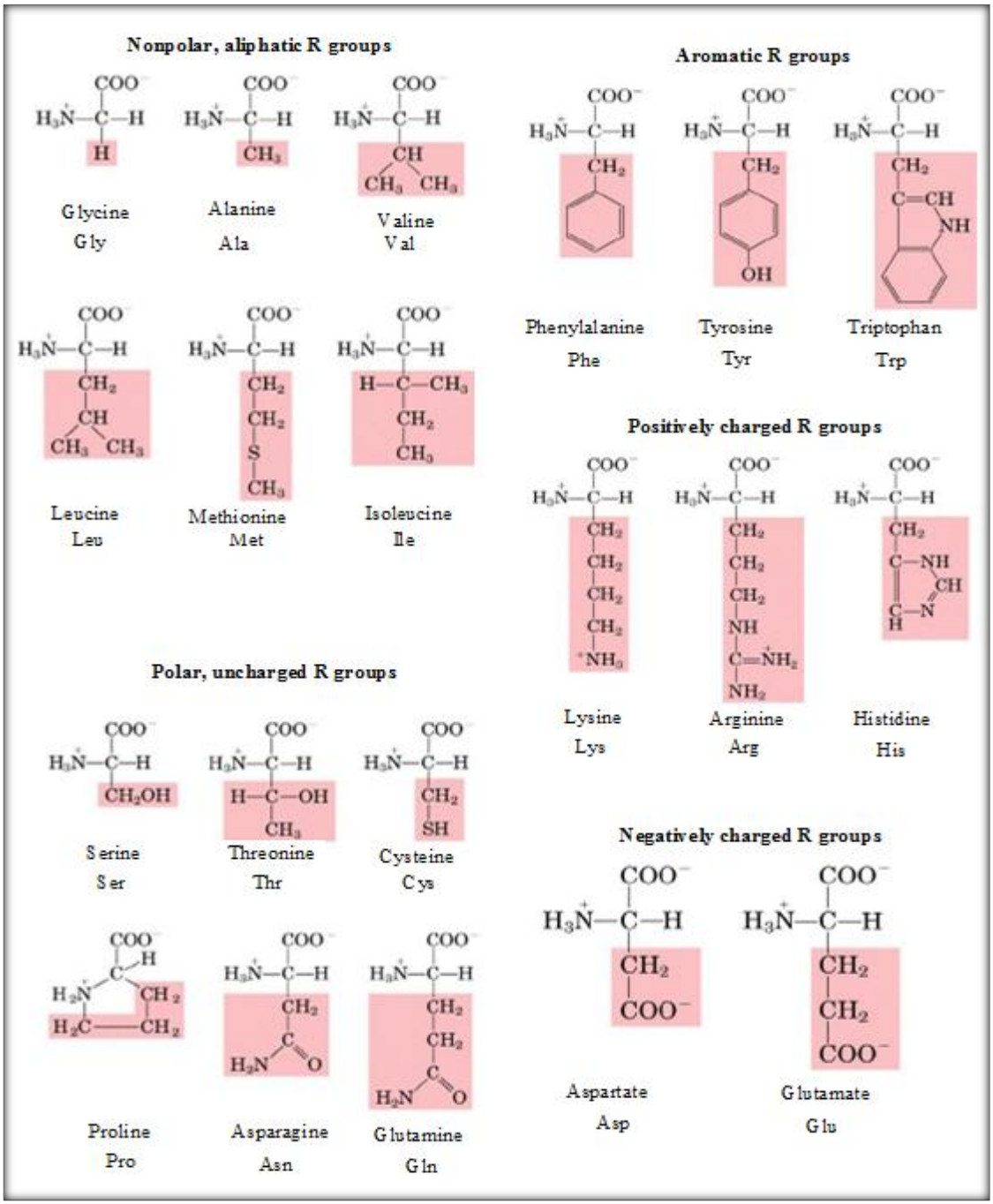

Fig. 1.3.2. The twenty standard amino acids [adapted from 19].

A peptide bond is a covalent bond [1] resulting from the association of the carboxylic group of one amino acid to the amino group of another amino acid releasing a water molecule. The remaining parts of the original amino acids are amino acid residues. If a biopolymer is composed of charged residues, it is known as a polyelectrolyte [1].

1.4. Proteins

Proteins possess four structural degrees which confer them their individual characteristic properties such as solubility and rigidity (or the lack of these) and their biological functions.

Their primary structure is the amino acid sequence. By convention, the first amino acid is the only one with a free amino group, or N-terminal, and it is always written on the left. The last amino acid is written on the right and it is the only one with a free carboxyl group or C-terminal [20].

The secondary structure is determined by the spatial arrangement of backbone segments, i.e. the peptide linkages and the α-carbons, which is strongly influenced by the order followed by the amino acids in the primary structure [1].

Two of the most common secondary structures are the right-handed α-helix and the pleated β-sheet. These make use of all possible hydrogen bonds of the backbone [6] by associating different parts of the same backbone (α-helix) or from different backbones (β-sheet). If no periodicity exists, a random chain results [1].

A turn in the α-helix extends 5.4 Å in length and contains 3.6 amino acid residues. Three turns is approximately the average length of a protein α-helix [6]. The β-sheet can be parallel or antiparallel, depending on whether the hydrogen bonding sites of the two associated chains extend in the same direction or not. One pleated unit extends 7 Å in length corresponding to the length of two amino acid residues. A protein β-sheet contains 2 to 22 strands with up to 15 residues per strand [6].

The stability of the secondary structure is affected by the bonds formed between the side chains and with other macromolecules or a solvent [1]. The hydrophobic moieties

attempt to escape contact with polar solvents by rotating around the allowed degrees of freedom thus leading to the folding of the structure.

The tertiary structure is conferred by the constraints imposed by the side chains and the quaternary structure is the spatial arrangement due to the association of various polypeptide chains or subunits.

The information of the overall protein structure is contained within the amino acid sequence or primary structure. Whether this information is the only condition necessary to fold the protein into its functional state is at present a matter of debate [1, 21]. A denatured protein that is allowed to refold may not adopt the conformation that allows it to regain its functionality [22].

Misfolding of the secondary structure can result in amyloid diseases in which proteinaceous structures composed of twisted β-sheets supplant the functional proteins necessary to carry out a specific biological function thus disrupting the latter. Prevalent diseases like Alzheimer's or spongiform encephalopathies are known to be related to the formation of amyloids [1, 22].

Proteins are sometimes categorized by their morphology. Two common groups are globular and fibrous proteins. Examples of globular proteins are myoglobin, bovine serum albumin (BSA) and lysozyme. Known fibrous proteins are keratin and collagen, both possessing highly elongated structures due to the dominance of only one type of secondary structure [6].

Proteins are amphiphilic molecules and their surface activity is related to the ratio of hydrophobic to hydrophilic residues. Nevertheless, knowledge of the amino acid sequence alone is sometimes insufficient to determine their surface activity. Thus, the distribution pattern of the charges is related to the flexibility or rigidity of the polypeptide chain and the ease of adaptability to changes in the environment. Therefore, the surface activity of proteins is related to their adopted conformation [23].

Protein solubility is altered with different protein conformations and decreases with higher incidence of exposed hydrophobic patches. Hydration is also affected not only by the charges present in the molecule but by the protein conformation [23].

1.5. Collagen

The primary structure of collagen is the repetition of blocks of three amino acid residues, Glycine (Gly), X and Y, in the sequence Gly-X-Y (see Figure 1.5.1). X and Y are often proline (Pro) and hydroxyproline (Hyp). The latter is almost exclusively found in collagen and used to identify it [24]. Hydroxyproline is synthesized by the enzyme prolyl hydroxylase from proline residues in the presence of ascorbic acid (vitamin C) [6].

The secondary structure is known as tropocollagen; three parallel left-handed helical polypeptide chains coil around each other in a right-handed conformation due to the hydrogen bonds linking the Gly N-H (amine) bonds to the Pro C=O (carbonyl) bonds in an adjacent polypeptide. Glycine is the smallest of the standard amino acids and the only one capable to fit in the centre of the triple helix [6].

There are nearly 40 distinct polypeptide chains that form the known 20 collagen types. The most abundant of these, is type I. This tropocollagen of molecular weight ~285 KDa has a length of ~300 nm and a width of ~14 nm [6, 25]. It is found in skin, tendons, ligaments, vascular tissue, organs and bone [6, 25]. As an example, type I collagen from tendons is composed of approximately 33% Gly, 15% Pro and 15% Hyp [24].

Several tropocollagen molecules self-assemble to form fibrils (tertiary structure) [8]. The quaternary structure consists of further cross-linking and close-packing of several collagen molecules to form ordered structures such as networks (formed by type IV collagen) or fibers (formed by types I, II, III) [6].

Mimicking the structure of collagen is a technique used in biotemplates due to the improved qualities offered by its intricate structure [26].

Collagen-related diseases, such as scurvy, lathyrism, osteogenesis imperfecta or the Ehlers-Danlos syndromes [1, 6], result from alterations of the hierarchical structure of collagen by inactivation of enzymes like prolyl hydroxylase or genetic mutations. In addition, collagen is used in many cosmetic products. Thus, improving our knowledge of the collagen structure at every level is important for the development of biomimetic materials and to further understand the occurrence of misfolds leading to defects in its structure which are responsible for the different physical behaviour encountered in defective collagen.

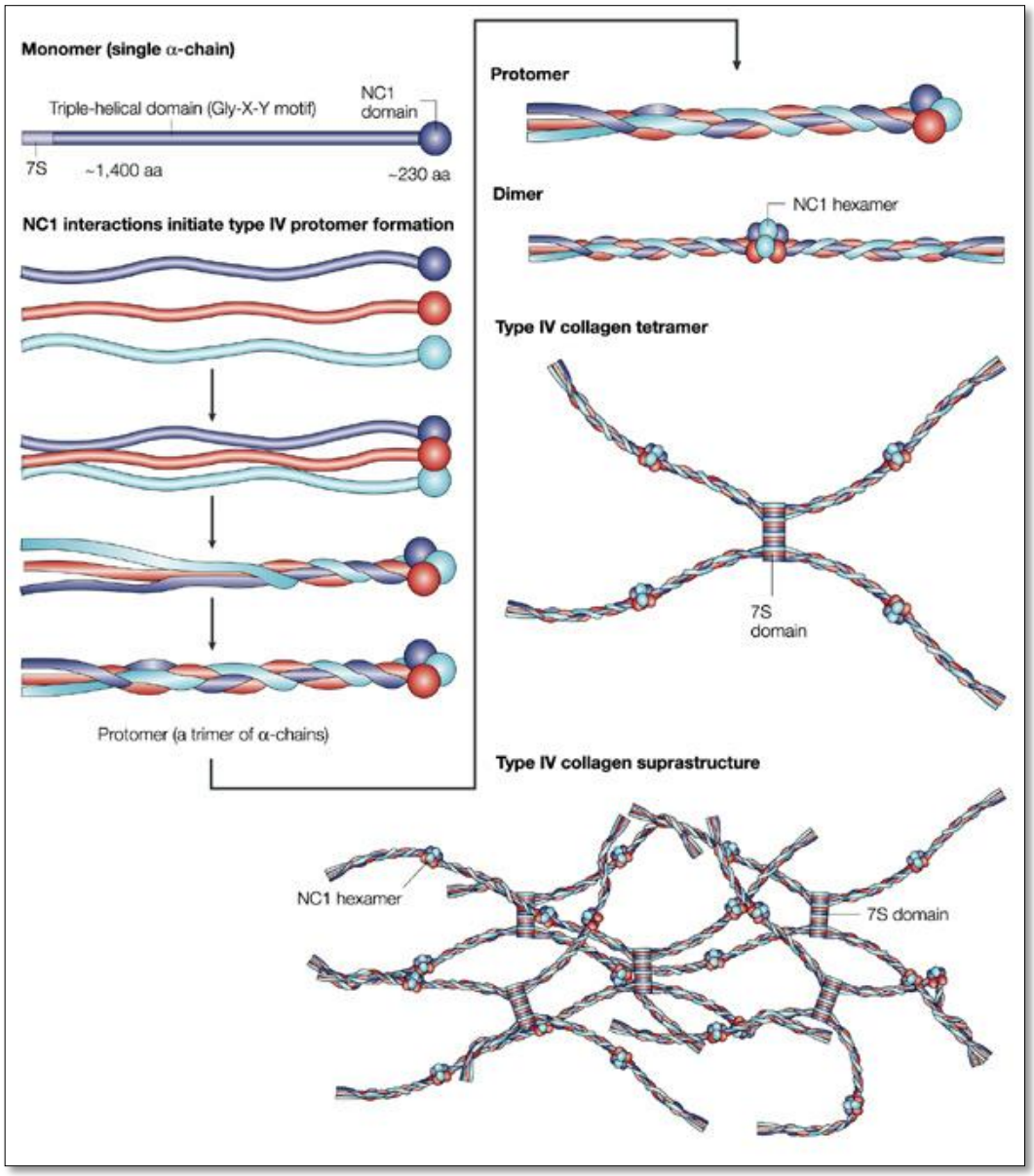

Fig. 1.5.1. Hierarchical structure of type IV collagen [27].

The collagen present in the chicken eggshell membrane belongs to types I, V and X [9, 14]. The eggshell membrane is divided into an outer layer and an inner layer. Both contain a ratio of 100:1 of type I to type V collagen [28]. Types I and V are fibril-forming collagens with different subunits (heterotrimers). Type X is a hexagonal-network forming collagen composed of three identical subunits (homotrimer) [29].

1.6. Thesis Chapter plan and strategy

Since the egg membrane collagen (aka 40 KDa polypeptide) is surface active, the first step conducted in this project was to characterise its adsorption properties. As it was found that the charge in the polypeptide influenced the interfacial adsorption, ζ-potential measurements were used to complement the surface studies. Direct observations of the foams stabilised by the polypeptide were made to test their foaming behaviour and stability. These are known to be a result of the dynamic adsorption properties. At this juncture other surfactants were introduced to try to understand the nature of the adsorbed species and how it could be modified.

In addition to surface tension and ζ-potential measurements in mixtures, neutron reflection was used to further investigate the structure of the adsorbed interfacial layer. The interfacial adsorption properties are also related to the solute behaviour in solution and formation of micellar aggregates. Hence, small angle neutron scattering (SANS) was applied to investigate the formation of these aggregates.

The behaviour of the biosurfactant in combination with LMWs surfactants was also investigated. Hence, the procedure described above was also followed for mixed solutions of polypeptide with ionic LMW surfactants, SDS and DTAB. The main motivation here was to establish a basic understanding of how different type of surfactants affected the pattern of binding to the polypeptide and how such surface complexation processes affected surface tension changes and foam stability. The results highlighted synergistic effects manifested by a possible electrostatic component between the polypeptide and the ionic surfactants and hydrophobic association. Thus, equilibrium and dynamic surface tension measurements of mixed solutions of polypeptide with non-ionic surfactant, $C_{10}E_8$, were also conducted in order to prove the crucial role of electrostatic interactions in the mixtures involving ionic surfactants.

Chapter 1 offers the necessary general background information and presents an introduction to the subject under study. Chapter 2 offers an account of the relevant techniques and theories used in this project. The materials employed are listed in Chapter 3. In this Chapter, the experimental methodology followed is explained.

The results obtained are categorized according to the type of solutes present in solution. Thus, Chapter 4 presents the results obtained with solutions containing the 40 KDa polypeptide. Chapter 5 contains the results of mixing the 40 KDa polypeptide with the anionic surfactant SDS. Chapter 6 contains the results of mixing the 40 KDa polypeptide with the cationic surfactant DTAB. And finally, Chapter 7 contains the results of mixing the 40 KDa polypeptide with the non-ionic surfactant $C_{10}E_8$.

The overall results are discussed in Chapter 8 where the conclusions reached and the proposed further work are also presented.

References

[1] P.R. Bergethon (1998) "The physical basis of biochemistry. The foundations of molecular biophysics", Springer-Verlag.

[2] D. Myers (2006), "Surfactant science and technology", 3rd ed., John Wiley and Sons.

[3] A. Cooper, M.W. Kennedy (2010) "Biofoams and natural protein surfactants", Biophys. Chem., 151(3), pp. 96-104.

[4] H.L. Halliday (2008) "Surfactants: past, present and future", J. Perinatol., 28, S47-S56.

[5] K. Hill (2007) "Industrial development and application of biobased oleochemicals", IUPAC, Pure Appl. Chem., 79 (11), pp. 1999-2011.

[6] D. Voet, J.G. Voet, C.W. Pratt (2006) "Fundamentals of biochemistry. Life at the molecular level", 2nd ed., John Wiley and Sons.

[7] A.M. Kingori (2011) "A review of the uses of poultry eggshells and shell membranes", Int. J. Poultry Sci., 10 (11), pp. 908-912.

[8] M.J. Buehler (2006) "Nature designs tough collagen: explaining the nanostructure of collagen fibrils", PNAS, 103 (33), pp. 12285-12290.

[9] Y. Zhao, Y. Chi (2009) “Characterization of collagen from eggshell membrane”, Biotechnology, 8 (2), pp. 254-258.

[10] C. Sonenklar (1999) “Famous for egg waste”, The Pennsylvania State University, Research/Penn State, 20 (3).

[11] V. Vlad, (BIOVA L.L.C.), (07/06/2011) “Eggshell membrane separation method”, US Patent and Trademark Office, 7954733 (Patent).

[12] S. Ishikawa, K. Suyama, I. Satoh (1999) “Biosorption of actinides from dilute waste actinide solution by egg shell membrane”, Appl. Biochem. Biotechnol., 77-79, pp. 521-533.

[13] S. Ishikawa, S. Sekine, N. Miura, K. Suyama, K. Arihara, M. Itoh (2004) “Removal of selenium and arsenic by animal biopolymers”, Biol. Trace Elem. Res., 102, pp. 113-127.

[14] F. Yi, Z. Guo, L. Zhang, J. Yu, Q. Li (2004) “Soluble eggshell membrane protein: preparation, characterization and biocompatibility”, Biomaterials, 25, pp. 4591-4599.

[15] Cheng, S. Takenaka, S. Aoki, S. Murakami, K. Aoki (2009) “Purification and characterization of an eggshell membrane decomposing protease from Pseudomonas aeruginosa strain ME-4”, J. Biosci. Bioeng., 107 (4), pp. 373-378.

[16] K. Takahashi, K. Shirai, M. Kitamura, M. Hattori (1996) “Soluble egg-shell membrane protein as a regulating material for collagen matrix reconstruction”, Biosci., Biotech., Biochem., 60 (8), pp. 1299-1302.

[17] T. Ino, M. Hattori, T. Yoshida, S. Hattori (2006) “Improved physical and biochemical features of a collagen membrane by conjugating with soluble egg shell membrane protein”, Biosci. Biotech. Biochem., 70 (4), pp. 865-873.

[18] J.L. Meikle (1997) “American plastic: a cultural history”, Rutgers University Press.

[19] M.A. Rodriguez Rius (2009) “Characterization of two peptides derived from eggshell membrane”, MPhil Thesis, University of Manchester.

[20] J.L. Hansen, T.M. Schmeing, P.B. Moore, T.A. Steitz (2002) “Structural insights into peptide bond formation”, Proc. Natl. Acad. Sci. USA, 99 (18), pp. 11670-11675.

[21] R.L. Baldwin, B.H. Zimm (2000) “Are denatured proteins ever random coils?”, PNAS, 97 (23), pp. 12391-12392.

[22] K. Kar, P. Amin, M.A. Bryan, A.V. Persikov, A. Mosh, Y. Wang, B. Brodsky (2006) “Self-association of collagen triple helix peptides into higher order structures”, J. Biol. Chem., 281 (44), pp. 33283-33290.

[23] O.R. Fennema (1996) “Food chemistry”, 3rd ed., CRC Press.

[24] Y.C. Fung (1993) “Biomechanics: mechanical properties of living tissues”, 2nd ed., Springer.

[25] P. Fratzl (2008) “Collagen: structure and mechanics”, Springer Science+Business Media, LLC.

[26] D. Dong, Y. Wu, X. Zhang, J. Yao, Y. Huang, D. Li, C. Li (2011) “Eggshell membrane-templated synthesis of highly crystalline perovskite ceramics for solid oxide fuel cells”, J. Mater. Chem., 21, pp. 1028–1032.

[27] R. Kalluri (2003) “Basement membranes: structure, assembly and role in tumour angiogenesis”, Nature Reviews Cancer, 3, pp. 422-433.

[28] M. Wong, M.J.C. Hendrix, K. von der Mark, C. Little, R. Stern (1984) “Collagen in the eggshell membranes of the hen”, Dev. Biol., 104 (1), pp. 28-36.

[29] K. Gelse, E. Poschl, T. Aigner (2003) “Collagens-structure, function and biosynthesis”, Adv. Drug Deliv. Rev., 55, pp. 1531-1546.

Chapter 2. Theoretical Background of Molecular Processes and Relevant Techniques

This Chapter encompasses the theory behind molecular processes such as surface adsorption and colloidal aggregation that take place at the air/liquid interface, in solution and/or in foams, and describes the relevant instrumental and theoretical principles on which the techniques applied in this work rely.

2.1. Surface adsorption

The boundary between water and a gas phase, commonly referred to as the interfacial layer [1, 2], arises as a consequence of the attractive van der Waals forces acting upon the molecules in the liquid phase. At a planar interface, the van der Waals forces act to contract the surface thereby separating the liquid layer from the molecules that remain in the gas phase. The molecules in this layer thus experience only half of the attractions. A surface active agent lessens the strain suffered by this layer by adsorbing on it with the hydrophobic tail oriented towards the gas phase and the polar head group oriented towards the liquid phase. This interrupts the intermolecular interactions between the liquid molecules initially present at the surface and increases the surface area. The arrangement of surface active molecules at this interface is depicted in cartoon form in Figure 2.1.1.

Surface tension is the measure of the work needed, *U*, to produce this increase in surface area, *A*, isothermally and reversibly by a unit amount [3, 4] and it is expressed via

$$\gamma = \frac{U}{2A} \qquad Eq.\ 2.1.1$$

In the case of a flat pure water surface, the surface tension at a fixed temperature of 25°C is ~72 $mN \cdot m^{-1}$. This value is temperature dependent and reduces with increasing temperature [1].

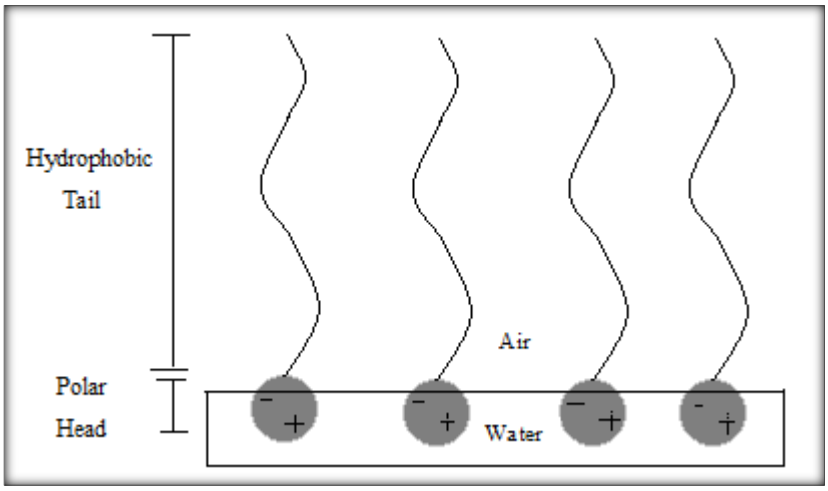

Fig. 2.1.1. Orientation of a surface active agent at the air/liquid interface.

Similarly, the surface pressure is defined as the difference in surface tension between an air-pure water surface, γ_0, and the surface tension resulting after adsorption of a molecule [5], i.e.

$$\Pi = \gamma - \gamma_0 \qquad Eq.\,2.1.2$$

2.1.1. Equilibrium surface adsorption: Gibbs Equation

From a thermodynamics point of view, the interfacial layer can be assumed to be an infinitesimally small layer dividing the gas (g) and liquid (l) bulk phases, which characteristics are fully known, thus avoiding the description of the interfacial parameters so the process in which the variation in the characteristics occurs from one bulk phase to the other is unimportant. The choice of the dividing (Gibbs) plane is arbitrary as long as it accounts for the material encountered at the interface [6, 7].

The total internal energy of the system U, is the sum of the internal energies of both phases in equilibrium, U_g and U_l, and that of the interface, U_i,

$$U = U_g + U_l + U_i \qquad Eq.\,2.1.3$$

The differential internal energy of a bulk phase is given by

$$dU_i = TdS - PdV + \sum_j \mu_j dn_j \qquad Eq.\,2.1.4$$

where *T, S, P, V,* μ_j and n_j are the usual thermodynamics parameters that describe the equilibrium state, i.e. temperature, entropy, pressure, volume, chemical potential and particle number of species j, respectively. The internal energy for the two-dimensional interface after replacement of the expansion work, $-PdV$, by the work needed to change the surface area, i.e. γdA, is given by

$$dU_i = TdS + \gamma dA + \sum_j \mu_j dn_j \qquad Eq.\,2.1.5$$

Differentiating Equation 2.1.5 gives

$$dU_i = TdS + SdT + \gamma dA + Ad\gamma + \sum_j \mu_j dn_j + \sum_j n_j d\mu_j \qquad Eq.\,2.1.6$$

Subtracting Equation 2.1.5 from Equation 2.1.6 leads to

$$0 = SdT + Ad\gamma + \sum_j n_j d\mu_j \qquad Eq.\,2.1.7$$

Furthermore, if constant temperature is assumed, this further reduces to the general form of the Gibbs Equation,

$$d\gamma = -\sum_j \Gamma_j d\mu_j \qquad Eq.\,2.1.8$$

with the amounts adsorbed at the interface or surface excess defined according to unit area or as

$$\Gamma_j = \frac{n_j}{A} \qquad Eq.\,2.1.9$$

As the position of the dividing Gibbs plane is arbitrary only the adsorbate is pertinent [6]. Thus, substituting the chemical potential in Equation 2.1.8 by its general form, i.e.

$$\mu_j = \mu_j^0 + RTlna_j \qquad Eq.2.1.10$$

where μ_j^0 is the standard chemical potential of species j and $a_j = X_j \cdot f_j$ is the product of the mole fraction, X_j, and the activity coefficient, f_j, and it is known as the activity of the species, the Gibbs Equation becomes

$$\Gamma_{eq} = \frac{-1}{nRT}\frac{d\gamma}{d(lna_j)} \qquad Eq.2.1.11$$

In the dilute regime, the activity of a species j for the case of uni-univalent electrolytes such as SDS and C_{16}TAB [6], can be considered approximately equal to the concentration of solute X_j in the bulk. The parameter n adopts a value of 1 for zwitterionic and non-ionic surface active agents, and a value of 2 for 1:1 ionic surfactants in the absence of electrolyte. If a sufficient amount of electrolytes is added to ionic surfactants, n approaches a value of 1 [8].

2.1.2. Measuring the surface adsorbed amounts

Measuring the surface tension of a surfactant solution as a function of the natural logarithm of solute concentration in the bulk offers the opportunity to calculate the surface excess through Gibbs Equation. When monomers adsorb at the interface the surface tension is lowered. The drop in surface tension is related to the concentration of solute and there is a concentration above which the surface adsorbed amount is constant and the surface tension reaches a plateau as in Figure 2.1.2.1. This point is known as the critical micelle concentration or CMC. Below this concentration, the curve can be modelled and the model's derivative substituted in Equation 2.1.11 so the equilibrium surface excess is obtained. A common choice of model for this curve is a quadratic form [9, 10].

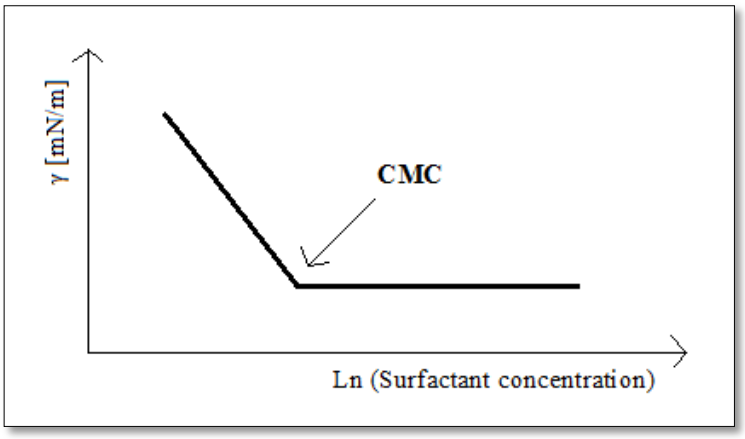

Fig. 2.1.2.1. Surface tension as a function of the concentration of a pure surfactant.

If the solution contains impurities that are more surface active than the main component, a minimum appears just below the CMC where the impurities adsorb strongly at the interface. At higher concentrations the micellisation process of the main component results in the solubilisation of the impurities and their removal from the interface [11]. Thus, when the minimum does not appear, the surface active agent is assumed to be pure although this may not be true in certain cases as Elworthy et al. [12] demonstrated using octane as a non-polar impurity.

Nevertheless, when the minimum does appear the impurities are adsorbed at the surface as explained before. Hence, using chelating agents and foam fractionation it is possible to remove them from the surface and increase the surface tension to purity levels [8, 12].

2.1.3. Surface adsorption of mixed solutions

When more than one component is present in the solution, the γ *vs. ln C* curve may differ from the behaviour exhibited by the individual compounds alone, i.e. Figure 2.1.2.1. The surface tension curves for these mixed systems depend on the strength and type of interaction between the individual species. Furthermore, the components may bind to each other and present a synergistic (cooperative) behaviour. There may also be a process in which individual components compete to reach the interface and adsorb. Mixed surfactants tend to either mix, mix non-ideally or demix. Polymers have distinctly different interactions depending on the nature of the association.

The inset in Figure 2.1.3.1 describes the surface tension behaviour in mixtures where there are no competitive interactions. In this case, different components, A and B, bind to each other and their interaction results in a displacement of the CMC generally towards lower surface tension values with increasing amount of B in the bulk phase if the concentration of A in the bulk phase is fixed. In this case, the activity of the species, a_j, is equal to the mole fraction of the species, X_j. This is termed "ideal mixing", where the new value of CMC, or CMC*, can be calculated through the expression

$$\frac{1}{CMC^*} = \frac{X_A}{CMC_A} + \frac{1 - X_A}{CMC_B} \qquad Eq.\,2.1.12$$

In the above Equation, CMC_A and CMC_B are the critical micelle concentrations of the individual components and X_A is the mole fraction of component A [11, 13]. Sehgal et al. [14] observed this phenomenon in mixtures of the zwitterionic dimethyldodecylammoniopropane sulfonate (DPS) and the phospholipid 1,2-diheptanol-sn-glycero-3- phosphocholine (DHPC).

When the activity of the species does not correspond to their mole fractions, and it depends on the concentration of the components in the mixed micelle, α_j, Equation 2.1.12 becomes

$$\frac{1}{CMC^*} = \frac{X_A}{f_A \cdot CMC_A} + \frac{1 - X_A}{f_B \cdot CMC_B} \qquad Eq.\,2.1.13$$

where f_A and f_B are the activity coefficients in this model known as Regular Solution Theory [15] and can be expressed as

$$f_A = e^{\beta(1-\alpha_1)^2} \qquad Eq.\,2.1.14$$

$$f_B = e^{\beta(\alpha_1)^2} \qquad Eq.\,2.1.15$$

Thus, the interaction parameter β accounts for the departure from the ideal mixing case.

Figure 2.1.3.1 also shows below the inset three different types of surface tension curves for polymer/surfactant mixtures as functions of the bulk surfactant concentration. The thick black line follows the usual pattern of a surfactant in solution with the CMC as the critical point where the plateau representing formation of micellar structures commences. For a polymer/surfactant system, competition to occupy the interface occurs. If the interaction is weak, the curve tends to exhibit two plateau areas rather than one.

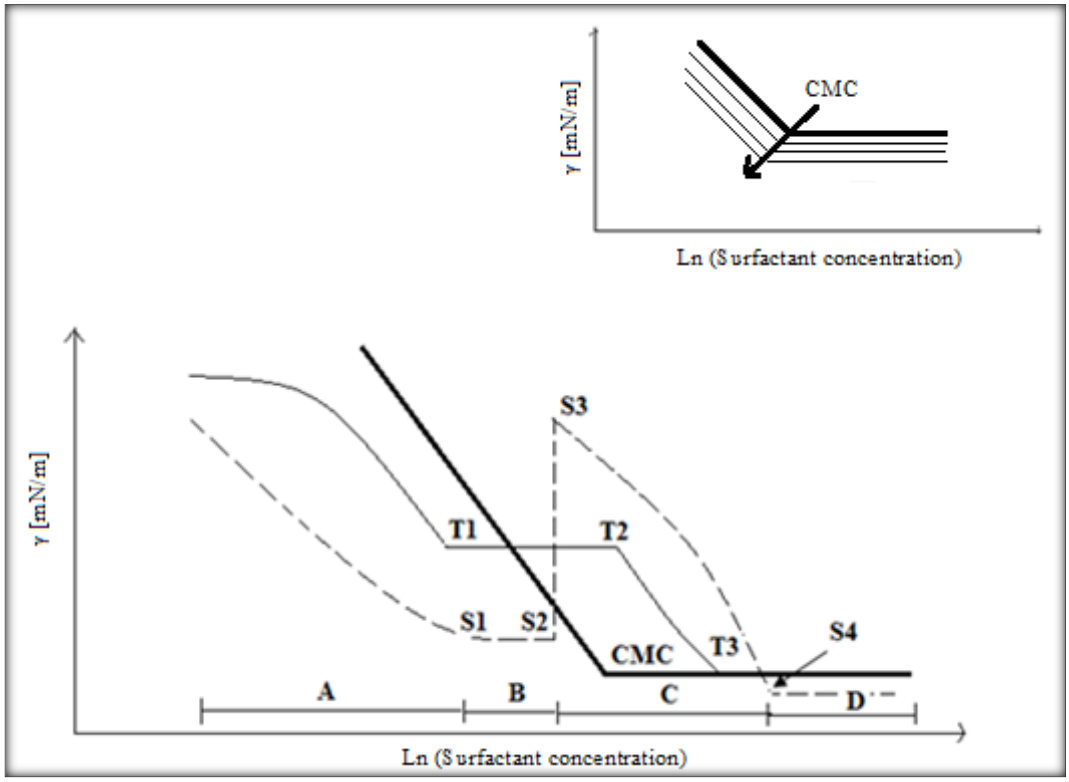

Fig. 2.1.3.1. Typical adsorption curves obtained with mixed solutions of two or more components.

The thin black line with 'T'-labelled points represents the typical behaviour observed in weakly interacting systems of polymer/surfactant mixtures. This is the expected behaviour for neutral polymers. From left to right, in the region up to T1 or critical aggregation concentration (CAC), monomers adsorb at the interface and some degree of cooperation between the polymer and the surfactant already takes place as stated in the lower values of surface tension obtained when compared to the surfactant-only curve.

This interaction is driven by a hydrophobic affinity increasing in strength with higher degree of polymer hydrophobicity [16]. From T1 to T2, the interaction between the components results in the adsorption of surfactant onto the polymer forming necklace-like complexes in the bulk that adsorb at the interface; a metastable plateau is reached, the length of which increases linearly with polymer concentration [16]. The interface is saturated of complexes capable of modifying the activity coefficients therefore rendering the Gibbs isotherm useless as a method to calculate the surface adsorbed amounts.

With increasing surfactant concentration, from T2 to T3, free surfactant monomers start replacing the complexes at the interface, i.e. the polymer is saturated. From T3 onwards, the CMC value of the surfactant is reached and the curve becomes a stable plateau meaning that the interface is saturated with more energetically favoured surfactant micelles. The mixture of poly(vynilpyrrolidone) or PVP and sodium dodecyl sulfate or SDS constitutes an example of this behaviour [4, 17]. Another example is the SDS/PEO system [18].

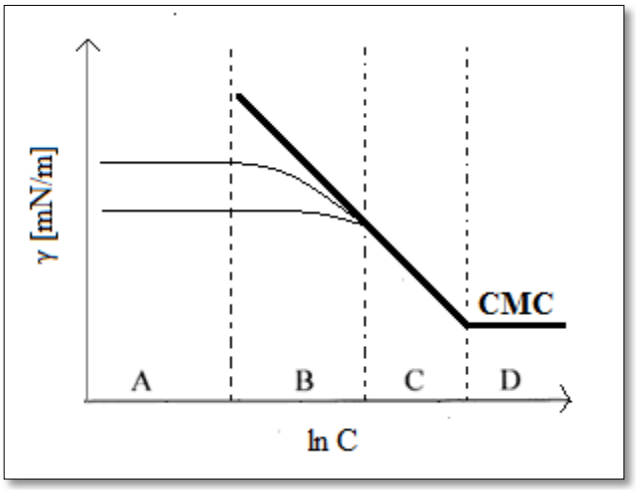

Fig. 2.1.3.2. Adsorption curve obtained with systems such as lysozyme/$C_{12}E_5$.

For weakly interacting systems, in contrast to the explanation given in relation to Figure 2.1.3.1, there is also a possibility that no cooperative interaction takes place at low surfactant concentrations. This is region A in Figure 2.1.3.2. The thick black line corresponds to a surfactant only curve; the thin black lines represent two different

concentrations of polymer added to the surfactant. The lowest belongs to the highest polymer concentration.

Green et al. [19] showed that this is the case for the mixed lysozyme/$C_{12}E_5$ system. With an increase in concentration the surfactant co-adsorbs on the polymer (region B). This is true over a relatively short range of surfactant concentrations that vary according to polymer concentration. With even more surfactant, the system behaves as if only surfactant was present at the interface suggesting a competitive adsorption where the polymer gets replaced by the surfactant (regions C, D). Nonetheless, this behaviour is only exhibited in the surface tension experiments whereas their neutron reflection results point towards a possible conformational change in the lysozyme at low concentrations of $C_{12}E_5$. Blomqvist et al. [20] observed similar behaviour mixing the non-ionic triblock copolymer PEO_{99}-PPO_{65}-PEO_{99} (F127) and the protein β-lactoglobulin.

Finally, the dashed line with 'S'-labelled points shows the behaviour of strongly interacting systems such as mixtures of charged polymers and charged surfactants.

2.1.4. Models of S-labelled curves

Since the Gibbs adsorption Equation on its own is not valid to describe the 'T'- and 'S'-labelled curves due to the change in species activities through aggregate formation, different attempts have been made to explain the experimental data that follows these shapes.

2.1.4.1. Orogenic model

Mackie et al. [21] proposed a model which they called 'orogenic displacement' in an attempt to describe the adsorption mechanism followed by mixtures of protein and surfactant. Although initially they experimented with solid/liquid interfaces, their theory was later expanded to account for air/liquid interfaces [20, 22, 23] and different types of surfactants and proteins. This led them to the conclusion that their orogenic model is generic [24]. Different experimental techniques like atomic force microscopy and Brewster angle amongst others [25] also support their model.

The orogenic model is based in the mechanical properties of a protein network adsorbed at an interface. Broadly speaking, it states that a protein adsorbs at an interface and due to its heterogeneity, a surfactant follows by adsorbing at defects found in the adsorbed protein network until protein displacement from the interface is reached. Mackie et al. then argue that the differences observed between the adsorption of mixtures with non-ionic or ionic surfactants arise from the difference in elastic response with respect to one or other kind of surfactant. Thus, for a non-ionic surfactant, adsorption at defects is the first step. This creates a surfactant domain in the protein network, i.e. nucleation, which grows with increasing surfactant concentration until it reaches a break point leading to the collapse of the protein network.

However, if the surfactant is ionic, after adsorption at defects, the growth of the domain created is limited by electrostatic interactions with the protein network. Therefore, the protein network does not collapse because of the growth of a hole but rather due to the increasing number of nucleation sites with increasing concentration.
In both cases, the elastic resistance of the protein network against displacement by the surfactant determines the final outcome of the competition with the latter [22].

2.1.4.2. S-labelled curves according to Bell et al.

According to Bell et al. [26], in order of increasing concentration, up to S1 (region A), synergistic behaviour already shows by lowering the surface tension; the surfactant monomers bind onto the polymer forming surface active complexes. Thus, Gibbs Equation does not describe the system as previously explained for the 'T'-labelled curve.

S1 can be considered the CAC in this curve at first glance. However, no surfactant micelles are associated with the polymer at this stage, only surfactant monomers. Thus, the real CAC should take place at higher surfactant concentrations [26, 27] that do not necessarily relate to any feature in the curve since the strong interaction at the surface screens the bulk effect of the CAC. As opposed to weakly interacting systems, the synergy in this case is assumed to be caused mainly by electrostatic interactions. For the strongly interacting systems there is a dependence on the type of charges that the surfactant head group carries. It is generally accepted that anionic surfactants interact

with polymers more strongly than cationic surfactants [16, 28, 29]. This could be explained in terms of the interactions between the surfactant charges and the polymer dipole [16].

From S1 to S2 (region B), a metastable plateau appears. A sublayer of surfactant aggregates bind onto the polymer/monomer complexes already adsorbed at the surface causing conformational changes. In this region, even though no apparent changes are observed in the curve, it is assumed that the composition of the complexes varies at different surfactant concentrations leading to the formation in the bulk phase of non-surface active complexes of polymer and surfactant micelles adopting a 'necklace' structure.

An increase in solubility (S2 to S3) arises due to hydrophobic parts of the polymer associating with surfactant chains to avoid exposure to the solvent; this results in complexes returning to the bulk solution and consequently a higher value of surface tension.

In region C, from S3 to S4, the amount of surfactant monomers increases contributing to a decrease in surface tension. Replacement of the polymer/monomer complexes at the interface starts from S4 onwards (region D), where the curve reaches an equilibrium state or plateau area and mainly surfactant only aggregates are present. S4 is therefore the CMC of the mixture. This point can appear below or above the concentration corresponding to the CMC of the surfactant-only solution depending on whether the association with the polymer facilitates or hinders the aggregation of the surfactant. The surface tension value beyond this point is also affected by the interaction with the polymer resulting in a lower value when the polymer facilitates the aggregation of the surfactant. This type of interaction can be observed in the mixed lysozyme/SDS system [28]. The results were also supported by Alahverdjieva et al. [30] using dynamic surface tension measurements and ellipsometry.

Other examples are the mixtures of SDS with the cationic polymer PDMDAAC [31, 32], DTAB with the anionic polymer NaPSS [33,34] and the hydrophobically modified anionic polymer PMAOVE with DTAB [35]. Of particular interest for this work are the studies of the polyethylenimine (PEI)/SDS and PEI/C_{16}TAB systems [36-38] which are

the systems that more closely resemble two of the mixtures studied here. This shall be explained in later Chapters. It is worth noticing that the polymers in these examples are not very surface active (including PEI which does not adsorb at the air/liquid interface [39]) and no interaction of this kind was found in the literature involving surface tension measurements of polymers that are more surface active than the surfactant.

Nevertheless, different techniques have probed this particular case. For instance, the interaction between hydrophobin HFBII and ionic surfactants C_{16}TAB and SDS was studied by neutron reflection by Zhang et al. [40]. They reported different behaviour at different pHs. At pH 3, close to the neutralization condition for the protein [40] and concentrations just below the CMC of the surfactant, the HFBII/SDS mixture produces a complex adsorbed layer. This was attributed to complex formation at the interface. At pH 7 however, the protein dominates the interface below the surfactant's CMC.

Bell et al. [16, 26] developed a mathematical description of the 'S'-labelled curve based on the application of the Gibbs Equation and the Langmuir isotherm, in combination with a model proposed earlier by Gilanyi and Wolfram [41]. The latter aimed to explain the interaction between neutral polymers and surfactants (i.e. weakly interacting systems) through the law of mass action. The application of their model in terms of surface tension experiments succeeded in explaining the 'T'-labelled curves. Nevertheless, to describe the 'S'-curves, Bell at al. [16, 26] followed the hypothetical model already proposed by Taylor et al. [34, 42] in which the appearance of a peak is attributed to the relative stability of the polymer/monomer complex (S1 to S2) and the polymer/micelle complex (S2 to S3).

Taylor et al. stipulated that the peak is more likely to appear with higher polymer concentration and with minimal difference in relative stability of the polymer/monomer and polymer/micelle complexes. In Bell's description, for surfactant concentrations up to S1, they assumed the cooperation between polymer and surfactant is a single-step reaction; this however, fails to describe the experimental data at low concentrations. The fact that they use the Langmuir isotherm also implies the assumption that the excluded area at the interface is exactly the same for every component whether it is a free surfactant monomer or a complex. This also fails to account for polydispersity effects.

Another assumption leading to possible deviations when applied to real data is that the maximum surface excess corresponds to that calculated for the surfactant-only curve and the number of free surfactant monomers contained in the micelles, *N*, forming the polymer/micelle complexes is the same as for surfactant-only micelles. Despite the many simplifications encountered in this model, a relation between the amount of surfactant in the bulk, S_b, and the free surfactant at the interface, *S*, was obtained [26] and it follows

$$S_b = S + S_{CMC}\left(\frac{S}{S_{CMC}}\right)^N + P_b\left(\frac{nM\left(\frac{S}{S_{CAC}}\right)^{nM} + L\left(\frac{S}{S_{ELE}}\right)^L}{1 + \left(\frac{S}{S_{CAC}}\right)^{nM} + \left(\frac{S}{S_{ELE}}\right)^L}\right) \qquad Eq.\,2.1.16$$

where n is the number of surfactant micelles containing *M* surfactant monomers in the polymer/micelle complex and *L* is the number of surfactant monomers in the polymer/monomer complex. The terms S_{CMC}, S_{CAC} and S_{ELE} relate to the concentrations at the surfactant CMC, the CAC and the formation of surface polymer/monomer complexes, respectively. Similar expressions for every component were also obtained.

Hence, Bell et al. were able to formulate a criterion for the appearance of the peak in the hope to devise tailor-made surfactant systems. They concluded that the peak depends not only on the parameters that appear in Equation 2.1.16 but also on the difference in surface activities of the surfactant and the polymer/monomer complex. In reaching this criterion, they assume that $S_{ELE} < S_{CAC} < S_{INT} < S_{CMC}$, where S_{INT} is a function of the difference in stability in polymer/monomer and polymer/micelle complexes.

Although this model has proved useful in describing the DTAB/NaPSS system amongst others, its many assumptions lead to a failure for other systems like the C_{16}TAB/NaPSS. Consequently, further improvements are necessary to achieve a full description of strongly interacting systems.

2.1.4.3. S-labelled curves according to Campbell et al.

Campbell et al. [43], through the study of PDMDAAC/SDS, generalised their findings for strongly interacting systems. According to this group, the appearance of a peak in a 'S'-labelled curve is not due to relative surface activities of different complexes; the peak can be switched on and off by altering the pH of the solution so the colloidal stability is restablished, or by resuspending surface active material in the solution so the depletion causing the appearance of the PDMDAAC/SDS-style peak vanishes.

Through turbidity and gravimetric studies of the PDMDAAC/SDS mixture, they arrived to the conclusion that the peak is the product of the slow depletion of surface active material from the bulk solution via precipitation in the phase separation region, which in turn causes depletion at the interface and the appearance of the peak. The measurements of the precipitated material at concentrations around the peak formation suggest a relation between both since the minimum proportion of precipitated material found was 85%.

The changes produced with pH were observed through electrophoretic mobility measurements. The results indicate a charge reversal passing through a zero point at or around the surfactant concentrations causing the appearance of the peak. This also holds true in the case of the PEI/SDS system [44].

2.1.5. Dynamic surface tension

Notice the surface excess subscript 'eq' referring to adsorbed amounts under equilibrium conditions in Equation 2.1.11; the Gibbs Equation describes the equilibrium situation. However, the adsorption of molecules at the interface is a dynamic process that is never final and molecules continue moving in and out of the interfacial layer. Thus, when referring to equilibrium in this context, it refers to the flux of monomers adsorbing at the surface equalling the flux of monomers desorbing or returning to the bulk phase.

If a subsurface of a few molecular diameters is assumed to exist between the interface and the liquid phase, two models exist that can describe the adsorption of surfactants to the interface and explain the decay in the value of surface tension with time [8].
Initially, the interfacial layer is just composed of water molecules and acts as if no other components were present. This is followed by the diffusion of monomers from the bulk onto the subsurface from where they may either freely adsorb at the interface or they have to overcome an adsorption barrier impeding their direct diffusion into the interface and causing them to diffuse back into the bulk. The barrier may be caused by a lack of empty spaces at the interface or by an increase in surface pressure as well as due to electrostatic or conformational constraints.

The diffusion of monomers into the subsurface determines the rate of adsorption in the diffusion-only model whereas the barrier overcoming process is the rate determinant step in the mixed kinetic-diffusion controlled model.

In the absence of a barrier, the process can be explained mathematically via the Fick's Equations or via the Ward-Tordai Equation. The latter describes the amounts of material adsorbed at the surface or surface excess, Γ, as a function of time. With the bulk and subsurface concentrations given by C_0 and C_s, respectively, and D the diffusion coefficient, the Ward-Tordai Equation is written as

$$\Gamma = \Gamma(t) = 2C_0\left(\frac{Dt}{\pi}\right)^{1/2} - 2\left(\frac{D}{\pi}\right)^{1/2}\int_0^{t^{1/2}} C_s\, d(t-\tau)^{1/2} \qquad Eq.\,2.1.17$$

where τ is a variable of integration and t is time. The first term describes the initial diffusion and adsorption of monomers into a newly formed interface. The second term accounts for the back diffusion of monomers that do not find a free interfacial space to adsorb into due to the presence of other previously adsorbed molecules and are therefore forced to move back into the bulk. Both terms are dependent on time.
If the adsorption from the subsurface is hindered, it is possible to think of an energy barrier (ε_a) that needs to be overcome before adsorption occurs [45-48]. In this case, the diffusion coefficient in Equation 2.1.17 becomes

$$D^* = De^{\left(-\frac{\varepsilon_a}{RT}\right)} \qquad Eq.\,2.1.18$$

In general, to model dynamic surface tension data, an adsorption isotherm (i.e. Langmuir's if a limiting value for monomers reaching the interface is assumed; or Frumkin's if solute-solvent interactions are considered) is chosen to be incorporated in the Ward-Tordai Equation described above after substitution in Gibbs Equation.

Limiting solutions are then calculated and these offer a direct relation between surface tension and time dependence of the adsorption process. Thus, on the one hand, at short times the monomers adsorb at the interface and no back diffusion occurs. Since the back diffusion is expressed in the second term of the Equation, this can be neglected.
The Henry's isotherm (Eq. 2.1.19) [9], defined as the product of the bulk concentration, *C*, by the Henry's equilibrium adsorption constant K_H, constitutes the simplest example:

$$\Gamma = K_H C \qquad Eq.\,2.1.19$$

The equilibrium description of the system, i.e. Gibbs Equation, then leads to the following Equation of state:

$$\Pi = \gamma - \gamma_0 = -nRT\Gamma \qquad Eq.\,2.1.20$$

corresponding to the short-time condition when the change in interfacial tension is minimal. Substituting this expression in Equation 2.1.17 results in

$$\gamma_{t\to 0} = \gamma_0 - 2nRTC_0\left(\frac{Dt}{\pi}\right)^{1/2} \qquad Eq.\,2.1.21$$

On the other hand, when enough time has been given to the system, the concentration at the subsurface can be considered close to that of the bulk and thus from the Ward-Tordai Equation it is possible to obtain the relation

$$\Delta C_{t\to\infty} = C_0 - C_s = \Gamma\left(\frac{\pi}{4Dt}\right)^{1/2} \qquad Eq.\,2.1.22$$

By substituting in Gibbs Equation the result is now

$$\gamma_{t\to\infty} = \gamma_{eq} + \frac{nRT\Gamma_{eq}^2}{C_0}\left(\frac{\pi}{4Dt}\right)^{1/2} \qquad Eq.\,2.1.23$$

The above Equation allows checking whether the system is following a diffusion-only model or a mixed model with an energetic barrier [7, 8, 49]. If the resulting γ vs. $t^{-1/2}$ plot agrees with a diffusion-only model (i.e. Equation 2.1.23), the relationship should be linear. Generally, for LMW surfactants at $t > 0.25$ s or equivalently $t^{-1/2} < 2$ s$^{-1/2}$, the diffusion-only model is followed [8].

Equations 2.1.21 and 2.1.23 [50] clearly demonstrate how the initial bulk concentration and particle number affect the modification of the interface.

2.2. ζ-potential

2.2.1. The electrical double layer

When a solid particle is placed in an aqueous solution the charges at its surface interact with the nearby solvent charges. For the system to be at equilibrium the latter are either attracted to or repelled from the surface causing an electrical layer to form around the surface of the particle to shield its charges. This layer is known as the electrical double layer (EDL). The self-explanatory adjective 'double' indicates the existence of two different regions within the electrical layer formed at the particle surface. Helmholtz offered a rough description of the electrical double layer consisting of two rigid layers: a first region (inner Helmholtz layer) where the charges are highly packed and in close proximity to the particle surface and a second region immediately after (outer Helmholtz layer) of similar characteristics but opposite charge due to counterion presence [2, 51-54].

Unlike Helmholtz, Gouy and Chapman believed the counterion region could not be simply defined as a rigid body of opposite charge but the Brownian thermal motion of the ions also needed to be accounted for. Thus, in their model, the counterions are in the liquid phase and their concentration, c_i, follows a Boltzmann distribution function to describe the probability of finding a particular state of the system at a temperature T:

$$c_i = c_{i,\infty} e^{-z_i e\psi / k_B T} \qquad Eq.\,2.2.1$$

where z_i is the valence of the ions, e is the electron charge, k_B is Boltzmann's constant and ψ is the electric potential. The ion concentration in the bulk is $c_{i,\infty}$. This second layer is known as the diffuse layer.

The Gouy-Chapman model assumes the particle surface and the ions are ideal, no ion-ion interaction (other than the electrostatic) occurs, the activity is equal to the molar concentration and there is no specific adsorption of ions [2, 51-54]. Experimental results proved the EDL to be thicker than Gouy and Chapman predicted. Thus, Otto Stern further contributed to the Gouy-Chapman model by introducing a few constraints.

Firstly, ions are only allowed to come as close as distance δ from the surface and the plane situated at this distance is known as the Stern layer. This distance is of the order of their hydrated atomic radii. Secondly, within the δ distance, ions can adsorb at the particle surface and the electric potential decays almost linearly (see Figure 2.2.1.1). Furthermore, the specific adsorption of ions can lead to charge neutralization and ultimately to charge reversal [2, 51-54].

In general, the electric field E generated by an electric potential ψ is defined as the negative gradient of the potential and can be related to the charge density $\rho = \sum_i z_i e c_i$ by applying Gauss' law for electricity. The result is Poisson's Equation:

$$\nabla^2 \psi = -\frac{\rho E}{\varepsilon} \qquad Eq.\,2.2.2$$

where ε is the permittivity of the medium.
A combination of the Boltzmann distribution function with Poisson's Equation leads to the Poisson-Boltzmann Equation [2, 51-54],

$$\nabla^2 \psi = -\frac{e N_A}{\varepsilon} \sum_i c_{i,\infty}\, z_i e^{-z_i e\psi / K_B T} \qquad Eq.\,2.2.3$$

(N_A: Avogadro's constant)

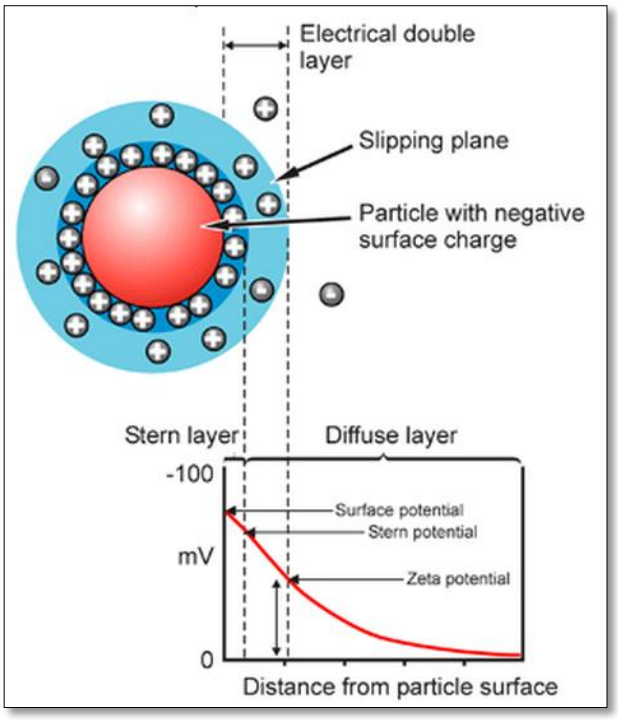

Fig. 2.2.1.1. Electrical double layer [56].

which in the Stern model is used to describe the electrical double layer through its one-dimensional linearised form and for the case when $z_i\psi \ll k_BT$. This is known as the Debye-Hückel approximation. Hence, the condition to apply this approximation is imposed by the limiting thermal voltage $V = k_BT/e \approx 26\,mV$, which is the minimum voltage or potential a colloidal system may present in a stable dispersed state [55].

For the given case, the exponential term of the Poisson-Boltzmann Equation is treated mathematically using a Taylor expansion ($e^x \approx 1 + x$) to obtain

$$\nabla^2\psi = K^2\psi \qquad Eq.\,2.2.4$$

The characteristic thickness of the electrical double layer (EDL), also called the Debye screening length, represents the change in the potential in the double layer as a function of the distance from the particle surface. Thus, it accounts for screening effects between the charges which are stronger at shorter distances. When a system is electrically neutral, Equation 2.2.4 leads to the definition of the Debye length [55]:

$$K^{-1} = \frac{\sqrt{\varepsilon RT}}{FI^{1/2}} = \frac{\sqrt{\varepsilon V/e}}{I^{1/2}} \qquad Eq.\,2.2.5$$

where R is the gas constant; F is Faraday's constant $F = N_A e = 96485\ C/mole$; and I is the ionic strength, $I = \frac{1}{2}\sum z_i^2 c_i$.

2.2.2. Electrokinetic effects

In a system consisting of particles in suspension in an aqueous medium, the application of an electric field results in electrokinetic effects due to the charges at the particle surfaces. These effects are known under different names depending on the relative position of the liquid to the particle [51, 53, 56].

Electrophoresis results from the movement of a particle relative to a stationary liquid and produces an electric field known as sedimentation potential.

Electroosmosis results from the movement of a liquid relative to a stationary particle and produces an electric field known as streaming potential [51, 53, 56].

2.2.3. Electrophoresis and relation to ζ-potential

When a particle travels through a liquid, the charges in the electrical double layer move accordingly. The slipping or hydrodynamic shear plane is then defined as the plane that separates the moving charges attached to the particle surface from those that do not follow the movement of the particle. It is the potential at this plane that is used to determine the surface charge experimentally using electrophoresis and it is known as the zeta potential or ζ [51, 53, 56].

2.2.4. DLVO

When a real colloidal system is under study it is necessary to use a model not only for the individual interactions of the electrical double layers with the aqueous medium but also for a possible overlapping or repulsion of EDLs accompanying the different existing particles in the suspension.

The Derjaguin-Landau-Verwey-Overbeek theory is such a model [2]. The DLVO theory (see Figure 2.2.4.1) attempts to describe the colloidal stability in a solution of suspended particles. Under the Derjaguin approximation a spherical particle of radius a is thought of as the sum of many parallel disks. Two spherical particles in solution separated by a distance d interact repulsively if their electrical double layers overlap and attractively due to the van der Waals forces acting between them. The overall energy of the interaction U_{DLVO} is then, using the Derjaguin approximation ($a >> d$), given by [2, 57],

$$U_{DLVO} = 2\pi\varepsilon a\zeta^2 e^{-Kd} - \frac{Aa}{12d} \qquad Eq.\,2.2.6$$

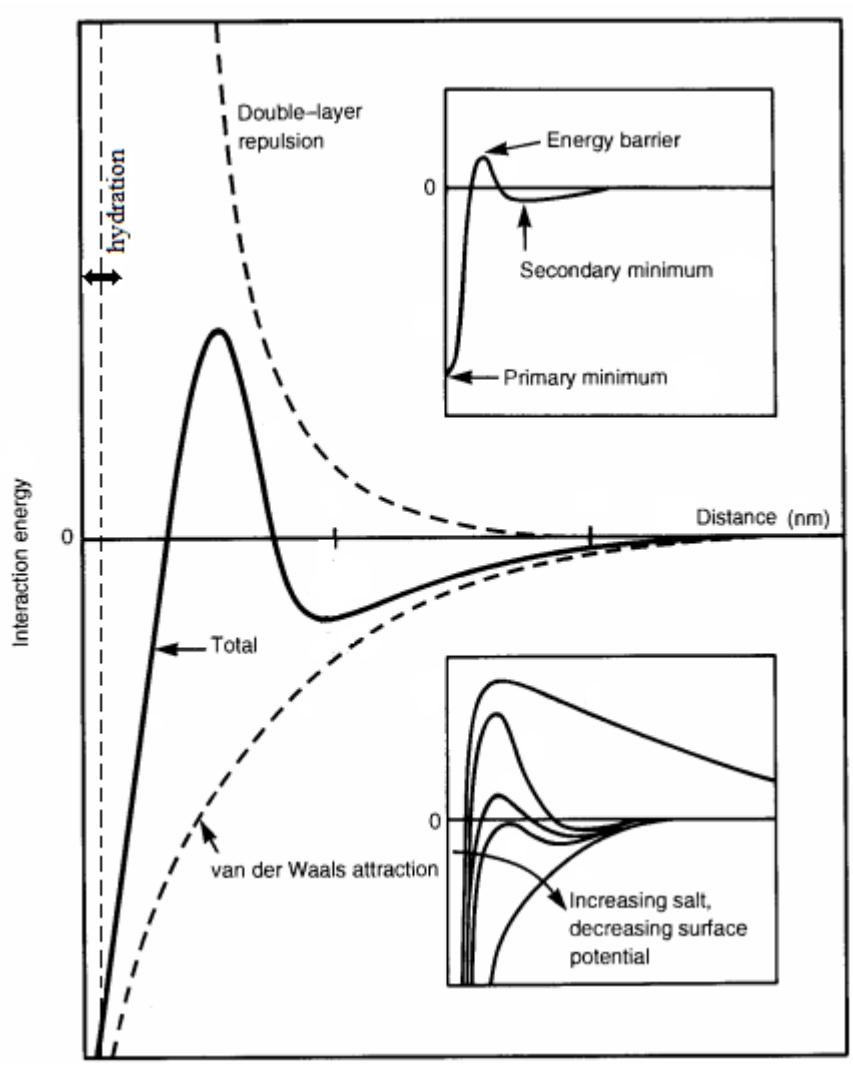

Fig. 2.2.4.1. DLVO theory (adapted from [58]).

The first term relates to the electrostatic repulsion (i.e. Coulomb type) and the second term describes the van der Waals attractive interaction (together with hydration (see 2.2.5.) as a Lennard-Jones type potential) where *A* is known as the Hamaker constant, which accounts for each van der Waals macroscopic pair potential [58].

As seen in Figure 2.2.4.1, the combined effect of both interactions presents an energy barrier to aggregation which can only be overcome by Brownian motion in the absence of external actions. Towards the left side of the barrier, the combined potential curve falls into a primary minimum leading to the aggregation of the particles. Aggregation may also occur towards the right side of the energy barrier where there may exist a secondary minimum in the curve. The position of the minimum in which aggregation takes place determines whether aggregation is termed coagulation (primary minimum) or flocculation (secondary minimum).

The left side potential well is due to short range repulsion between particles and it is thought of as being critical to the repeptization or restoration of the aggregates [2].

2.2.5. Repeptization

Repeptization is hindered by the time dependency of aggregation. However, aggregation is sometimes reversible although with polyvalent ions is a rare occurrence. Thus, even though the restoration of the colloidal stability is not easily explained, several postulates attempt to do so by trying to justify the existence of the Hofmeister series [2].

On the one hand, the possibility that a monolayer of water (i.e. ~0.2 nm) exists at the surface of a particle implicates that the proximity between two particles is limited by the repulsion produced by the hydration of these layers. This repulsion overlaps the curve representing the combined attractive and repulsive interaction in the region tending towards the primary potential well in Figure 2.2.4.1. Thus, the thicker the bound solvent layer is, the closest the energy barrier is and the easier it is to overcome it.

On the other hand, the rate of relaxation of the double layer if diluting the solution can lead to a temporary alteration in the available energy to overcome the energy barrier whilst equilibrium is being restored. During this time repeptization may occur [2].

Hence, extended versions of the DLVO theory exist which introduce different terms (i.e. hydration forces, hydrophobic forces…) into Equation 2.2.6 in order to tackle the deviations of the theory from experimental observations.
The aggregation process is influenced by the size of the particles and the amounts of electrolyte present in the solution. Temperature also affects the repulsive term; however, this effect is negligible. Thus, manipulation of these parameters can aid aggregation [2].

2.2.6. Particle size

From Equation 2.2.6, it is clear that particle size has a direct relation with the attractive and the repulsive terms. Whilst the thermal energy needed to overcome the energy barrier remains unaffected by particle size, for a solution with smaller particles the energy barrier is lowered [2].

2.2.7. Addition of electrolyte

Because the exponential in the repulsive term in Equation 2.2.6 depends on the inverse Debye screening length, an increase in electrolyte concentration leads to a decrease in the repulsive interaction (see Figure 2.2.4.1) expressed by a lower value of ζ-potential; that is, a less stable colloidal system. Addition of electrolyte therefore leads to a collapse of the combined potential curve and aggregation at the critical coagulation concentration or CCC [2].

Since the surface charge of a particle varies with the relation between the dissociation of the surface functional groups and pH, it can be concluded that the ζ-potential is pH dependant. Thus, a plot of the ζ-potential versus pH (see Figure 2.2.7.1) reveals the pHs at which the colloidal system can be regarded as stable, i.e. $\zeta \geq |\pm 26\, mV|$. The region comprised between -26 mV and 26 mV represents unstable colloidal systems and maximum instability is reached at a ζ-potential value equal to 0 mV, known as the isoelectric point (pI) or point of zero charge (pzc); that is, no repulsive forces act between particles due to the absence of surface charges [53, 59]. Nevertheless, steric effects may hinder the aggregation process. The adsorption of a steric stabiliser layer (i.e. polymers adsorbed on the surface of particles) leads to an increase in the repulsive

forces between particles which in turn also results in a lower value of ζ-potential without necessarily manifesting itself through a decrease in electrostatic interactions [2, 53, 54].

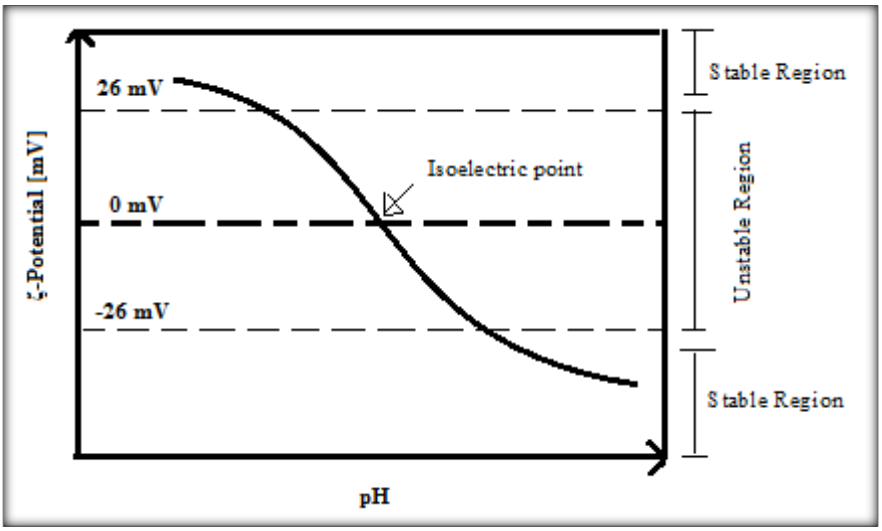

Fig. 2.2.7.1. A typical ζ-potential curve.

It is worth noticing that the isoelectric point and the point of zero charge are not always coincident and specific ion adsorption may result in a difference in these values. Specific adsorption of cationic species shifts the pI to a higher pH and lowers the pH at which the pzc occurs. If specific adsorption of anionic species occurs, the shifts in pH follow the opposite trend [2, 59].

2.2.8. Hofmeister series

We have so far established that addition of electrolyte to a solution may cause aggregation. However, aggregation depends on whether the added electrolytes are monovalent or polyvalent and even when comparing two monovalent electrolytes, the quantities leading to aggregation vary and the CCC is generally found in the 50-250 mM region [2]. It has been found that electrolyte adsorption depends on its hydrated size. Thus, adsorption of electrolytes is related to the pH of the solution as explained earlier. The valence also seems to play a role.

Moreover, when more than one kind of electrolyte is present in solution there may be different compounds formed and their properties may affect the adsorption of ions on the surface of the particles.
Generally, larger ions adsorb more strongly even when present in small amounts.
An experimental classification of the strength different electrolytes have in the aggregation process are the Hofmeister series. The following are the Hofmeister series showing some monovalent cations and anions [60]:

$$(Cations) \qquad Li^+ < Na^+ < K^+ < H_3O^+ < NH_4{}^+ < Rb^+ < Cs^+$$

$$(Anions) \qquad F^- < OH^- < Cl^- < Br^- < I^- < SCN^-$$

The differences in the effect of adding different electrolytes to the solution do not affect the interpretation of the DLVO theory since it uses the ζ-potential to describe the vicinity of the particle's surface and not the surface potential [2].

2.2.9. Debye-Hückel approximation relation to Henry's Equation

In the dilute regime, the EDLs of different particles do not overlap when the system is stable. Every EDL presents a maximum potential of approximately 26 mV corresponding to the thermal voltage; that is, for repulsive and attractive interparticle interactions to be in equilibrium, the maximum Debye screening length depends only on thermal Brownian motion as the ionic strength is low enough to consider the probability of interactions between particles occurring as negligible [2, 51]. This particular case is known as the Debye-Hückel approximation and it allows calculating the ζ-potential through measurement of the electrophoretic movement of particles in solution while neglecting interparticle effects; that is, the attractive term in Equation 2.2.6 is zero.

The Navier-Stokes Equation, which describes the flow of incompressible fluids, leads to a description of the electrophoretic mobility U_E of a particle in a solution under a weak applied electric field and in the low Reynold number's regime (particles moving slowly in a viscous medium [61]), where any convection is neglected [55], through an expression known as Henry's Equation

$$U_E = \frac{2\varepsilon\zeta F(Ka)}{3\eta} \qquad Eq.\,2.2.7$$

where η is the viscosity of the medium and $F(Ka)$, known as Henry's function, is a dimensionless correction factor to account for the effect of resistance to mobility due to local electric fields through the EDL and hydrodynamic friction [56, 62]. $F(Ka)$ is dependent upon the inverse Debye screening length and the particle radius, a. For a spherical non-conductive particle,

$$F(Ka) \approx \frac{2}{3}\left[1 + \frac{{}^{1}/_{2}}{\left(1 + \frac{2.5}{{}^{a}/_{K^{-1}}}\right)^{3}}\right] \qquad Eq.\,2.2.8$$

Henry's function will determine whether the solution to the analysis of the electrophoretic mobility follows a Hückel approximation, a Smoluchowski approximation or is in between both approximations [53].

In the Hückel approximation, $F(Ka)$ = 1, and it is employed when the electrical double layer is thick and the particle is small in comparison, i.e. $a \leq 0.1\,nm$. There may be local electric fields through the EDL. This approximation is used for non-polar fluids. In the Smoluchowski approximation, $F(Ka)$= 1.5, and it is employed when the electrical double layer is thin and the particle is big in comparison, i.e. $a \geq 200\,nm$. This approximation is commonly used for polymers in aqueous solutions [53, 56, 62].
From Equation 2.2.7, it is clear that for the many-particles case the Debye screening length and the ζ-potential play a crucial role in the description of the system.

2.3. Foam studies

2.3.1. Definition of foam

Foam is a metastable structured system composed of gas pockets or cells supported by a continuous matrix. The matrix can be a solid or a liquid.

Examples of naturally found foams are pumice stones, bone structures, wood and honeycombs. Artificially created foams are also commonly encountered, i.e. beer heads, polyurethane (in insulation and upholstery), polyethylene (in insulation and packaging), fire extinguisher foams… [2, 63-66].

The vast importance of foams derives from the many different applications based in their properties. They are used in transport of materials in metal drillings and oil processes [67]. The low weight and high performance as supportive structures of some foams is exploited on a daily basis; for instance, in a mattress.

What follows in this Chapter is mainly concerned with foams of liquid matrixes (solutions of surfactants and/or polypeptides) and air pockets. These are employed in personal care products (i.e. detergency) and throughout the food industry (aerated food, i.e. a meringue).

2.3.2. Geometry of foam and viscoelasticity

The air pockets or cells in foams are surrounded by the supporting matrix due to a thermodynamically driven process [65] in which work is done to expand the surface area, *A*. This requires a certain amount of energy *U* that depends on surface tension, γ:

$$U = 2\gamma A \qquad Eq.\,2.3.1$$

The matrix forms a barrier between air pockets and at the same time allows transport processes to take place within.

Each pocket adopts a geometrical shape where the sides of the geometrical Figure separating two cells constitute the lamella region containing a two-dimensional thin film [2]. The plateau borders are the connecting points between two lamella regions (i.e. the vertices) [67]. In two dimensions, the plateau borders connect three lamellae at an angle of 120° (Steiner angle). In three dimensions, the plateau borders connect four lamellae at 109° [2].

This is better seen through a picture shown in Figure 2.3.2.1 obtained from a sample of 18 mM DTAB in 10 mM NaCl solution at pH 5.

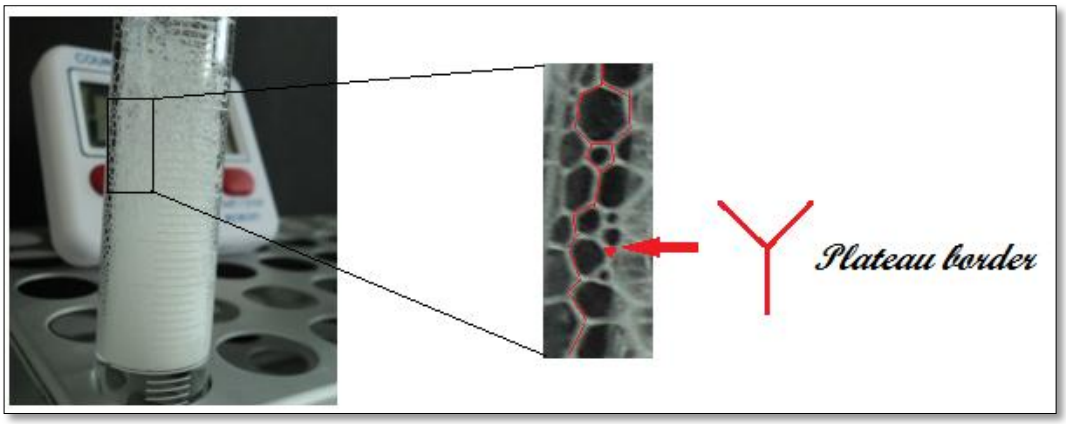

Figure 2.3.2.1. Foam obtained from 18 mM DTAB in 10 mM NaCl solution at pH 5. The straight red lines highlight the lamellae and the arrow points to a plateau border.

An isolated air pocket can be compared to a soap bubble. Its geometry arises as a consequence of the forces acting upon it (minimizing surface area in an attempt to achieve equilibrium or minimum energy) and constitutes a prediction of the system behaviour (if the 'correct' shape is adopted, the system is more durable).
However, minimizing the energy does not mean forming fully spherical shapes as could be expected based on mathematical arguments of minimal surfaces. The rigidity or viscoelasticity and shear history of the soap film also plays a role in determining its shape.

Likewise, the cells formed in foam are not spherical but curved in nature (or more exactly, they are almost regular polyhedral [2]) and their viscoelastic behaviour is fundamental for understanding the reasons behind foam collapse. The elasticity or rigidity of the cell is crucial to maintain the pressure difference, or Laplace pressure [68], between cells.

Hence, we introduce the elastic modulus ε_0 and its relation to the Gibbs elasticity E_G, in the limiting case of thin films, and define it as the "ability of increase tension during stretching" [69]

$$\frac{1}{2}E_G = \frac{\varepsilon_0}{1 + \left(\frac{h}{2}\right)\left(\frac{dc}{d\Gamma}\right)} \qquad Eq.\,2.3.2$$

The term $dc/d\Gamma$ is the slope of the surfactant's equilibrium adsorption isotherm and h is the thickness of the film [70]. The Gibbs elasticity is given by

$$E_G = \frac{2d\gamma}{dlnA} \qquad Eq.2.3.3$$

and in the case of incompressible fluids (i.e. liquids) it becomes

$$E_G = 2A\frac{d\gamma}{dA} \qquad Eq.2.3.4$$

where $d\gamma$ can be interpreted as the stress (i.e. compression) and dA as the strain (i.e. elongation) [71].

Furthermore, the overall behaviour of the foam matrix is given by the dilatational and shear viscoelastic moduli. Both viscoelasticities can be defined as a complex quantity expressed through the sum of a storage modulus and a loss modulus which correspond to the real and imaginary terms, respectively. The storage modulus in the dilatational viscoelasticity is the dilational elasticity o elastic modulus and the loss modulus is the dilational viscosity arising from internal relaxation and diffusive transport of surface active material between the bulk and the surface [65, 70-73].

Figure 2.3.2.2 is a general representation of the viscoelastic behaviour of foams. If an area is disturbed enough to reach the yield stress point, foams collapse and become liquid. Yield stress is strongly dependent on the liquid fraction present in the matrix.
Just below this point, the matrix behaves as a plastic solid; that is, the effect caused by the disturbance is irreversible and its viscosity is not constant. This is manifested through a structural rearrangement. Small disturbances however, leave foams in the elastic limit where any effect caused is reversible and the viscosity is constant [74].

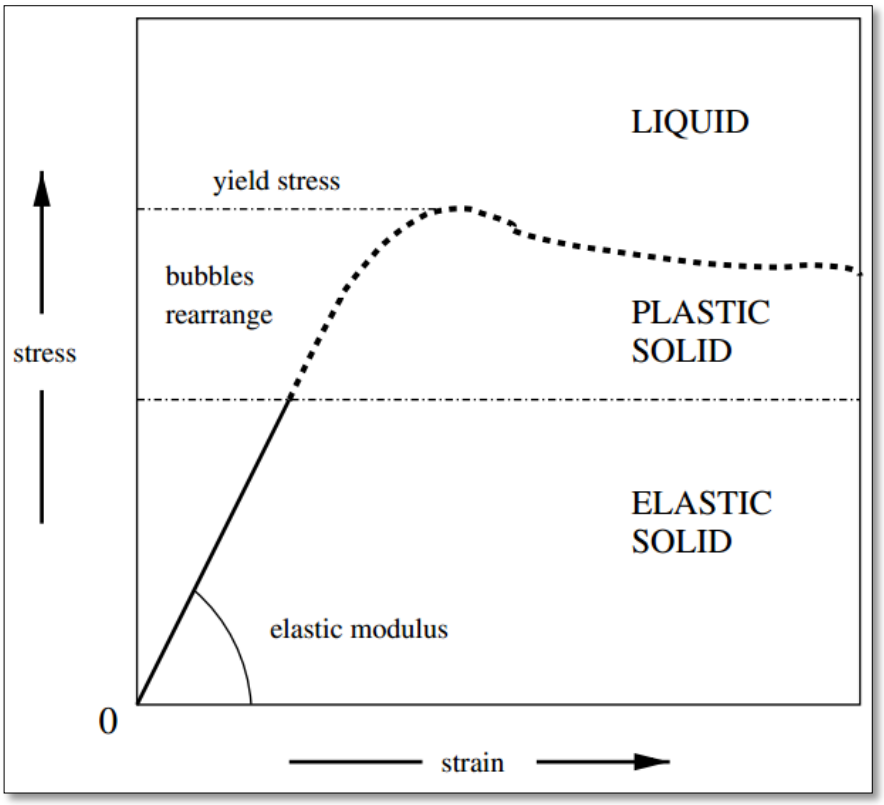

Figure 2.3.2.2. Description of the stress/strain relation in liquid foams [74].

2.3.3. Foam formation and stability

The formation and stability of foams depend on several factors related to composition of the liquid phase, many of which can be manipulated to enhance the properties of interest for a particular application.

External manipulation methods, others than those related to composition, can also be applied (i.e. irradiation) [75].

In any case, to enhance foam properties it is necessary to understand how foams are formed and the mechanisms that stabilize or collapse them.

This is not an easy task due to the non-equilibrium nature of foams. Formation and destabilization processes may occur simultaneously.

2.3.3.1. Foam formation

The ability of a solution to foam relies on several factors [64]. The most important is the need to exert some vigorous movement onto the liquid/gas phase separation [67]. This

is done through a variety of mechanisms ranging from a simple shake to the use of most sophisticated devices where parameters such as gas flow, bubble size, temperature and pressure can be controlled. The chosen mechanism and the liquid composition determine the volume of foam produced.

Another requirement is the addition of material to a chemically pure liquid, usually in the form of surface active agents. It is well known that a chemically pure liquid does not produce foam and therefore foam formation depends on the composition of the liquid phase and a lowering of the interfacial tension [67].

The rate of adsorption of surface active agent to the air/liquid interface is also a determinant condition for foaming [65, 67]. Note that although foams form at low surface tension, how much the surface tension is lowered is not relevant per se [66]. The gas pockets need to be covered in a layer of adsorbed surfactant and this can only happen with the adsorption process taking place in a rapid manner.

If the adsorbed material is not capable of undergoing conformational changes, the air pockets do not form. Thus, a certain degree of flexibility (i.e. viscoelasticity) in the adsorbed layer is a prerequisite.
Hence, foam formation is linked to the electrokinetic properties of the interface and surface charge, i.e. optimal surface adsorption occurs in a rapid manner at the isoelectric point or pI. Under pH conditions far from the pI adsorption is hindered. At the pI, the yield stress point increases and therefore elasticity also increases (see fig. 2.3.2.2). Thus, manipulation of foams trough addition of electrolytes is possible [65, 72].

Once the air pockets are formed they are arranged in a higher order structure with viscoelastic properties. The formation of this structure depends on the molecular packing of surfactant micelles present in the lamellae. Hence, the molecular packing and micelle structure affect the flow of surfactant through the lamellae and plateau borders [20].

Finally, since it is necessary to exert some vigorous movement onto the liquid/gas phase separation for it to foam, it is logical to think that the way in which this action is undertaken impacts on the molecular packing and ultimately in the matrix structure.

2.3.3.2. Foam stability

Once foam is produced it can collapse due to the lack of resistance of the matrix structure to interfacial changes and although it is unrelated to the concept of thermodynamic stability (foam is a non-equilibrium state), this is termed foam stability [64].
Like the ability to foam, foam stability depends on the composition of the liquid, the molecular packing and its evolution with time, and the electrokinetic properties of the interface [20].

Foam stability can be short-lived or long-lasting. The rheological properties of the foam (i.e. viscoelasticity) are associated with the composition of the matrix and therefore they also depend on the original liquid phase.

An important parameter when referring to foams is their relative density or *R*. If the matrix is a one polymer solution, *R* is defined as the ratio between the density of the foam and the density of the polymer, and its porosity is given by 1-*R*. The relative density is also the volume fraction of polymer in the foam and the porosity is the air fraction. The relative density of typical low density foam is $R < 0.1$ [76].

In liquid foams, gravity affects foam stability through drainage [65, 77]. Gravity pulls the material contained within the matrix creating a flow to oppose any emerging surface tension gradient between the lamella region and the plateau borders that can cause localized depletion of surface active agents. Hence, low density foams are less affected by gravity than high density foams.
The opposing flow is known as the Gibbs-Marangoni effect and it can also oppose surface tension gradients arising from lateral stretching of a lamella region [2, 20, 66, 77].

Common factors in foam collapse are coarsening processes like coalescence or disproportionation.
Coalescence is a randomly distributed process [78] based on two cells merging through rupture of the lamella separating region due to the formation of thermally activated

holes [79]. Because foam cells differ in size, the rupture of different size cells results in different magnitude effects [78, 80].
Disproportionation is a diffusion process. Foams suffering this process experience a transfer of gas or liquid from the smaller cells to the largest ones to equilibrate the pressure difference between cells [65, 66, 72, 79].
Lowering the surface tension reduces the chances of disproportionation [81].

Foam stability also depends on the viscoelastic layer opposing collapse via steric repulsion within the matrix to avoid too much film thinning or via electrostatic interactions caused by the double layers [20, 65].

2.3.4. Foam behaviour of conventional low molecular weight surfactants

Not all conventional low molecular weight (LMW) surfactants are capable of foaming [64] regardless of their ability to lower the surface tension of liquids what is an indicative of the foaming process being dependant on other parameters like the rate of adsorption or the ability to desorb amongst others. However, for those that do produce foams, the ability to foam is at its highest at or above the CMC [2].

Although LMW surfactants like C_nTAB [82] stabilize foams through steric repulsion and electrostatic interactions, it is mainly the lateral transport of material adsorbed at the matrix, i.e. Gibbs-Marangoni effect, that is responsible for foam stability in this type of foam. The lateral transport also causes adsorption from the bulk. The film thickness is restored due to transport of material within the matrix and also from the bulk [20]. Thus, mobility and speed in the adsorption process are the main mechanisms to withstand collapse.

The increase in stability due to the electrostatic repulsions existent in foams of ionic surfactants means these are better foamers than non-ionic surfactants [2].
In general, it can also be said that the longer the hydrocarbon chain is, the more foam that is produced. However, chain branching or any other mechanism that increases area cross-section results in a decrease in volume of foam produced [2].

2.3.5. Foam behaviour of proteins

A protein solution foams if rapid adsorption followed by conformational changes or denaturation occurs. Contrary to LMW surfactants, foam made from a protein solution is stable because a viscoelastic layer forms at the interface thus resulting in rigid plateau borders [82]. The foam stability is thickness dependent and is aided by steric resistance to coalescence [65, 81].
The matrix viscosity helps decreasing drainage as in the case of whey protein isolate [65]. Thus, protein foams need to lower the surface tension, adsorb rapidly, rearrange at the interface and suffer conformational changes and they also depend on the film thickness and viscosity to counteract collapse and stabilise the foam.

Proteins are known to lower the surface tension to values typically in the 45 mN/m region [65]. However, as in the case of LMW surfactants, some proteins are better foaming agents than others. The main reason behind these differences lies on their structure. Globular proteins like lysozyme, BSA or β-lactoglobulin show a higher degree of matrix viscoelasticity than other more flexible proteins like β-casein. This translates in differences in magnitude of transmitted forces and therefore in different overall resistance to collapse [65, 83]. Unlike LMW surfactants, proteins rely mostly on their adopted structure in the matrix to prevent collapse.

2.3.6. Foam behaviour of mixtures

Some proteins have proved to be effective foaming agents. Nevertheless, high amounts of protein are generally needed to achieve stable foams unless they are mixed with some LMW surfactants [81].

The latter disrupt protein-only foams by adsorbing at defects encountered within the matrix [20] and therefore the right equilibrium in concentrations of both components must be found if stable foam is the outcome sought after.
At the appropriate concentrations, the combination of both can result in a synergistic increased viscosity opposing film rupture (protein foam behaviour) and an increased ability to transport molecules within the matrix and from the bulk to replenish any depleted area (LMW surfactant behaviour), thus avoiding collapse mechanisms.

The interaction between a protein and a surfactant, and therefore their synergistic effect, depends mainly on the surfactant nature and its concentration.
For a protein/non-ionic surfactant, the surfactant gradually displaces the protein from the surface in a competitive adsorption process.

For a protein/ionic surfactant at low surfactant concentrations, electrostatic interactions dominate. With increasing surfactant concentration the charges in the protein and surfactant interact by forming molecular complexes which may differ in surface tension related capabilities from those of the protein or the surfactant on their own [81] (an example of high ability to foam is observed in mixtures of SDS/β-casein [82]).

Therefore, different surfactants result in different foam properties. With even more surfactant, the complexes need to compete with the unbound surfactant to reach the interfaces. Finally, the surfactant replaces the complexes at the interface.

2.4. Neutron scattering theory

The Schrödinger Equation is the basic vehicle that allows us to apply principles of non-relativistic quantum mechanics to understand the behaviour of a thermal neutron (thermal neutrons correspond to 25 meV energies and 1.8 Å wavelength [84]) being scattered from a target composed of many nucleons (protons and neutrons). This is essentially the principle on which neutron scattering techniques are based.

In its stationary form, for a particle of mass *m* under the influence of a square well interaction potential *V(r)* and using a radial function $u(r) = r\psi(r)$ to represent the system (where ψ is the wave function representing the wave form of the particle), the Schrödinger Equation is expressed as

$$\frac{d^2u}{dr^2} + \frac{2m}{\hbar^2}\left[E - V(r) - \frac{l(l+1)\hbar^2}{2mr^2}\right]u = 0 \qquad Eq.\,2.4.1$$

In the above Equation E is the allowed energy states of the system; $l = \hbar k R_0$ is the angular momentum quantum number; k is the wavenumber; R_0, the distance between the nucleons and $\hbar$, Planck's constant [85].

This form of Schrödinger Equation involves a plane incident wave and a spherical scattered wave. Its solution is

$$\psi(r) = A\left[e^{ikr} + f(\theta)\frac{e^{ikr}}{r}\right] \qquad Eq.\,2.4.2$$

where $f(\theta)$ is the scattering amplitude and it is proportional to the Fourier transform of the interaction potential, $V(r)$.

For slow neutrons (i.e. $\lambda >>$ nuclear radius), it is acceptable to believe that the process occurs primarily under no angular dependence, or $l = 0$, and if temporal dependence is included in the previous Equations, then $f(\theta)$ at $k \rightarrow 0$ becomes [85]:

$$f(\theta) = -a \qquad Eq.\,2.4.3$$

The constant a is the scattering length of the incident particle and can be defined through the expression

$$a = \pm \lim_{k \to 0} \frac{\delta_0}{k} \qquad Eq.\,2.4.4$$

where δ_0 is the phase shift of the scattered wave with respect to the incident wave. The scattering length is related to the scattering cross-section σ, or the total probability of an incident particle to be scattered in any direction [85], through the expression

$$\lim_{k \to 0} \sigma = 4\pi a^2 \qquad Eq.\,2.4.5$$

Due to the short-ranged character of the interaction, $kr << 1$, and the wavefunction becomes

$$\psi(r) \approx A\left(1 - \frac{a}{r}\right) \qquad Eq.\,2.4.6$$

The implications of this solution are dependent upon the sign of a [85]. Whether it is positive or negative would reflect in the behaviour of the wavefunction with respect to the nucleus. With the boundary conditions being imposed on the radial function, a becomes [84, 85]

$$a = R_0\left(1 - \frac{tan(kR_0)}{kR_0}\right) \qquad Eq.\,2.4.7$$

Very relevant to the current study, this highlights a most powerful aspect of neutron scattering which is the ability to selectively highlight the different features we are interested in studying in a material through the use of isotopic labelling via simple exchange of deuterium for hydrogen [86, 87].

However, since our neutron is being scattered by many nuclei, the Schrödinger Equation and its solution have to be adapted to the present case. Hence, a is now called the free scattering length and b is the bound coherent scattering length:

$$b = \frac{m}{m_r}a \qquad Eq.\,2.4.8$$

where m_r is the reduced mass of the system [85].
For example, in Figure 2.4.1 a hydrogen atom lies in the negative area of the b/R_0 axis whereas a deuterium atom lies in the positive area. This is the result of a 180^{o} phase shift between waves scattered by hydrogen and those scattered by deuterium [89].

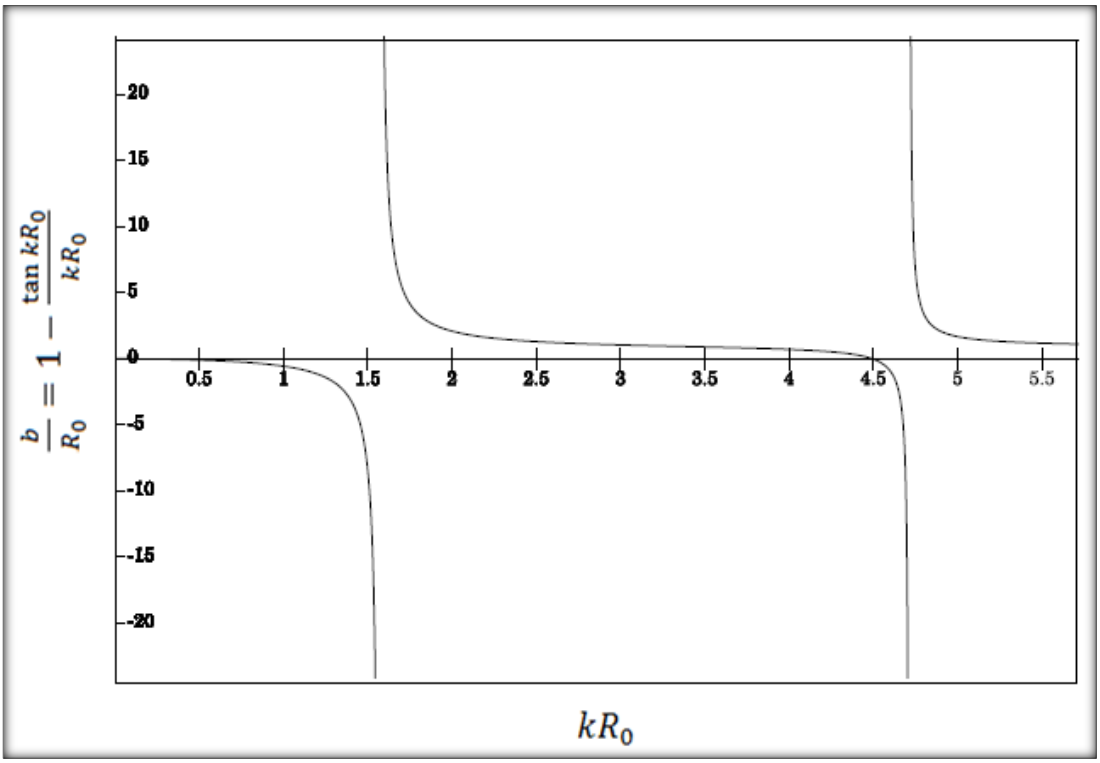

Fig. 2.4.1. Isotopic labelling.

The following Table (2.4.1) contains some of the scattering length values used in this work:

Isotope [90]	b [fm]		Solvent	b [fm]
H	-3.7406		H_2O	-1.678
D	6.671		D_2O	19.145
C	6.6511		NRW	0.0
O	5.803		Surfactant	
S	2.804		h-SDS ($C_{12}H_{25}O_4SNa$)	15.9442
Br	6.795		d-SDS ($C_{12}D_{25}O_4SNa$)	276.2842
N	9.36		h-DTAB ($C_{15}H_{34}BrN$)	-11.3354
Na	3.63		d-DTAB ($C_{15}D_{25}H_9BrN$)	243.9856

Table 2.4.1. Scattering lengths of materials used in this project.

2.4.1. Neutron Reflection

Neutron reflection is an in-situ depth profiling technique. Whether on its own or in conjunction with other spectroscopic techniques (i.e. spectroscopic ellipsometry), it is a powerful mean to obtain information about surface adsorbed amounts and layer structure at the interface through the analysis of the elastic scattering of neutrons from a surface. Despite it being a penetrative technique, it is unlike X-ray techniques, non-destructive due to the weakly interacting nature of neutrons with matter.

It covers a vast range of concentrations from dilute solutions to solutions concentrated to several times the critical micelle concentration in the case of a surfactant and it helps us visualize the changes that take place when monomers become micelles. It has also proved useful in demonstrating the effect of electrolytes on the solutions studied.

2.4.1.1. Specular Neutron Reflection

Specular neutron reflection occurs when the incident and scattered angles are equal, $\theta_i = \theta_f = \theta$, as shown in Figure 2.4.2.

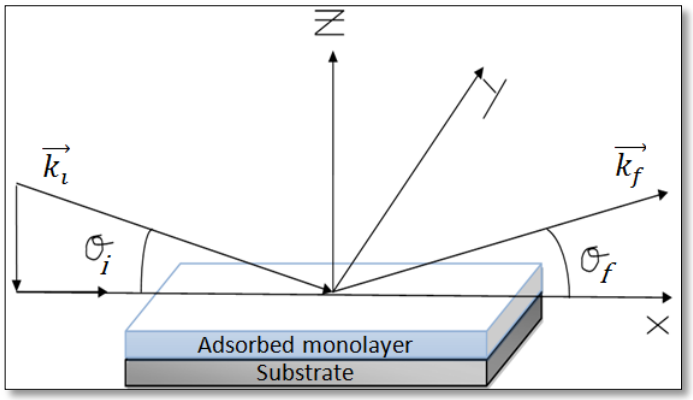

Fig. 2.4.2. Schematic representation of specular neutron reflection.

The difference between the final and the initial wave vectors $\overrightarrow{k_f}$ and $\overrightarrow{k_i}$ at a wavelength λ defines the momentum transfer or scattering vector *Q* in the z-direction perpendicular to the interface (x-y plane) as

$$Q = Q_z = \overrightarrow{k_f} - \overrightarrow{k_i} = \left(\frac{4\pi}{\lambda}\right)\sin(\theta) \qquad Eq.\,2.4.9$$

Specular neutron reflection can be analyzed by applying either particle scattering theory or a classical thin film optics approach.

2.4.1.2. Optical model

The phenomenon of elastic nuclear scattering is identical to that of light being diffracted by an opaque disk. However, in nuclear scattering there are no equivalent intensity minima due to the diffuseness (or lack of sharp edges) of the nuclei. Hence, an optical model can be used to describe elastic scattering in the presence of absorptive effects in a nuclear reaction by choosing a complex potential with a nuclear potential term and another term *W(r),* to explain the absorptive effects [94]:

$$U(r) = V(r) + iW(r) \qquad Eq.\,2.4.10$$

The description of the system is complete after solving Schrödinger Equation if *U(r)* has a square-well form and choosing *V(r)* to be the Fermi pseudopotential [95]:

$$V(r) = \frac{2\pi\hbar^2}{m}b \qquad Eq.\,2.4.11$$

In specular neutron reflectivity, a monochromatic neutron beam is directed towards its target at a grazing angle. As in thin film optics, the refractive index of neutrons is

$$n_r = \frac{k_f}{k_i} \qquad Eq.\,2.4.12$$

In the case of neutrons, it can also be written as a complex function where the complex term depends on the cross-sections of the absorptive σ_a, and incoherent effects, σ_i:

$$n_r = 1 - \lambda^2\frac{nb}{2\pi} - i\lambda n\frac{\sigma_a + \sigma_i}{4\pi} \qquad Eq.\,2.4.13$$

Since the absorptive effects are generally much weaker than the elastic component, it is generally accepted that they should be ignored [88, 94].

The scattering length *b* (recall it is related to the Fourier transform of the interaction potential *V(r)*) is a positive value for most materials leading to a refractive index value less than 1. This produces total external reflection and constitutes the condition for the determination of the critical grazing angle of incidence in the instrumental setup (typically less than 3°) [94].

Following the above Equation, the refractive index can be related to the scattering length density through the expression

$$n_r^2 = 1 - \frac{\lambda^2}{\pi}\rho \qquad Eq.\,2.4.14$$

with the scattering length density $\rho = \rho(z)$ being defined by

$$\rho = \sum_i b_i n_i \qquad Eq.\,2.4.15$$

and n_i representing the number density of nucleon i.

In the optical model [88, 94] the reflectivity is then expressed as

$$R(Q) = \frac{16\pi^2}{Q^4}\Delta\rho^2 \qquad Eq.\,2.4.16$$

If the adsorbed material forms several layers at the interface, then using the Abeles matrix method it can be expressed as the product of the individual matrices C_{ij} defining each layer through the Fresnel coefficients r_{ij} at the ij interface,

$$R(Q) = \prod C_{ij} \qquad Eq.\,2.4.17$$

with

$$C_{ij} = \begin{pmatrix} e^{i\beta_i} & r_j e^{i\beta_i} \\ r_j e^{-i\beta_i} & e^{-i\beta_i} \end{pmatrix} \qquad Eq.\,2.4.18$$

where

$$r_{ij} = \frac{p_i - p_j}{p_i + p_j} \qquad Eq.\,2.4.19$$

and

$$p_i = n_i \sin\theta_i \qquad Eq.\,2.4.20$$

and

$$\beta_i = \left(\frac{2\pi}{\lambda}\right) n_i \tau \sin\theta_i \qquad Eq.\,2.4.21$$

τ is the thickness of the adsorbed material.

2.4.1.3. The kinematic form-factor approximation

Within quantum mechanics, it is common to talk about the expectation value. This is the average value of a parameter *f* and it is calculated through

$$\langle f \rangle = \int \psi^* f \psi dx \qquad Eq.\,2.4.22$$

where Ψ^* is the complex conjugate of Ψ.
In a similar approach [85], the quantum mechanical matrix element *M*,

$$M = \int \psi_Y^* \psi_b^* V_w \psi_X \psi_a dv \qquad Eq.\,2.4.23$$

where V_w is a weak perturbing potential affecting the stationary state of a particle, acts as a substitute of the Schrödinger Equation in its function to describe a system going from the initial state (X + a) to the final state (Y + b).The transition or scattering amplitude is now governed by Fermi's Golden Rule [85]:

$$f(\theta) = \frac{2\pi}{\hbar} |M|^2 \cdot den(E_f) \qquad Eq.\,2.4.24$$

with *den(E_f)* being the density of final states or number of states per unit energy interval at the final state, E_f.

The plane-wave Born approximation uses this description of the system and assumes the scattering takes place only at the surface of a nucleus.

This model considers Ψ_a and Ψ_b to be plane waves resulting from the superposition of incident spherical waves [84, 95]. This assumption results in a wavefunction proportional to a combination of Bessel's functions and Legendre's polynomials. Therefore, unlike the optical model, it contains information about the angular dependence.

The kinematic expression for reflectivity is derived from the first order Born approximation (i.e. first order perturbation theory) and although scattering by thermal neutrons is not appropriately described by this approximation on its own, "in combination with the Fermi pseudopotential, it gives the required result of isotropic scattering for a single fixed nucleus" [84].

Crowley [96] showed that the kinematic reflectivity for a flat surface can be expressed as

$$R(Q) = \frac{16\pi^2}{Q^2}\left|\int \rho(z)e^{-iQz}dz\right|^2 \qquad Eq.\,2.4.25$$

Thus, the reflectivity can be expressed through self-partial structures h_{ii} or cross-partial structures h_{ij}:

$$R(Q) = \frac{16\pi^2}{Q^2}[b_a^2 h_{aa} + b_b^2 h_{bb} + b_s^2 h_{ss} + 2b_a b_a h_{ab} + 2b_a b_s h_{as} + 2b_b b_s h_{bs}] \qquad Eq.\,2.4.26$$

The subscripts *a* and *b* refer to different components of the adsorbed material and *s* refers to the solvent used in the solution [97].

The partial structures are the one dimensional Fourier transforms of the number density distributions of individual components, n_i.

$$h_{ii} = |n_i(Q)|^2 \qquad Eq.\,2.4.27$$

$$h_{ij} = Re\left|n_i(Q)n_j(Q)\right| \qquad Eq.\,2.4.28$$

The h_{ii} terms relate to the distribution of individual components at the interface and the h_{ij} relate to their relative positions.

If the h_{ii} and h_{ij} factors have been already determined experimentally, the kinematic approximation does not need to make model assumptions to fit the data [91, 92] thus, offering a more precise analysis of the layer than the optical model. The structure factors can be expressed as a function of the distance between the centres of distribution δ_{ij}. Their distances from the centre can be seen as an even function

$$h_{ij} = \pm\sqrt{h_{ii}h_{jj}cos\left(Q\delta_{ij}\right)} \qquad Eq.\,2.4.29$$

or an odd function

$$h_{ij} = \pm\sqrt{h_{ii}h_{jj}sin\left(Q\delta_{ij}\right)} \qquad Eq.\,2.4.30$$

When plotting the h_{aa} structure factor against the square of the momentum transfer Q, a Gaussian model centred at position z can be fitted to the experimental data [91]:

$$n_z = n_0 e^{-\left(4z^2/\sigma^2\right)} \qquad Eq.\,2.4.31$$

where σ is the full width at 1/e of the maximum for which the reflectivity is

$$Q^2R = \frac{16\pi^2 b^2 N_a^2 \Gamma^2}{10^{40}} e^{\left(-Q^2\sigma^2/8\right)} \qquad Eq.\,2.4.32$$

(with b in Å and Γ in mol·m^{-2}). The exponential term accounts for departures from ideally flat surfaces due to thermal motions, i.e interfacial roughness, and it was calculated by Nevot and Croce [as explained in ref. 88]

It is possible to plot $ln\ (h_{ii})$ versus Q^2 by applying logarithms to both sides of Equation 2.4.32 to obtain an equation of type y = ax + b where the intercept is linked to the

adsorbed amount at the interface. If only one component is present, the resulting equation is

$$\ln h_{ii} \approx 2ln\Gamma - \frac{Q^2\sigma^2}{8} \qquad Eq.\,2.4.33$$

2.4.1.5. Null Reflecting Water and isotopic substitution

The use of Null Reflecting Water (NRW), also known as Air Contrast Matched Water (ACMW), in combination with deuterium isotopic labelling has become an essential tool to uncover structural and conformational details of a layer adsorbed at the air/liquid interface. NRW is composed of 8% D_2O and 92% H_2O and the calculation of its scattering length density shows it is, as its name indicates, non-reflecting. Thus, a layer of material adsorbed at the interface between a solution in NRW and air produces a reflectivity signal with structural information arising only from the material at the interface (see Figure 2.4.1.5.1) [98].

Using the reflectivity data obtained experimentally, *R(Q)*, a best fit model is chosen to describe the data from a combination of variables that fulfil any physical limitations we may know about the system under analysis. These are thickness τ and scattering length density ρ. The reflectivity curve may present characteristic features such as a Bragg peak that are helpful when establishing a first model approach.

When total external reflection occurs, the signal appears flat and *R(Q)* = 1. The signal then decays until reaching background levels. The value of *Q* where this happens is known as the critical edge, or $Q_{c,}$ and following Equation 2.4.25,

$$Q_c = \sqrt{16\pi\Delta\rho} \qquad Eq.\,2.4.34$$

At the air/liquid interface, a critical edge appears when examining a sample in D_2O solvent at Q_c = 0.0179 $Å^{-1}$. Thus, the critical edge offers an opportunity to check whether the reflectivity signal received has been scaled correctly or not to give an appropriate interpretation of the signal.

The appearance of a Bragg peak in the curve offers a direct way to estimate the spacing in a repeated structure, i.e. a multilayer. Combining Bragg's law

$$\lambda = 2\tau sin\theta \qquad Eq.2.4.35$$

with the momentum transfer, Equation 2.4.9, the spacing (or *d)* is given by [100]

$$d = \frac{2\pi}{Q} \qquad Eq.2.4.36$$

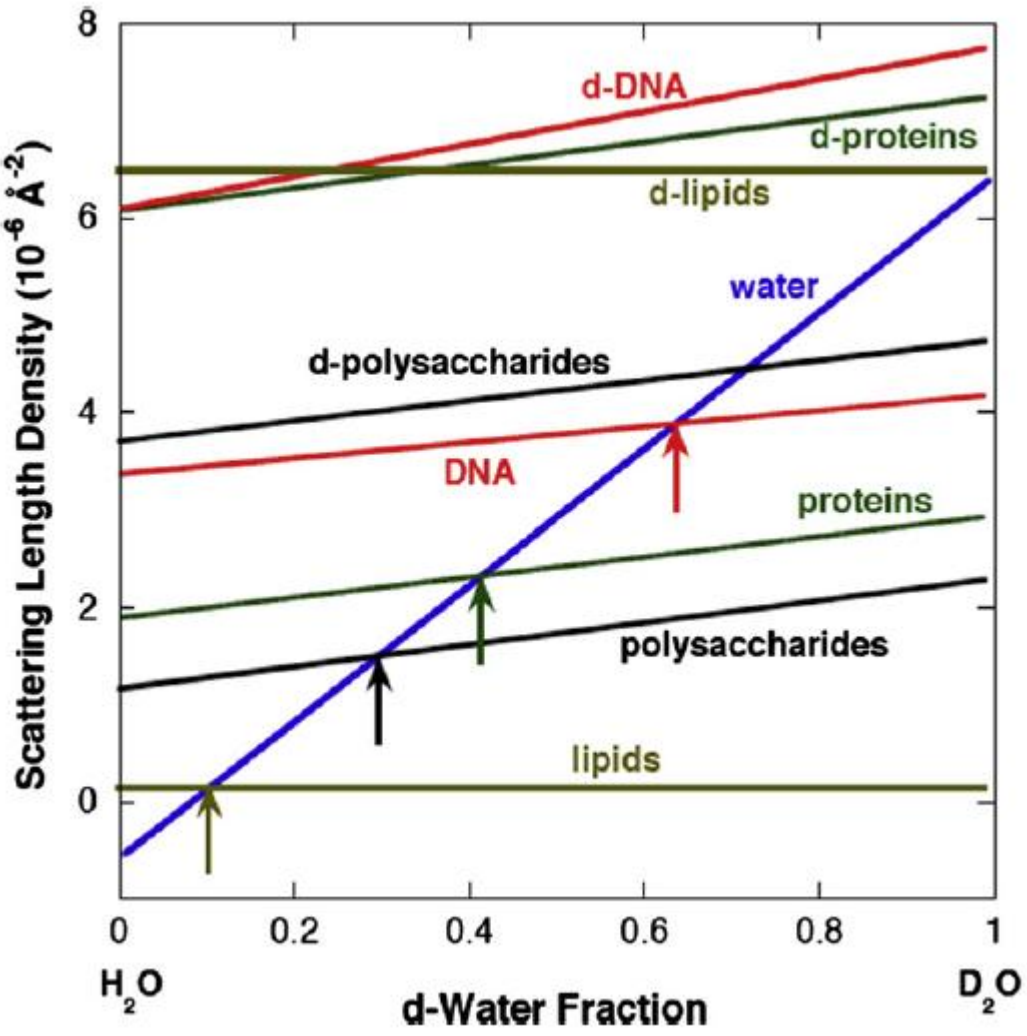

Fig.2.4.1.5.1. H2O / D2O scattering length density as a function of deuterium present. Notice how the y-axis corresponding to the values of ρ starts with negative values for 0% D_2O and at 8% D_2O, ρ = 0 (i.e. NRW) [99].

2.4.2. Small angle neutron reflection (SANS)

The elastic scattering of neutrons at small angles from colloidal particles in solution offers an opportunity to study not only the structure of one individual colloid but also its interactions with the surrounding media.
Small angle neutron scattering or SANS, has proved so far an important tool in the study of molecular aggregates such as micelles, microemulsions and liquid crystal structures [100].

The range of wavelengths used in this technique allows the study of length scales out of reach for other techniques, i.e. light and X-ray scattering, and the fact that neutrons barely interact with matter combined with their penetrative capabilities make it suitable to study biological materials like proteins without the need for crystallization [89].

Its importance gets emphasized when considering the in vivo relation of proteins with their surrounding environment. The electrolyte concentration and type present in the environment plays an important role in the protein behaviour and many physiological phenomena hinge on the existent protein/electrolyte interaction [89, 101].

2.4.2.1. Theory of small angle neutron scattering

To obtain structural information at macroscopic levels, it is necessary to introduce the macroscopic cross-section or $\Sigma = \sigma/V$, which is expressed in terms of V, the volume of one scattering centre; and σ, the microscopic scattering cross-section.
This can be separated into a coherent term dependant on the scattering vector Q and a incoherent term independent of Q.
In a neutron reflection experiment the reflectivity or *R(Q)* is the intensity measured. Similarly, in a SANS experiment, the scattered intensity *I(Q)* is measured.

Isotopic substitution is used in both techniques to discriminate some parts of the molecules being scattered and by using several substitutions, a more elaborated model of the system under study can be obtained (recall section 2.4.1.5). The appearance of Bragg peaks is also a common feature shared with neutron reflection. However, the scattering vector at low angles is now defined as

$$Q = \left(\frac{4\pi}{\lambda}\right)\sin\left(\frac{\theta}{2}\right) \qquad Eq.\,2.4.37$$

The signal observed in SANS is related to the macroscopic coherent cross-section via the following Equation

$$I(Q) = I_0(\lambda)\Delta\Omega\eta(\lambda)T(\lambda)V_{sample}\frac{d\Sigma(\mathrm{Q})}{d\Omega} \qquad Eq.\,2.4.38$$

where $\mathrm{I}_0(\lambda)$, $\Delta\Omega$, $\eta(\lambda)$ are the incident neutron flux, solid angle element defined by the detector/sample geometry and detector efficiency, respectively. These quantities are all dictated by the instrumental setup. $\mathrm{T}(\lambda)$ is the transmission from the sample and $\mathrm{V}_{\mathrm{sample}}$ is the volume of sample illuminated by the neutron beam [100].

Through the Rayleigh-Gans Equation and following the kinematic theory or Born approximation [102], the macroscopic differential cross-section is given by

$$\frac{d\Sigma(\mathrm{Q})}{d\Omega} = NV^2(\Delta\rho)^2P(Q)S(Q) + bgd \qquad Eq.\,2.4.39$$

where $\Delta\rho$ is the difference in scattering length densities of two scatterers and it is commonly known as contrast. *P(Q)* is a shape defining function known as the form factor, *S(Q)* or structure factor is a function of the inter-particle interactions and *bgd* is the background signal. The latter, as in neutron reflection, also arises mainly from incoherent effects.

Figure 2.4.2.1.1 is a representation of the form and structure factors as functions of the scattering vector. The product of both is the result of the modulation of $d\Sigma(\mathrm{Q})/d\Omega$ by interference effects between neutrons scattered off different parts of the same nucleus and different nuclei [100].

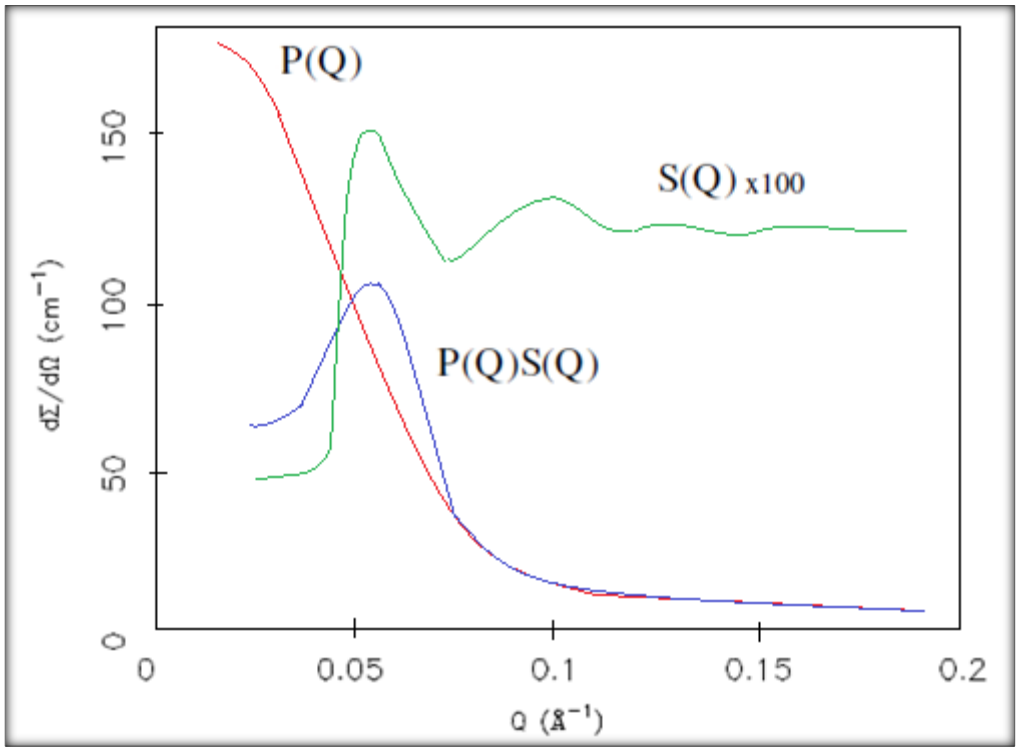

Fig.2.4.2.1.1. Data obtained in a SANS experiment.

2.4.2.2. Form factor

The interference effects caused by scattering of neutrons from different parts of the same nucleus are expressed through the form factor [100]:

$$P(Q) = \left|\frac{1}{V}\int dV e^{-iQr}\right|^2 \qquad Eq.\,2.4.40$$

Due to the complexity arising from solving this Equation in its general form, numerical methods are common place amongst SANS experimenters. The form factor is in this way, adapted to calculations for specific shapes. Some of the most common form factors are presented next [103].

For a sphere model:

$$P(Q) = \frac{scale}{V}\left(\frac{3V(\Delta\rho)(\sin(QR) - QRcos(QR))}{QR^3}\right)^2 + bgd \qquad Eq.\,2.4.41$$

(*R*: radius of the sphere).

For a spherical core/shell model:

$$P(Q) = \frac{scale}{V_s}\left(3V_c(\rho_c - \rho_s)\frac{(\sin(QR_c) - QR_c cos(QR_c))}{{QR_c}^3} + 3V_s(\rho_s - \rho_w)\frac{(\sin(QR_s) - QR_c cos(QR_s))}{{QR_s}^3}\right)^2 + bgd \qquad Eq.\,2.4.42$$

(subscripts *c, s, w* stand for core, shell and water (solvent)).

For a random Gaussian coil:

$$P(Q) = \frac{2}{QR_g}\left(e^{-Q^2R_g^2} + Q^2R_g^2 - 1\right) \qquad Eq.\,2.4.43$$

(R_g: radius of gyration).

2.4.2.3. Structure factor

The stability of a colloid is traditionally given by expressions derived from the Poisson-Boltzmann distribution function or the DLVO theory, both explained in section 2.2.

However due to the multiple failures encountered in these analytical approaches, the use of integral Equations has become more common in recent years [54]. In particular, the Ornstein-Zernike integral Equations (2.4.44 and 2.4.45, helps us resolve the expression for $g(r)$, known as the pair correlation function or radial distribution function,

$$h(r_{12}) = c(r_{12}) + \rho \int dr_3 c(r_{13})h(r_{23}) \qquad Eq.\,2.4.44$$

$$h(r) = g(r) - 1 \qquad Eq.\,2.4.45$$

(where $r = r_{ij}$ is the distance between a pair of particles, *h(r)* is the total correlation function and *c(r)* is the direct correlation function and ρ in this case, represents the number density or number of molecules per $Å^3$ [54, 101]).

Hayter and Penfold [104] showed that the result is given by using the above Equations in conjunction with the Mean Spherical Approximation or MSA [101, 104],

$$c(r_{12}) = -U(r)/k_BT \qquad \text{for r > 2R} \qquad Eq.\,2.4.46$$

$$h(r_{12}) = -1 \qquad \text{for r < 2R} \qquad Eq.\,2.4.47$$

and so the radial distribution function becomes,

$$g(r) = e^{-U(r)/k_BT} \qquad Eq.\,2.4.48$$

where *U(r)* is the interparticle interaction potential [86, 87].

The Ornstein-Zernike Equation also treats the particles as point scatterers and therefore does not take into account the excluded volume and the MSA considers the pair correlation function *g(r)* as equal to 0 [104].

The structure factor obtained in a SANS experiment is then the representation of "the interference effects caused by scattering of neutrons from different nuclei" [54, 84, 100],

$$S(Q) = 1 + \frac{4\pi N}{QV_s}\int_0^\infty (g(r) - 1)rsin(QR)dr) \qquad Eq.\,2.4.49$$

and it "is related to the interactions between particles and is independent of the neutron characteristics or its interaction with the particles in the scattering system [84]". This factor is also numerically treated to simplify the calculations. Thus, what follows is one of the most common numerical forms encountered throughout the literature. It gives an expression for *U(r)* to substitute in Eq. 2.4.48 and it is known as the Hayter-Penfold model [104] for the structure factor.

$$U(r) = \pi\varepsilon_0\varepsilon\sigma^2\psi_0^2 e^{(-K(r-\sigma)/r)} \qquad Eq.\,2.4.50$$

where K^{-1} is the Debye length; σ is the particle diameter; ε_0 is the permittivity of free space and ε is the dielectric constant. The surface potential is related to the electronic charge z_m and it is given by

$$\psi_0 = \frac{z_m}{\pi\varepsilon_0\varepsilon\sigma(2+K\sigma)} \qquad Eq.\,2.4.51$$

2.4.2.4. Polydispersity

When the system under study is composed of a distribution of sizes x_i, correction factors can be included in the calculations of form and structure factors to reach a better agreement with the experimental data. In this text, the chosen correction factor is the Schultz distribution [86, 87, 100],

$$f(x) = \frac{1}{Norm}(Z+1)^{(Z+1)}\left(\frac{x}{x_{mean}}\right)^2 \frac{e^{-(Z+1)x/x_{mean}}}{x_{mean}\Gamma(Z+1)} \qquad Eq.\,2.4.52$$

where Z is the width of the distribution , x_{mean} is the mean of the distribution, Γ is the gamma function and *Norm* is a normalization factor. Hence, the polydispersity index is given by $p = \sigma/x_{mean}$.

References

[1] P.W. Atkins, J. de Paula (2006) "Atkins' Physical Chemistry", 8th ed., Oxford University Press.

[2] L.L. Schramm (2005), "Emulsions, foams, and suspensions. Fundamentals and applications", Wiley-VCH.

[3] D. Myers (1991), "Surfaces, interfaces and colloids", VCH.

[4] I.P. Purcell, J.R. Lu, R.K. Thomas (1998) "Adsorption of sodium dodecyl sulfate at the surface of aqueous solutions of poly(vynilpyrrolidone) studied by neutron reflection", Langmuir, 14, pp. 1637-1645.

[5] V.B. Fainerman, E.V. Aksenenko, S.V. Lylyk, J.T. Petkov, J. Yorke, R. Miller (2010) "Adsorption layers characteristics of mixed sodium dodecyl sulphate/C_nEO_m solutions 1. Dynamic and equilibrium surface tension", Langmuir, 26 (1), pp. 284-292.

[6] P. Ghosh (2009) "Colloid and Interface Science", PHI Learning Pvt. Ltd.

[7] G. Barnes, I. Gentle (2011), "Interfacial science: an introduction", 2nd ed., Oxford University Press.

[8] J. Eastoe, A. Bankin, R. Wat. C. Bain (2001) “Surfactant adsorption dynamics”, Int. Rev. Phys. Chem., 20 (3), pp. 357-386.

[9] J. Eastoe, J.S. Dalton (2000) “Dynamic surface tension and adsorption mechanisms of surfactants at the air-water interface”, Adv. Colloid Interface Sci., 85, pp. 103-144.

[10] M. Yaseen, J.R. Lu, J.R. Webster, J. Penfold (2005) “Adsorption of single chain zwitterionic phosphocoline surfactants: effects of the length of alkyl chain and head group linker”, Biophys. Chem., 117 (3), pp. 263-273.

[11] J. Clint (1975) “Micellization of mixed non-ionic surface active agents”, J. Chem. Soc., Faraday Trans., 1 (71), pp. 1327-1334.

[12] P.H. Elworthy, K.J. Mysels (1966) ″The surface tension of sodium dodecylsulfate solutions and the phase separation model of micelle formation", J. Colloid Interface Sci., 21, pp. 331-347.

[13] V.B. Fainerman, E.V. Aksenenko, S.V. Lylyk, J.T. Petkov, J. Yorke, R. Miller (2010) “Adsorption layers characteristics of mixed sodium dodecyl sulphate/C_nEO_m solutions 3. Dynamic of adsorption and surface dilational rheology of micellar solutions”, Langmuir, 26 (4), pp. 2424-2429.

[14] P. Sehgal, H.D., M.S. Bakshi (2003) “Interfacial and micellar properties of binary mixtures of surfactant and phospholipid in an aqueous medium”, Colloid Polym. Sci., 281, pp. 275-282.

[15] D.N. Rubingh in K.L. Mittal (ed). (1979) “Solution chemistry of surfactants”, Plenum Press.

[16] C.G. Bell, C.J.W. Breward, P.D. Howell, J. Penfold, R.K. Thomas (2007) “Macroscopic modelling of the surface tension of polymer-surfactant systems”, Langmuir, 23, pp. 6042-6052.

[17] G. Masutani, M.K. Stenstrom (1984) “A review of surface tension measuring techniques, surfactants, and their implications for oxygen transfer in wastewater treatment plants”. Water resources program, School of Engineering and Applied Sciences, UCLA, Los Angeles, CA.

[18] D.J. Cooke, C.C. Dong, J.R. Lu, R.K. Thomas, E.A. Simister, J. Penfold (1998) “Interaction between poly(ethylene oxide) and sodium dodecyl sulfate studied by neutron reflection”, J. Phys. Chem. B, 102, pp. 4912-4917.

[19] R.J. Green, T.J. Su, J.R. Lu, J. Webster, J. Penfold (2000) “Competitive adsorption of lysozyme and $C_{12}E_5$ at the air/liquid interface”, Phys. Chem. Chem. Phys., 2, pp. 5222-5229.

[20] B.R. Blomqvist,, M.J. Ridout, A.R. Mackie, T. Warnheim, P.M. Claesson, P. Wilde (2004) “Disruption of viscoelastic β-lactoglobulin surface layers at the air-water interface by non-ionic polymeric surfactants ”, Langmuir, 20, pp. 10150-10158.

[21] A.R. Mackie, A.P. Gunning, P.J. Wilde, V.J. Morris (1999) "Orogenic displacement of protein from the air/water interface by competitive adsorption", J. Colloid Interface Sci., 210, pp. 157–166.

[22] J. Maldonado-Valderrama, N.C. Woodward, A.P. Gunning, M.J. Ridout, F. A. Husband, AR. Mackie, V.J. Morris, P.J. Wilde (2008) "Interfacial characterization of β-lactoglobulin networks: displacement by bile salts", Langmuir, 24 (13), pp. 6759-6767.

[23] A.R. Mackie, A.P. Gunning, P.J. Wilde, V.J. Morris (2000) "Competitive displacement of β-lactoglobulin from the air/water interface by sodium dodecyl sulfate", Langmuir, 16, pp. 8176-8181.

[24] N.C. Woodward, P.J. Wilde, A.R. Mackie, A.P. Gunning, P.P. Gunning, V.J. Morris (2004) "Effect of processing on the displacement of whey proteins: applying the orogenic model to a real system", J. Agric. Food. Chem., 52, pp. 1287-1292.

[25] A.R. Mackie, A.P. Gunning, M.J. Ridout, P.J. Wilde, V.J. Morris (2001) "Orogenic displacement in mixed β-lactoglobulin/β-casein films at the air/water interface", Langmuir, 17, pp. 6593-6598.

[26] C.G. Bell, C.J.W. Breward, P.D. Howell, J. Penfold, R.K. Thomas (2010) "A theoretical analysis of the surface tension profiles of strongly interacting polymer–surfactant systems", J. Colloid Interface Sci., 350, pp. 486–493.

[27] D.J.F. Taylor, R.K. Thomas, J.D. Hynes, K. Humphreys, J. Penfold (2002) "The adsorption of oppositely charged polyelectrolyte/surfactant mixtures at the air/water interface: neutron reflection from dodecyl trimethylammonium bromide/sodium poly(styrene sulfonate) and sodium dodecyl sulfate/poly(vinyl pyridinium chloride)", Langmuir, 18, pp. 9783-9791.

[28] R.J. Green, T.J. Su, H. Joy, J.R. Lu (2000) "Interaction of lysozyme and sodium dodecyl sulphate at the air/liquid interface", Langmuir, 16, pp. 5797-5805.

[29] Y. Nozaki, J.A. Reynolds, C. Tanford (1974) "Interaction of a cationic detergent with bovine serum-albumin and other proteins", J. Biol. Chem., 249 (14), pp. 4452-4459.

[30] V.S. Alahverdjieva, V.B. Fainerman, E.V. Aksenenko, M.E. Leser, R. Miller (2008) "Adsorption of hen egg-white lysozyme at the air–water interface in presence of sodium dodecyl sulphate", Colloids and Surfaces A: Physicochem. Eng. Aspects, 317, pp. 610–617.

[31] E. Staples, I. Tucker, J. Penfold, N. Warren, R.K. Thomas, D.J.F. Taylor (2002) "Organization of polymer-surfactant mixtures at the air-water interface: sodium dodecyl sulphate and poly(dimethyldiallylammonium chloride)", Langmuir, 18, pp. 5147-5153.

[32] J. Penfold, I. Tucker, R.K. Thomas, D. J. F. Taylor, X.L. Zhang, C. Bell, C. Breward, P. Howell (2007) "The interaction between sodium alkyl sulfate surfactants and the oppositely charged polyelectrolyte, polyDMDAAC, at the air-water interface:

the role of alkyl chain length and electrolyte and comparison with theoretical predictions", Langmuir, 23 (6), pp. 3128-3136.

[33] D.J.F. Taylor, R.K. Thomas, J. Penfold (2002) "The adsorption of oppositely charged polyelectrolyte/surfactant mixtures: neutron reflection from dodecyl trimethylammonium bromide and sodium poly(styrene sulfonate) at the air/water interface", Langmuir, 18 (12), pp. 4748-4757.

[34] D.J.F. Taylor, R.K. Thomas, P.X. Li, J. Penfold (2003) "Adsorption of oppositely charged polyelectrolyte/surfactant mixtures. Neutron reflection from alkyl trimethylammonium bromides and sodium poly(styrenesulfonate) at the air/water interface: The effect of surfactant chain length", Langmuir, 19, pp. 3712-3719.

[35] P. Deo, N. Deo, P. Somasundaran, A. Moscatelli, S. Jockush, N. Turro, K. P. Ananthapadmanabhan, M. Francesca Ottaviani (2007) "Interactions of a hydrophobically modified polymer with oppositely charged surfactants", Langmuir, 23, pp. 5906-5913.

[36] X.L. Zhang, D.J.F. Taylor, R.K. Thomas, J. Penfold (2011) "Adsorption of polyelectrolyte/surfactant mixtures at the air-water interface: modified poly(ethyleneimine) and sodium dodecyl sulfate", Langmuir, 27, pp. 2601–2612.

[37] A.G. Bykov, S.Y. Lin, G. Loglio, R. Miller, B.A. Noskov (2010) "Dynamic surface properties of polyethylenimine and sodium dodecylsulfate complex solutions", Colloids and Surfaces A: Physicochem. Eng. Aspects, 367, pp. 129–132.

[38] H. Comas-Rojas, E. Aluicio-Sarduy, S. Rodriguez-Calvo, A. Perez-Gramatges, S. J. Roser and K. J. Edler (2007) "Interactions and film formation in polyethylenimine–cetyltrimethylammonium bromide aqueous mixtures at low surfactant concentration", Soft Matter, 3, pp. 747–753.

[39] R.A. Campbell, M. Yanez Arteta, A. Angus-Smyth, T. Nylander, I. Varga (2011) "Effects of bulk colloidal stability on adsorption layers of poly(diallyldimethylammonium chloride)/sodium dodecyl sulfate at the air–water interface studied by neutron reflectometry", J. Phys. Chem. B,115 (51), pp 15202–15213.

[40] X.L. Zhang, J. Penfold, R.K. Thomas, I.M. Tucker, J.T. Petkov, J. Bent, A. Cox, R.A. Campbell (2011) "Adsorption behaviour of hydrophobin and hydrophobin/surfactant mixtures at the air/water interface", Langmuir, 27, pp. 11316-11323.

[41] T. Gilanyi, A. Wolfram (1981) "Interactions of ionic surfactants with polymers in aqueous solutions", Colloids Surf., 3 (2), pp. 181-198.

[42] D.J.F. Taylor, R.K. Thomas, J.D. Hines, K. Humphreys, J. Penfold (2002) "The adsorption of oppositely charged polyelectrolyte surfactant mixtures at the air-water interface: neutron reflection from dodecyl trimethylammonium bromide/sodium poly(styrene sulfonate) and sodium dodecyl sulphate/poly (vinyl-pyridinium chloride)", Langmuir 18 (25), pp. 9783-9791.

[43] R.A. Campbell, A. Angus-Smyth, M. Yanez Arteta, K. Tonigold, T. Nylander, I. Varga (2010) "New perspective on the cliff edge peak in the surface tension of oppositely charged polyelectrolyte/surfactant mixtures", J. Phys. Chem. Lett., 1, pp. 3021–3026.

[44] A. Dedinaite, R. Meszaros, P. Claesson (2004) "Effect of sodium dodecyl sulfate on adsorbed layers of branched polyethylene imine", J. Phys. Chem. B, 108, pp. 11645-11653.

[45] S. Lin, R. Tsay, L. Lin, S. Chen (1996) "Adsorption kinetics of $C_{12}E_8$ at the air-water interface: adsorption onto a clean interface", Langmuir, 12, pp. 6530-6536.

[46] J. Eastoe, J.E. Dalton, P.G.A. Rogueda, E.R. Crooks, A.R. Pitts, E.A. Simister (1997) "Dynamic surface tension of non-ionic surfactants", J. Colloid Interface Sci., 188, pp. 423-430.

[47] H. Chang, C. Hsu, S. Lin (1998) "Adsorption kinetics of $C_{10}E_8$ at the air-water interface", Langmuir, 14, pp. 2476-2484.

[48] J. Eastoe, J.E. Dalton, P.G.A. Rogueda, P. Griffiths (1998) "Evidence for activation-diffusion controlled dynamic surface tension with a non-ionic surfactant", Langmuir, 14, pp. 979-981.

[49] V.B. Fainerman, S.A. Zholob, J.T. Petkov, R. Miller (2008) "$C_{14}E_8$ adsorption characteristics studied by drop and bubble profile tensiometry", Colloids and Surfaces A: Physicochem. Eng. Aspects, 323, pp. 56–62.

[50] D. Mobius, R Miller (editors) (1995) "Studies in interface science. Volume 1. Dynamics of adsorption at liquid interfaces", Elsevier.

[51] J.C. Berg (2010), "An introduction to interfaces and colloids. The bridge to nanoscience", World Scientific Publishing Co Pte. Ltd.

[52] P.R. Bergethon (1998) "The physical basis of biochemistry. The foundations of molecular biophysics", Springer-Verlag.

[53] B.J. Kirby (2010) "Micro and Nanoscale fluid mechanics. Transport in microfluidics devices", Cambridge University Press.

[54] L.L. Lee (2008) "Molecular thermodynamics of electrolytes solutions", World Scientific Publishing Co Pte. Ltd.

[55] A.T. Conlisk (2005) "The Debye-Hückel approximation: Its use in describing electroosmotic flow in micro- and nanochannels", Electrophoresis, 26, pp. 1896–1912.

[56] Malvern instruments (2003) "Zetasizer Nano series user manual".

[57] H. Ohshima (Editor) (2012), "Electrical phenomena at interfaces and biointerfaces: fundamentals and applications in nano-, bio-, and environmental sciences", John Wiley & Sons, Inc.

[58] J. Israelachvili (1992) “Intermolecular and surface forces”, 3rd ed., Academic Press.

[59] G. Sposito (1998) “On points of zero charge”, Environ. Sci. Technol., 32 (32), pp. 2815-2819.

[60] H. Tanaka, Y. Oka (2005) “Chaotropic ions and multivalent ions activate sperm in the viviparous fish guppy *Poecilia reticulata”,* Biochim. Biophys. Acta, 1724 (1-2), pp. 173-180.

[61] S.H. Lam (2004) “Low Reynolds Number Flows”, ME351B Fluid Mechanics (Winter 2003/2004), Stanford University.

[62] E.M. Cadena, J. Garcia, T. Vidal, A.L. Torres (2009) ”Determination of zeta potential and cationic demand in ECF and TCF bleached pulp from eucalyptus and flax. Influence of measuring conditions”, Cellulose, 16, pp. 491–500.

[63] Y. Di, E. Di Maio, C. Marrazzo, S. Iannace (2005) “Rheology in processing of polymer foams”, Annu. Trans. Nordic Rheol. Soc., 13, pp. 37-43.

[64] M.H. Amaral, J. das Neves, A.Z. Oliveira, M.F. Bahia (2008) “Foamability of detergent solutions prepared with different types of surfactants and waters”, J. Surf. Detergents, 11, pp. 275-278.

[65] E.A. Foegeding, P.J. Luck, J.P. Davis (2006) “Factors determining the physical properties of protein foams”, Food Hydrocolloids, 20, pp. 284-292.

[66] A. Berthold, H. Schubert, N. Brandes, L. Kroh, R. Miller (2007) “Behaviour of BSA and of BSA-derivatives at the air/water interface”, Colloids and Surfaces A: Physicochem. Eng. Aspects, 301, pp. 16-22.

[67] D.D. Joseph (1997) “Questions in Fluid Mechanics: Understanding Foams and Foaming”, J. Fluids Eng., 119 (3), pp. 497-499.

[68] J. Guven (2006) “Laplace pressure as a surface stress in fluid vesicles”, J. Phys. A: Math. Gen. 39, pp 3771-3785.

[69] A.I. Rusanov and V.V. Krotov (2003) “Gibbs elasticity of free thin liquid films”, Doklady Phys. Chem., 393 (4-6), pp. 350-352.

[70] E.H. Lucassen-Reynders, A. Cagna, J. Lucassen (2001) “Gibbs elasticity, surface dilational modulus and diffusional relaxation in non-ionic surfactant monolayers”, Colloids and Surfaces A: Physicochem. Eng. Aspects 186, pp. 63-72.

[71] V.B. Faineman, J.T. Petkov, R. Miller (2008) “Surface dilational viscoelasticity of $C_{14}EO_8$ micellar solution studied by bubble profile analysis tensiometry”, Langmuir, 24, pp. 6447-6452.

[72] A. Phianmongkhol, J. Varley (2003) ”ζ potential measurements for air bubbles in protein solutions”, J. Colloid Interface Sci., 260, pp. 332-338.

[73] F. Han, Y. Chen, Y. Zhou, B. Xu (2012) “A surface rheological study of Silwet L-77 surfactant at the air/water interface”, J. Dispersion Sci. Technol., 33, pp 396-402.

[74] D. Weaire, S. Hutzler, S. Cox, N. Kern, M.D. Alonso, W. Drenckhan (2003) “The fluid dynamics of foams”, J. Phys.: Condens. Matter, 15, pp. S65-S73.

[75] X.D. Liu, R.X. Han, H. Yun, K.C. Jung, D.I. Jin, B.D.Lee, T.S. Min, C. Jo (2009) “Effect of irradiation on foaming properties of egg white proteins”, Poultry Sci., 88, pp 2435-2441.

[76] N.J. Mills (2007), “Polymer foams handbook. Engineering and Biomechanics Applications and Design Guide”, Elsevier Ltd.

[77] S.N. Tan, D. Fornasiero, R. Sedev, J. Ralston (2005) “Marangoni effects on aqueous polypropylene glycol foams”, J. Colloid Interface Sci. 286, pp 719-729.

[78] D. Monin, A. Espert, A. Colin (2000) “A new analysis of foam coalescence: from isolated films to three-dimensional foams”, Langmuir, 16, pp 3873-3883.

[79] D. Georgieva, A. Cagna, D. Langevin (2009) “Link between surface elasticity and foam stability”, Soft Matter, 5, pp 2063-2071.

[80] A. Myagotin, L. Helfen, T. Baumbach (2009) “Coalescence measurements for evolving foams monitored by real-time projection imaging”, Meas. Sci. Technol., 20, pp 055703.

[81] V.S. Alahverdjieva, K. Khristov, D. Exerowa, R. Miller (2008) “Correlation between adsorption isotherms, thin liquid films and foam properties of protein/surfactant mixtures: lysozyme/C_{10}DMPO and lysozyme/SDS”, Colloids and Surfaces A: Physicochem. Eng. Aspects, 323, pp 132-138.

[82] A. Saint-Jalmes, M.L. Peugeot, H. Ferraz, D. Langevin (2005) “Differences between protein and surfactant foams: microscopic properties, stability and coarsening”, Colloids and surfaces A: Physicochem. Aspects, 263, pp 219-225.

[83] S.H. Kim, J.E. Kinsella (1985), “Surface activity of food proteins: relationships between surface pressure development, viscoelasticity of interfacial films and foam stability of bovine serum albumin”, J. Food Sci., 50, pp 1526-1530.

[84] G.L. Squires (1978), “Introduction to the theory of thermal neutron scattering”, Dover.

[85] K.S. Krane (1988) “Introductory Nuclear Physics”, John Wiley and Sons.

[86] B. Hammouda (1995) “SANS from Polymer Tutorials”, NIST Centre for Neutron Research Report.

[87] G.V. Schultz (1939) “Uber Die Kinetik der Kettenpolymerisationen. V Der Einfluss Verschiedener Reakions- Arten auf Die Polymolekularitat", Z. Phys. Chem. 43, pp. 25-46.

[88] J. Penfold, R.K. Thomas (1990) "The application of the specular reflection of neutrons to the study of surfaces and interfaces", J. Phys.: Condens. Matter, 2, pp 1369-1412.

[89] B. Jacrot (1976) "The study of biological structures by neutron scattering from solution", Rep. Prog. Phys., 39, pp 911-953.

[90] V.F. Sears (1992) "Neutron Scattering Lengths and Cross Sections", Neutron News, 3 (3), pp. 26-37.

[91] J.R. Lu, R.K. Thomas (1998) "Neutron reflection from wet interfaces", J. Chem. Soc., Faraday Trans., 94 (8), pp. 995-1018.

[92] J.R. Lu, R.H. Ottewill, A.R. Rennie, (2001) "Adsorption of ammonium perfuorooctanoate at the air–water interface", Colloids and Surfaces A: Physicochem. Eng. Aspects, 183–185, pp. 15–26.

[93] J.R. Lu (1999) "Neutron reflection study of globular protein adsorption at planar interfaces", Annu. Rep. Prog. Chem., Sect. C, 95, pp. 3-45.

[94] IAEA (2006) "Neutron Reflectometry. A probe for materials surfaces. Proceedings of a technical meeting. Vienna, 16-20 August 2004". IAEA.

[95] G. Fragneto-Cusani (2001) "Neutron reflectivity at the solid/liquid interface: examples of applications in biophysics", J. Phys.: Condens. Matter, 13, pp 4973–4989.

[96] T.L. Crowley (1993) "A uniform kinematic approximation for specular reflectivity", Physica A, 195, pp. 354-374.

[97] J.R. Lu, Z.X. Li, R.K. Thomas, J. Penfold (1996) "Structure of hydrocarbon chains in surfactant monolayers at the air/water interface: neutron reflection from dodecyl trimethylammonium bromide", J. Chem. Soc., Faraday Trans., 92 (3), pp. 403-408.

[98] J.R. Lu, R.K. Thomas (2000) "Surfactant layers at the air-water interfaces: structure and composition", Adv. Colloid Interface Sci., 84, pp. 143-304.

[99] A. Lopez-Rubio, E. P-Gilbert (2009) "Neutron scattering: a tool for food science and technology research", 20, pp. 576-586.

[100] R.A. Pethrick, J.V. Dawkins (Editors) (1999), "Modern techniques for polymer characterization", John Wiley and Sons.

[101] F. Zhang, M.W.A. Skoda, R.M.J. Jacobs, R.A. Martin, C.M. Martin, F. Schreiber (2007) "Protein interactions studied by SAXS: effects of ionic strength and protein concentration for BSA in aqueous solutions", J. Phys. Chem., 111, pp. 251-259.

[102] T.L. Spehr, D.Phil thesis, Darmstadt 2010, "Water dynamics in soft confinement: neutron scattering investigations on reverse micelles".

[103] DANSE/SANS Project. Sansview software version 2.1.0. 2009-2012, University of Tennessee, http://www.sasview.org/
Last accessed on 06/07/2012.

[104] J.B. Hayter, J. Penfold (1981) “An analytic structure factor for macroion solutions”, Mol. Phys., 42, pp. 109-118.

Chapter 3. Methodology

This Chapter offers a brief description of the experimental methods followed to obtain and analyse the data presented in this thesis. The materials and techniques used in the sample preparation are also presented here.

3.1. General information

Surface adsorption measurements, foam studies and the ζ-potential measurements were conducted at either the Biological Physics department, School of Physics and Astronomy, University of Manchester or at Unilever Research and Development Laboratory, Port Sunlight (Wirral). Neutron reflection experiments were performed using the SURF and INTER beamlines at the ISIS pulsed spallation neutron source, Chilton, Didcot, UK. Small angle neutron scattering was carried out using the ISIS LOQ beamline. In all cases ultra high quality water (UHQ) was used. SDS-PAGE and UV-Vis spectrophotometry were also carried out at Manchester.

The solution-containing glassware was cleaned with a dilute solution (~ 1%) of Decon 90 from Decon Laboratories Limited and repeatedly rinsed with tap water followed by deionized or UHQ water as were the Teflon troughs used in neutron reflection; the exception being the folded capillary cells used for ζ-potential measurements which were flushed with ethanol and ultrapure water.
Deuterium oxide, D_2O, was obtained from the ISIS facilities.

3.2. Equilibrium surface tension

The measurement of equilibrium surface tension can be done with a tensiometer following two common methods: the du Noüy ring and the Wilhelmy plate. Both rely in the measurement of the tensional force experienced by a suspended piece of metal (i.e. a ring or a plate) from a precision balance when in contact with the surface of the liquid. The liquid is contained in a vessel (commonly a hydrophilic Pyrex vessel).

Two different tensiometers from KRUSS were involved in the equilibrium surface tension measurements, a K11 and a K100. Both were temperature controlled by Haake baths set at 25°C. The volume of the samples loaded were ~50 ml in the KRUSS 100 and 15-20 ml in the KRUSS 11. The sole reason for using two different tensiometers was their availability at different locations where other experiments were being performed at the same time. The following sections give a more detailed explanation of both methods.

3.2.1. The ring method

In the ring method (see Figure 3.2.1.1), a ring typically made of a platinum-iridium alloy, is positioned parallel to the liquid phase and then immersed in it. The liquid containing vessel is pulled downwards following the direction of gravity until a stretched interface is formed. During this process, a column of liquid is lifted by the ring. The total force experienced by the ring is the difference in magnitude between the pulling force *F*, and the weight of the column, *W*.

Following Equation 2.1.1 surface tension can be expressed as the total force *F*-*W* experienced throughout the wetted length, *L*. The wetted length is twice the perimeter of the ring and using the mean radius *R*,

$$R = \frac{R_i + R_o}{2} \qquad Eq.\,3.2.1$$

where R_i is the inner ring radius and R_o is the outer ring radius, then *L* is given by

$$L = 2 \cdot 2\pi R \qquad Eq.\,3.2.2$$

The column of liquid lifted is however not entirely cylindrical and thus the wetted length should account for the contact angle formed at the edges of the ring. Thus the surface tension measured is

$$\gamma = \frac{F - W}{L\cos\theta} \qquad Eq.\,3.2.3$$

This corresponds to a maximum value for *F* at which the contact angle becomes zero. The same procedure is followed several times until the value at equilibrium is found. This value is obtained when the mean of a certain number of measurements approaches zero.

Unfortunately, the surface tension value obtained through this method suffers from errors associated with the correct calculation of the volume of liquid lifted. Two different values for the total force are measured depending on whether the volume corresponds to that of the inner or the outer side of the ring.

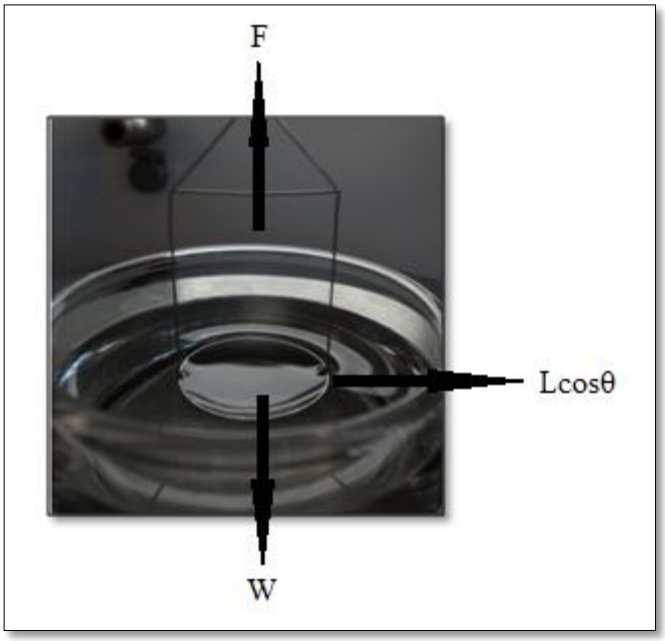

Fig. 3.2.1.1. The ring method.

Harkins and Jordan gave an empirical correction factor *F*, that agrees with experimental values within a 0.25% precision [1-3] and thus the surface tension can be expressed as

$$\gamma = \gamma^* F \qquad Eq.\,3.2.4$$

where γ^* is the measured value of surface tension and *F* is dependent upon the corrected volume *V*,

$$V = \frac{4\pi R\gamma^*}{(D-d)g} \qquad Eq.\,3.2.5$$

with *D*-*d*, the density difference between the involved phases.
By extrapolating the data from Harkins and Jordan, Zuidema and Waters [4]: presented the following correction factor:

$$F = 0.725 + \sqrt{\frac{0.01452\gamma^*}{0.25U^2(D-d)} + 0.04534 - \frac{1.679}{R/r}} \qquad Eq.\,3.2.6$$

Zuidema et al. [4] concluded that for samples with density close to the density of water, the ring method loses precision.

In this work, the ring method was used with the K11 tensiometer and corrected with the Harkins and Jordan formula. The ring, a platinum-iridium alloy (RI01 from KRUSS), had a wetting length of 119.95 mm, a cross-sectional radius of 0.185 mm and a radius of 9.545 mm. The vessel had an outer diameter of 5 cm.
The data obtained with the ring method corresponds to surface tension variations of less than 1 mN/m in an hour or after an upper limit of 6000 seconds (1.66 hours).

3.2.2. The plate method

The theoretical description of the plate method is very similar to that of the ring method. Nevertheless, there are a few differences. For instance, the plate is vertically immersed in the liquid phase until a meniscus is formed at the lower edge of the plate. Once the plate has been positioned it is not moved throughout the remaining length of the measurement so there is no volume of liquid being lifted in this case.

Also, the plate is made of a roughened material, typically platinum, to ensure complete wetting, i.e. the contact angle is zero. Therefore, Equation 3.2.3 becomes

$$\gamma = \frac{F}{Lcos\theta} \approx \frac{F}{L} \qquad Eq.\,3.2.7$$

However, the wetted length in this case is the perimeter of the plate. More importantly, since there is no volume of liquid to lift, there are no associated errors that need to be corrected.

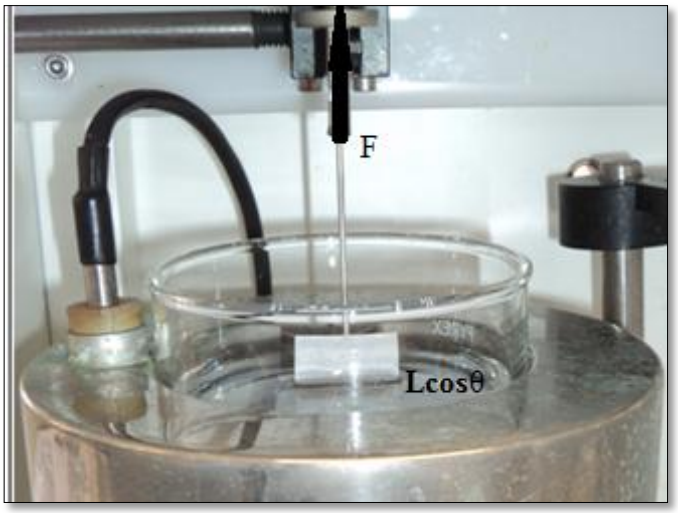

Fig. 3.2.2.1. The plate method.

In this work, the K100 tensiometer was used with a platinum plate (PL01 from KRUSS) of 19.9 mm in length and 0.2 mm thick. The wetted length is 40.2 mm. The vessel had a 7 cm outer diameter. The plate and the ring were rinsed with deionized water and flamed dry before and after every measurement.
Equilibrium with the plate method was considered established when the surface tension varied less than 1 mN/m in an hour or after an upper limit of 57600 seconds (16 hours).

3.3. Dynamic surface tension

To test the dynamic adsorption of solute at the interface, maximum bubble pressure measurements were made with a BPA-1S SINTERFACE maximum bubble pressure tensiometer at room temperature. The following section details the operative mechanism of this apparatus.

3.3.1. Maximum bubble pressure

The maximum bubble pressure (MBP) method is regarded as [5] one of the most reliable methods to study the time dependence of surface tension. In this method, a gas flows under controlled conditions through a capillary of known dimensions immersed in the solution under study creating bubbles in the tip of the capillary (with r_c, capillary radius; h, length of capillary immersed in liquid). The maximum pressure necessary to create a bubble at the capillary tip is then measured from its creation until its detachment (see Figure 3.3.1.1), i.e. the total surface age,

$$t_{total} = t_{life} + t_{dead} \qquad Eq.\,3.3.1$$

The pressure, P, is affected by adsorption of surface active molecules. Most of the surface adsorption occurs in the interval between the fresh creation of a layer at the capillary tip and it becoming a hemisphere with the same diameter as the capillary. This is the lifetime of the bubble, t_{life} [6].

The dead time, t_{dead}, corresponds to a rapid period of bubble growth (therefore hindering adsorption) from the end of the lifetime until the bubble detachment.

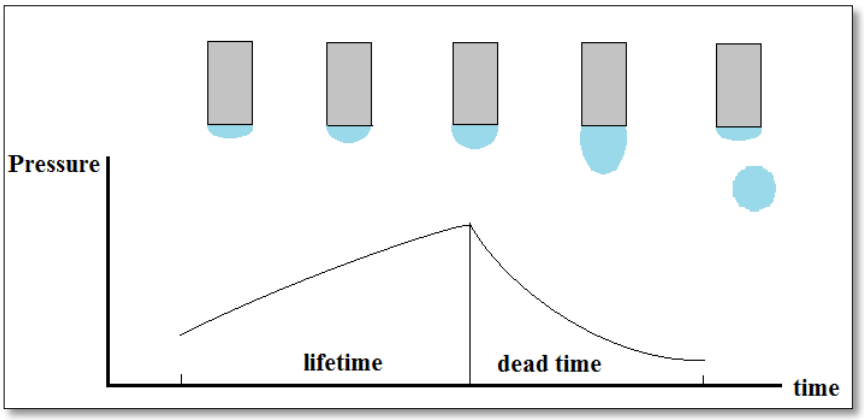

Fig. 3.3.1.1. Formation and detachment of a bubble.

In this experimental method, it is necessary to separate t_{life} from t_{dead} in order to obtain the relation between surface tension and time. Poiseuille's Law dictates [7] that the

viscous resistance of a laminar flow of viscosity η passing through a capillary of radius r_c and length l, is

$$F = \frac{\pi r_c^4}{8l\eta} \qquad Eq.3.3.2$$

It also states that the volume flow rate, L, is

$$L = FP \qquad Eq.3.3.3$$

A plot of the pressure against the flow rate shows the existence of a critical point (L_C, P_C) at which the behaviour of the flow-pressure curve changes from the jet region (i.e. in agreement with Poiseuille's Law) to the bubble formation region as seen in Figure 3.3.1.2.

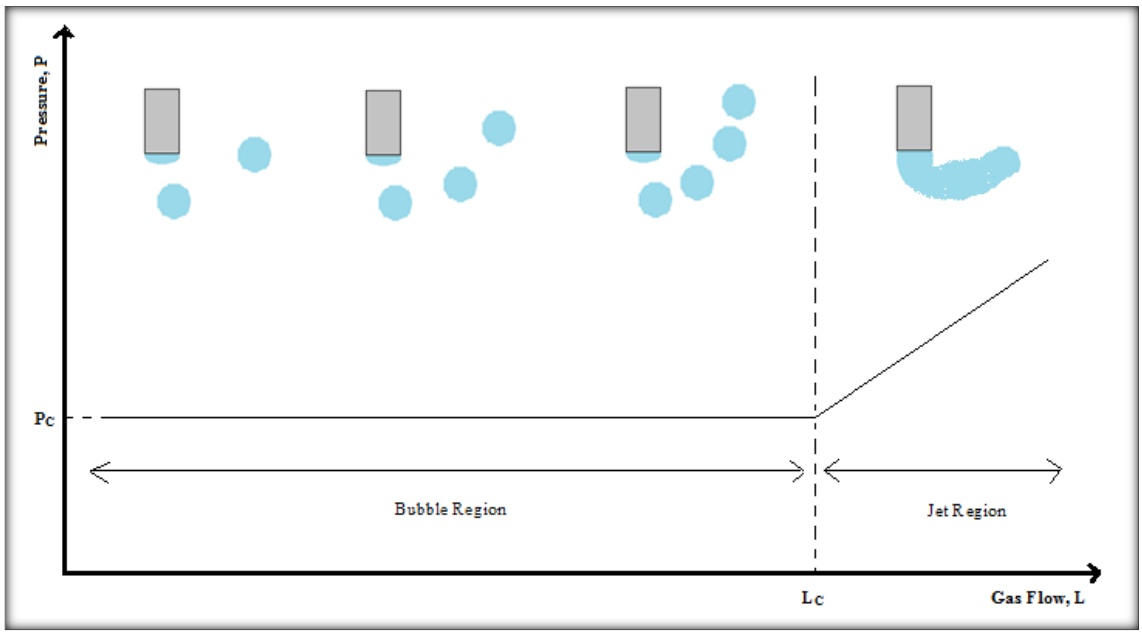

Fig. 3.3.1.2. Transition between the continuous jet flow region and the bubble formation region.

It is at this point that the lifetime of a bubble of radius R begins and its radius and volume remains constant throughout the bubble region [8].

Fainerman et al. (as referenced in [8]) made use of these relations to express the dead time of a bubble at constant pressure through the following expression:

$$t_{dead} = \frac{Lt_{total}}{FP}\left(1 + \frac{3r_c}{2R}\right) \qquad Eq.\,3.3.4$$

Using the critical point parameters, Equation 3.3.4 becomes

$$t_{dead} = \frac{t_{total}(P_C \cdot L)}{L_C \cdot P} \qquad Eq.\,3.3.5$$

The pressure is obtained through the Laplace Equation taking into account the experimental setup; that is,

$$P = \frac{2\gamma}{R} + \rho g h + \Delta P \qquad Eq.\,3.3.6$$

(ρ is the density of the solvent, g is the acceleration due to gravity and ΔP is the pressure difference due to hydrodynamic effects).
When $\Delta P < 0$, the difference in observed values of surface tension is given by [8]:

$$\Delta\gamma = \frac{3}{2}\frac{\eta R}{t_{total}} \qquad Eq.\,3.3.7$$

Fainerman et al. [6, 8] also concluded that if the lifetime of a bubble is less than 0.65 s, then the dead time is approximately equal to the lifetime of the bubble. This statement was also asserted by Kloubek et al [9, 10] who also found that the volume of the bubble is independent of the depth of immersion of the capillary tip but it decreases with increasing frequency of bubble formation and the capillary diameter and orientation determine the diameter of the bubble and influences the detachment from the capillary tip. They also found that the relation between pressure and surface tension is not followed beyond a value of maximum bubble frequency that coincides with the existence of dead time only; i.e. in the jet regime.

In this work, the capillary (of radius 0.130 mm), was cleaned by immersing it in ethanol and running the instrument until a surface tension value of approximately 22 mN/m [11] was obtained. This procedure was followed before and after every measurement. The vessel containing the samples was filled with 25 ml.

3.4. ζ-potential

ζ-potential measurements were performed either at Manchester using a standard setup or in later work, using a hybrid Malvern Zetasizer Nano ZS [12] in Unilever R&D optimised to measure ζ-potential using Phase Analysis light scattering [13, 14] of small colloids. This, combined with long integration times boosts the coherent scattering from weakly scattering systems thereby allowing more reliable measurements of small electrophoretic mobilities that otherwise would be masked by the scattering from dust particles. A schematic representation of the experimental setup is shown in Figure 3.4.1. In particular, systems with ζ-potential values close to 0 mV are the least stable [15] and the optimised Zetasizer offers better results when analyzing a possible charge reversal.

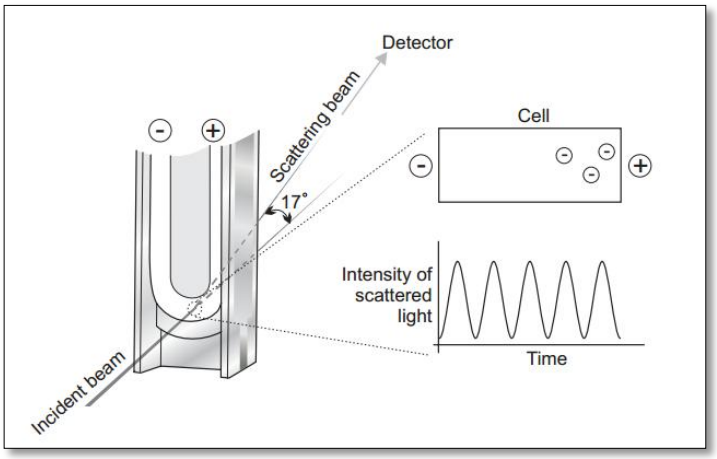

Fig. 3.4.1. A ζ-potential experiment [13].

The cell is a narrow square section capillary and is arranged at the crossover of a Mach-Zender Interferometer. In the forward direction the interference pattern formed “beats” with the frequency of the light modulated by the movement of particles. If this is controlled by an external electrical field, the modulation of the light is in direct proportion to the degree to which the particle is “dragged” by the applied electric field

and the frequency response of the modulated light is akin to a Doppler effect. Given that the source is folded back into the interferogram, it follows that a cumulants analysis of the heterodyne scattering yields the frequency response which is directly transformed into mobility via [16],

$$f = \frac{2U_E sin(\theta/2)}{\lambda} \qquad Eq.\,3.4.1$$

Where f is the frequency shift, U_E is the mobility and θ and λ have their usual meanings. This translates into ζ-potential via Henry's Equation (Eq. 2.2.7).

The applied field needs to be reversed periodically during a measurement to keep the particles from accumulating at the electrodes. This is done in two time modes (see Figure 3.4.2): the fast field reversal (or FFR) gives us a mean value of the velocity of the particle; and the slow field reversal (or SFR) offers better resolution due to longer run times. The results from both modes are contrasted to detect electroosmosis contributions. The combination of these two modes is known as the M3 technique [13]. Because FFR measurements are done at the centre of the sample containing cell, only the phase shifts produced by the FFR are summed to obtain the beat frequency due to the negligible effects that electroosmosis have on these [13].

In experiments, three different types of commercial cells (from Malvern Instruments Ltd.) were used; however, the result is the same irrespective of the cell type; the polycarbonate disposable capillary cell DTS1061, and the universal dip cell kit ZEN1002 with a PCS1115 glass cuvette, and latterly the ZEN1010 higher concentration cell (because of its improved optics and durability). In all cases the cells were filled with at least 1 ml of the sample solution after being flushed with ethanol and ultrapure water.

All measurements were made in the Smoluchowski limit thus assuming a thin electrical double layer in comparison to the size of the particle.

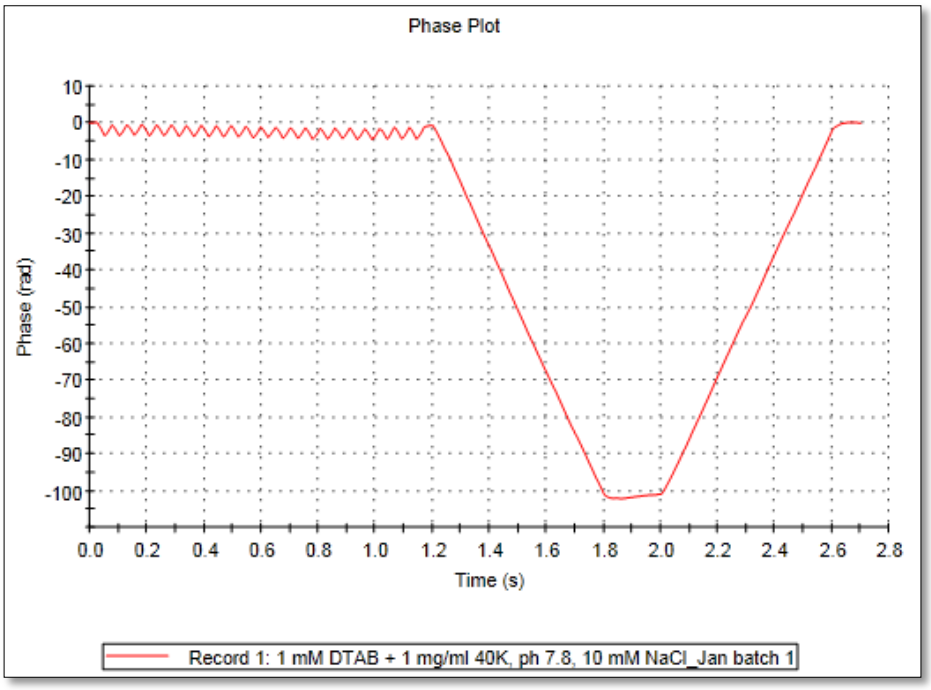

Fig. 3.4.2. Two times mode field reversal phase plot obtained experimentally for a mixture of 1 mg/ml 40K + 1 mM DTAB at pH 7.8 in a 10 mM NaCl solution. The signal represented at times 0.0-1.2 s corresponds to the FFR and the signal obtained from 1.2-2.8 s is given by the SFR.

3.5. Foam studies

Foaming was assessed using similar empirical methods to those followed by Tripp et al. [17] and Amaral et al. [18]. Calibrated test tubes of 20 ml of volume were carefully filled with 10 ml of solution in order to avoid foaming. The test tubes were then shaken up and down by hand three times whilst trying to keep a constant movement and subsequently positioned in a test tube rack where they were allowed to stand for the remaining experimental time. A commercial digital camera was used to record pictures of the solutions before and after the shaking and at regular intervals thereafter to investigate the decay of the volume of foam produced with time.

The test tubes were thoroughly cleaned beforehand and rinsed several times with deionized water. The measurements were performed at room temperature and atmospheric pressure.

The volume of foam produced was visually assessed from the pictures and taken to be the volume produced on top of the initial 10 ml and any additional foam produced

below the 10 ml level when applicable. When foam was encountered at the cylinder walls but not at the centre, the best efforts were made to estimate the total volume of foam without evidently empty spaces at the centre.
Every sample was tested three times and the results here presented correspond to the average of the three values obtained.

3.6. Specular neutron reflection

Neutron reflectivity measurements were performed on both the SURF and INTER reflectometers at the ISIS pulsed neutron source, Chilton, Didcot, UK, [19, 20]. These reflectometers use the white beam time of flight method where polychromatic cold thermal neutrons illuminate a sample and are reflected by the differential neutron scattering length density in the adsorbed layer. The reflected beam is recorded using a detector at a fixed angle. The angles used in order to probe a maximum *Q*-range from 0.01 $Å^{-1}$ to 0.5 $Å^{-1}$ with wavelengths from 1 to 16 Å, were 1.5° in the case of SURF, 0.8° and 2.3° in the case of INTER.

For both reflectometers an initial direct transmission of the beam and a sample of D_2O were run to obtain total reflection and thus calibrate the reflectivity signal received. The resolution in *Q* was approximately 4% in all experiments.

All samples were allowed to adsorb freely for at least 1 hour prior to measurement and these were effected at 25°C.

The reflectivity data were analysed using the MULF routines within the OpenGenie software package [21], fitting the reflectivity data to a single adsorbed layer, a slab of uniform composition, or a double layer when pertinent.

This provides a thickness, τ, and scattering length density, ρ, which can be linked to the adsorbed amounts, Γ, of material at the interface probed [22] through the Equation

$$\Gamma = \frac{\rho\tau}{N_a \sum_i b_i} = \frac{Mw}{N_a A} \qquad Eq.\,3.6.1$$

where N_a is the Avogadro's number, M_W is the molecular weight of the material under study and b_i, its scattering length. The area occupied per molecule is given by

$$A = \sum_i m_i b_i / \rho\tau \qquad Eq.\,3.6.2$$

where m_i is the mass of component i.

The modelled scattering length density ρ_{expt} can be described as the sum of the scattering length densities of every individual component adsorbed at the layer multiplied by the volume fraction Φ_i occupied by each component. If a layer is composed of a mixture of surfactant (s) and peptide (p) in water (w), then

$$\rho_{expt} = \Phi_p\rho_p + \Phi_s\rho_s + \Phi_w\rho_w \qquad Eq.\,3.6.3$$

If the liquid phase is NRW, the scattering length density of such layer is also described by

$$\rho_{expt} = \frac{b_p + n \cdot b_s}{A \cdot \tau} \qquad Eq.\,3.6.5$$

where n is the number of surfactant molecules associated per peptide molecule.
Two reflectivity profiles are obtained from the same system at the air/liquid interface using either the h-surfactant (hs) or the d-surfactant (ds) so n can be calculated from Equation 3.6.5. From Equation 3.6.3, obtaining Φ_p is then straightforward. However, to calculate Φ_s

$$\Phi_s = V_s/V_p \qquad Eq.\,3.6.6$$

it is necessary to know the volumes of the peptide and the surfactant molecules, V_p and V_s, respectively. Hence,

$$V_p = \tau \cdot A \qquad Eq.\,3.6.7$$

and

$$V_s = 27.4 + 26.9 \cdot n_c \qquad Eq.3.6.8$$

as defined by Tanford et al. [23], where n_c is the number of carbon atoms in the surfactant chain. The volume of the polar head also needs to be taken into account.
The adsorbed amount of surfactant at the interface can then be obtained through Equation 3.6.1 using the area of one surfactant molecule, $A_s = A/n$.

To corroborate the chosen model fitted to the experimental data, the two measurements made in NRW are replicated in a solvent of different scattering length density; i.e. in D_2O. Thus, the reflectivity data now consists of two layers: a layer in air where the hydrophobic moieties are usually found and a layer in water where the hydrophilic moieties are usually found. Equation 3.6.3 and the NRW data already obtained give us an expected value for the new data. Consequently, if the expected values are matched by the experimental data, the model can be assumed to be correct.

Since the amino acid sequence of the 40 KDa polypeptide is not known, the scattering length densities and volumes of two common proteins, i.e. lysozyme and bovine serum albumin (BSA) were used as an approximation when necessary (in neutron reflection and small angle neutron scattering). Table 3.6.1 contains these values.

Protein	Volume/Å^3	ρ (in NRW)/10^{-6} Å^{-2}	ρ (in D_2O)/10^{-6} Å^{-2}
Lysozyme [24]	16717	2.17	3.60
BSA [25]	79110	2.01	3.25

Table 3.6.1. Typical protein parameters used in the modelling of the 40 KDa polypeptide.

3.7. Small angle neutron scattering

The small angle neutron scattering measurements were performed using the LOQ diffractometer at the ISIS pulsed neutron source, Rutherford Appleton Laboratory, Chilton, Didcot, UK [26]. Data were recorded at a sample to detector distance of 4.5 m using 2–10 Å wavelength neutrons over an angular range of 0.008 to 0.3Å $^{-1}$. A 12 mm diameter cadmium mask defined the illumination at the sample in 5 mm path length

spectrophotometer cells. SANS data were collected for 15 μA of source current and transmission runs for 10 μA, corresponding to 10 and 7 minutes collection time. Subsequently data were converted from time of flight to intensity versus scattering vector, and both converted to absolute scale, (reference to a standard scatterer and corrected for transmission) and radially averaged using the open source Mantid software package [27]. Subsequent analysis of the reduced SANS data was performed with the Sansview 2.1.0. software [28].

3.8. Surfactants

Sodium dodecyl sulfate (SDS) of purity ≥ 99% and molecular weight 288.38 g/l was purchased from Sigma-Aldrich and used as received (Figure 3.8.1). Its molecular volume is 412.2 $Å^3$ [29].

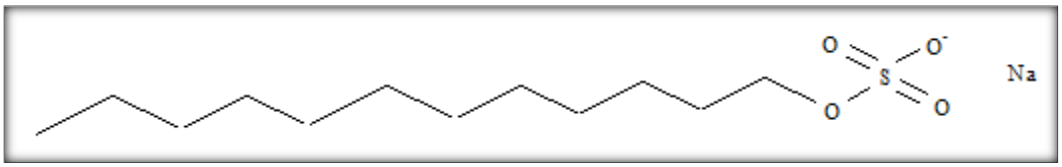

Fig. 3.8.1. Sodium dodecyl sulfate.

Dodecyl trimethylammonium bromide (DTAB) of purity ≥ 99% and molecular weight 308.34 g/l was obtained from Sigma-Aldrich and used as received (Figure 3.8.2). Its molecular volume is 485 $Å^3$ [30].

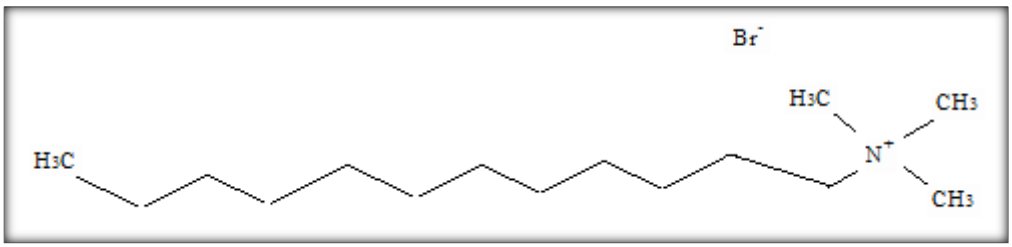

Fig. 3.8.2. Dodecyl trimmethylammonium bromide.

The chain-deuterated SDS and DTAB were obtained from the isotope unit in the Physical and Theoretical Chemistry Laboratory in the University of Oxford. The molecular weights after deuteration are 313.53 g/l and 333.49 g/l for d-SDS and d-DTAB, respectively. The volume of the dodecyl chains is 350 $Å^3$ [31].
Octaethylene glycol monodecyl ether ($C_{10}E_8$) of purity ≥ 98% was obtained from Sigma-Aldrich and used as received (Figure 3.8.3). Its molecular weight is 510.70 g/l.

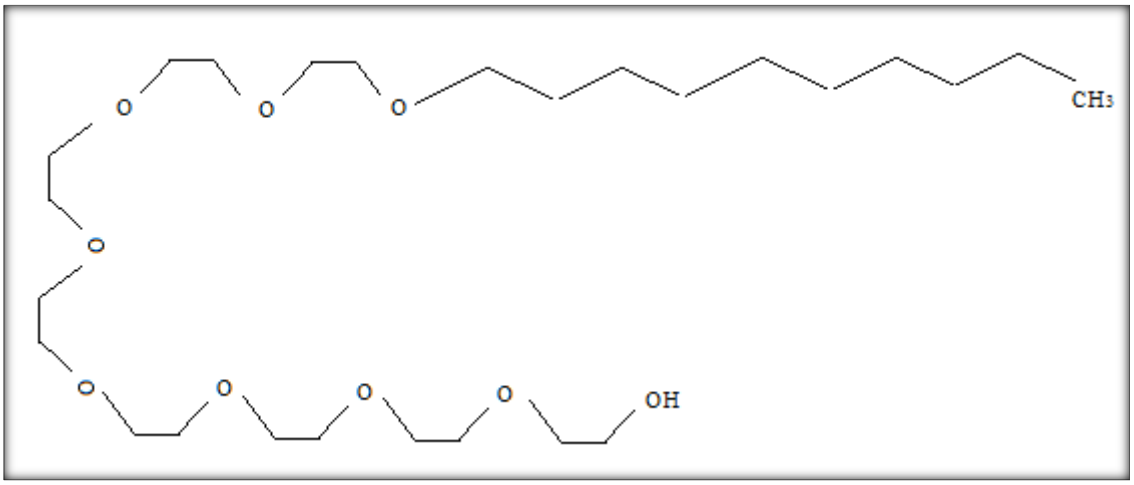

Fig. 3.8.3. Octaethylene glycol monodecyl ether.

3.9. Other materials

The lysozyme from chicken egg white (purity 95%) used in the ζ-potential experiments with the non-ionic $C_{10}E_8$ was obtained from Sigma and used as obtained.
Sodium chloride (NaCl) of 99.9% purity was obtained from Fisher Scientific.

Hydrochloric acid (HCl) and sodium hydroxide (NaOH) at 1 M were added to the solutions when the pH needed to be adjusted. The pH was checked with a Pocket Checker1 HI-98103 pH Tester calibrated with Hanna buffer solution sachets of pHs 4.01, 7.01 and 10.01.

3.10. Sample preparation

Stock solutions of concentrated surfactants and polypeptide, unless otherwise stated, were prepared independently with ultrapure water containing 10 mM NaCl and adjusted

to the relevant pH for every measurement. Despite not keeping a fixed ionic strength, the latter is always approximately 0.01 M. A stock solution of ultrapure water with 10 mM NaCl was also prepared. The mixtures were carried out by adding polypeptide stock solution to an appropriate amount of surfactant stock solution and diluted to the relevant concentrations with the stock of ultrapure water. These were lightly stirred and allowed to mix for at least 30 minutes before any measurement.

Fresh samples were prepared when possible and old samples were discarded after two to three days and never beyond a maximum of one week only if stored in a fridge. Samples that had been stored in a fridge were given time to reach room temperature before being used. Some of the samples used in the plate method were also used in the maximum bubble pressure measurements and in foam studies.

For the ring method, individual solutions of mixed polypeptide/surfactant were prepared by adding polypeptide in powder form to a solution of surfactant containing 10 mM NaCl. These were pH adjusted, lightly stirred and left to mix for a minimum of 30 minutes.

References

[1] A.W. Adamson (1967) "Physical chemistry of surfaces", 2nd ed., John Wiley and Sons.

[2] Processor Tensiometer K12/User Manual, KRUSS, Hamburg, 1994, pp. 66–73.

[3] M.A. Rodriguez Rius (2009) "Characterization of two peptides derived from eggshell membrane", MPhil Thesis, University of Manchester.

[4] H. Zuidema, G. Waters (1941) "Ring method for determination of interfacial tension", Ind. Eng. Chem., Anal. Ed., 13 (5), pp 312–313.

[5] J. Eastoe, J.S. Dalton (2000) "Dynamic surface tension and adsorption mechanisms of surfactants at the air-water interface", Adv. Colloid Interface Sci., 85, pp. 103-144.

[6] G. Masutani, M.K. Stenstrom (1984) "A review of surface tension measuring techniques, surfactants, and their implications for oxygen transfer in wastewater treatment plants". Water resources program, School of Engineering and Applied Sciences, UCLA, Los Angeles, CA

[7] S.P. Sutera, R. Skalak (1993) “The history of Poiseuille’s Law”, Annu. Rev. Fluid Mech., 25, pp. 1-19.

[8] D. Mobius, R Miller (editors) (1995) “Studies in interface science. Volume 1. Dynamics of adsorption at liquid interfaces”, Elsevier.

[9] J. Kloubek (1972) “Measurement of the dynamic surface tension by the maximum bubble pressure method. III. Factors influencing the measurement at high frequency of bubble formation and an extension to zero age of surface”, J. Colloid Interface Sci., 41 (1), pp. 7-16.

[10] J. Kloubek (1972) “Measurement of the dynamic surface tension by the maximum bubble pressure method. IV. Surface tension of aqueous solutions of sodium dodecyl sulfate”, J. Colloid Interface Sci., 41 (1), pp. 17-22.

[11] F.A.M.M. Goncalves, A.R. Trindade, C.S.M.F. Costa, J.C.S. Bernardo, I. Johnson, I.M.A. Fonseca, A.G.M. Ferreira (2010) “PVT, viscosity and surface tension of ethanol: New measurements and literature data evaluation”, J. Chem. Thermodynamics, 42, pp. 1039-1049.

[12] personal communication from Dr. I. M. Tucker, Unilever Research & Development.

[13] Malvern instruments (2003) “Zetasizer Nano series user manual”.

[14] J.F. Miller, K. Schatzel, B. Vincent (1991) “The determination of very small electrophoretic mobilities in polar and nonpolar colloidal dispersions using phase analysis light scattering”, J. Colloid Interface Sci.143, 2, pp. 532-554.

[15] S. Patila, A. Sandberg, E, Heckert, W. Self, S. Seal (2007) “Protein adsorption and cellular uptake of cerium oxide nanoparticles as a function of zeta potential”, Biomaterials, 28, pp. 4600–4607.

[16] D. Colegate (2009) “Structure-kinetics relationships in micellar solutions of nonionic surfactants”, PhD Thesis. University of Durham.

[17] B.C. Tripp, J.J. Magda, J.D. Andrade (1995) “Adsorption of globular proteins at the air/water interface as measured via dynamic surface tension: concentration dependence, mass-transfer considerations, and adsorption kinetics”, J. Colloid Interface Sci., 173, pp. 16-27.

[18] Maria Helena Amaral, Jose das Neves, Angela Z. Oliveira, M. Fernanda Bahia (2008) “Foamability of detergent solutions prepared with different types of surfactants and waters”, J. Surf. Detergents, 11, pp 275-278.

[19] D.G. Bucknall, J. Penfold, J.R.P. Webster (1996) “SURF-A second generation reflectometer”, ICANS 13 Proceedings.

[20] J. Webster, S. Holt, R. Dalgliesh (2006) "INTER-The chemical interfaces reflectometer on target station 2 at ISIS", Physica B: Condensed Matter, 385, pp. 1164-1166.

[21] http://www.opengenie.org/Main_Page
Last accessed on 02/08/2012.

[22] J.R. Lu, R.K. Thomas (2000) "Surfactant layers at the air-water interfaces: structure and composition", Adv. Colloid Interface Sci., 84, pp. 143-304.

[23] C. Tanford (1972) "Micelle Shape and Size", J. Phys. Chem., 76 (21), pp. 3020-3024.

[24] T. Su, J.R. Lu, R.K. Thomas, J. Penfold, J. Webster (1998) "Structural conformation of lysozyme layers at the air/water interface studied by neutron reflection", J. Chem. Soc., Faraday Trans., 94, pp. 3279-3287.

[25] J.R. Lu, T. Su, R.K. Thomas (1999) "Structural conformation of bovine serum albumin layers at the air/water interface studied by neutron reflection", J. Colloid Interface Sci., 213, pp. 426 – 437.

[26] R.K. Heenan, J. Penfold, S.M. King (1997) "SANS at pulsed neutron sources: present and future prospects", J. Appl. Cryst., 30, pp. 1140-1147.

[27] MANTID Project. Mantid Software version 2.1.,
http://www.mantidproject.org/Main_Page
Last accessed on 06/07/2012.

[28]] DANSE/SANS Project. Sansview software version 2.1.0. 2009-2012, University of Tennessee, http://www.sasview.org/
Last accessed on 06/07/2012.

[29] J.F. Berret (2005) "Evidence of overcharging in the complexation between oppositely charged polymers and surfactants", J. Chem. Phys. 123 (16), pp. 164703-164712.

[30] D.J.F. Taylor, R.K. Thomas, J. Penfold (2002) "The adsorption of oppositely charged polyelectrolyte/surfactant mixtures: neutron reflection from dodecyl trimethylammonium bromide and sodium poly(styrene sulfonate) at the air/water interface", Langmuir, 18 (12), pp. 4748-4757.

[31] D.J. Lyttle, J.R. Lu, T.J. Su, R.K. Thomas, J. Penfold (1996) "Structure of a dodecyltrimethylammonium bromide layer at the air/water interface determined by neutron reflection: comparison of the monolayer structure of cationic surfactants with different chain lengths", Langmuir, 11, pp. 1001-1008.

Chapter 4. Characterization of the 40 KDa polypeptide

In this first experimental results Chapter, the extraction and initial characterization of the 40 KDa polypeptide via SDS-PAGE and UV-Vis spectroscopy are described.

This section also reports the surface adsorption of the 40 KDa polypeptide characterized through the use of the plate and the maximum bubble pressure methods. These measurements together give useful indications of dynamic and equilibrated surface adsorption behaviour through surface tension changes. In contrast, the behaviour of the polypeptide in the bulk solution under different pH conditions was investigated via ζ-potential. Neutron reflection was undertaken to offer a deeper understanding of the conditions under which this biopolymer adsorbed at the interface and SANS provided us with an initial model of the aggregation of this material in solution. An attempt was made to correlate surface properties to foaming behaviour.

4.1. Origins of the 40 KDa polypeptide

The collagenous polypeptide that occupies the central position in this work was obtained from Qingdao Ecole Biotech Ltd. (Qingdao, China). The process according to this company follows several steps. These are described next.

Firstly, after dissolution of the membrane of chicken eggs, the resultant material is treated at ambient temperature with sodium hydroxide (NaOH) during 8 to 10 hours. After this time, hydrochloric acid (HCl) is added to neutralize the solution. Secondly, the solution is filtered using porous membranes of sizes 100, 30 and 5 KDa. Finally, the solution is concentrated to remove any salt and a powder is obtained by freeze-drying.

The appearance of the powder is a yellow to brown colour and it can be more or less coarse depending on the batch. The material contained within the same batch was used when possible although different batches gave similar results in a variety of tests.
The polypeptide was initially characterized through SDS-PAGE and UV-Vis spectroscopy. The findings of these experiments follow.

4.2. Molecular weight determination via SDS-PAGE

The average molecular size of a protein can be determined using SDS-polyacrylamide gel electrophoresis. In this technique, the protein is mixed with SDS and cast into a polyacrylamide gel; voltage is applied and this draws the now charged complex down the gel. Size exclusion effects retard the motion of the charged unstructured material and by comparison with a broad range protein marker for known protein sequences the molecular weight of the protein is deduced.

The average molecular size of the powder material has been tested by SDS-PAGE and compared with a broad range protein marker for known protein sequences (see Table 4.2.1).

Protein	**Source**	**Mw (KDa)**
Myosin	rabbit muscle	212
MBP-β-galactosidase	E. coli	158
β-galactosidase	E. coli	116
Phosphorylase b	rabbit muscle	97.2
Serum albumin	bovine	66.4
Glutamic dehydrogenase	bovine liver	55.6
MBP-β-galactosidase	E. coli	42.7
Thioredoxin reductase	E. coli	34.6
Triosephosphate isomerase	E. coli	27
Trypsin inhibitor	soy bean	20
Lysozyme	chicken egg white	14.3
Aprotinin	bovine lung	6.5
Insulin A	bovine pancreas	3.4
B chain	bovine pancreas	2.3

Table 4.2.1. Reference points for SDS-PAGE [1, 2].

The results of this experiment (conducted by Dr. Fang Pan) can be seen in Figure 4.2.1 where the left column corresponds to the reference protein and the right column belongs to the polypeptide under study. The denser stretch of material is found between 6.5 and 20 KDa. However, the results for the polypeptide cover a wider molecular size range following a polydisperse distribution of sizes with an approximate 200 KDa upper limit.

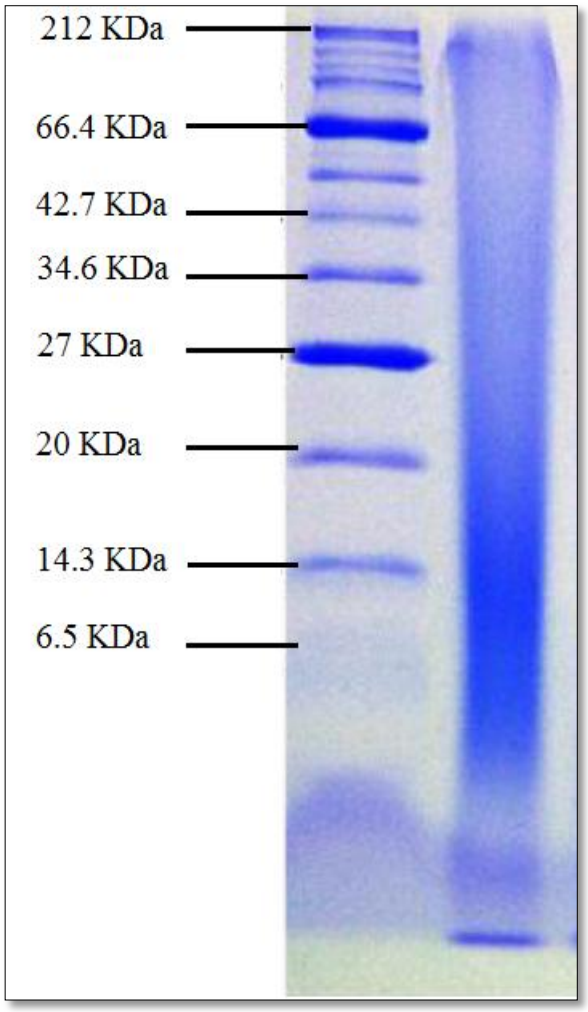

Fig. 4.2.1. Molecular size detection of the polypeptide by SDS-PAGE. The left column is a ~2 μg/protein marker and the column to the right is a 10 μg/lane.

Due to the polydispersity of the peptide, it is difficult to establish a precise average size. Nonetheless, a 40 KDa limit was chosen as a nominal molecular weight and thus, we refer to the polypeptide as the 40 KDa polypeptide or 40K throughout the length of this work.

4.3. Optimal solution conditions for maximum adsorption

Previous studies have shown that surface adsorption of the 40 KDa polypeptide is not greatly affected by addition of small quantities of NaCl [3]. Thus, the remaining experiments performed to characterize this material were conducted in 10 mM NaCl solutions in order to mimic conditions closer to those found in living cells.

Surface adsorption tends to be at its maximum at the isoelectric point [4] so preliminary ζ-potential studies of the 40 KDa polypeptide as a function of pH were conducted with a standard setup in order to determine the isoelectric point of the polypeptide and thus establish the conditions under which the main experiments were going to be performed. In 10 mM NaCl this was established as the point of zero charge (see Figure 4.3.1) which was found close to pH 5.

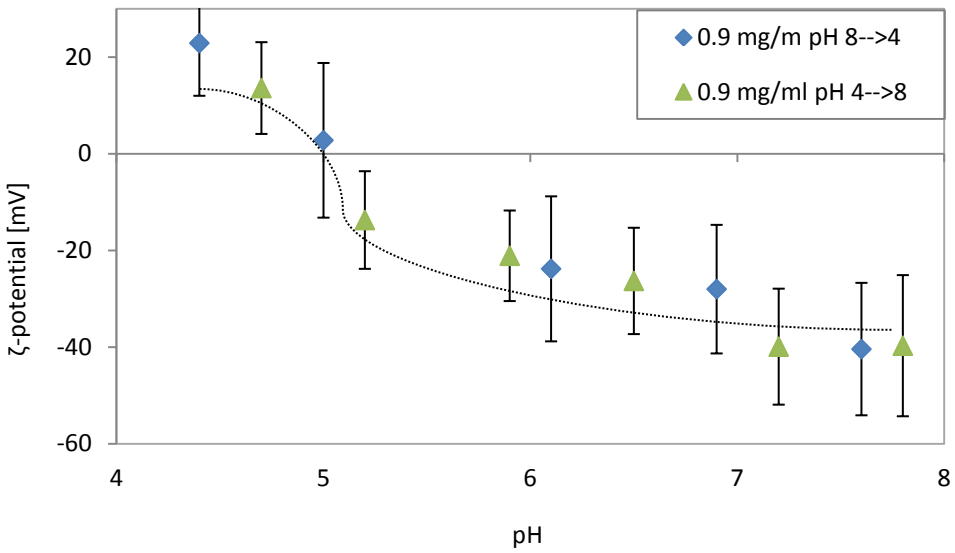

Fig. 4.3.1. Determination of the isoelectric point of the 40 KDa polypeptide. The arrows in the legend indicate the direction in which the pH was adjusted. Error bars obtained after averaging three experimental readings.

This pH was used in the following adsorption studies with and without the presence of LMW surfactants, and thus we refer to this pH whenever the isoelectric point of the polypeptide is mentioned in this work unless otherwise stated.

4.4. Verification of the collagenous nature of the 40 KDa polypeptide

The UV-Vis absorption spectrum of the 40 KDa polypeptide at different concentrations was obtained with a Thermo Spectronic GENESYS 6 UV-Visible Spectrophotometer. The results were then compared with the known spectrum of collagen from the rat tail tendon (see Figure 4.4.1) [5] in order to verify the collagenous nature of the polypeptide.

The 40 KDa polypeptide was prepared in UHQ water with 10 mM NaCl and adjusted to pH 5. The solution was then centrifuged for 3 minutes at 6000 rpm to remove any dust particles present in solution.

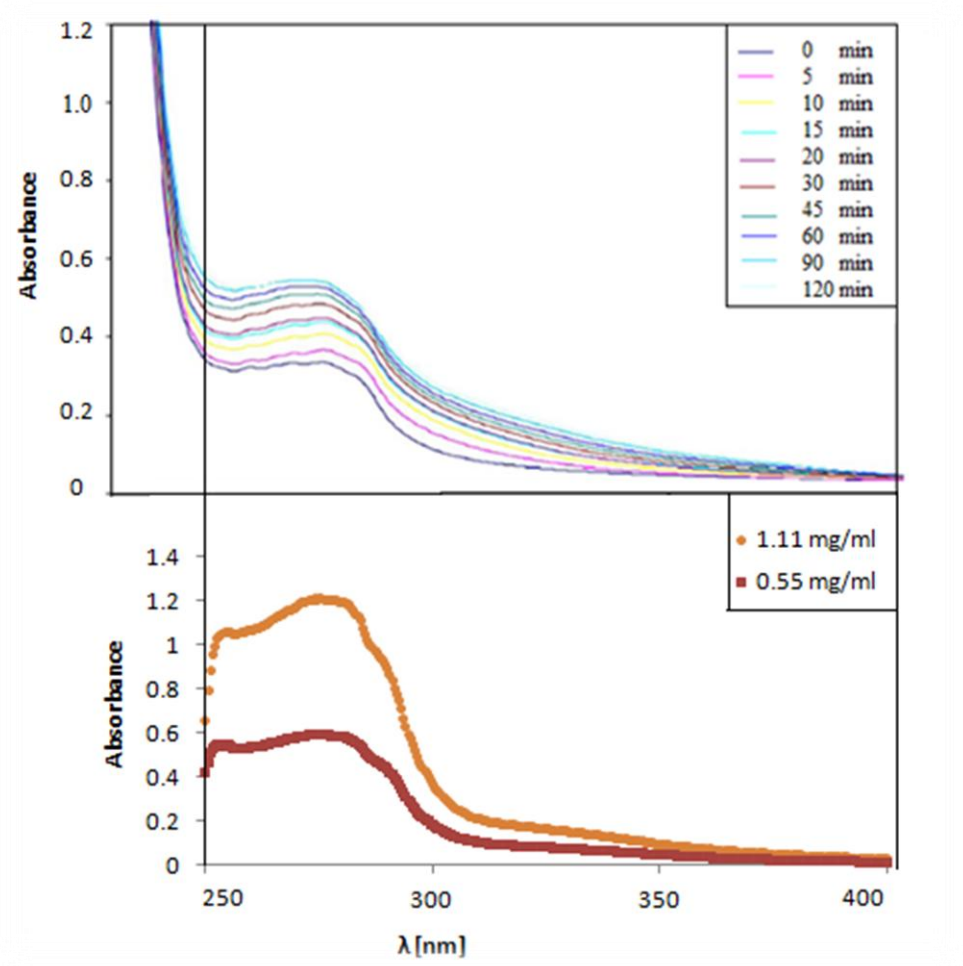

Fig. 4.4.1. Comparison of rat tail tendon collagen [5] (top) and the 40 KDa polypeptide (bottom).

The spectrum of 0.9 mg/ml of rat tail tendon collagen is shown after different irradiation times [5]. Clearly, UV irradiation in their case caused structural deterioration of the molecules in the absence of ascorbic acid. The spectra for the 40 KDa polypeptide are limited in the lower wavelength area to 250 nm due to instrumental constraints.

Both materials exhibit similar absorption peaks in the 275 nm vicinity. This similarity signifies their collagenous nature in basic molecular structure. Thus, although the polypeptide has undergone a denaturation treatment it still shows characteristics typical

of collagen structures. But note that the absorption curves follow the same overall trend but differ in absorption intensity, indicating clear differences between them.

4.5. Equilibrium surface tension

The Wilhelmy plate method was employed to measure the surface tension from a set of aqueous solutions containing different amounts of the 40 KDa polypeptide at pH 5 with 10 mM NaCl. Since this pH is close to the isoelectric point and thus maximum adsorption should occur under these conditions, there was no interest in conducting surface adsorption measurements under different pH conditions.

The surface tension values used to plot Figure 4.5.1 were taken from the readings that were equilibrated for up to 16 hours to account for time dependent changes. The position of the critical aggregation concentration (CAC) as can be seen in Figure 4.5.1 is marked by the clear break point. It corresponds to a value of $\gamma_{CAC} = 32 \pm 1$ mN/m at the CAC concentration of 1 mg/ml of 40 KDa polypeptide.

It is worth noticing that whereas for LMW surfactants the CMC is easily identified by the break point and the surface coverage is similar at concentrations around the CMC, the CAC in the case of polymers cannot be immediately identified as the break point from the surface tension profile alone. This feature may be the result of changes in the activity coefficients, the ionization of the polymer in the micelle or changes in the surface structure [6]. Nevertheless, the position of the CAC was later verified by neutron reflection as will be explained later in this Chapter.

The Gibbs Equation (Equation 2.1.11) has been widely used to derive surface adsorbed amount or surface excess from surface tension variation below the CMC (critical micellar concentration); its practical relevance is limited to systems whose solution behaviour can be approximated to be ideal by thermodynamic definition. For small surfactant molecules under concentrations below or close to their CMCs, their solution activity coefficients can be approximated to 1 and their solution activities are thus effectively equal to their concentrations. In contrast, for polymeric materials, this is less obvious as the activity coefficients are highly deviated from 1, making it difficult to extract useful information from such systems.

On the other hand, it is useful to explore what the outcome would be if the Gibbs Equation is applied. The surface tension values below the CAC were modelled using a second order polynomial presented in Figure 4.5.1 (from the γ vs. ln C plot and using SI units). The equation was differentiated and substituted into Equation 2.1.11 by taking n = 1 (under a constant salt concentration with [NaCl] = 10 mM). The results are presented in Figure 4.5.2.

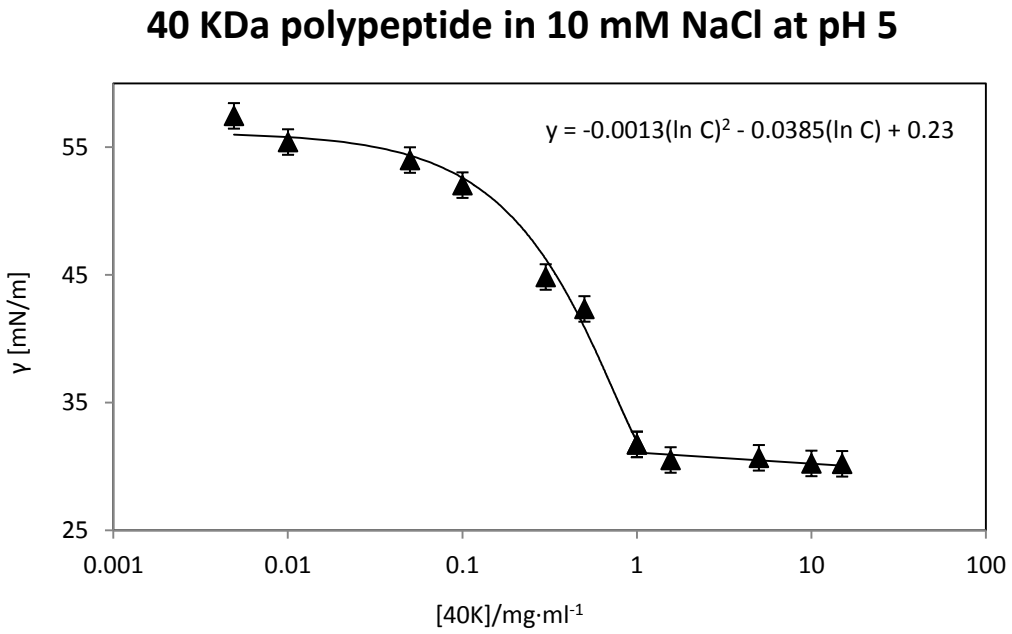

Fig. 4.5.1. Equilibrium surface tension as a function of polypeptide concentration. The lines have been added as a visual aid. The critical aggregation concentration was found at γ = 32 ± 1 mN/m at a concentration of 1 mg/ml of 40 KDa polypeptide. The Equation is the second order polynomial fitted to surface tension values below the CAC.

The limited applicability of Gibbs Equation in the study of surface adsorption of biopolymers was exposed through the low value of area occupied per molecule obtained from the equilibrium surface tension.

The surface excess obtained at the CAC was $(4.4 \pm 0.3) \cdot 10^{-6}$ mol·m^{-2} (assuming the molecular weight of the polypeptide is 40 KDa) and the area occupied per molecule at this concentration is ~ 38 Å^2, which is rather too small for such a large polymer.

Clearly, the theoretical treatment followed to obtain this value does not offer a physically feasible description of the polypeptide. To put this result into context, we examine the dimensions of some globular proteins of different molecular sizes. For instance, lysozyme is an ellipsoid of molecular weight 14.2 KDa and dimensions 30 x 30 x 45 $Å^3$ [7]. Thus, the area per molecule occupied by one lysozyme molecule ranges from a minimum limit of 900 $Å^2$ to an upper limit of 1350 $Å^2$ when the layer reaches close packing.

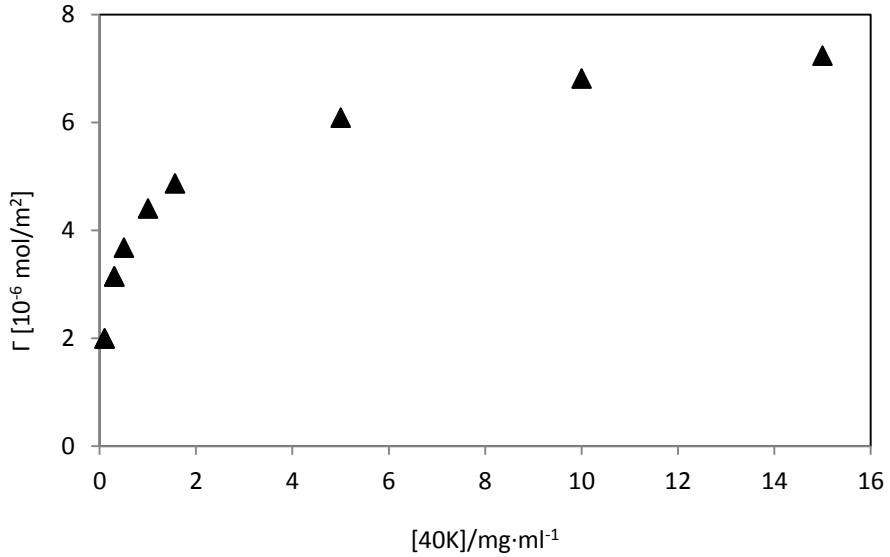

Fig. 4.5.2. Surface adsorbed amounts of 40 KDa polypeptide as calculated from equilibrium surface tension.

Bovine serum albumin (or BSA), a protein of approximately 66 KDa, adopts a cylindrical conformation of dimensions 40 x 40 x 120 $Å^3$ [8] and it was found to occupy an area of 3800 $Å^2$ at the interface of air with an aqueous solution at pH 5 and a concentration of 1 mg/ml. The isoelectric point of BSA is also close to pH 5 so this value represents the highest possible surface adsorption under the conditions specified. However, this area is below the minimum possible area for a BSA molecule. Hence, it was concluded that the molecule had undergone some changes in the projection of globular fragments resulting into their further projection along the surface normal direction and lateral intermixing. Such interfacial processes must be highly associated with structural reorganisation and loss of bioactivities in general.

Previously, the polypeptide was shown to absorb UV-Vis light in the same manner as the collagen from the rat tail. Thus, if we also compare the results of the 40 KDa polypeptide with a fibrous collagen molecule of type I which consists of a triple helix of 300 nm in length and 14 Å wide [9], the calculated area occupied per molecule of 40 KDa polypeptide seems rather small in comparison to all these molecules. The resultant area per molecule for the collagen is 616 $Å^2$ assuming this molecule adsorbs with the minimum area possible at the air/water interface retaining its structural properties.
The area per molecule calculated via the Gibbs Equation seems to be at least one order of magnitude smaller than expected; this could be due to several factors.

An initial approach could lead us to consider the effect of the 40 KDa polypeptide being comprised of mixed peptides of different sizes and sequences, i.e. the effect of polydispersity. Nevertheless, the difference in peptide sizes will alter the n prefactor in Gibbs Equation but also the molar adsorbed amount accordingly, thus the combination of these parameters remains relatively constant.

Also, assuming such inhomogeneous distributions are left aside, the assumption that the concentration of the polypeptide in solution is approximately equal to the activity is generally applied for small uni-univalent electrolytes only. Therefore it may not be suitable for the polypeptide since at this stage we have little information regarding the chemical composition and behaviour of this molecule.

Furthermore, the derivation of the Gibbs Equation is possible only if the adsorption process is reversible. Many proteins adsorb at the air/liquid interface in an irreversible manner due to the denaturation process suffered with greater unfolding rates related to lower adsorption rates. Precipitation instead of solubilization may occur with lateral compression of the surface [10].

The above discussion seems to be excessive or artificial given that the polypeptide is known to us to be a mixture and is most likely not to follow the Gibbs Equation.

However, similar treatments via the Gibbs Equation for protein and polypeptide systems have often been adopted in the open literature [6], where the systems either are impure, mixed or suffer from the non-ideal nature. It is hence useful to enforce the

understanding at this stage that such simple treatment is unrealistic and could lead to wrong conclusions.

4.6. Maximum bubble pressure

Dynamic surface tension changes at different polypeptide concentrations were recorded using the maximum bubble pressure method. The solutions were prepared in 10 mM NaCl and the results are presented in Figure 4.6.1. From this Figure it is possible to observe the decay in surface tension as a function of the lifetime of the bubbles formed at the tip of the capillary. In agreement with previous studies of proteins [10, 11] the decay only occurs after an induction period or lag time during which the surface tension decay is negligible. This period is reduced with increasing polypeptide concentration. As expected, the decay in surface tension is also faster at higher concentration. With 5, 10 and 15 mg/ml, the induction period has already finished at 0.01 s so the surface tension values at these concentrations are lower than the surface tension of pure water.

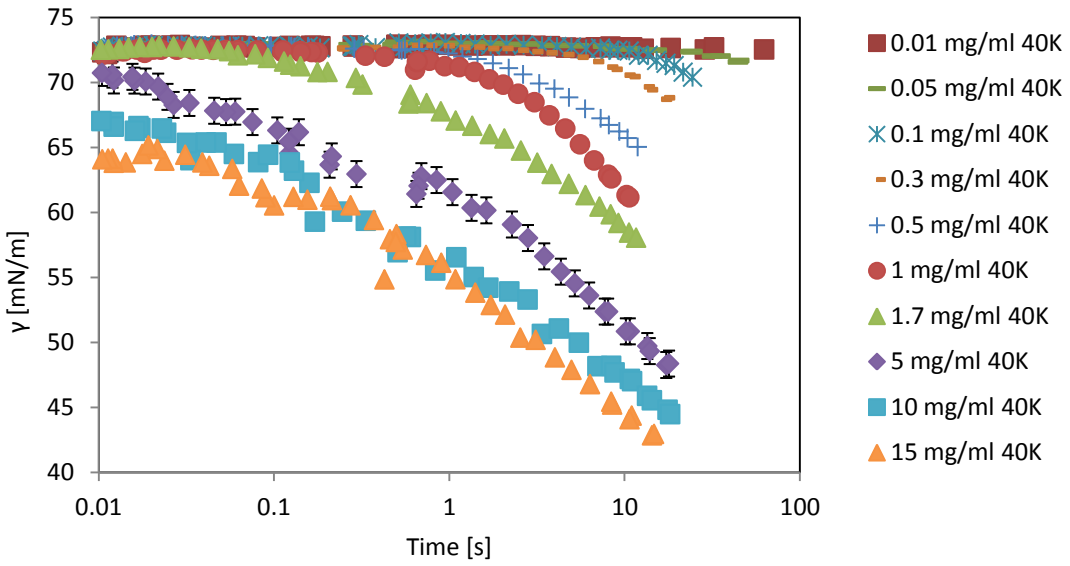

Fig. 4.6.1. Dynamic surface tension results obtained with different concentrations of the 40 KDa polypeptide. For clarity, error bars are only shown in one curve.

Figure 4.6.2 shows the concentration dependence of this induction period. Following the different time curves from top to bottom of the plot, it is possible to observe that the induction period has finished for almost every concentration of polypeptide after 10 s. However, for the lowest concentrations studied, 0.05 and 0.01 mg/ml, the surface tension remains at high values equal to the value obtained with the pure water. For 0.1 mg/ml, the surface tension starts decaying just after 10 s and for 1 mg/ml (the CAC), just before 1 s.

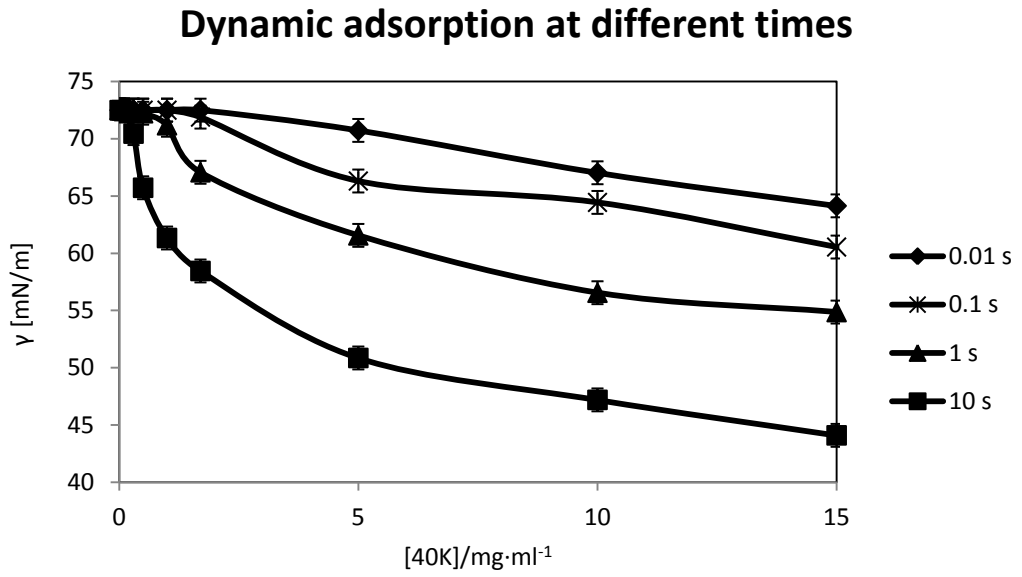

Fig. 4.6.2. Concentration dependence of the surface tension decay induction period and consequent adsorption.

During the induction period the surface adsorption dynamics are governed by a diffusion only process in which the solute is transported to the surface from the bulk phase in the absence of an energy barrier to adsorption [11]. The surface coverage for globular proteins in this time period was found to be 25%-50% [10, 11]. Once the solute needs to travel from distances further away from the interface than the distance at which the diffuse limit is located, it needs to overcome an energy barrier for which convection in the liquid is responsible [11].

Proteins usually follow a three step model of surface adsorption; transport from the bulk phase to a subsurface, transport from the subsurface to the interface and conformational

rearrangements to accommodate themselves in the interface where a mesoequilibrium plateau region appears in the dynamic adsorption profile. During the second step, surface coverage increases to ~100% of its equilibrium value [10].
As seen in Figure 4.6.1, the polypeptide does not reach the mesoequilibrium region within the times and concentrations probed nor does it reach the equilibrium surface tension values. Thus, after 10 s, surface coverage is not yet complete and molecular reorientation has not occurred.

The end of the induction time at a concentration of 0.01 mg/ml is not seen within the 10 s interval. At the same concentration, the induction period for BSA has already finished; for lysozyme, it lasts 40 minutes [10]. The difference in duration of this time interval stems in the different molecular sizes and different degrees of flexibility in protein structure with BSA representing a flexible structure and lysozyme, a hard structure. The duration of the induction period for the 40 KDa polypeptide is situated between those of BSA and lysozyme. Hence, it is possible to assume that the polypeptide is not as flexible as BSA.

4.7. ζ-potential

The colloidal stability of polypeptide solutions was tested via ζ-potential studies at five different pHs: 2.2, 3, 5, 7 and the natural pH of the polypeptide, i.e. pH 7.8. The pH was adjusted with addition of HCl. The solutions were prepared at three different polypeptide concentrations: below, at and above the CAC. The polypeptide concentrations used were 0.5 mg/ml, 1 mg/ml and 2 mg/ml. The results are presented in Figure 4.7.1.

The results for 0.5 mg/ml and 1 mg/ml overlap at pHs 3 to 7.8 and the results for 2 mg/ml are not too far from each other except for the results at pH 5 where the 2 mg/ml solution falls just outside the unstable region ($\zeta < -25$ mV) and the 0.5 and 1 mg/ml solutions are above the stability limit at $\zeta \approx -35$ mV.

The results from these ζ-potential measurements show almost identical values across the entire range of pH studied, showing little trend of concentration dependence. This

observation would imply that ζ-potentials were not affected by aggregation behaviour with respect to concentration dependent changes.

The aggregation of solutions of 40 KDa polypeptide at pH 2.2 and pH 3 is observable by naked eye at the three polypeptide concentrations studied.

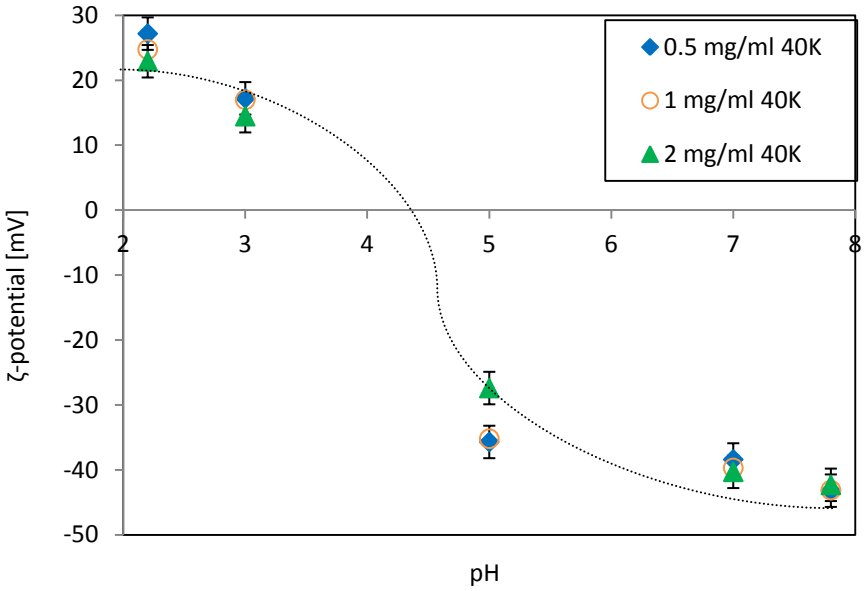

Fig. 4.7.1. ζ-potential of polypeptide as a function of pH in 10 mM NaCl solutions. The sigmoidal curve is only added as a visual aid.

The polypeptide forms stable solutions at pH > 5 for concentrations below the CAC and at the CAC. For 2 mg/ml, stability was only observed at pHs 7 and 7.8.

These results point towards an isoelectric point (pI) located between pH 4 and pH 5.
The ζ-potential is known to follow a sigmoidal shape when suffering a charge reversal as in the present case. Thus, a line has been added to the plot to aid visually with the determination of the point of zero charge or pI. The observed formation of polypeptide aggregates at concentrations over the CAC at pHs immediately below pH 5 and the results in Figure 4.7.1 suggest the pI is located close to pH 5 tending towards a slightly lower pH, as previously observed.

4.8. Foam studies

From the equilibrium and dynamic surface tension results, we know that the polypeptide is capable of lowering the surface tension and starts adsorbing at the interface at relatively short times at high enough concentrations.

Thus, the question remained whether the polypeptide would be able to produce foams and if so, how durable are they? Foam formation is dependent upon rapid surface adsorption and low surface tension. At the isoelectric point, maximum adsorption occurs and so it is at this pH that the foams produced by the polypeptide were studied.

Solutions prepared in 10 mM NaCl at pH 5 containing 0.1 mg/ml and 1 mg/ml, i.e. the CAC of the polypeptide, were hand shaken three times. The decay of the volumes of foam produced was observed at different time intervals. Pictures of the foam produced in this procedure are shown below in Figure 4.8.1.

As seen in the pictures, the volumes of the foams obtained were very small. Nonetheless, their response with respect to time was observed and the results are presented in Figure 4.8.2.

Despite the very low volumes produced at the CAC, the foam volume remained intact after 50 minutes from the time of shaking.

For a concentration ten times lower, 0.1 mg/ml, the amount of foam was stable during the first five minutes after shaking time. This was followed by a slow decay that ended in collapse between 35 and 50 minutes. The resilience to collapse shown by these foams suggested the strong ability of the molecular films formed at the interface to withstand draining and destabilisation.

Previously, it was established that the polypeptide's behaviour resembles more that of lysozyme than that of BSA.

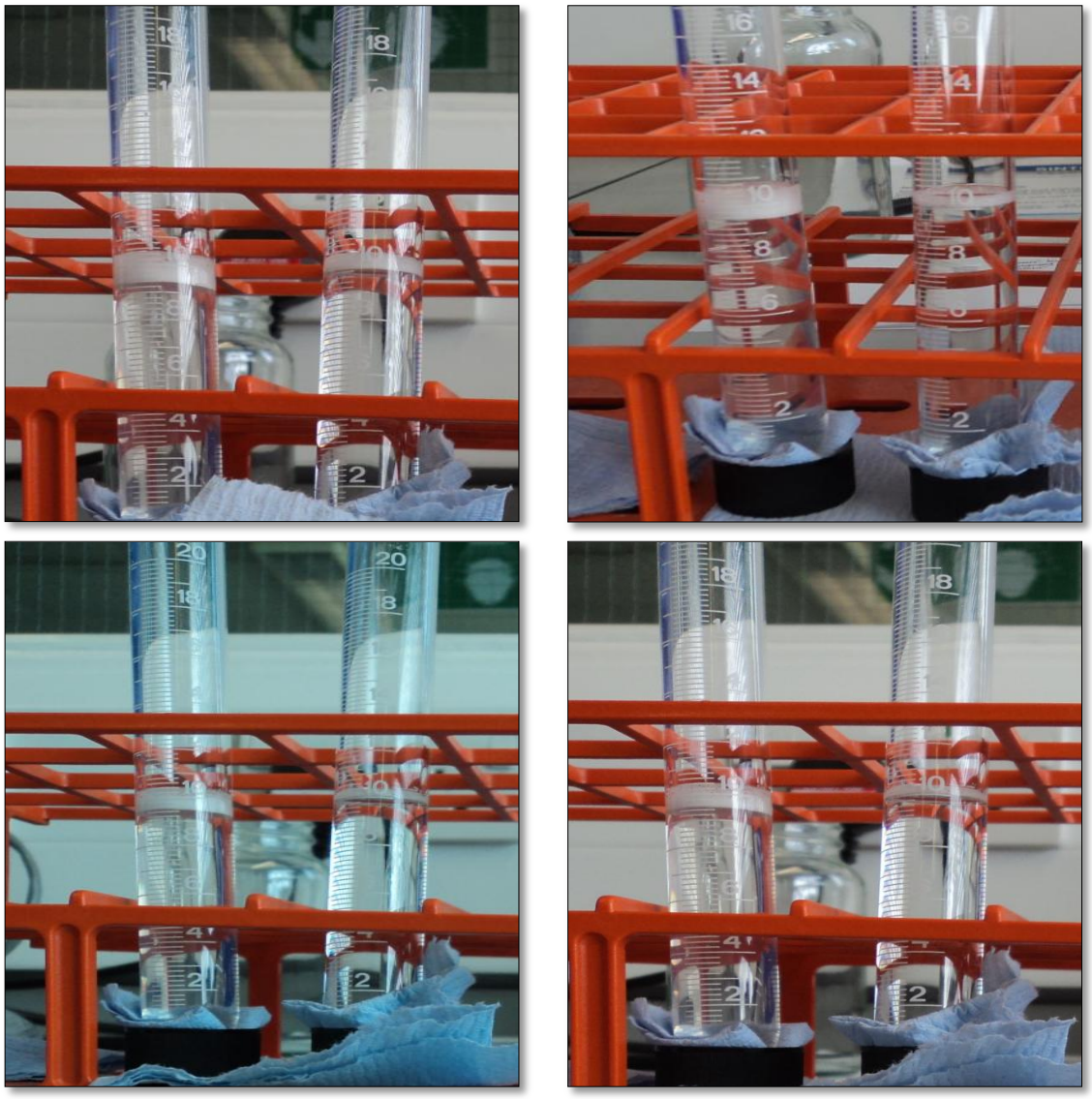

Fig. 4.8.1. Top left: (left to right) 1 mg/ml 40K and 0.1 mg/ml 40K after shaking. Top right: (left to right) 1 mg/ml 40K and 0.1 mg/ml 40K after 5 min.
Bottom left: (left to right) 1 mg/ml 40K and 0.1 mg/ml 40K after 15 minutes.
Bottom right: (left to right) 1 mg/ml 40K and 0.1 mg/ml 40K after 35 minutes.

For comparison, when BSA and lysozyme were foamed under similar conditions from an initial volume of 5 ml in a different experiment [10], the observed height of the foam columns in a 20 ml glass scintillation vial (radius ~14 mm) after 30 seconds from the stirring process were 15 and 0.1 mm, respectively, showing significantly low foam stability.

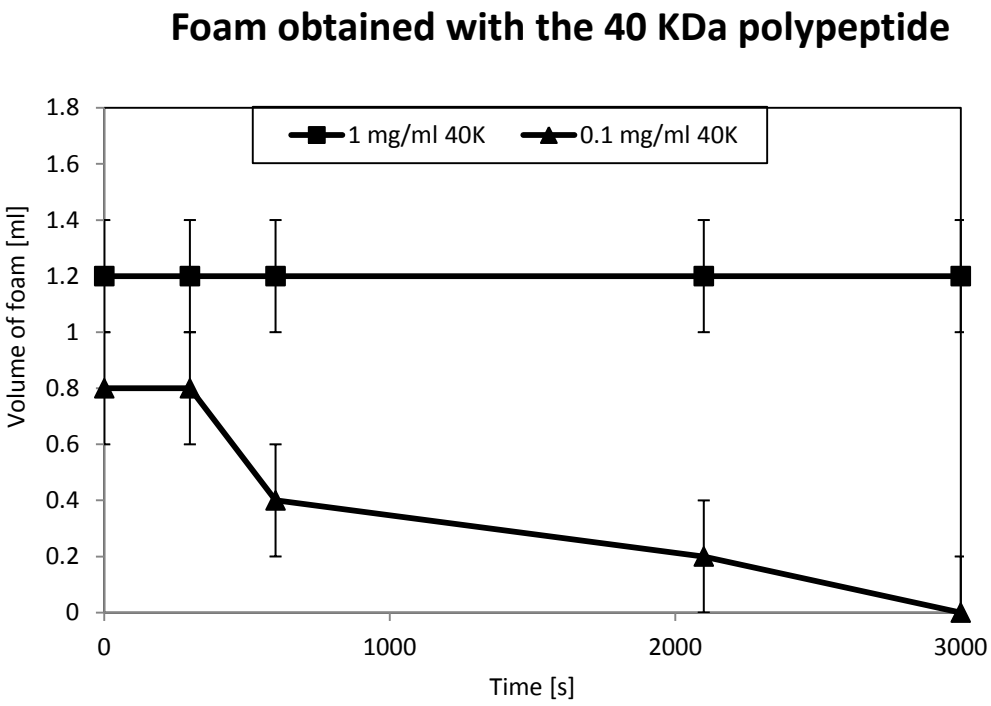

Fig. 4.8.2. Decay of polypeptide foams with time.

4.9. Neutron reflection

The adsorption of polypeptide at the air/liquid interface was further tested using neutron reflection to corroborate the values of surface adsorbed amounts already obtained with the plate method and to investigate the effects produced by changes in pH and amounts of NaCl in the solutions of polypeptide.

4.9.1. Effect of polypeptide concentration

Several concentrations of polypeptide were prepared in NRW with 10 mM NaCl and at pH 5. Their reflectivity profiles were measured and can be seen in Figure 4.9.1.1.

For concentrations equal to or lower than the polypeptide CAC, a monolayer model was appropriate to fit the reflectivity data measured. At 2 mg/ml, a two-layer fitting model had to be used to produce a suitable fit. The second layer is assumed to be spreading out

in the air from the first layer, adsorbed at the surface. The fitting parameters and the results for area per molecule and surface excess are presented in Table 4.9.1.1.

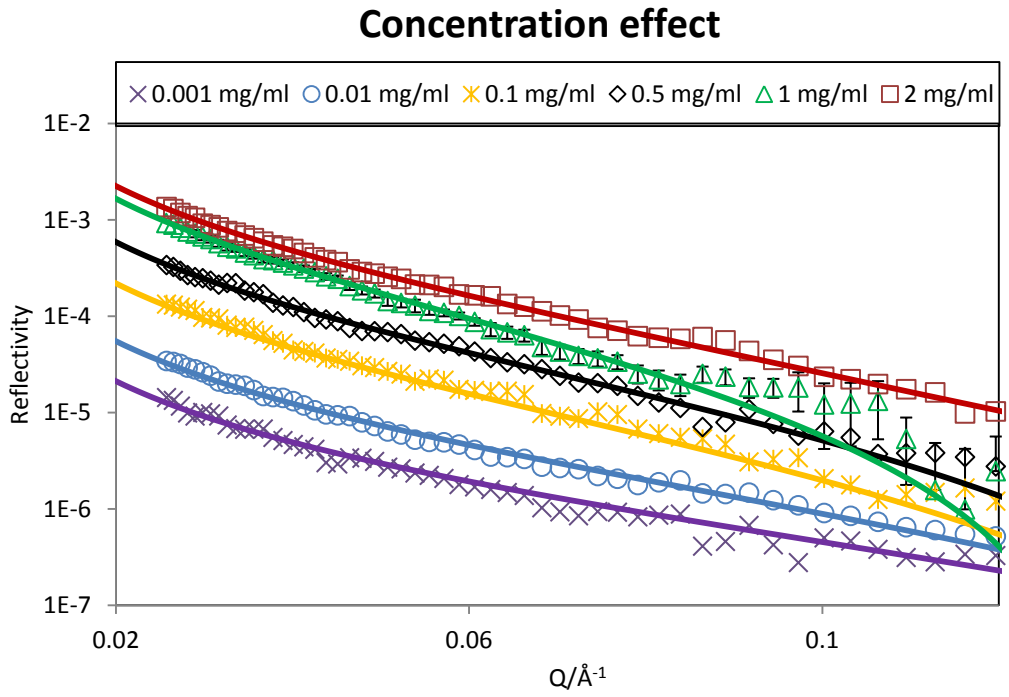

Fig. 4.9.1.1. Polypeptide concentration effect. The lines correspond to the model fits for the data of the same colour and symbol. Results have been scaled with respect to 0.1 mg/ml and error bars are only included in one of the curves for clarity.

From table 4.9.1.1, it is possible to observe how the adsorbed amounts of the polypeptide at the interface increase rapidly at concentrations lower than 0.5 mg/ml reaching values close to 2 mg·m^{-2}. At the CAC of 1 mg/ml, the surface has already reached a steady amount of peptide verified by the measurement of a concentration at 2xCAC. Hence, the previous assumption (CAC ~ 1mg/ml) derived from the surface tension data is shown to be correct.

This upper limit of adsorption corresponds to a surface adsorbed amount of 2.33 ± 0.14 mg·m^{-2}. As noted already, the reflectivity data at 2xCAC forces the fitting model into a two layer rather than a single monolayer, showing a clear structural transition.

C/mg/ml	τ / Å	ρ/ x10^{-6} Å^{-2}	Φ	A ± 6 %/ Å^2	Γ ± 6 %/mg·m^{-2}
2 layer 1	29	0.95	0.47	5394	2.03
2 layer 2	20	0.20	0.10	37150	0.30
2	49				2.33
1	45	0.70	0.35	4717	2.32
0.5	40	0.70	0.35	5307	2.07
0.1	37	0.70	0.35	5737	1.91
0.01	32	0.75	0.37	6192	1.77
0.001	27	0.55	0.27	10007	1.10
0.0001	0	0.00	0.00	0	0.00

Table 4.9.1.1. Neutron reflection data for different concentrations of 40K in NRW at pH 5, 10 mM NaCl. In the model analysis, the scattering length of BSA in NRW was used to calculate the surface excess or area per molecule due to the fact that the molecular weight of the 40kDa polypeptide and sequence are unknown. This treatment should not cause any significant deviation in estimating surface excess.

As the concentration is increased by two orders of magnitude from 0.01 mg/ml to 1 mg/ml, the thickness of the monolayer also increases from some 32 Å to 45 Å whilst maintaining an almost constant scattering length density. At a concentration of 10^{-3} mg/ml, neutron reflection shows how the material is adsorbed at the interface in a highly spread distribution. In contrast, the adsorbed layer at the CAC of 1 mg/ml is about the thickest and most dense packed monolayer with area per molecule of 4700 Å^2. At 2xCAC, the monolayer fit becomes worse and the adsorbed layer is better to be described by a 2-layer model reflecting increased inhomogeneity across the interface. However, the total layer thickness and the adsorbed amount are close to those obtained from the single layer fit.

Hence, we incur that no adsorption takes place at any lower concentration than 10^{-4} mg/ml and therefore it is not presented in Figure 4.9.1.1.

As neutron reflection determines the surface adsorbed amount without any major assumption, the concentration dependent adsorption is best illustrated from the neutron study. The overall results indicate an increase in surface excess with increasing concentration and an inverse relation with respect to the areas occupied per molecule.

Figure 4.9.1.2 shows the variation in surface excess with increasing polypeptide concentration. At 1 and 2 mg/ml, it is essentially unaltered therefore suggesting that the

critical aggregation concentration is indeed at 1 mg/ml. However, the total amount of material adsorbed at the surface is substantially lower than the value obtained via the plate method.

As explained in Chapter 2, the value of surface excess obtained through NR is not subject to model errors and thus from this point on, the accepted value for surface excess at 1 mg/ml of polypeptide at pH 5 is accepted to be 2.32 ± 0.14 $mg \cdot m^{-2}$. The corresponding area per molecule is 4717 ± 283 $Å^2$, a much more realistic value when considering the average molecular weight of the polypeptide is 40 KDa. This order of magnitude is in the same region as the values found for lysozyme and BSA [7, 8].

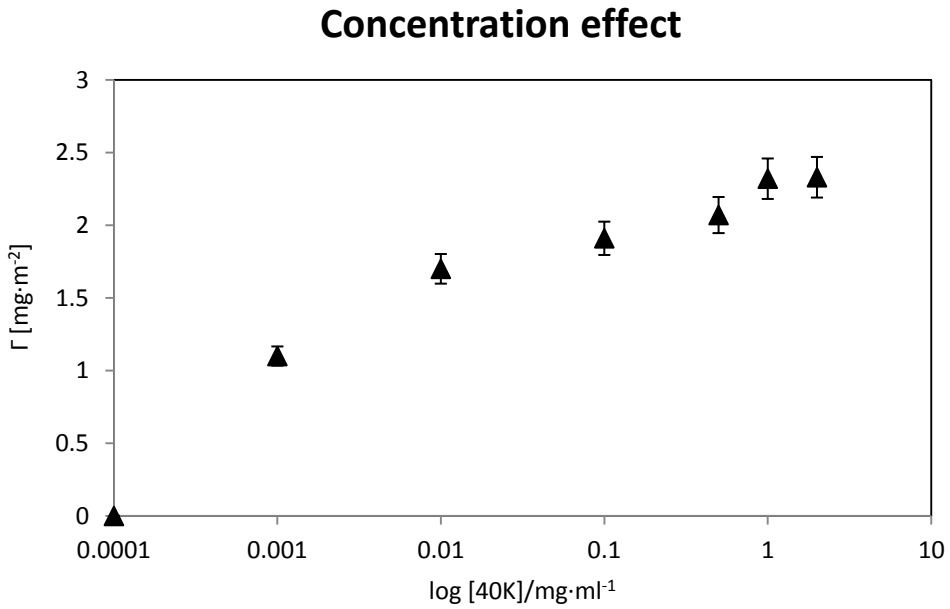

Fig. 4.9.1.2. Surface adsorbed amounts of polypeptide at different concentrations as obtained via neutron reflection.

Measurement of three of the polypeptide concentrations were also performed in solution prepared in D_2O instead of NRW. The fitted parameters and the calculated scattering length densities can be seen in Table 4.9.1.2. The reflectivity data and model fits are found in Figure 4.9.1.3.

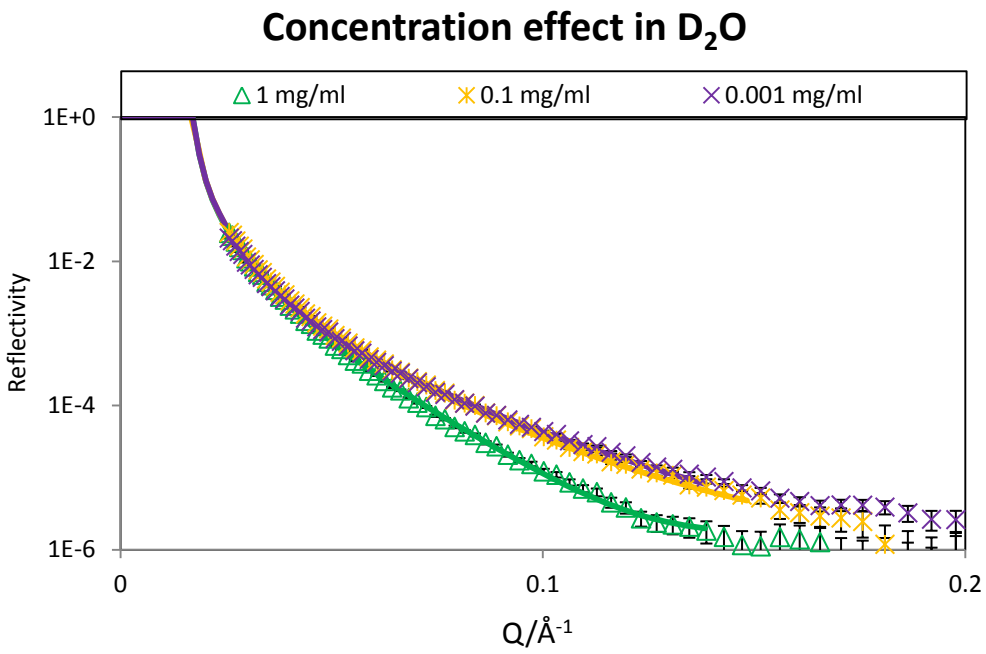

Fig. 4.9.1.3. Polypeptide reflectivity profiles measured from adsorption at different polypeptide concentrations in D_2O samples. The straight lines represent the model fits.

C/mg/ml	layer	τ / Å	P_{exp}/ x10^{-6} Å^{-2}	P_{calc}/ x10^{-6} Å^{-2}
1	**air**	20	0.70	0.70
1	**D_2O**	25	4.83	4.83
0.1	**air**	20	1.15	0.70
0.1	**D_2O**	17	6.20	4.83
0.001	**air**	15	0.54	0.54
0.001	**D_2O**	12	5.18	5.18

Table 4.9.1.2. Neutron reflection data obtained for different concentrations of the 40K in D_2O at pH 5, 10 mM NaCl. The error in thickness is ± 3 Å and the error in scattering length density is ± 0.05 x10^{-6} Å^{-2}.

Since the total thickness adsorbed at the interface must be equal in NRW and D_2O, these were kept constant in the modelling of the D_2O data. The expected scattering length densities can be obtained from Equation 3.6.3 using the parameters already obtained with the samples prepared in NRW, taking into account the additional contributions from D_2O mixing into the layer immersed. Thus, the basic additional consideration in fitting the D_2O profiles was to assume that the top layer in air contained

no water and the bottom layer in water was fully immersed, with the total thickness equal to or close to the full thickness obtained in the matching NRW profile.

The results in Table 4.9.1.2 support the findings in Table 4.9.1.1. The only deviation from the theoretical values expected is presented by 0.1 mg/ml for which the air layer is denser than expected and the D_2O layer is more loosely packed than expected. This could be interpreted as the polypeptide adopting different orientations and surface packing at intermediate concentrations between the very dilute regime (0.001 mg/ml) and the CAC (1 mg/ml) due to adsorption being hindered by previous surface occupancy.

Figure 4.9.1.2 supports this idea. At 0.1 mg/ml there is inflexion point from where the polypeptide adsorption to the interface slows down and heads for a plateau with increasing concentration. The beginning of the plateau marks the CAC.

As explained earlier in Chapter 2, the use of the kinematic approximation provides an alternative and model-independent path to calculate the surface adsorbed amounts and layer thicknesses. The calculated values obtained using equation 2.4.33 are in agreement with those exhibited in Table 4.9.1.1 within a 6% error variation. Figure 4.9.1.4 shows the linear plots from the matching values of surface excess and layer thickness calculated. The almost perfect fitting to each set of measured data confirms the high quality of the structural parameters obtained from direct model fitting to reflectivity profiles measured. The plots shown in fig 4.9.1.5 represent a different way of presenting the partial structural factors versus Q.

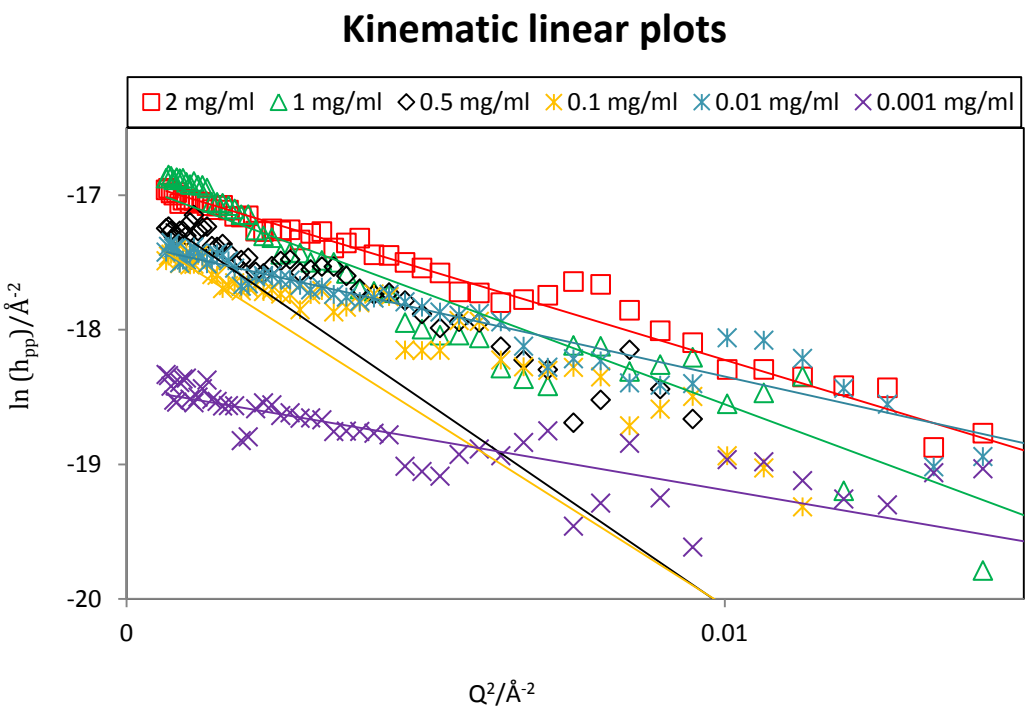

Fig. 4.9.1.4. Use of the kinematic approximation to calculate surface adsorbed amount and layer thicknesses.

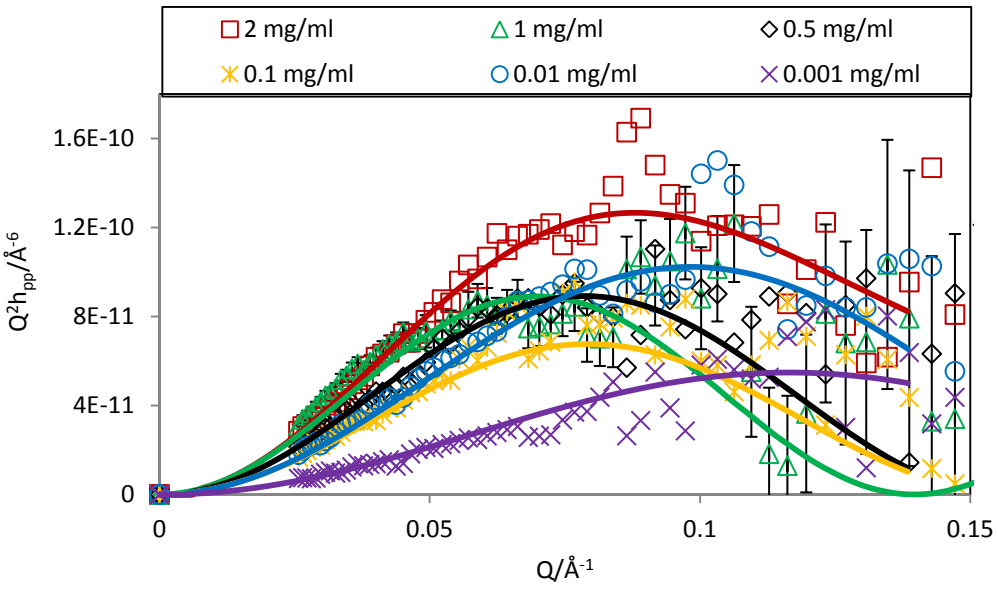

Fig. 4.9.1.5. Use of the kinematic approximation to calculate the self-partial structure factors for the polypeptide adsorbed under different concentrations.

4.9.2. Effect of different pHs on the polypeptide

The responses of 0.1 and 1 mg/ml to pHs 3.6, 5 and 7 were studied in solutions of 10 mM NaCl in NRW. The results and fitting parameters can be seen in Figures 4.9.2.1, 4.9.2.2 and Table 4.9.2.1. The obtained surface excesses are presented in Figure 4.9.2.3. Using a monolayer model, the lowest adsorbed amounts were encountered at pH 7; the highest, at pH 3.6.

Although the isoelectric point as determined by ζ-potential reports is close to pH 5 and therefore at this pH there should be optimal adsorption at the surface, the highest amounts of material are found at pH 3.6. This was expected due to the previously observed aggregation process taking place at pH below 5. That is, for soluble molecules minimum solubility usually occurs at the isoelectric point due to the reduced electrostatic repulsion and thus, maximum adsorption follows. However, in the case of the 40 KDa polypeptide, solubility was noticeably reduced at a pH less than 5 reflecting a conformational change, and surface adsorption increased accordingly.

The differences in adsorbed amounts at 0.1 and 1 mg/ml are negligible at pHs 3.6 and 7 but not at pH 5 where the lowest polypeptide concentration resulted in a difference of 0.51 $mg \cdot ml^{-2}$.

If comparing to BSA (pI ~ 5), an area per molecule of 3800 $Å^2$ was considered physically unattainable with the globular structure of the protein [8]. Thus, this low value of area occupied per molecule indicates, in the case of BSA, that the protein has unfolded to some extent. At pH 3.6, the polypeptide occupies a similar area per molecule both, at the CAC and below it. Also, aggregates formed at this pH are visually observable. This change in behaviour can be related to the polypeptide rearranging its conformation, i.e. unfolding.

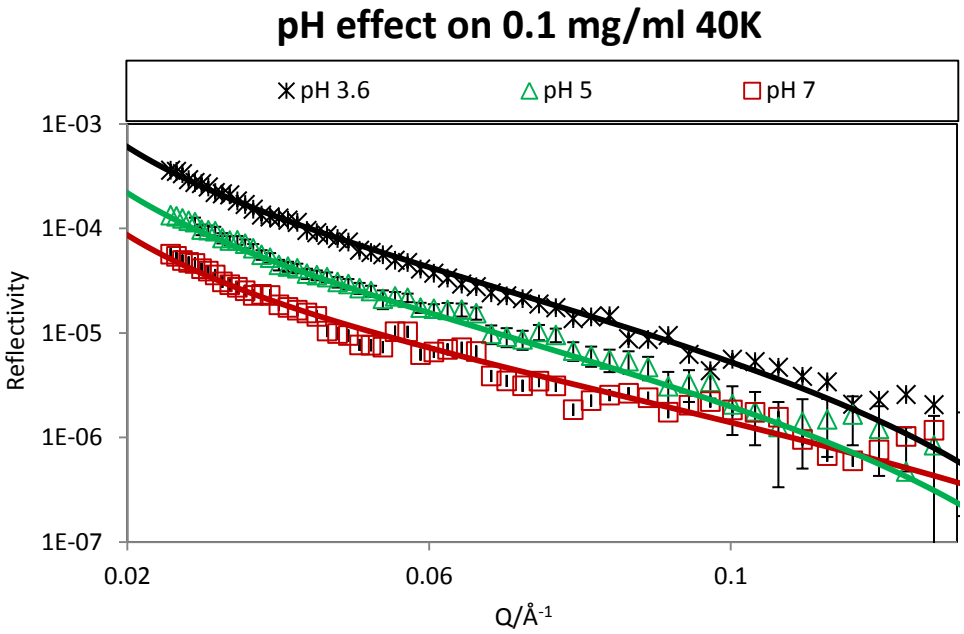

Fig. 4.9.2.1. Effect of pH on neutron reflectivity profiles measured for 0.1 mg/ml polypeptide solutions. The lines correspond to the model fits for the data of the same colour and symbol. Error bars are only included in one of the curves for clarity.

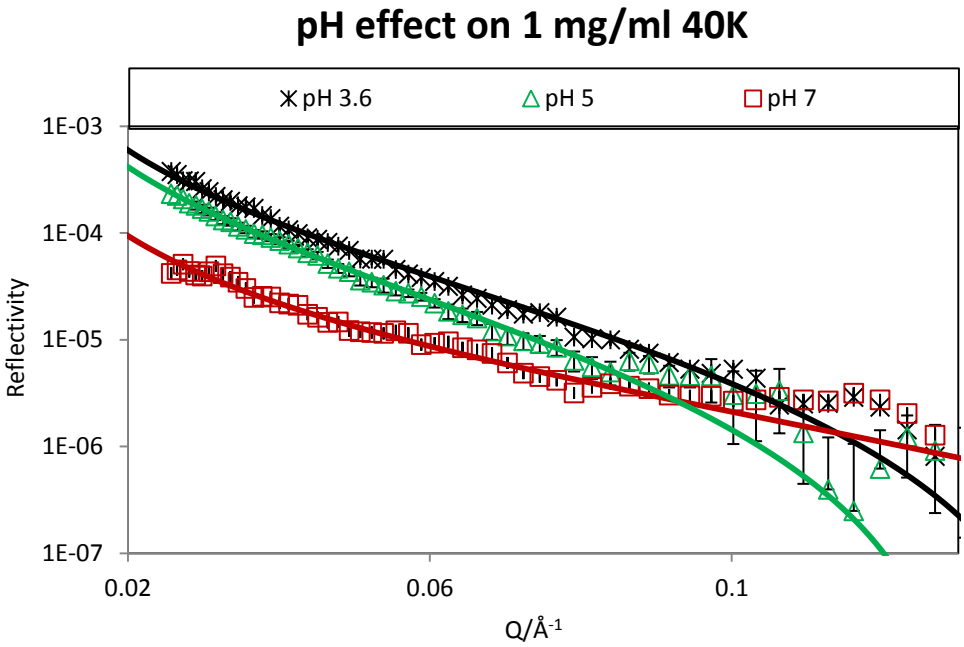

Fig. 4.9.2.2. Effect of pH on neutron reflectivity profiles measured for 1 mg/ml polypeptide solutions. The lines correspond to the model fits for the data of the same colour and symbol. Error bars are only included in one of the curves for clarity.

C/mg/ml	pH	τ / Å	ρ/ x10^{-6} Å^{-2}	Φ	A ± 6 %/ Å^{2}	Γ ± 6 %/mg·m^{-2}
0.1	**3.6**	42	0.95	0.47	3724	2.94
0.1	**5**	37	0.70	0.35	5737	1.91
0.1	**7**	32	0.47	0.23	9880	1.11
1	**3.6**	43	0.93	0.46	3716	2.95
1	**5**	45	0.70	0.35	4717	2.32
1	**7**	26	0.60	0.30	9526	1.15

Table 4.9.2.1. Neutron reflection data for 0.1 mg/ml and 1 mg/ml of 40K in NRW under different pH conditions, 10 mM NaCl. All the fitted models are monolayers.

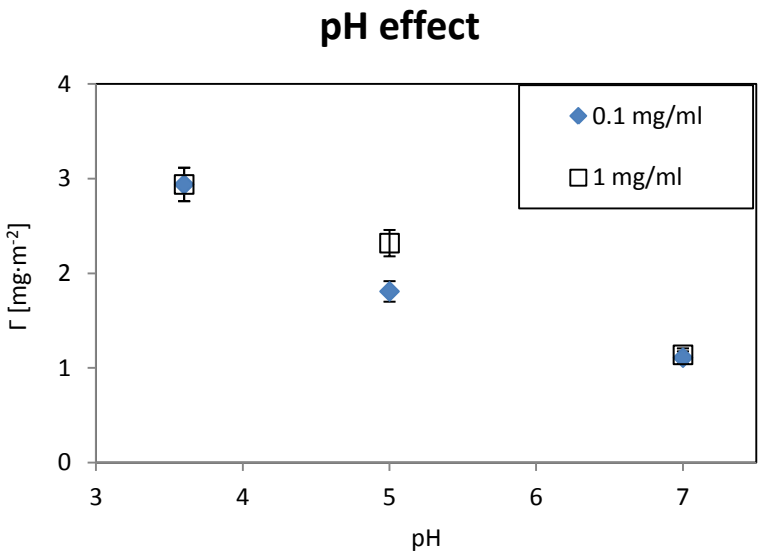

Fig. 4.9.2.3. Surface adsorbed amounts of polypeptide under different pH conditions as obtained via neutron reflection.

4.9.3. Effect of salt addition

The effect of adding different amounts of NaCl to a 1 mg/ml solution of polypeptide at pH 5 was also tested with this technique. The fitted parameters and numerical results are found in Table 4.9.3.1 and can be seen in Figure 4.9.3.1. Graphic results for the surface excess are shown in Figure 4.9.3.2.

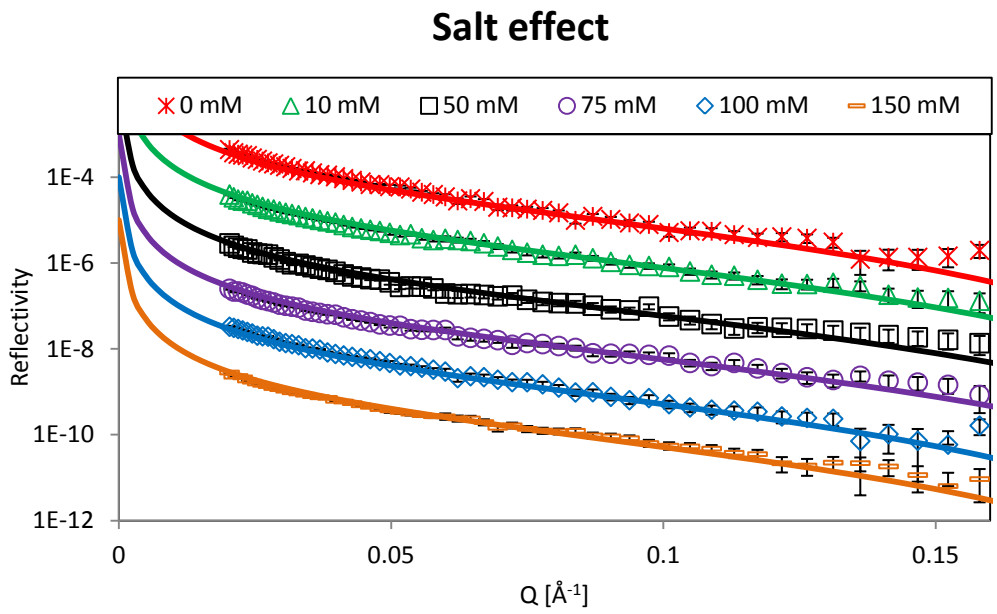

Fig. 4.9.3.1. Effect of addition of NaCl to polypeptide solutions. The lines correspond to the model fits for the data of the same colour and symbol. Results have been scaled with respect to 0 mM NaCl by multiples of 10.

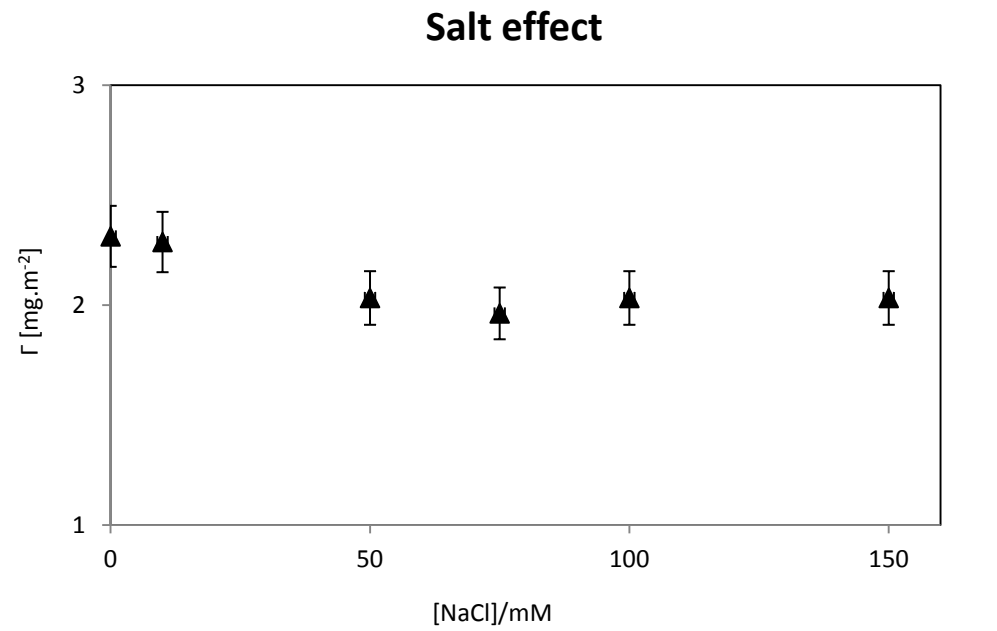

Fig. 4.9.3.2. Variation of surface excess of polypeptide with addition of different amounts of NaCl.

C NaCl/mM	τ / Å	ρ/ x10^{-6} Å^{-2}	Φ	A ± 6 %/ Å^{2}	Γ ± 6 %/mg·m^{-2}
0	33	0.95	0.47	4740	2.31
10	31	1.00	0.35	4794	2.29
50	29	0.95	0.47	5394	2.03
75	28	0.95	0.47	5586	1.96
100	29	0.95	0.47	5394	2.03
150	29	0.95	0.47	5394	2.03

Table 4.9.3.1. Neutron reflection data for 1 mg/ml of 40K in NRW with different NaCl concentrations, pH 5.

As seen in the Figure above, salt concentration does not impact majorly in the surface adsorption of the 40 KDa polypeptide.

In a range from 0 to 50 mM NaCl there was a decrease in surface excess which albeit small, can be considered the result of binding and/or the demonstration of the screening effect that NaCl has on the charged segments of the polypeptide. With a further increase to 150 mM NaCl the surface excess tended to a constant value within error.

In this case, the net effect of salt addition is some minor weakening of surface adsorption through ion binding and association. This differs from the behaviour observed for lysozyme and BSA at the same protein concentration where an increase in ionic strength from 0.02 M to 1 M through addition of NaCl and at their respective isoelectric points resulted in a marked decrease of the adsorbed amounts at the surface [7, 8].

4.10. Small angle neutron scattering

SANS is capable of revealing the structure the polypeptide adopts in solution and tells us whether any aggregation occurs under different solution conditions. Polypeptides are usually water-soluble and the polypeptides chains may adopt different structural conformations. Models proposed and developed for polymeric systems can be directly applied to these biopolymers. At present, it is often assumed that a denatured biopolymer adopts a random Gaussian coil conformation. But there are also counter-arguments, so the matter remains to be in controversy due to the lack of reliable

techniques to unravel the true states of polypeptides in solution. It is particularly unclear how the secondary structures, often unique to peptides and proteins, assume their roles in adopting different tertiary and quaternary structures. Again, with the current techniques available, it remains unknown how primary and secondary structures affect higher-order structures in solvent based aggregation [12-14].

To gather some knowledge about the relation between the structure of the 40 KDa polypeptide at the air/water interface with their structure in the bulk phase, a SANS experiment was performed. Due to limitations in the time access to neutron beam time, only one concentration and pH sample of polypeptide was analyzed with SANS. This was 10 mg/ml at pH 5 and in 10 mM NaCl, i.e. 10 times over the CAC. Figure 4.10.1 shows the data obtained and three different model fits corresponding to a Gaussian coil, a cylinder and a disk, as previously explained in Section 2.4.2.

The straight featureless line characterizing the aggregates of polypeptide formed in the bulk offers a variety of interpretations. Usually, for an unfolded biopolymer a Gaussian or random coil is the expected result in the absence of surfactant [15, 16]. For the 40 KDa polypeptide, the Gaussian coil seen in Figure 4.10.1 has a radius of gyration of 90 Å. Much better fits are obtained increasing this radius to 150 ± 10 Å if the polydispersity index is decreased from 2 to 1. The radius of gyration for a molecule of N amino acid residues according to Tanford [17, 18] is given by

$$R_g = \sqrt{15(N-1)} \qquad Eq.\,4.8.1.$$

Flory offered an alternative expression to calculate the radius of gyration [19] in which solvation is reflected in the parameter v (0.6 for fully solvated chains),

$$R_g = R_o N^v \qquad Eq.\,4.8.2.$$

In Equation 4.8.2, R_0 is a constant related to the persistence length and has a value of 2.40 [18].
Hence, considering N = 129 for lysozyme and N = 582 for BSA [9], R_g is ~44 Å for lysozyme and ~93-109 Å for BSA.

Given that the radius of gyration for a BSA or a lysozyme aggregate ranges between ~44 and ~109 Å, and that R_g depends on the number of amino acid residues in the molecule and therefore depends on its molecular size, any higher value of R_g can be considered as not reasonable from a physical point of view when assuming the name 40 KDa polypeptide is indeed descriptive of this material.

At this point it is worth recalling the high degree of polydispersity observed through SDS-PAGE where positive readings at much higher molecular sizes were obtained. A molecule of bigger size than a BSA molecule could result in a coil with a radius of gyration greater than the calculated upper BSA limit, i.e. $R_g > 109$ Å. Thus, a radius of gyration of 150 Å would indicate that the polypeptide acts as if it was bigger than 40 KDa.

On the other hand, a cylinder shape of length of 7 ± 1 Å and a radius similar to the R_g of BSA was modelled. Since it is possible to argue that a short wide cylinder (or sheet) is akin to a disk shape based on geometrical arguments, a disk shape (or sheet) of thickness 7 ± 1 Å and similar radius to that of the cylinder model was also tested. The fits using the cylinder and the disk model are in good agreement between them and with the scattering data whereas the Gaussian coil, within physically reasonable limits, departs from the scattering data in the low Q-range.
The relevant fitting parameters are presented in Table 4.10.1.

Model	length/ thickness	R	p
Gaussian coil	-	90 Å (=R_g)	2
Disk	7 ± 1 Å	110 ± 30 Å	0.7
Cylinder	7 ± 1 Å	90 ± 20 Å	1

Table 4.10.1. SANS fitting parameters for 10 mg/ml of 40 KDa polypeptide. The scattering length density used for the polypeptide is (3.6 ± 0.4) ·10^{-6} Å^{-2}.

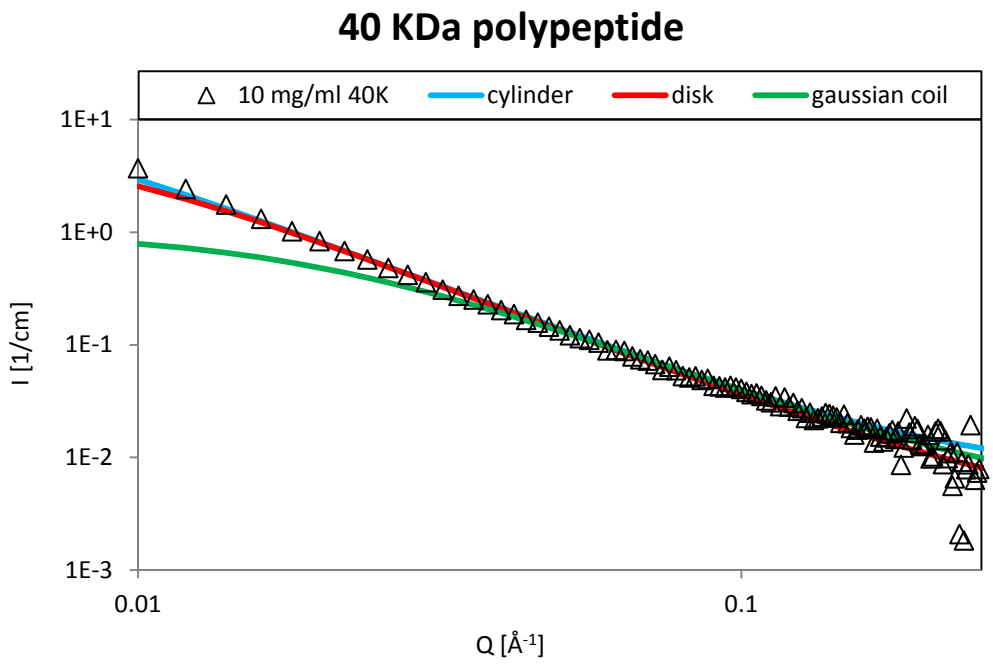

Fig. 4.10.1. Small angle neutron scattering results for 10 mg/ml of 40 KDa polypeptide at pH 5 in 10 mM NaCl. Error bars are omitted for clarity.

Summary

The collagenous nature of the biopolymer under study has been verified by comparison with a known collagen molecule. The molecular size of this molecule was analyzed with SDS-PAGE and although a broad distribution of sizes was obtained, a nominal 40 KDa value was assigned to it.

The results from the foam studies (low volumes of foam) and dynamic surface tension (induction period longer than 10 seconds) point towards a behaviour more typical of lysozyme than of BSA. However, equilibrium surface tension for 1 mg/ml of lysozyme remains at pure water levels whereas for BSA, it drops below 65 mN/m [20]. The 40 KDa polypeptide reaches the CAC at this concentration with a surface tension value of ~32 mN/m.

ζ-potential suggests a pI close to pH 5 and shows that concentration has little effect on the colloidal stability. The solutions of polypeptide are stable at pHs ≥ 5 and unstable below this pH according to visual observations too.

Neutron reflection was used to study the effect of concentration, pH and NaCl concentration on the surface adsorption of the polypeptide. The CAC was found at a concentration of 1 mg/ml (as previously seen with equilibrium surface tension) corresponding to a surface excess of 2.32 ± 0.14 $mg \cdot ml^{-2}$ and an area occupied per molecule of 4717 ± 283 $Å^2$. Adsorbed amounts with different concentrations showed almost no variation with respect to each other at different pHs. Changes with pH manifest through a lower area occupied per molecule with decreasing pH and a possible rearrangement of the molecule at pH 3.6. This indicates that although precipitation occurs at pH 3.6, the remaining solute adsorbs into the surface and its more tightly packed than at pH 5. Variations due to addition of NaCl are negligible.

Su et al. [6] demonstrated through the study of block and statistical copolymers that the slopes obtained from the surface tension plots are determined by the ion absorption and desorption and thus, the calculated surface coverage from Gibbs Equation can deviate from the true values in the presence of electrolyte. The apparent surface coverage obtained from the surface tension experiments is (1+n) times the true surface coverage. Neutron reflection however, offers the true surface coverage and hence, a mean to estimate the n prefactor in the Gibbs Equation.

Given that the areas occupied per molecule as calculated from surface tension and neutron reflection experiments differ by approximately two orders of magnitude at the CAC, and recalling that the surface excess is inversely proportional to the area occupied per molecule (Equation 3.6.1), it is possible to establish a value for the n prefactor in Gibbs Equation of approximately 100, i.e. the polypeptide dissociates into ~100 ions.

With SANS it was possible to obtain a variety of interpretations. However, by comparison with BSA the scattering data obtained was modelled to a thin sheet (or cylinder).

References

[1] U.K. Laemmli (1970) “Cleavage of structural proteins during the assembly of the head of bacteriophage T4”, Nature, 227, pp. 680-685.

[2] J. Sambrook, E.F. Fritsch, T. Maniatis (1989) "Molecular cloning: a laboratory manual", 2nd ed., Cold Spring Harbor Laboratory Press.

[3] M.A. Rodriguez Rius (2009) "Characterization of two peptides derived from eggshell membrane", MPhil Thesis, University of Manchester.

[4] J.R. Lu, T.J. Su, J. Penfold (1999) "Adsorption of serum albumins at the air/water interface", Langmuir, 15, pp. 6975-6983.

[5] N.O. Metreveli, K.K. Jariashvili, L.O. Namicheishvili, D.V. Svintradze, E.N. Chikvaidze, A. Sionkowska, J. Skopinska (2010) "UV–vis and FT-IR spectra of ultraviolet irradiated collagen in the presence of antioxidant ascorbic acid.", Ecotoxicol. Environ. Saf., 73, pp. 448–455.

[6] T.J. Su, D.A. Styrkas, R.K. Thomas, F.L. Baines, N.C. Billingham, S.P. Armes (1996) "Neutron and X-ray reflectivity studies of water-soluble block and statistical copolymers adsorbed at the air-water interface", Macromolecules, 29, pp. 6892-6900.

[7] J.R. Lu (1999) "Neutron reflection study of globular protein adsorption at planar interfaces", Annu. Rep. Prog. Chem. C: Phys. Chem., 95, pp. 3-45.

[8] J.R. Lu, T.J. Su, R.K. Thomas (1999) "Structural conformation of bovine serum albumin layers at the air–water interface studied by neutron reflection", J. Colloid Interface Sci., 213, pp. 426 – 437.

[9] D. Voet, J.G. Voet, C.W. Pratt (2006) "Fundamentals of biochemistry. Life at the molecular level", 2nd ed. John Wiley and Sons.

[10] B.C. Tripp, J.J. Magda, J.D. Andrade (1995) "Adsorption of globular proteins at the air/water interface as measured via dynamic surface tension: concentration dependence, mass-transfer considerations, and adsorption kinetics", J. Colloid Interface Sci., 173, pp. 16-27.

[11] C. Ybert, J.M. di Meglio (1998) "Study of protein adsorption by dynamic surface tension measurements: diffusive regime", Langmuir, 14, pp. 471-475.

[12] R.L. Baldwin, B.H. Zimm (2000) "Are denatured proteins ever random coils?", PNAS, 97 (23), pp. 12391-12392.

[13] V.N. Uversky (2002) "Natively unfolded proteins: a point where biology waits for physics", Protein Sci., 11, pp. 739-756.

[14] R.V. Pappu, R. Srinivasan, G.D. Rose (2000) "The Flory isolated-pair hypothesis is not valid for polypeptide chains: Implications for protein folding", PNAS, 97 (23), pp. 12565–12570.

[15] P.C. Griffiths, Z. Khayat, S. Tse, R.K. Heenan, S.M. King, R. Duncan (2007) "Studies on the mechanism of interaction of a bioresponsive endosomolytic polyamidoamine with interfaces.1. Micelles as model surfaces", Biomacromolecules, 8, pp. 1004-1012.

[16] H. Comas-Rojas, E. Aluicio-Sarduy, S. Rodriguez-Calvo, A. Perez-Gramatges, S. J. Roser and K. J. Edler (2007) “Interactions and film formation in polyethylenimine–cetyltrimethylammonium bromide aqueous mixtures at low surfactant concentration”, Soft Matter, 3, pp. 747–753.

[17] N.C. Fitzkee, G.D. Rose (2004) “Reassessing random-coil statistics in unfolded proteins”, PNAS, 101 (34), pp. 12497-12502.

[18] C. Tanford, K. Kawahara, S. Lapanje (1966) “Proteins in 6 M Guanidine Hydrochloride. Demonstration of random coil behaviour”, J. Biol. Chem., 241, pp. 1921-1923.

[19] M.A. Basharov (2012) “Residual ordered structure in denatured proteins and the problem of protein folding”, Indian J. Biochem. Biophys., 49, pp. 7-17.

[20] A. Cooper, M.W. Kennedy, R.I. Fleming, E.H. Wilson, H. Videler, D.L. Wokosin, T. Su, R.J. Green, J.R. Lu (2005) “Adsorption of frog foam nest proteins at the air-water interface”, Biophys. J., 88, pp. 2114–2125.

Chapter 5. Mixtures with ionic surfactants I: SDS/40K mixtures

This Chapter describes the properties of the solutions containing the 40 KDa polypeptide and the anionic surfactant SDS, highlighting the impact of the interactions with the anionic surfactant on surface adsorption and solution aggregation. Surface adsorption from the binary mixtures was first investigated through the plate and the ring methods and the dynamic changes in surface tension were monitored through the maximum bubble pressure method. The charge of the polypeptide was studied through the ζ-potential measurements by following changes in ζ-potential against solution pH under different surfactant concentrations. Foam stability was then characterised using representative solutions to highlight the synergistic effects arising from interactions between the polypeptide and the surfactant. As for the polypeptide systems alone (results shown in Chapter 4), neutron reflection experiments were undertaken to outline the main changes in surface composition and layer thickness and SANS studies helped unravel the main structural features in the corresponding bulk solutions. These studies together helped corroborate surface tension, surface and solution structural changes with foam stability.

5.1 Surface tension

The equilibrium surface tension of SDS and its mixtures with different concentrations of polypeptide were evaluated using the plate method. The adsorption of SDS in 10 mM NaCl at pH 5 resulted in a CMC with $\gamma = 40 \pm 1$ mN/m at 4 mM (see Figure 5.1.1), exactly the same value given by Fainerman et al. [1] for SDS in 10 mM NaCl at 25°C. The surface adsorbed amount at this concentration calculated via Gibbs Equation was $(4.1 \pm 0.3) \cdot 10^{-6}$ mol·m^{-2} (see Figure 5.1.2) which corresponds to an area per molecule of 40 ± 3 Å^2. The limiting area per molecule is also in reasonable agreement with values obtained by Green et al. [2] and Cooke et al. [3], though attention needs to be paid to the different solution conditions including different SDS concentration, buffer type and temperature studied.

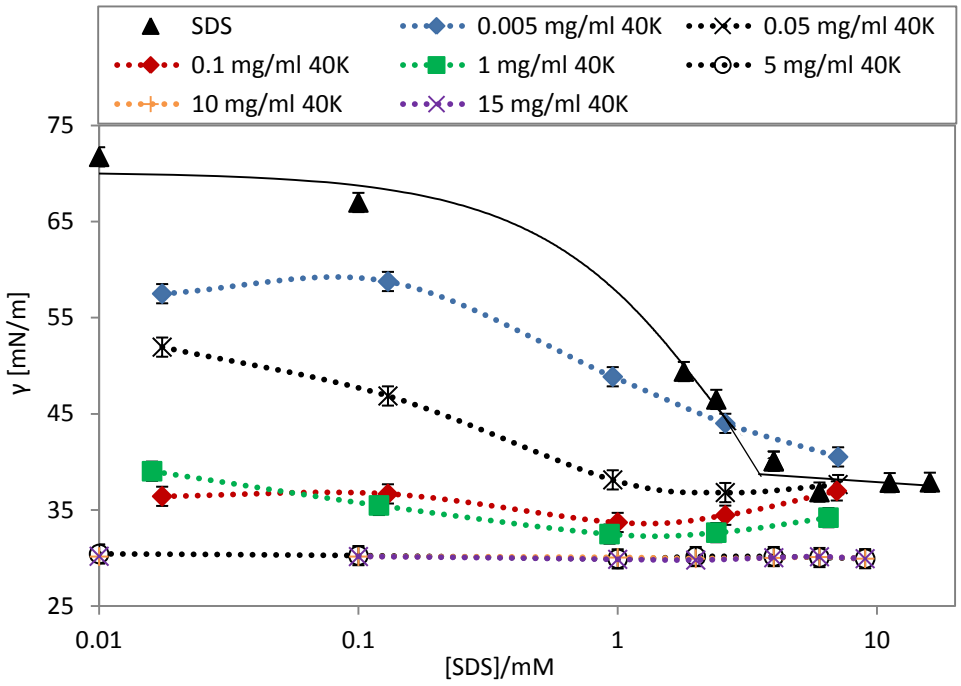

Fig. 5.1.1. Interfacial adsorption of 40K/SDS at the air/water interface. Lines are only added as a visual aid.

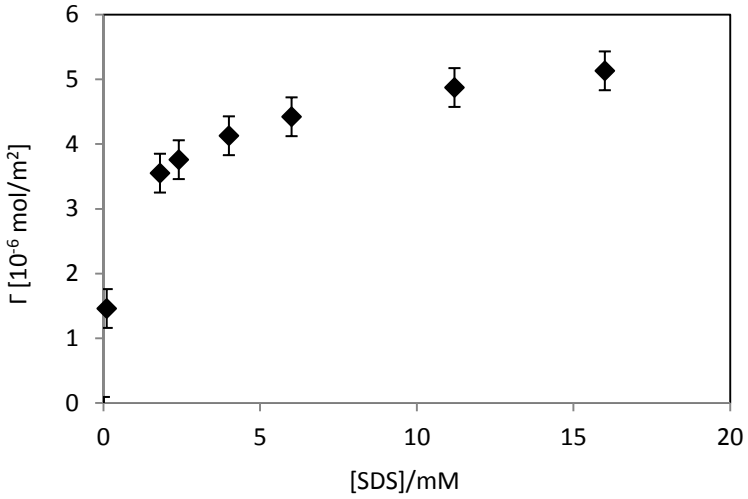

Fig. 5.1.2. SDS surface adsorbed amounts in 10 mM NaCl at pH 5 as calculated from equilibrium surface tension.

Once the CMC of the surfactant was established, different concentrations of the 40 KDa polypeptide were chosen in order to investigate the effects of mixing with SDS across a wide range of SDS concentration (see Figure 5.1.1).

The concentrations of the polypeptide correspond to values below the CAC, at the CAC and above the CAC. Note that changes in surface tension from the polypeptide alone are given in fig. 4.5.1.

At the lowest concentration of polypeptide, 0.005 mg/ml, and SDS concentrations lower than the CMC, lower surface tension values were obtained overall than those recorded with the individual components. The next lowest concentration of polypeptide, i.e. 0.05 mg/ml, decreased the surface tension values even further. At this concentration the value of the γ_{CMC} for the mixture is already obtained at a SDS concentration of 1 mM.

At a polypeptide concentration of 0.1 mg/ml the curve obtained not only lowered the values of surface tension with respect to both individual components, but also reduced surface tension for every point underneath the CMC of the pure SDS, achieving the lowest value, 34 ± 1 mN/m, at a SDS concentration of 1 mM. It is worth recalling that the surface tension value for 0.1 mg/ml of polypeptide is 52 ± 1 mN/m.

Despite a slightly lower value of surface tension at 6.5 mM (above the CMC of SDS), the curve obtained at the CAC of the polypeptide resembles the one just described. At the lowest concentration, γ is just above the value obtained for the mixture with 0.1 mg/ml.

At the three concentrations probed above the polypeptide critical aggregation concentration, i.e. 5, 10 and 15 mg/ml, respectively, the surface tension is further decreased reaching values comparable with those of the polypeptide on its own even at high SDS concentrations beyond the CMC. Within errors, the three curves overlap at every concentration of SDS and the overall curve is essentially a flat line located at a surface tension value of 30 ± 1 mN/m, just below the value obtained for the polypeptide at the CAC, 32 ± 1 mN/m.

The surface tension profiles obtained from the mixtures of SDS and polypeptide do not display any obvious association with any of the general surface tension patterns as described for polymer/surfactant mixtures in Section 2.1.8. Nevertheless, the lower surface tension values at very low SDS and polypeptide concentrations point towards a strongly interacting system, i.e. an 'S'-labelled curve, as already explained by Bykov et al. [4] who obtained a similar curve for a mixture of 0.02 mg/ml of branched PEI (25 KDa) with SDS under conditions of nearly total dissociation, i.e. pH 3.

Zhang et al. [5] also found similar shaped curves with the branched PEI (2KDa)/SDS system although they investigated modified PEI (also at 0.02 mg/ml).
In their study, different pHs resulted in differently-shaped adsorption profiles.
At pH 3, PEI is almost entirely dissociated [4], i.e. degree of dissociation approaches unity; at pH 10, the degree of dissociation is in the range 0.01 to 0.03 [6]; that is, almost completely uncharged. For the SDS mixed solutions with PEI-$(EO)_1$ and PEI-$(PO)_1$, the differences between pH 7 and 10 were minimal. However, at pH 3 the adsorption behaviour changed drastically. At this pH, the SDS mixtures with PEI-$(EO)_1$ and the PEI-$(PO)_1$ showed the pronounced negative peak followed by an also pronounced peak presenting higher values of surface tension.

All these features were encountered at SDS values between 0.01 and 1 mM. The curve features that Zhang et al. [5] found for the mixtures with PEI-$(EO)_1$ and PEI-$(PO)_1$ at pH 7 and pH 10 are almost identical to the shape that we found for the 40K/SDS system at a pH close to the isoelectric point of the polypeptide, i.e. pH 5.

The combination of a 25 KDa linear PEI with SDS is also pH-dependent and at pH 10 (in almost neutral charge conditions) presents a similar surface tension profile to that of the 40 KDa polypeptide/SDS system [7].
The results on pH dependence with different PEI leave no doubt that the strong electrostatic interaction plays an important role in the adsorption profile.

A comparison of the PEI systems with the mixed 40 KDa polypeptide with SDS suggests the possibility of the existence of a peak with positive surface tension values in the adsorption curve of the 40 KDa polypeptide /SDS that is dependent on the pH. In

other words, surface tension peaks may also occur from our system if studied at an appropriate pH.

Furthermore, Zhang et al. [5] used neutron reflection to probe the differently modified PEI mixtures with SDS and observed surface structural changes, i.e. a transition from monolayer to trilayer adsorption at high pH for the PEI-$(EO)_1$ and the PEI-$(PO)_1$, in agreement with the ion-dipole interaction model proposed by Penfold et al. [8] in their study of mixtures of surfactant and polyamine. The linear PEI/SDS system however, only showed a consistent monolayer at every SDS concentration studied [7].

Thus, the features encountered for the mixtures of SDS with linear and branched PEI were discussed in terms of an electrostatic interaction clearly seen at low pH. The interaction process then became transformed with pH changes, with an added strong hydrophobic interaction caused by the existence of an ion-dipole interaction between the SDS head group and the amine nitrogen present in the polymer that cooperates with the alkyl chains of the neighbouring surfactants [5]. The strong interaction dominates at a pH close to neutral conditions although according to Penfold [8] there remains an electrostatic component even in conditions close to neutrality.

The SDS/PEI-$(EO)_3$ system did not present any structural changes with different pH. This observation prompted Zhang et al. [5] to argue that this behaviour constituted a further prove of the existence of the ion-dipole interaction which they believed had been interrupted with the larger $(EO)_3$ group.

Since amines are found in amino acids, i.e. the building blocks of the 40 KDa polypeptide, the existence of a strong hydrophobic interaction of the kind described above also needs to be considered as a possible cause for strong interactions occurring in our system. The 40 KDa polypeptide/SDS system was also studied at a pH close to the isoelectric point and thus its adsorption curve can be thought of as a consequence of a cooperative ion-dipole interaction with the hydrophobic interaction between SDS chains dominating over the electrostatic interaction. However, it is worth recalling that Bykov et al. [4] obtained similar results at a degree of dissociation close to unity; where Zhang et al. [5] assume that the electrostatic interaction is stronger than the hydrophobic

interaction. Such differences are difficult to quantify and are likely to be system dependent.

In the present system and according to the model proposed by Bell et al. [9], region A corresponds to SDS concentrations below 1 mM; region B spans from 1 mM to around 2.5 mM; region C covers the concentrations between 2.5 mM and the surfactant CMC, i.e. ~ 4 mM; and finally, region D is occupied by SDS concentrations above the surfactant CMC.

In region A, cooperative interactions already take place and formation of polymer/surfactant monomer complexes starts. These complexes are very surface active and rapidly adsorb at the interface thus explaining the lowering of the surface tension in this region in comparison with the individual components. According to Bykov et al. however, the formation of the complexes only starts at S1 and not before, although cooperation occurs before S1. They identified S1 as the CAC of the system following the model proposed by Goddard et al. [10] in relation to the PNIPAM/SDS system, but Bell et al. [9] reached the conclusion that the CAC is not clearly defined in the surface tension curve as the bulk effects with regard to the formation of the bulk complexes are too weak compared to the surface phenomena taking place in strongly interacting systems.

In region B or S1 to S2, the polymer gets saturated with surfactant monomers thus leading to the formation of polymer/surfactant micelle complexes in the bulk phase due to the excess SDS available (S2 to S3). The polymer/micelle complexes are usually described as not very surface active and therefore they are often found responsible for a raise in surface tension values, i.e. the cliff edge peak in region C. For most systems of this kind, higher values of surface tension are found to be the consequence of surface active material being solubilised and returning to the bulk phase where they are free to associate in polymer/micelle complexes which are not as surface active as the polymer/monomer complexes. Thus, they remain in the solution rather than adsorbing at the interface. However, in the present case, the cliff edge peak is not observed. This phenomenon also occurs in the PEI/SDS systems mentioned earlier.

Penfold et al. [8] compared the surface tension profile of mixtures of small molecular weight amines and SDS, which lacks the cliff edge peak, with Bell's model. They discussed that the small amines were not capable of stabilizing the SDS micelles to a considerable extent and therefore no bulk amine/SDS micelle complexes were formed which in turn results in the no appearance of the cliff edge peak. The total surface adsorbed amounts were lower close to the isoelectric point for all the amines. However, the reduction in surface adsorbed amounts was less noticeable for the larger amines which presented a greater stability due to the more prevalent cooperative hydrophobic interaction with the ion-dipole interaction.

A major difference encountered in the 40 KDa polypeptide/SDS system as well as in the PEI/SDS systems is that the values of surface tension in regions A and B are already lower than the CMC of the surfactant. Also, regions B and C are not so clearly distinguished as far as surface changes are concerned. The polypeptide/surfactant micelle complexes that lead to re-solubilization of the polypeptide in Bell's model may be more surface active than expected (but not as much as the polymer/monomer complexes) which is reflected in the not-so-sharp raise in surface tension values at S2.

The surface activity of these complexes gradually decreases with increasing addition of SDS until the CMC of the surfactant is reached. The sharp S2 to S3 transition in Bell's model corresponding to the dissolution of the polypeptide/surfactant monomer complexes is therefore affected by the slower re-solubilization of polypeptide.

The high surface activity of the polypeptide results in the disappearance of large changes across the S3-S4 region boundary. The surface tension does not have to decrease to reach surfactant values due to the surface activity of the polypeptide/surfactant micelle complexes.

Bykov et al. on the other hand found that surface tension values rose to a local maximum before descending back to the CMC of the SDS. By looking at their surface tension curve one can argue that the local high peak is more likely to be caused by systematic errors than by any structural change in the aggregates as they explained.
However, their reasoning follows a local decrease in surface dilational elasticity at exactly the same point. Once again, it could be argued that that local minimum is only

an error associated with the measurement. Nonetheless, the overall trend that they found for surface dilational elasticity offers a clear explanation of the structural changes occurring at the surface in accordance with the formation of complexes of different surface activities. Hence, in region A they found the elasticity to increase to a maximum before starting to fall just before S1 in agreement with the concept of polymer/monomers formation below S1. In region B, a further change in the elastic behaviour of the surface is interpreted as the saturation of the polymer leading to a final change in elastic behaviour coincident with the region covering the top of the local maxima up to CMC surfactant levels. The local maximum was attributed to slow redistribution of material at the surface. This is consistent with the slower re-solubilization of the 40 KDa polypeptide.

Finally, in region D, the surfactant forms free micelles and eventually removes almost all the polymer complexes from the surface. It is reasonable to assume that some polymer remains since surface tension values are still generally lower than those for the surfactant alone.

In the system occupying the present study, the behaviour of the mixtures at very low polypeptide concentrations is also consistent with the general model presented by Zhang et al. and Bykov et al. As Bell et al. explained, "the higher the polymer concentration, the more likely a peak will form" [9]. Although in this case, the observed phenomenon is not the occurrence of the peak but the slow solubilisation leading towards it and only from concentrations higher than 0.05 mg/ml.

In the PEI/SDS systems no mention is made concerning the concentration at which the polymer PEI aggregates. In fact, both teams work with a concentration of 0.02 mg/ml of PEI. By observation of Figure 5.1.1 it is possible to conclude that the PEI/SDS systems are very likely to behave in a similar manner at PEI concentrations above the CAC, assuming 0.02 mg/ml is not already above this concentration.

Thus, at concentrations of 5 to 15 mg/ml of 40 KDa polypeptide, the interface is dominated by the polypeptide and no distinguishable signs of complex formation other than polypeptide aggregates are observable in the adsorption curves obtained. This does not necessarily mean that no changes in structure at the interface or within the

complexes take place along the whole range of SDS concentrations measured. It may simply indicate that the polymer does not saturate unless higher amounts of SDS are added.

Strongly interacting systems are generally associated with mixtures of polymer and oppositely charged surfactants that lead to phase separation at some surfactant concentrations. Campbell et al. [11] argued that the cliff edge peak, which is usually located in the phase separation region, in systems like the PEI/SDS are a product of the precipitation of bulk material which leads to depletion of surface active material at the interface with time. Thus, they argue that the phase separation is a consequence of the loss of bulk colloidal stability. In contrast to Bell's model, this group assumes that no polymer remains in solution and therefore the peak is not induced by the formation of non-surface active polymer/surfactant complexes.

Nevertheless, the linear PEI/SDS system did not show any cloudiness at any of the SDS concentrations studied [7]. And no phase separation or precipitation was observed for the 40 KDa polypeptide/SDS system at any of the surfactant concentrations studied either, even when the solutions were left untouched for several days close to the isoelectric point. The surface tension was lowered below that of the individual components by both systems, indicating the existence of a strong interaction that was not just electrostatic. Thus, we reject the assumption that there was no polypeptide in the bulk solution in the region where surface tension values rise.

5.1.1. Addition of NaCl

Driscoll et al. [12] found that addition of electrolyte to the DMDAAC/SDS system enhances the binding of the polymer to the surfactant micelles and reduces the values of CMC and CAC. Salt addition also enhances the formation of surface complexes, reducing the surface critical aggregation concentration and thus reducing surface tension further.

According to Penfold et al. [13], who also found enhanced adsorption with addition of NaCl to the mixed amine/SDS systems, salt screens the interaction between surfactant head groups. This promotes the lateral packing of the alkyl chains and strengthens the hydrophobic interaction without screening the ion-dipole interaction.

Some mixtures of SDS and polypeptide were initially measured using the ring method. However, due to the difficulties encountered during measurement of this system particularly at low polypeptide concentrations, the plate method became the preferred choice for evaluating them. Nonetheless, the study of variations in surface tension with addition of NaCl was obtained with the ring method.

It is necessary to clarify at this point that both compounds, the polypeptide and the SDS, belong to different batches from those used in the analysis with the plate method. Despite this fact and the fact that the volumes used for the correct functioning of both methods differ by a factor of 2 to 3, the comparison between solutions of the same concentrations from different sources resulted in similar values overall (see Figure 5.1.3), with only 2 points measured being out of the expected range. Thus, the two sets of data with the addition of 10 mM NaCl from both ring and plate methods were regarded the same, except 1 data point from the plate method measured at the lowest concentration.

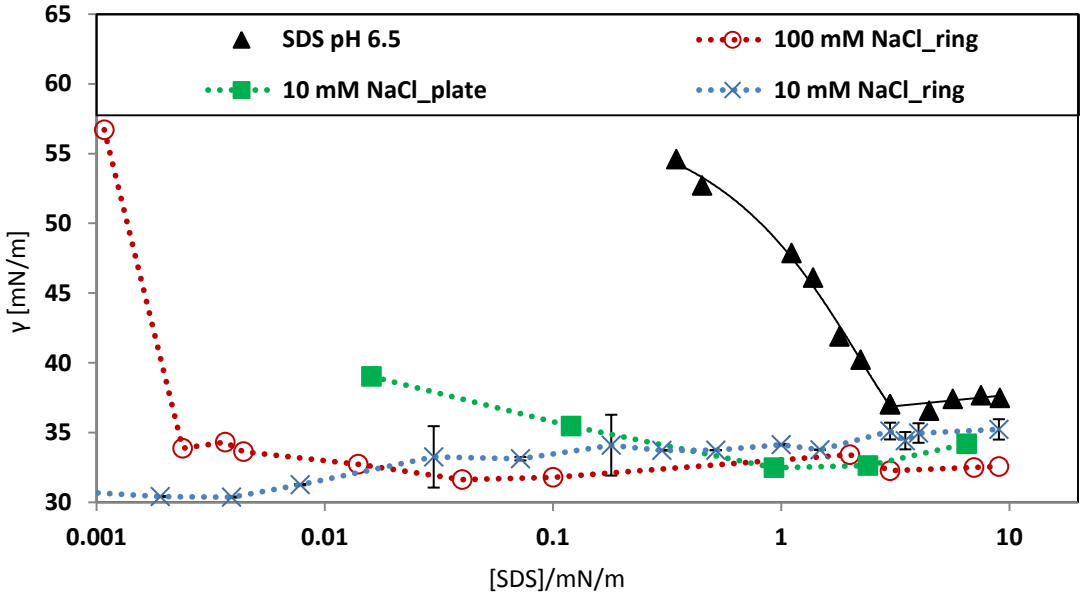

Fig. 5.1.3. Equilibrium surface tension profiles for 40K/SDS mixtures at different NaCl concentrations.

Addition of 100 mM NaCl did not result in enhanced adsorption but rather in earlier surface saturation of polypeptide/surfactant monomer complexes.

The range of surfactant concentrations studied did not result in phase separation or precipitation even at a 100 mM of NaCl (see Figure 5.1.4). This trend was again similar to the observations at 10 mM NaCl.

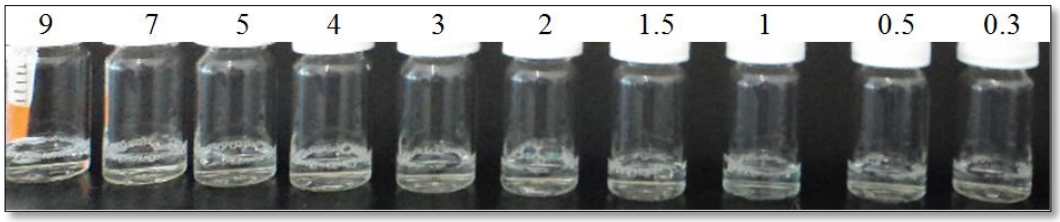

Fig. 5.1.4. Solutions of 1 mg/ml of polypeptide mixed with SDS at pH 5 in 100 mM NaCl. SDS concentrations are shown in mM by the numbers at the top of each bottle.

5.2. Maximum bubble pressure

The short-time dependent surface tension changes of the polypeptide mixtures with the anionic surfactant SDS were analyzed with the maximum bubble pressure method. Three different concentrations of SDS, below, at and above the CMC were mixed with concentrations below (0.1 mg/ml) and above the CAC of the polypeptide (5, 10, 15 mg/ml). The results are presented in Figures 5.2.1 to 5.2.12.

At the lowest SDS concentration (Figures 5.2.1 to 5.2.4), the decay of the surfactant adsorption curve within the first 10-100 seconds is considerably slow, reaching a value of 68.03 mN/m at 47 s. A concentration of 0.1 mg/ml of polypeptide behaves in a similar manner although there seems to be a change in behaviour at approximately 10 s which can be thought of as the end of the lag time or induction period. The decay of the mixture mimics the polypeptide shape but decreases the surface tension by a further ~2 mN/m at 17 s. For higher concentrations of 40 KDa polypeptide, the surface tension decay of the mixtures is identical to that of the polypeptide which at 5, 10 and 15 mg/ml, adopts a slightly concave shape that falls sharply reaching surface tension values between 42 and 49 mN/m at around 17 s when the SDS at 0.1 mM only reaches to ~69 mN/m.

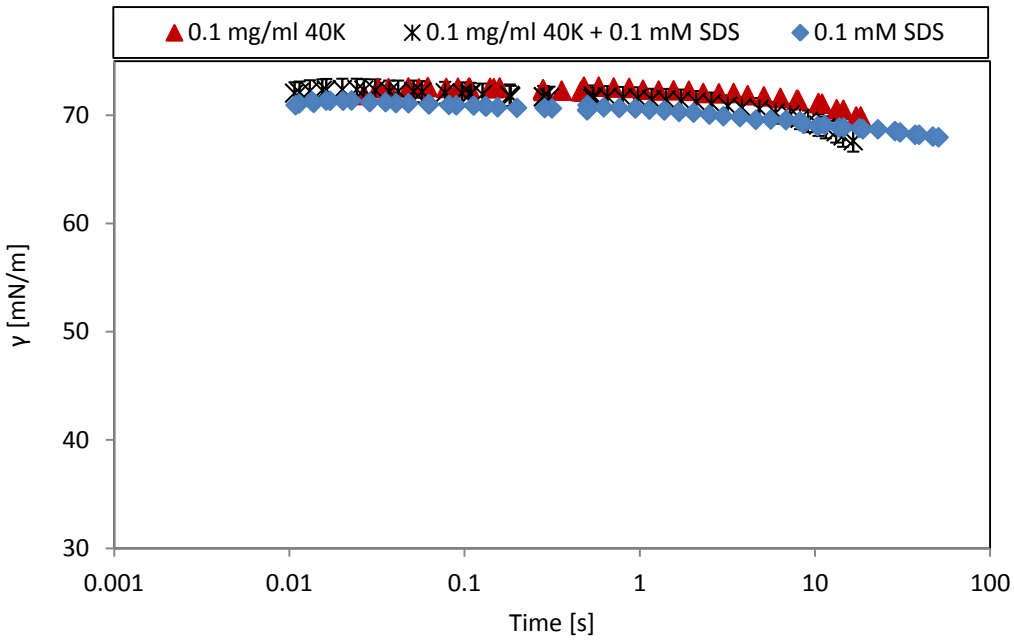

Fig. 5.2.1. Dynamic surface tension for 0.1 mg/ml 40K + 0.1 mM SDS.

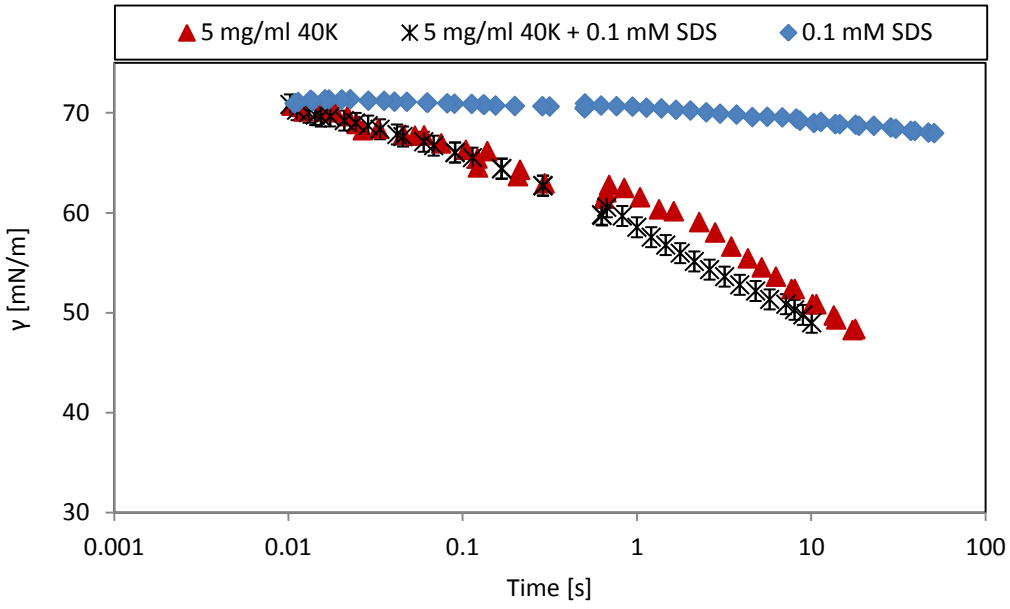

Fig. 5.2.2. Dynamic surface tension for 5 mg/ml 40K + 0.1 mM SDS.

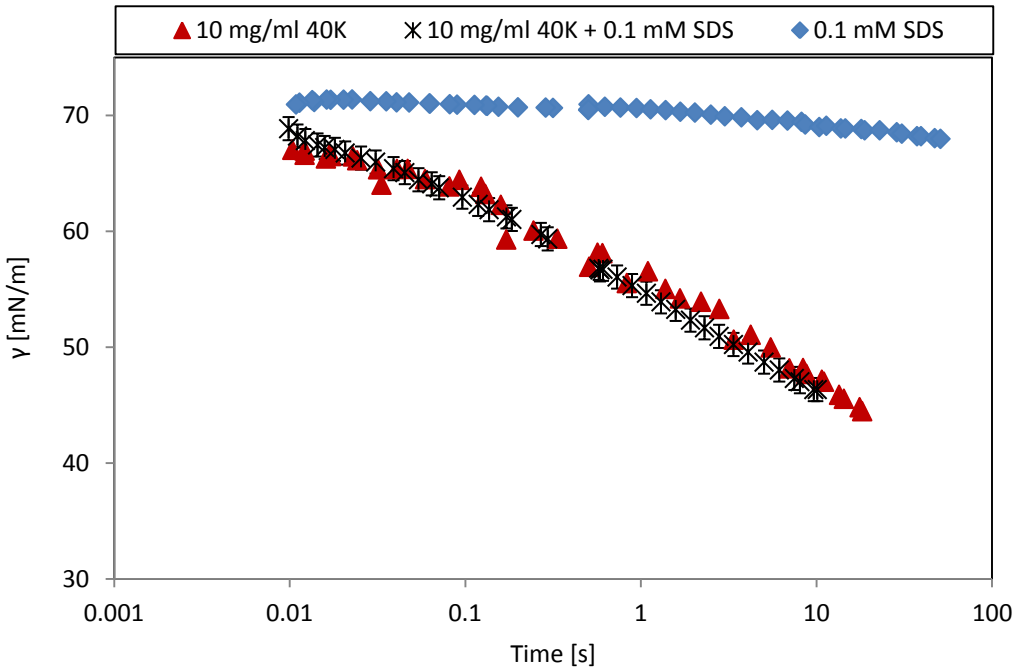

Fig. 5.2.3. Dynamic surface tension for 10 mg/ml 40K + 0.1 mM SDS.

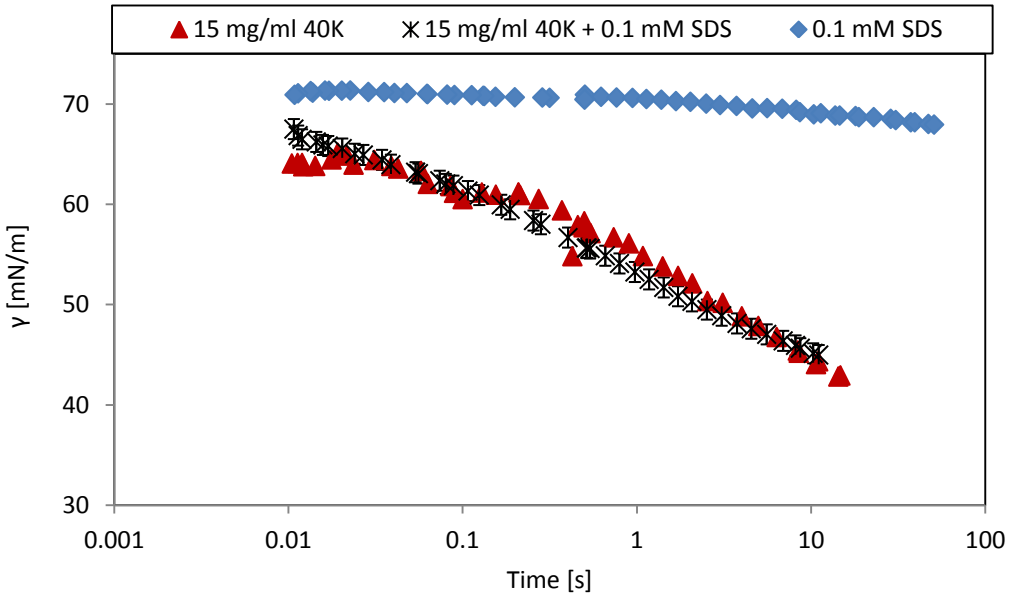

Fig. 5.2.4. Dynamic surface tension for 15 mg/ml 40K + 0.1 mM SDS.

When the SDS concentration is increased to near-CMC levels (Figures 5.2.5 to 5.2.8), the decay of the surfactant surface tension results in an inflexion point at ~ 0.01 s where the curve changes its shape from concave to convex. The mixtures with the polypeptide follow this trend at times below the 0.01 s inflexion point at concentrations 0.1 and 5 mg/ml. However, at 10 and 15 mg/ml, the shape of the curve for the mixed solutions is convex from the start, i.e. at ~0.003 s at $\gamma \approx \gamma$ (UHQ water).

The surface tension values of the mixture with 0.1 mg/ml of 40 KDa polypeptide are higher but still within a ~8 mN/m distance from the surfactant curve. In contrast, the surface tension values at higher polypeptide concentrations for the mixed curves are lower than those of the surfactant from the time when the inflexion point is seen in the surfactant curve and almost identical from 0.1 s onwards. Below the inflexion point, surface tension is higher than that of the surfactant showing the influence of the polypeptide which still remains at relatively high values, i.e. $\gamma \approx \gamma$ (UHQ water), of surface tension at these times.

For 5, 10 and 15 mg/ml of 40 KDa polypeptide, the curves attain a value of surface tension of ~36 mN/m at a time of ~20 s. This is a significant decrease since the equilibrium surface tension of the mixtures was found to be at ~30 mN/m for all three concentrations and the CMC of the SDS is at 40 mN/m.

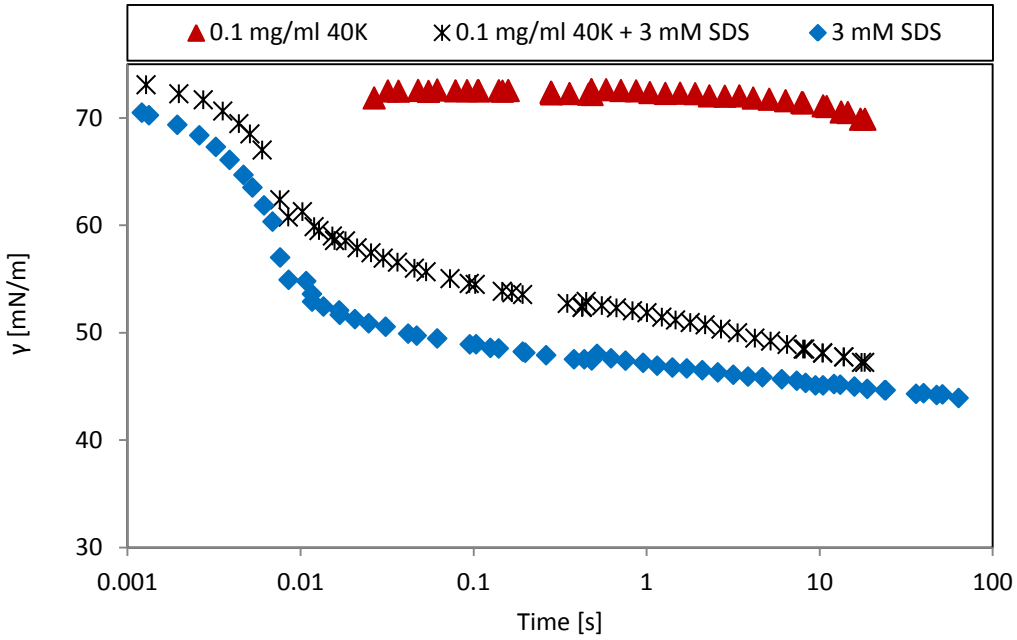

Fig. 5.2.5. Dynamic surface tension for 0.1 mg/ml 40K + 3 mM SDS.

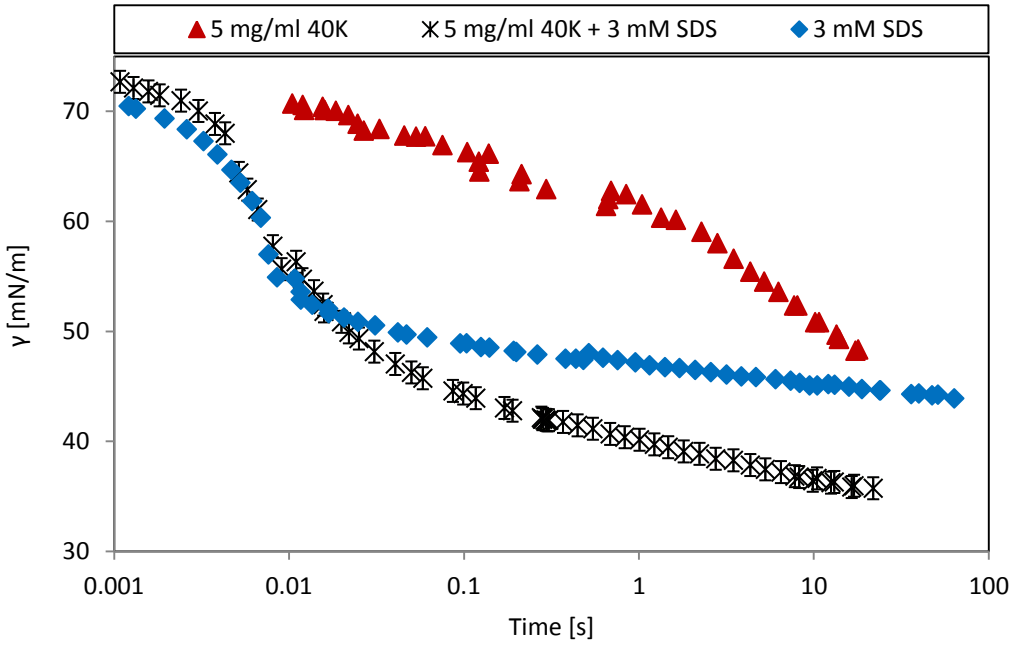

Fig. 5.2.6. Dynamic surface tension for 5 mg/ml 40K + 3 mM SDS.

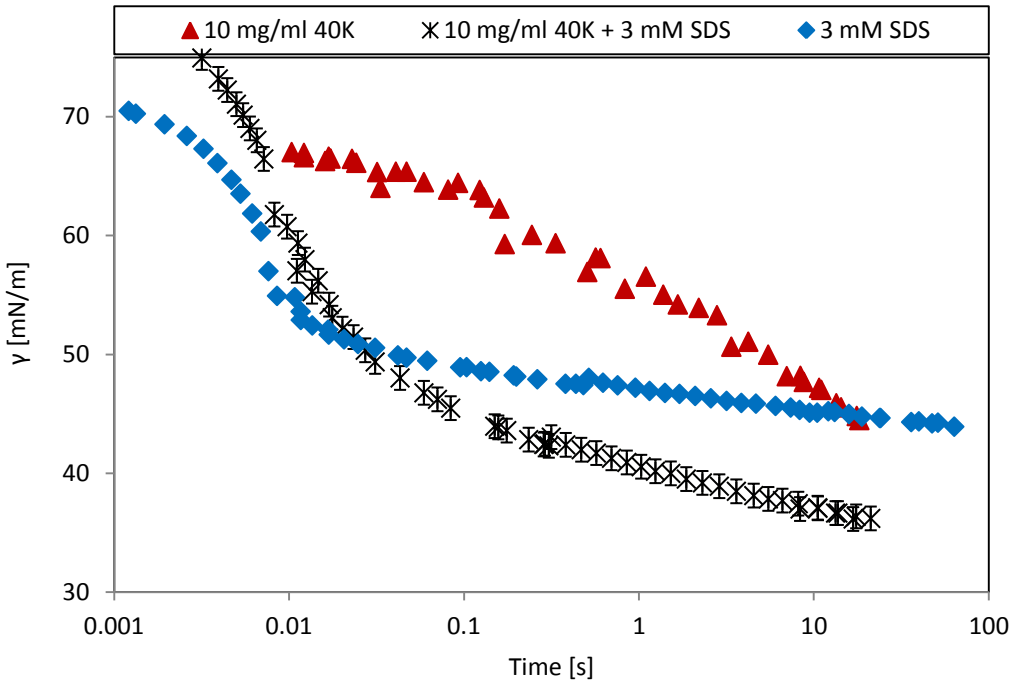

Fig. 5.2.7. Dynamic surface tension for 10 mg/ml 40 + 3 mM SDS.

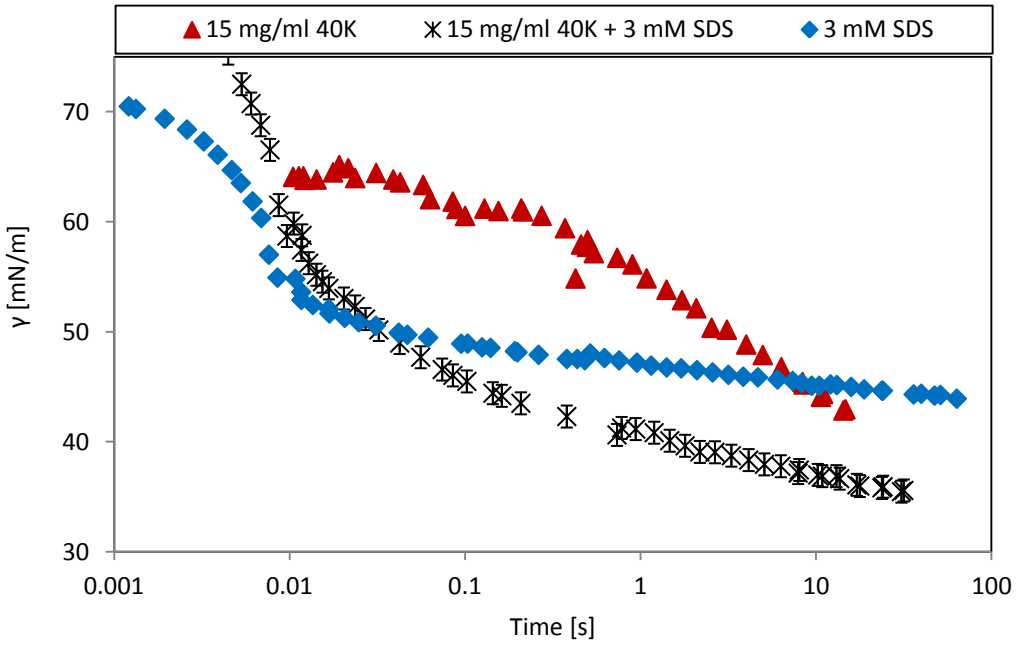

Fig. 5.2.8. Dynamic surface tension for 15 mg/ml 40K + 3 mM SDS.

At 9 mM SDS (Figures 5.2.9 to 5.2.12) and below 0.01 s, the mixed curves behave like the surfactant for 0.1, 5 and 10 mg/ml of polypeptide. In fact, with 0.1 mg/ml, the mixed curve is almost identical in the entire range up to 100 s.

Comparing the mixtures with 5, 10 and 15 mg/ml of the 40 KDa polypeptide, the curve shapes are very similar and the surface tension seems to decrease more with lower polypeptide concentrations at shorter times in contrast with polypeptide curves which decrease with higher concentration. This reflects the effect that the surfactant and the polypeptide have on these mixtures. Even though the polypeptide surface tension decays faster with increasing concentration, the otherwise low surfactant surface tension curves tend to delay the decay when mixed with polypeptide and show higher values of surface tension with increasing polypeptide concentration. Nevertheless, all three curves converge immediately after 20 s towards $\gamma \approx 32$ mN/m, i.e., equilibrium has not yet been reached.

Alahverdjieva et al. [14] studied the dynamic surface adsorption of SDS mixtures with lysozyme and attempted to model it. In their paper, the surface tension decay of SDS in phosphate buffer is described through a Langmuir isotherm and the results are used to describe the dynamic behaviour of the mixtures with lysozyme. It is now well established that mixing SDS with lysozyme results in complex formation and an equilibrium surface tension curve of type 'S' as described in the theory section [2, 14].
That is, at a fixed protein concentration γ decays with increasing surfactant concentration until the charges in the biopolymer are saturated. A further increase of surfactant in the bulk solution leads to more hydrophilic complexes that are more soluble thus depleting the interface from this material and increasing surface tension values. With even more surfactant added to the solution, the equilibrium adsorption curve tends towards the CMC of the surfactant where the surface is dominated by surfactant aggregates. Hence, Alahverdjieva et al. [14] observed the dynamic behaviour of the mixture and offered an explanation in relation to equilibrium surface adsorption based in the competitive nature of the protein/SDS system. They concluded that the switch in the overall shape of surface tension decay from a concave to a convex form is related to a transition from a diffusion-only surface adsorption mechanism to a mixed kinetic-diffusion controlled model dependent upon protein concentration. This

switching point, at a SDS concentration of 0.01 mM for a fixed lysozyme concentration of 0.01 mg/ml, coincides with concentrations at the start of region A in Figure 2.1.3.1.

In the present system, the switching point described for the lysozyme/SDS mixture occurs at concentrations between 0.1 and 3 mM of SDS (for all but the lowest polypeptide concentration), which in relation to the equilibrium surface adsorption is found somewhere in region A and not before as described in the lysozyme/SDS system. Since at 0.1 mM SDS the equilibrium surface tension of the 40 KDa polypeptide mixed with SDS is within region A where the polypeptide/surfactant monomer complexes are being formed, and the transition in adsorption mechanisms has not yet occurred (no change in the shape of the dynamic curve is observed), it is possible to argue that complexes of polypeptide and surfactant monomers are being formed in the diffusion-only region facilitated by electrostatic interactions. A consequence to this follows.

Bell et al. [9] assume that in region A (or up to S1), the cooperative interaction is a single step model although they admit that this is an oversimplification as demonstrated by the failure of their model at low surfactant concentrations. The change of the dynamic surface adsorption curve from concave to convex, and thus the transition from diffusion-only to mixed kinetic-diffusion adsorption mechanism, is consistent with the idea that at low concentrations one single step is not enough to describe the interactions in play. Indeed, an activation barrier related to protein desorption comes into play. As explained above, in the time scale investigated here this barrier appears between 0.1 mM and 3 mM of SDS, thus by looking into Figure 5.1.1 we may associate this event with the creation of a sublayer of surfactant aggregates adjacent to the polymer/monomer complexes adsorbed at the interface, i.e. S1 to S2 (the plateau region). The lack of intermediate experimental results in this region for the 40K/SDS system only allow us to speculate that the change in behaviour at S1 in equilibrium is related to the dynamic adsorption mechanism transition point.

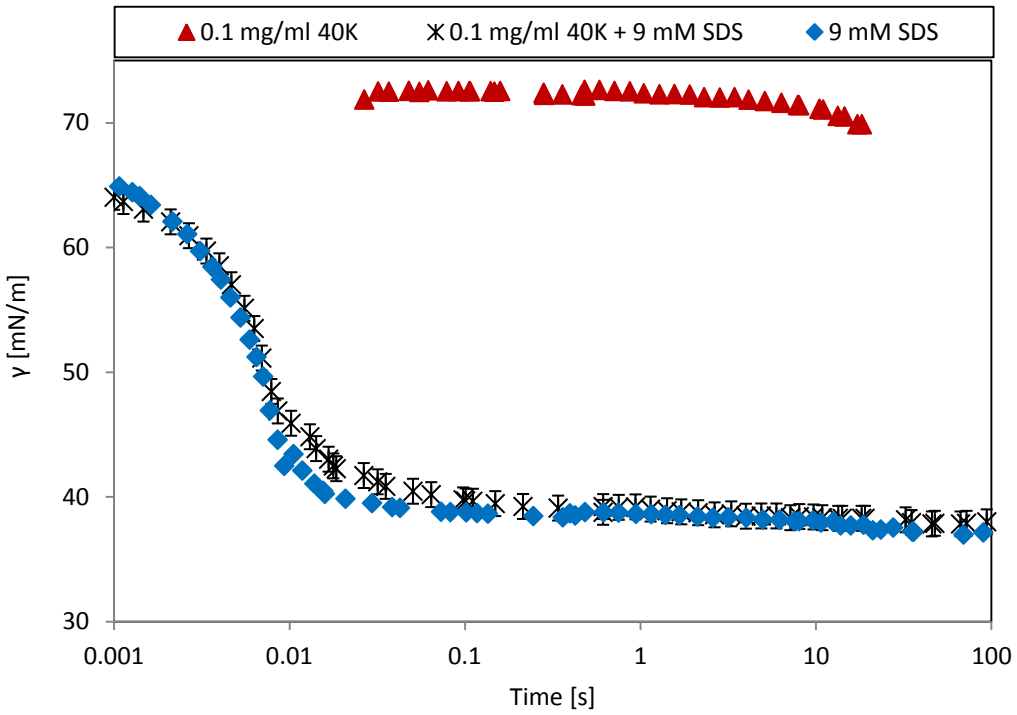

Fig. 5.2.9. Dynamic surface tension for 0.1 mg/ml 40K + 9 mM SDS.

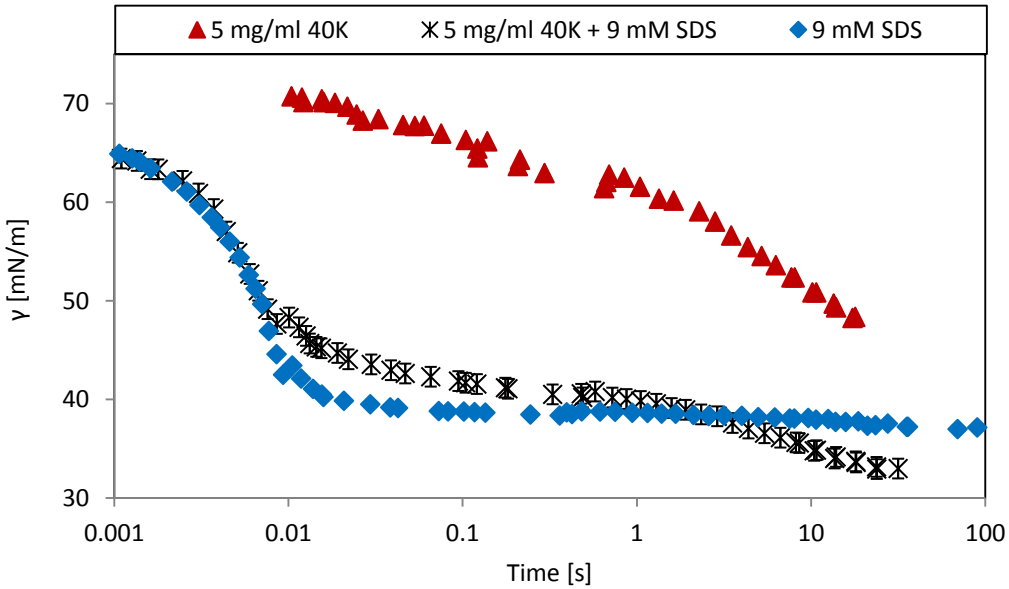

Fig. 5.2.10. Dynamic surface tension for 5 mg/ml 40K + 9 mM SDS.

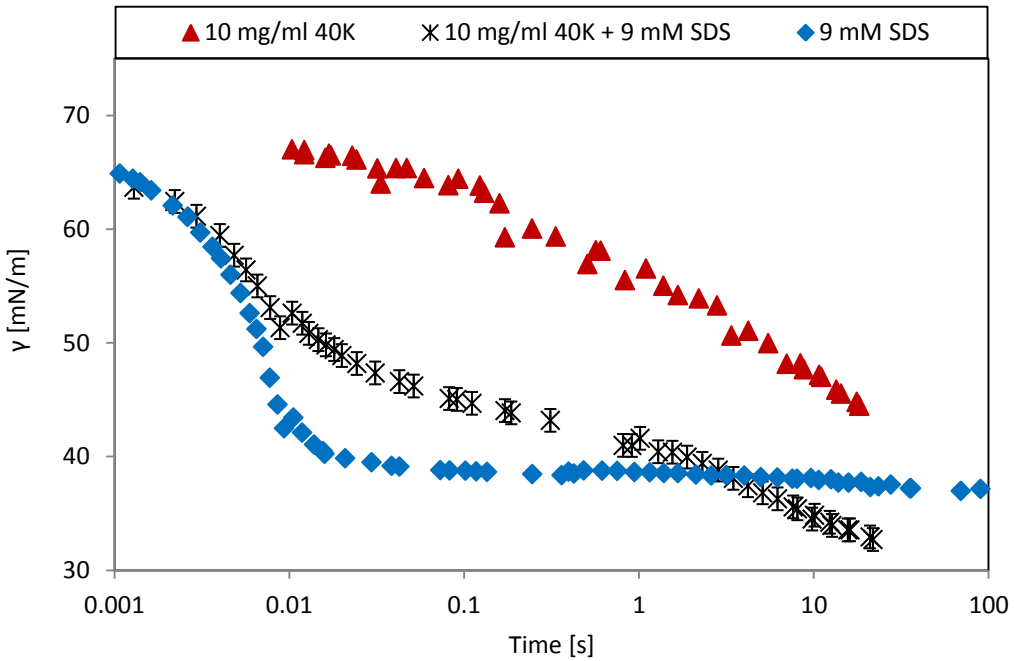

Fig. 5.2.11. Dynamic surface tension for 10 mg/ml 40K + 9 mM SDS.

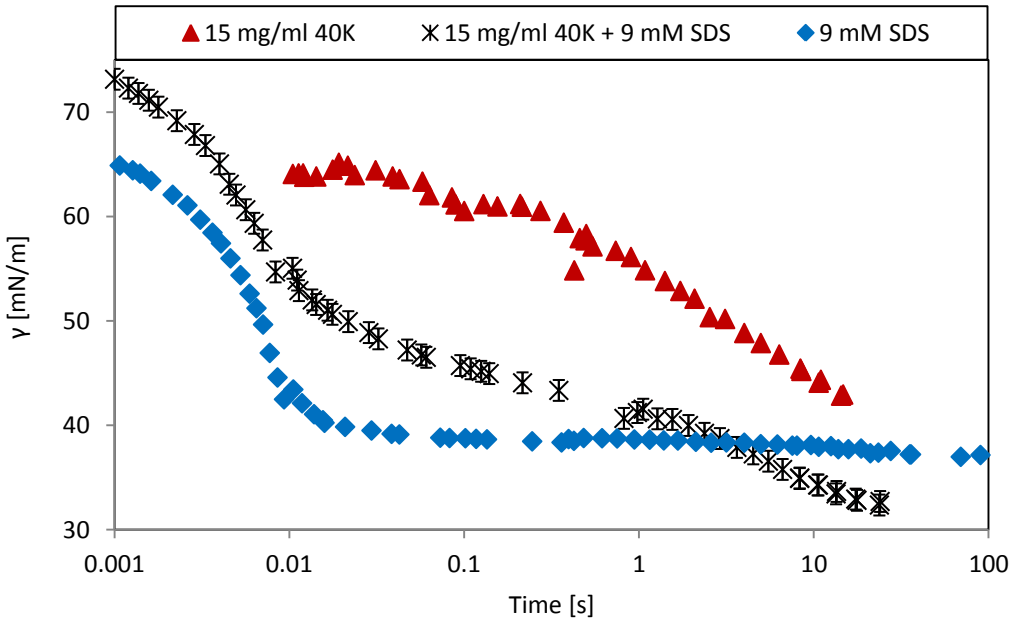

Fig. 5.2.12. Dynamic surface tension for 15 mg/ml 40K + 9 mM SDS.

The adsorption process can be explained at low SDS concentrations with the orogenic model [15]. At low SDS and low polypeptide concentrations, i.e. 0.1 mM SDS an 0.1 mg/ml of 40 KDa polypeptide, both individual components remain at high surface tension values close to that of pure water during the first 10 s of the adsorption process. After this time, the polypeptide rate of adsorption increases whereas the surface tension of SDS remains at high levels. Thus, the polypeptide occupies the interface preferentially in the short time range.

At low SDS concentrations and high polypeptide concentrations, the results of dynamic surface adsorption experiments show how the polypeptide adsorbs at the interface in the short time range while the SDS remains at pure-water level.
In the mixtures with low amounts of SDS, the polypeptide adsorbs first at the interface and the surfactant adsorbs into the protein network at defect sites.
The initial hole created is neutralizing the local charges. Hence, if another surfactant monomer arrives at the site, it is likely to interact at first via association of the hydrocarbon tails. This is also supported by Noskov et al. [16].
The surfactant head thus remains exposed in the solution forming the surfactant sublayer. This leads to the formation of hydrophobic dominated areas (surfactant tails close to hydrophobic sections of the polymer) surrounded by surfactant heads which could offer an explanation to the two dimensional surfactant coated polymer complexes encountered by Noskov et al. [16] at the interface.

At high SDS concentrations and low polypeptide concentration, the surfactant dominates the interface in the short time range and adsorption shows signs of a further increase when the polypeptide starts acting following its individual induction period. At this point, the rate of decay of the surfactant is already slowing down reaching close to equilibrium values, and the end of the polypeptide induction period coincides with values of surface tension for the mixture, which is now decaying in a faster manner, close to those of surfactant only.

At high SDS concentrations and high polypeptide concentration, the rapid surfactant adsorption at short times is quickly counteracted by the polypeptide surpassing the low SDS surface tension values after 10 seconds, or showing signs that this will occur soon after 10 s.

At high SDS, the surfactant arrives to the interface first at every polypeptide concentration but its rate of adsorption is slowed down due to the presence of polypeptide.

Figures 5.2.13 to 5.2.16 show the concentration dependence of the mixed curves at different times. From highest to lowest polypeptide concentration, we observe an almost identical behaviour with mixed solutions of SDS and 10 and 15 mg/ml of 40 KDa polypeptide at all times. With 5 mg/ml, the curve is similar to the ones just described although at 0.1 mM of SDS, the surface tension is slightly higher and at 9 mM, slightly lower except at times $\geq$ 10 s when it converges to the same values as the other two curves. This delay is only due to a lower amount of polypeptide present in solution and a higher and faster surfactant adsorption at the interface with high amounts of surfactant in solution.

Equilibrium surface tension shows no significant differences between these three curves. Hence, the mixtures with 5, 10 and 15 mg/ml continue decaying in a similar fashion until reaching equilibrium values, i.e. approximately 4 mN/m lower than those attained at 10 s.

The curves for SDS and SDS mixed with 0.1 mg/ml of 40 KDa polypeptide share the same starting point at all times and converge towards similar values at high surfactant concentration demonstrating the dominance of the surfactant at the interface. However, at 3 mM of SDS, i.e. close to the CMC of the surfactant, the mixture reaches higher surface tension values than the surfactant alone highlighting the occurrence of the synergism mechanism at short times, i.e. lower rate of decay leading to a lower interfacial adsorption but still lowering the surface tension greatly. These conditions are necessary to create stable foams.

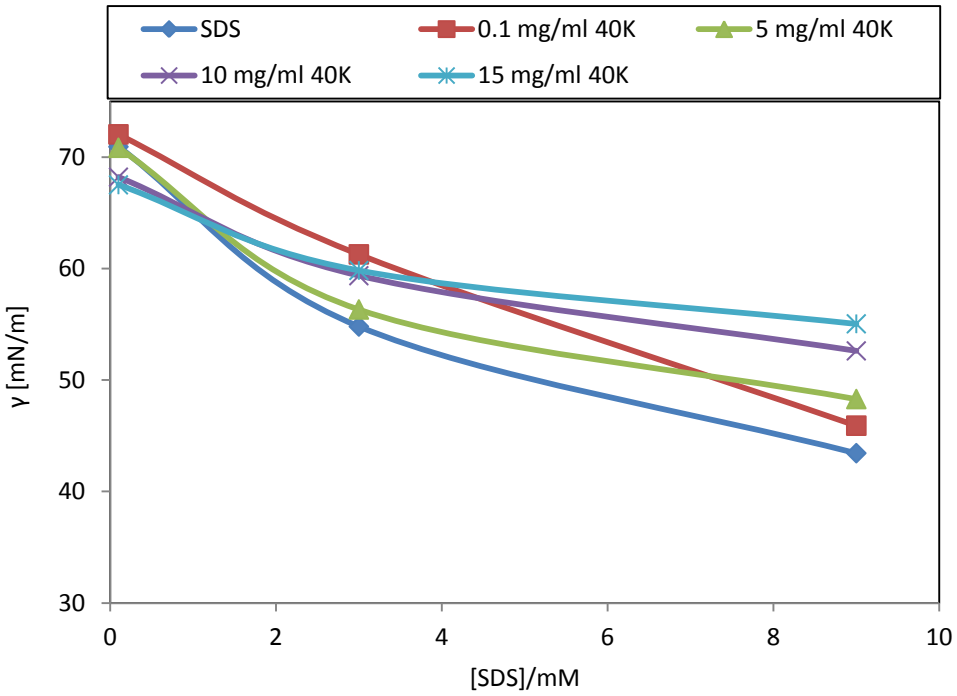

Fig. 5.2.13. Dynamic surface tension for the 40K/SDS system at 0.01 s.

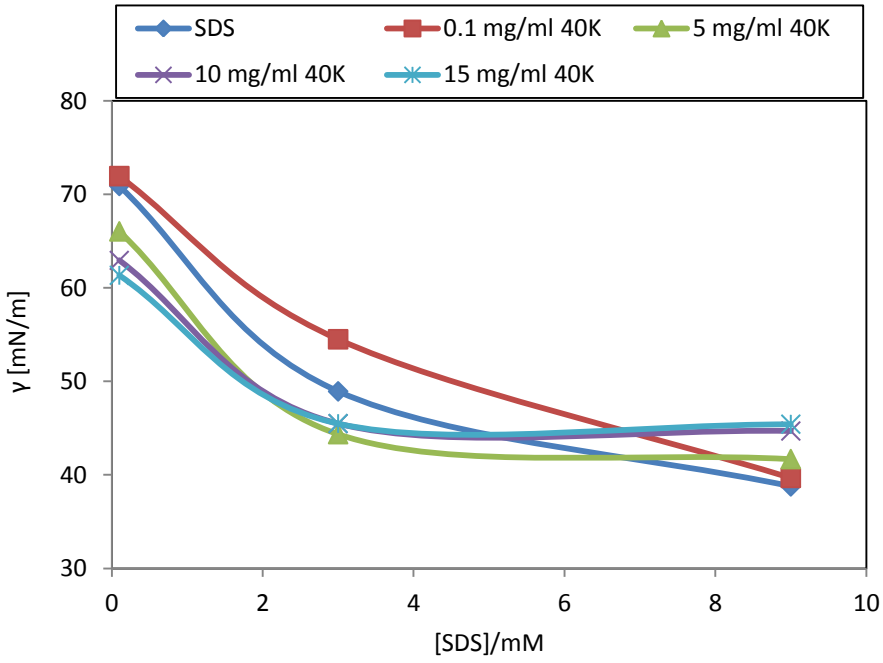

Fig. 5.2.14. Dynamic surface tension for the 40K/SDS system at 0.1 s.

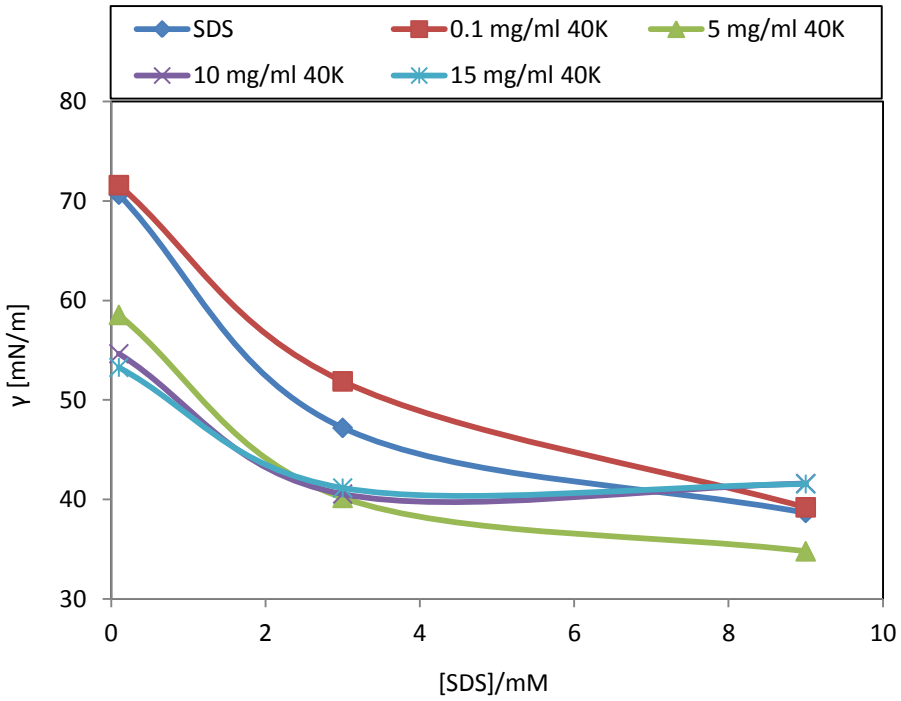

Fig. 5.2.15. Dynamic surface tension for the 40K/SDS system at 1 s.

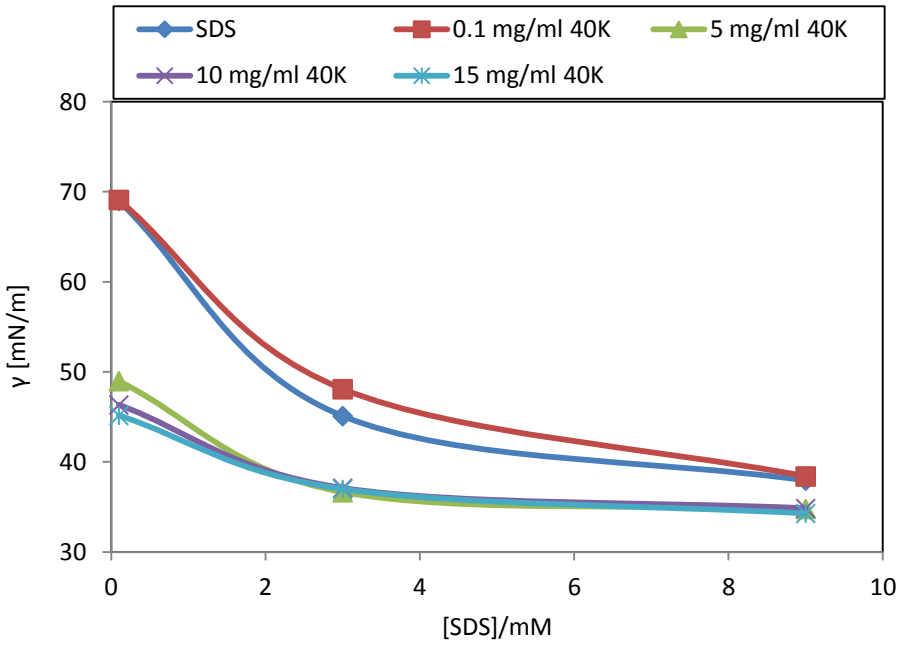

Fig. 5.2.16. Dynamic surface tension for the 40K/SDS system at 10 s.

5.3. ζ-potential

The ζ-potential of mixtures of polypeptide and SDS were investigated at different SDS concentrations (0.6 and 3 mM) and different polypeptide concentrations (0.5, 1 and 2 mg/ml). The results can be seen in Figures 5.3.2 to 5.3.5. Mixtures with 9 mM were also examined. However, the signal was too noisy to be investigated appropriately and although damping of the noise was attempted by adding electrolyte to the solutions, no reliable measurements were obtained. Nonetheless, in Figure 5.3.1 it is possible to visually observe colloidal aggregation with 2 mg/ml of 40 KDa polypeptide and 9 mM SDS at pHs 2.2 and 3. The resultant non-transparent solution indicates that the ζ-potential for these samples falls in the unstable region. In Chapter 4, it was mentioned that the colloidal aggregation of polypeptide solutions is visually observable below pH 5 from the polypeptide alone.

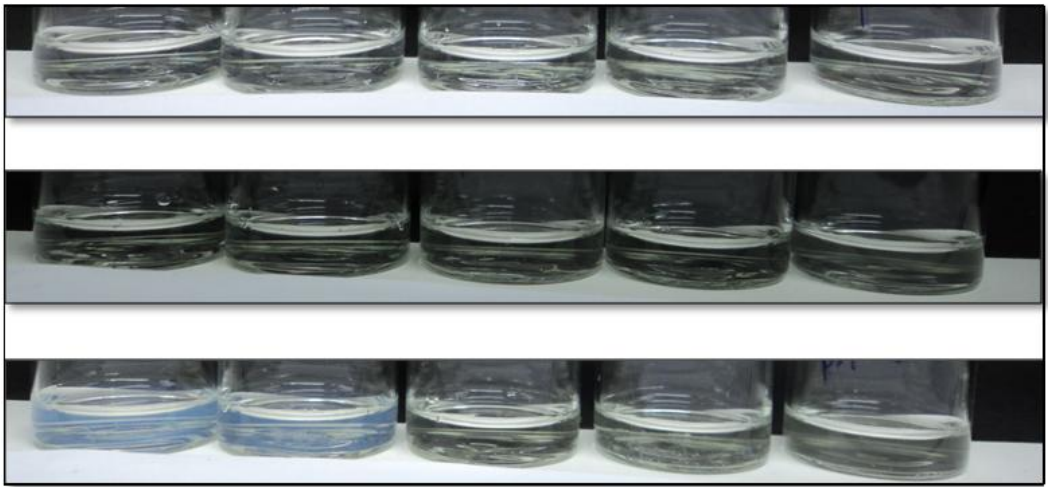

Fig. 5.3.1. Mixed solutions of 9 mM SDS with (top) 0.5 mg/ml of 40 KDa polypeptide, (middle) 1 mg/ml of 40 KDa polypeptide and (bottom) 2 mg/ml of 40 KDa polypeptide, at pH (from left to right) 2.2, 3, 5, 7 and 7.8, respectively. Colloidal aggregates can be visually observed at pH 2.2 and 3 with 2 mg/ml of 40 KDa polypeptide added to the solution.

At 9 mM of SDS, the equilibrium adsorption curves of the mixtures show the dominance of the SDS at the interface through free SDS micelles. Therefore, almost all the polypeptide has been resolubilized and is now present in the bulk solution as

demonstrated by the phase separation observed in Figure 5.3.1 at 2 mg/ml of 40 KDa polypeptide. At lower polypeptide concentrations, this visual effect does not appear in the presence of 0.6 or 3 or 9 mM of SDS.

For all the three tested concentrations of polypeptide, the addition of SDS resulted in lower ζ-potential values at pH 2.2 and pH 3. At pH 5 this effect was considerably reduced and at pHs above 5, SDS addition resulted in a pH-independent plateau with negligible differences for different amounts of polypeptide. This was also observed in mixtures of soy protein isolate and SDS [17]. In the latter case, it was suggested that the polymer reaches a critical level of charge beyond which no further surfactant can bind.

For pH 2.2 and pH 3, the effect of adding 0.6 mM SDS was more pronounced at lower polypeptide concentrations where the ζ-potential went from positive to negative values and the neutrality point was not found within the pH 2-pH 7.8 range. Thus, an increase in polypeptide buries some of the SDS charges indicating that the surfactant is effectively being coated by the polypeptide. Close to the CMC of the surfactant, i.e. at 3 mM, neutrality is not observed even with polypeptide concentrations above the CAC. Thus, albeit the encapsulation of the surfactant by the polypeptide, the particles remain negatively charged.

Addition of SDS to the polypeptide at different concentrations below the surfactant's CMC does not seem to alter the resultant ζ-potential of the mixture close to the isoelectric point of the polypeptide significantly, i.e. at pH 5, (see Figure 5.3.4). The absolute values remain outside the instability region. This was also the case for mixtures of SDS and soy protein isolates [17]. The polypeptide without surfactant is negatively charged at pHs above 5 and the addition of SDS negative charges only increases the absolute charge slightly. The greater effect is observed when the polypeptide was initially in the positively charged region.

According to Campbell et al. [11], the cliff edge peak observed in various surface tension profiles of mixed polymer/surfactant solutions is due to the precipitation of material in the bulk at the concentrations were the peak is observed, i.e. there is aggregate formation in the bulk.

As explained earlier, the model proposed by Bell et al. [9] also applies to the 40K/SDS system where no cliff edge peak is observed. This was attributed to the higher stability difference between polymer/monomer and polymer/micelle complexes. The SDS concentrations tested via ζ-potential, i.e. 0.6 and 3 mM, fall in the polymer/monomer and polymer/micelle regions, respectively. The equilibrium surface tension was performed at pH 5, where both surfactant concentrations have proved to produce stable colloidal solutions at different polypeptide concentrations as indicated by the ζ-potential results (fig. 5.3.5) and the lack of appreciable phase separation. Thus, the conclusions reached by Campbell et al. do not seem to fit the present case.

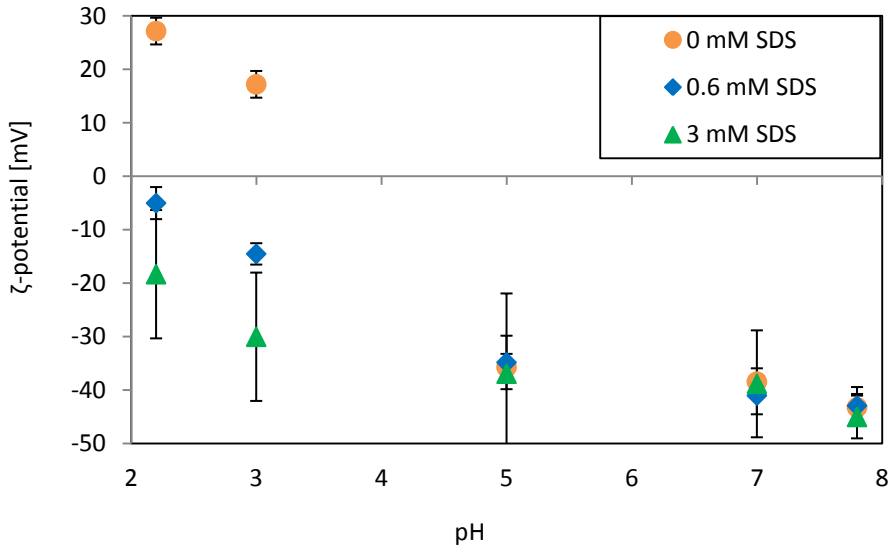

Fig. 5.3.2. ζ-potential for mixtures of 0.5 mg/ml of the 40 KDa polypeptide and SDS.

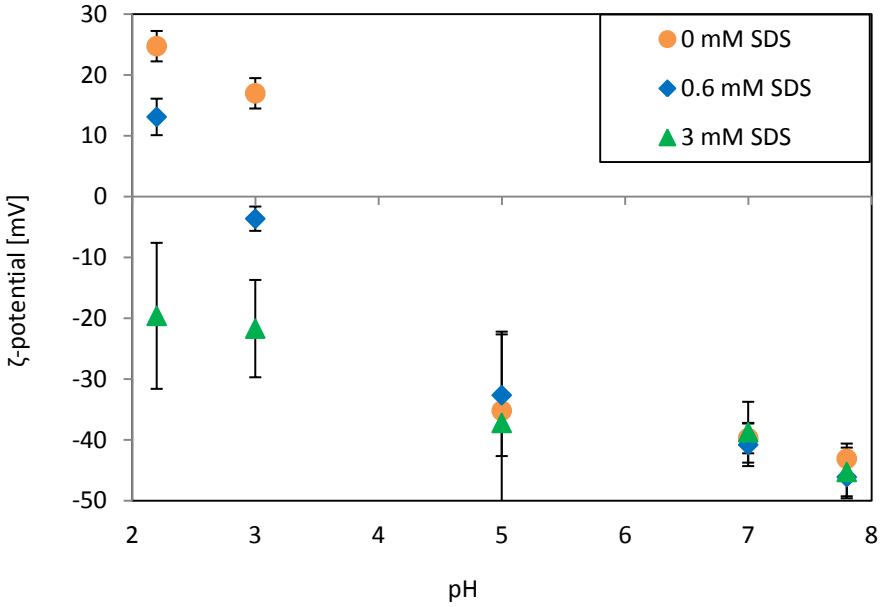

Fig. 5.3.3. ζ-potential for mixtures of 1 mg/ml of the 40 KDa polypeptide and SDS.

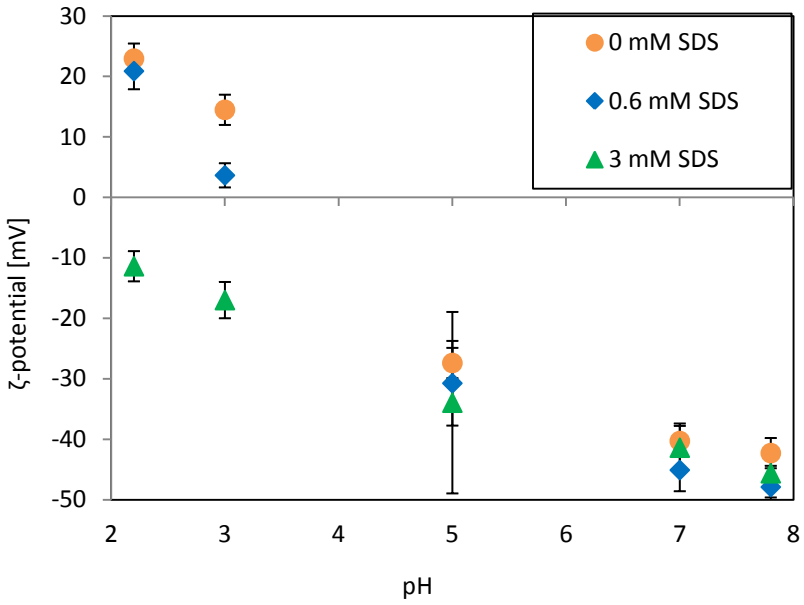

Fig. 5.3.4. ζ-potential for mixtures of 2 mg/ml of the 40 KDa polypeptide and SDS.

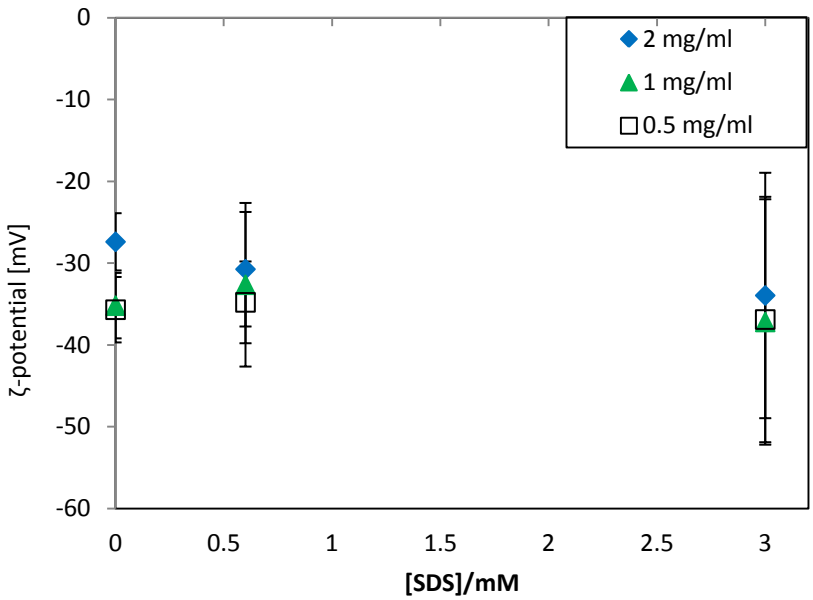

Fig. 5.3.5. ζ-potential for the 40 KDa polypeptide as a function of SDS concentration at pH 5.

5.4. Foam studies

Foams produced by the surfactant and its mixed solutions with 1 and 0.1 mg/ml of the 40 KDa polypeptide were studied at several SDS concentrations. Some pictures of these foams are presented in Figures 5.4.1 to 5.4.3.

Figure 5.4.1 shows how SDS concentrations below 0.1 mM produce almost no foam. For concentrations of 0.1 and 1 mM, SDS does produce high volumes of foam that are however, reduced at great rates after just 15 minutes from production.

In contrast, when adding 1 mg/ml of 40 KDa polypeptide to the solution (Figures 5.4.2 to 5.4.4), SDS concentrations 0.001 and 0.01 mM also produce high volumes of foam.

The mixtures with 0.001 to 0.1 mM of SDS do produce initially higher volumes of foam than in the absence of polypeptide. At 1 mM, this effect is not so noticeable initially. The foams produced by the mixtures are still present after 5 minutes but in the case of SDS concentrations lower than 0.1 mM, they are greatly reduced. For 0.1 and 1 mM, the foams remain stable after 5-15 minutes. These results prove that synergistic association of polypeptide and SDS takes place at SDS concentrations below the CMC.

The increased ability to foam and stability are due to the increased viscoelasticity of the foam matrix as Bykov et al. [4] found in the PEI/SDS system, and also to the ability to withstand collapse through an improved transport of material through the foam films when compared to the polypeptide-only foams. This proposition is supported to some extent by the more rapid adsorption observed with mixtures at the low polypeptide concentration.

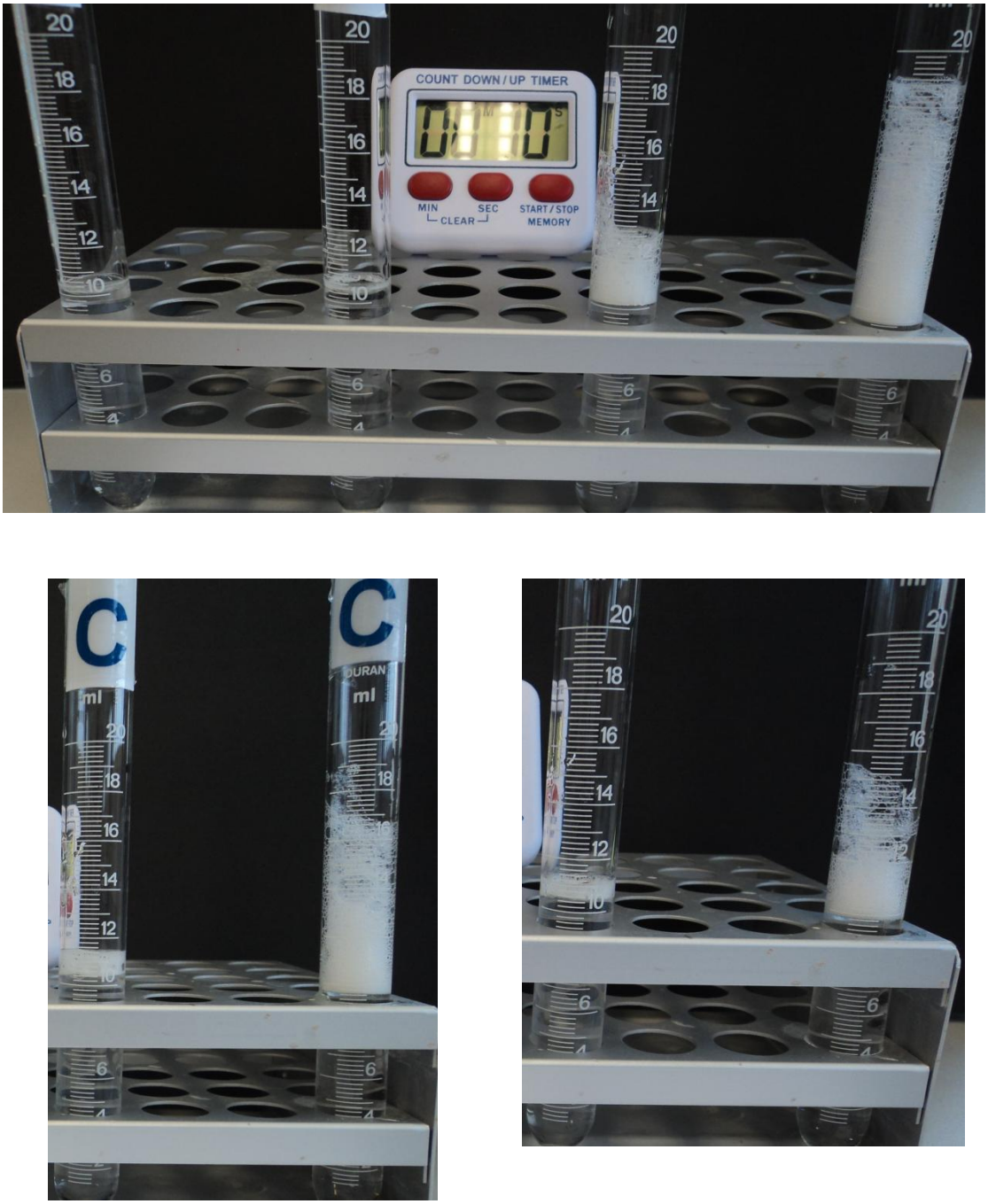

Fig. 5.4.1. Top: (left to right) 0.001, 0.01, 0.1, 1 mM SDS at 10 seconds after shaking.
Bottom left: (left to right) 0.1, 1 mM SDS after 5 minutes.
Bottom right: (left to right) 0.1, 1 mM SDS after 15 minutes.

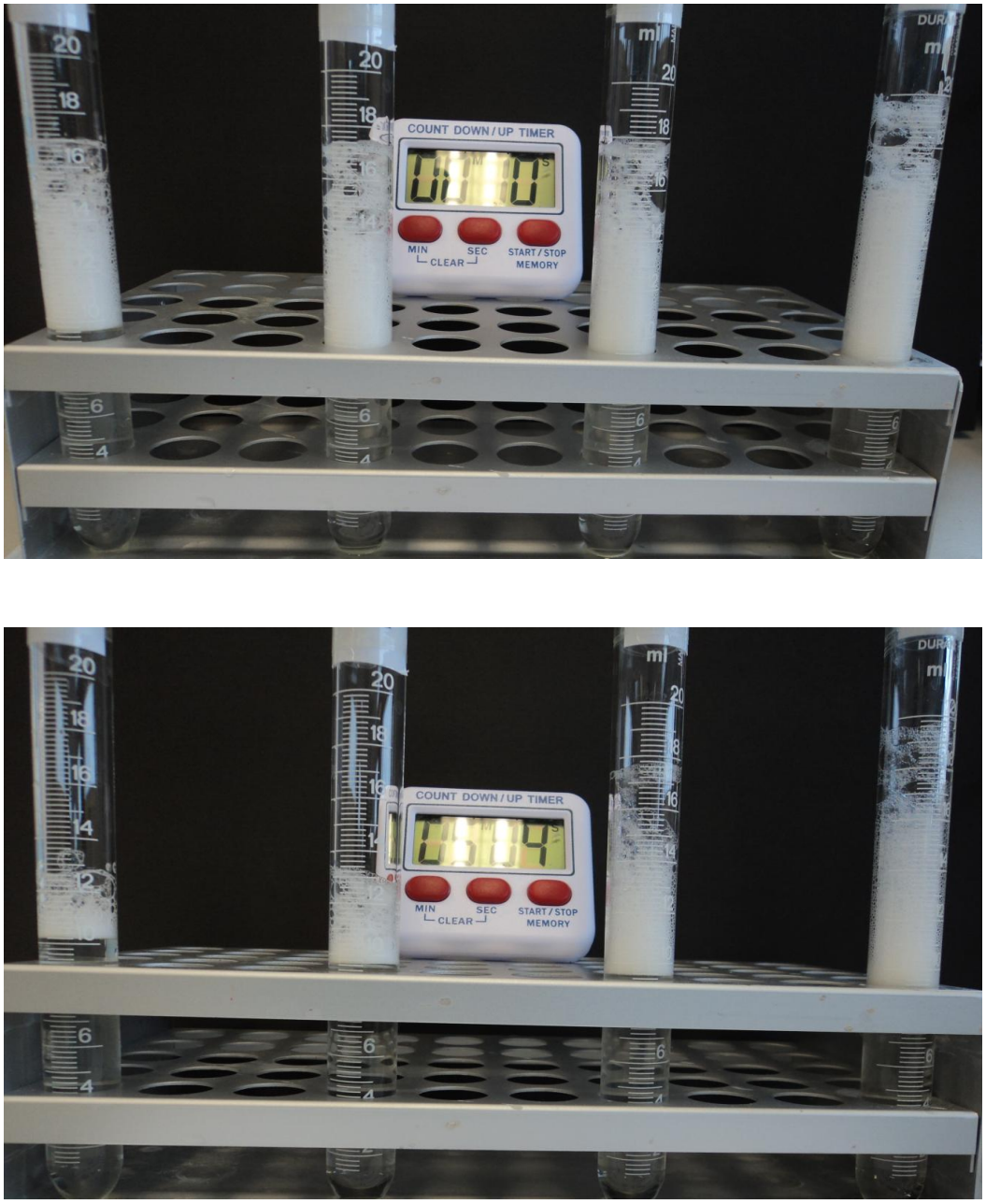

Fig 5.4.2. Top: 1 mg/ml 40K + (left to right) 0.001, 0.01, 0.1, 1 mM SDS at 10 seconds after shaking. Bottom: same samples after 5 minutes.

Fig 5.4.3. Top: 0.1 mg/ml 40K + (left to right) 0.1, 0.01, 0.001 mM SDS at 10 seconds after shaking. Middle: same samples after 5 minutes. Bottom left: 0.1 mg/ml 40K + 1 mM SDS at 10 seconds after shaking. Bottom right: 0.1 mg/ml 40K + 1 mM SDS after 5 minutes.

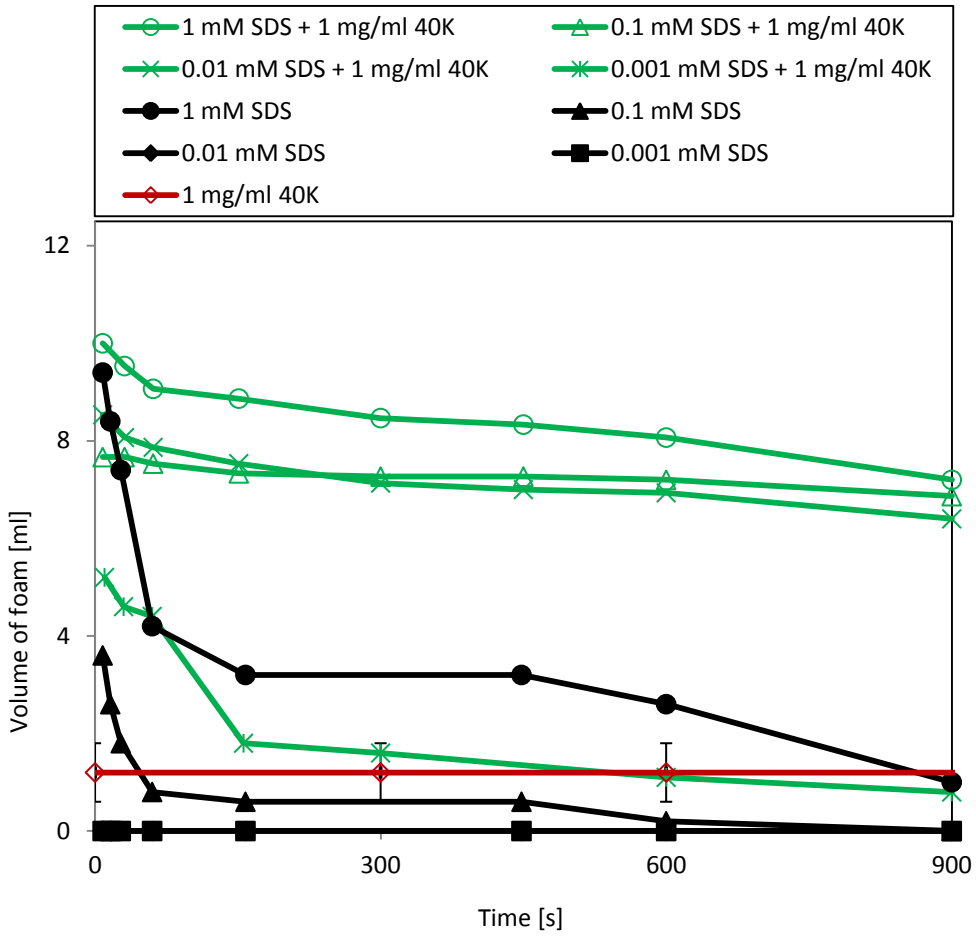

Fig. 5.4.4. Stability of foams resulting from mixed 40K/SDS solutions.

When the concentration of SDS is increased to near-CMC levels or above (see Figures 5.4.5 and 5.4.6), the foams produced initially are slightly higher than in the absence of polypeptide. Nevertheless, at these high SDS concentrations the volumes of the foams are similar to those of the surfactant even after 15 minutes. This can be interpreted as the surfactant causing the rupture of the protein network thus dominating the adsorption processes in the foam matrix.

Finally, if the polypeptide concentration is reduced to 0.1 mg/ml instead (see Figure 5.4.3), the volume of foam produced by the mixture with 0.01 mM SDS improves with respect to the results obtained with the surfactant. However, the volume of foam produced with polypeptide is still higher than that of the mixture (Figure 5.4.7). When the polypeptide is mixed with 0.1 and 1 mM (Figures 5.4.8 and 5.4.9), the foams improve vastly with respect to both of the individual components.

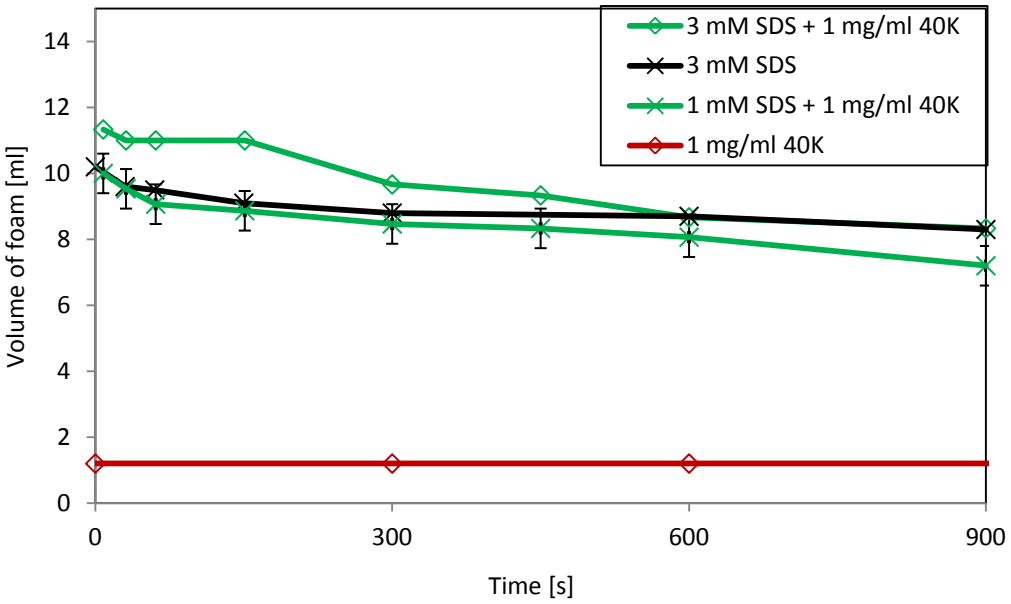

Fig. 5.4.5. Stability of foam produced by 3 mM of SDS mixed with 1 mg/ml of polypeptide.

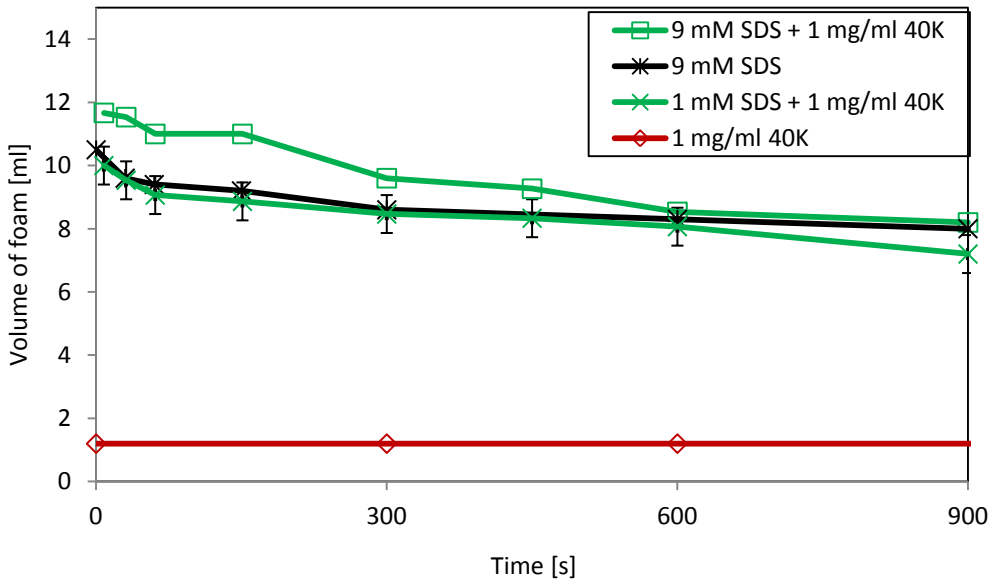

Fig. 5.4.6. Stability of foam produced by 9 mM of SDS mixed with 1 mg/ml of polypeptide.

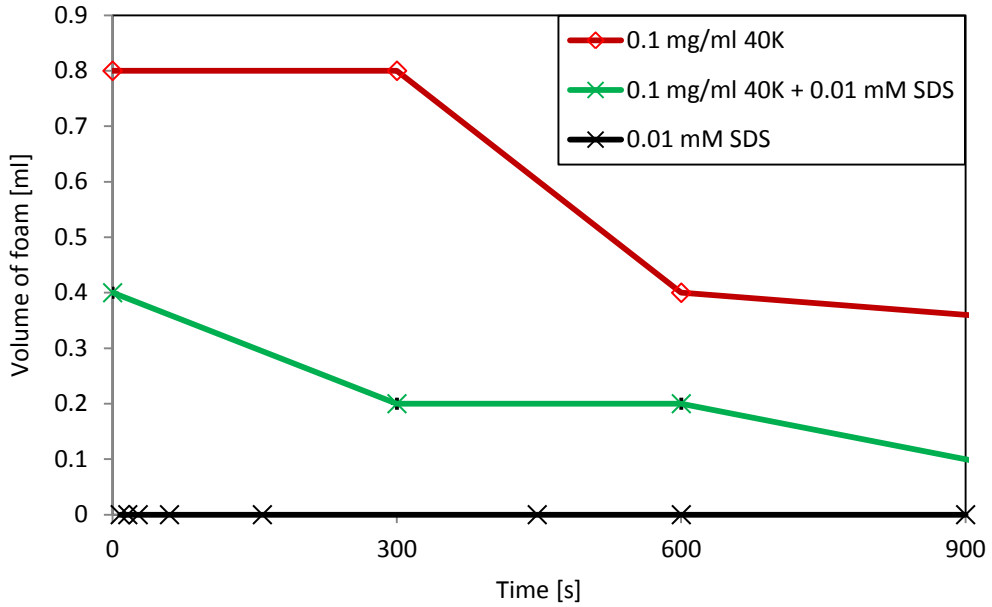

Fig. 5.4.7. Stability of foam produced by 0.01 mM of SDS mixed with 0.1 mg/ml of polypeptide. All data shown are within the error range of the mixed solution.

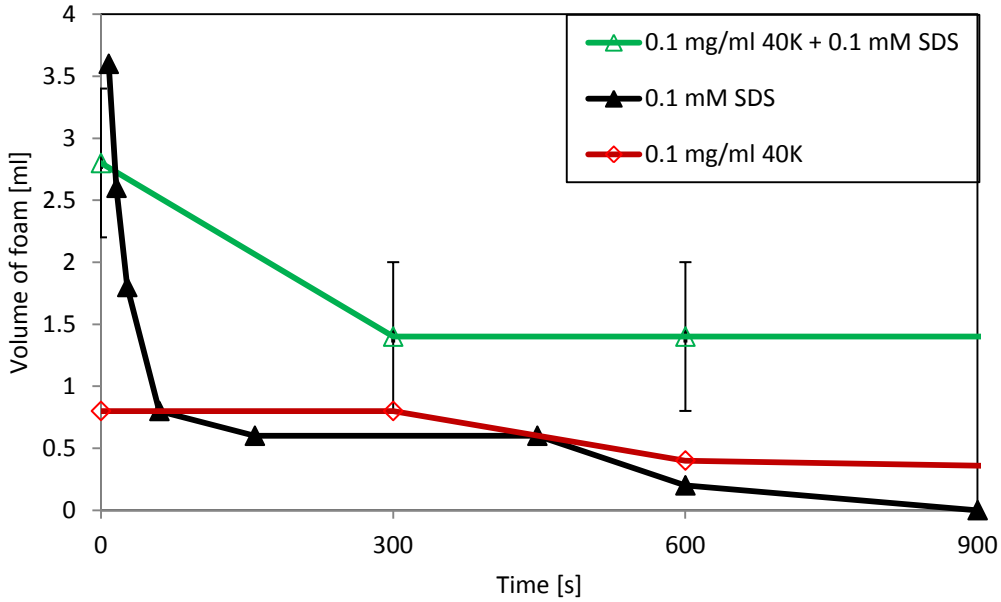

Fig. 5.4.8. Stability of foam produced by 0.1 mM of SDS mixed with 0.1 mg/ml of polypeptide.

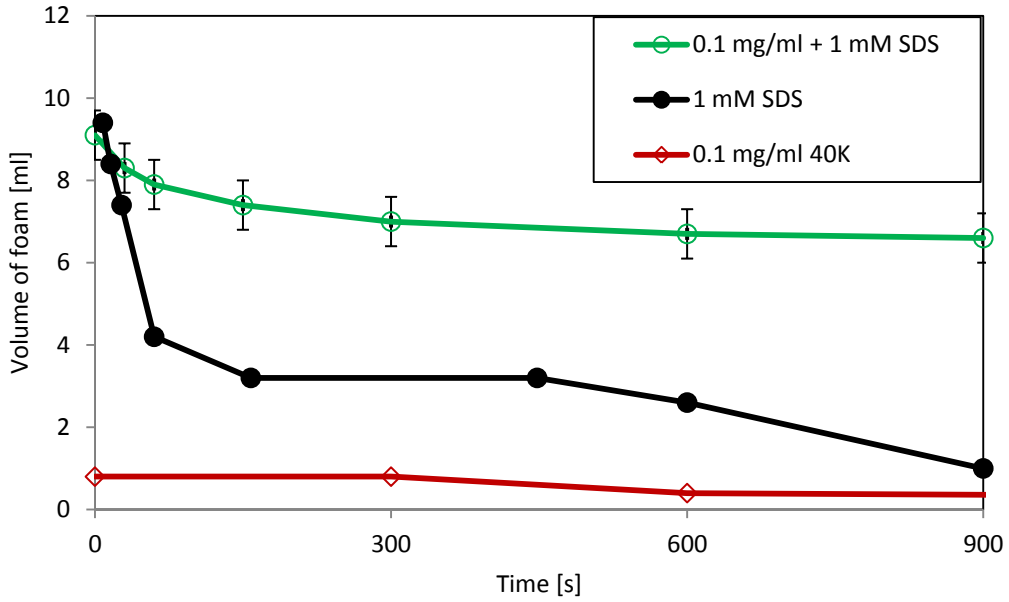

Fig. 5.4.9. Stability of foam produced by 1 mM of SDS mixed with 0.1 mg/ml of polypeptide.

Figures 5.4.10 and 5.4.11 clearly demonstrate the synergistic behaviour of the mixtures of 0.1 or 1 mg/ml of 40 KDa polypeptide with SDS concentrations below the CMC. From these Figures, it is possible to see that not only higher volumes of foam are produced at SDS concentrations below the CMC but also they remain stable after 15 minutes, when the SDS foams have disappeared or are about to.

At SDS concentrations close to the CMC and beyond, this synergy is not so observable anymore and the SDS foams remain stable after 15 minutes whereas the foams of the mixtures have decayed with respect to the initial formation suggesting that although the interfaces are dominated by the surfactant, there is some polypeptide present in the matrix. Nevertheless, foams of mixed solutions at these SDS concentrations still remain at high volumes.

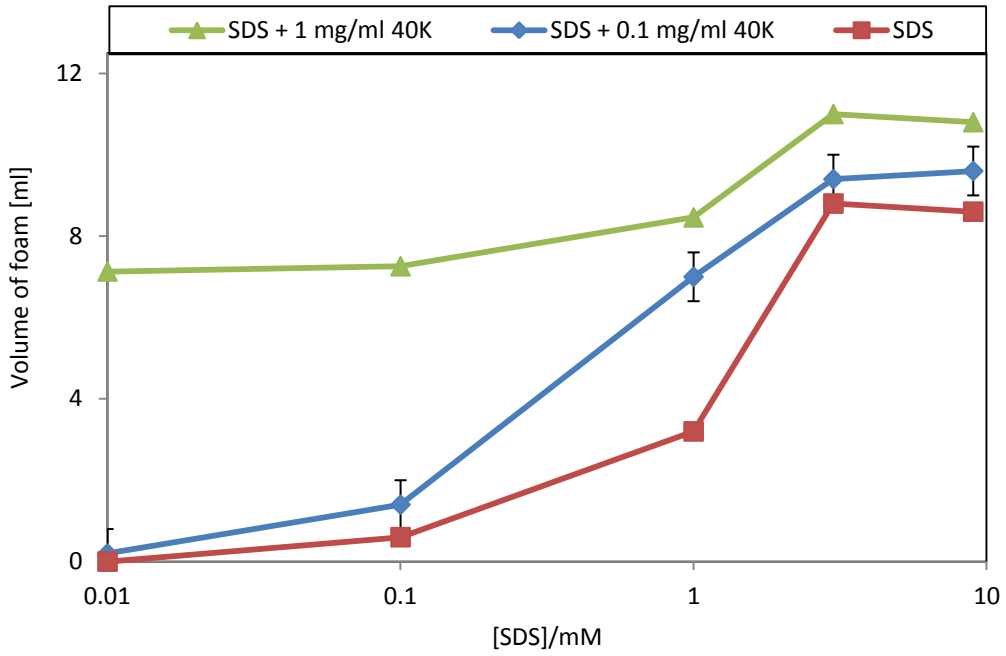

Fig. 5.4.10. Concentration dependence of foams as observed after 5 minutes.

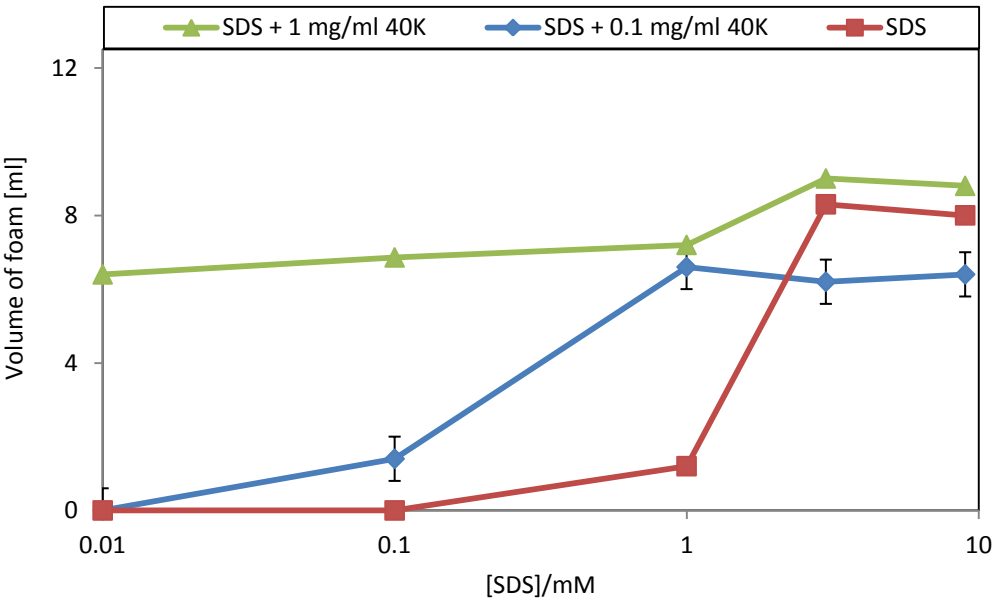

Fig. 5.4.11. Concentration dependence of foams as observed after 15 minutes.

5.5. Neutron reflection

As explained already in the study of the adsorption of the polypeptide alone, neutron reflection can be used to investigate the structure of the interfacial layer. Thus, a neutron reflection study was conducted using several concentrations of SDS and three concentrations of polypeptide. In all cases, two NRW contrasts were tested.

From Figures 5.5.1 to 5.5.7, it is clear that the idea of a single monolayer adsorbed at the interface is in agreement with the experimental data at SDS concentrations up to 4 mM mixed with 1 mg/ml of 40K in NRW, as judged by the visual overlap of both sets of data. The same reasoning can be applied to 0.1 mg/ml 40K at the SDS concentrations here presented (see Figures 5.5.9 to 5.5.12).

However, when we increase the peptide concentration to 2 mg/ml, twice its CAC, a different structure is observed (Figures 5.5.13 and 5.5.14). At 0.1 mM SDS, the adsorbed layer cannot be fitted to a single monolayer and a two layer structure needs to be modelled instead. This is in contrast to the branched PEI/SDS system which forms multilayers at low polymer concentrations. This effect is reflected in the appearance of a Bragg diffraction peak in the reflectivity profile [13].

No Bragg peaks were observed in any of the reflectivity profiles obtained with the 40 KDa polypeptide or the linear PEI/SDS system [7] which was also modelled to a monolayer at every SDS concentration studied.
The fitting parameters for a fixed polypeptide concentration of 1 mg/ml can be seen in Tables 5.5.1 to 5.5.4; for 0.1 mg/ml, in Tables 5.5.6 and 5.5.7; and for 2 mg/ml, in Table 5.5.8.

Three of the mixtures were analyzed in D_2O instead of NRW using h-SDS and d-SDS (Figures 5.6.15 to 5.5.20). This isotopic labelling technique aims, in conjunction with the results in NRW, to differentiate the structure of the adsorbed layer in air from that in solution.

Since the total thickness of the material adsorbed at the interface needs to remain constant for a given mixture, the structural parameters (total thickness, area per

molecules) calculated with the NRW data were kept constant within error when analysing the matching data in D_2O thus validating the model choice. From the D_2O data, it is also possible to calculate the scattering length density of the material adsorbed in the upper layer in air (assuming no water association) and in the lower layer in solution (assuming full space filling by water). To do so, the value of the volume fractions of the peptide and the surfactant calculated in NRW are used. Their constraint is that the total volume fraction of surfactant, peptide and water needs to be 1. Fitting parameters can be seen in Tables 5.5.11 to 5.5.13.

The mixtures studied in D_2O with 0.01 and 0.1 mM of SDS are fixed at 0.1 mg/ml of polypeptide. Both these concentrations fall in region A and thus they provide an insight into the structure of the polymer/monomer complexes.

The D_2O results for 0.1 mg/ml 40K + 0.01 mM SDS (Table 5.5.11) are in excellent agreement with the calculations derived from the NRW data. For the mixture of 0.1 mg/ml 40K + 0.1 mM SDS (Table 5.5.12), the results in the air layer also agree with the calculations. However, the layer in solution appears to have a higher scattering length density than calculated for both h-SDS and d-SDS. Hence, it is possible to conclude that the material encountered in the liquid phase is surrounded by water molecules, i.e. it is solvated.

For 1 mg/ml 40K mixed with 1 mM SDS (Table 5.5.13), the data obtained with d-SDS is also in agreement with the calculations. However, the scattering length density obtained experimentally for the air layer with h-SDS is lower than the calculations dictate by approximately $0.3 \cdot 10^{-6}$ $Å^{-2}$. The corresponding layer in D_2O fits a slightly larger value for the scattering length density but still close to the calculated value.

The origin in the discrepancies seen in these values is uncertain but the fact that the thicknesses remain constant and these values are not too distant from the calculated results highlights on the one hand, the repeatability of the measurements (same thicknesses obtained in NRW and D_2O with h- and d-SDS); and on the other hand, given that not one full set of data is in disagreement with the calculations, the assumption that complexes are being formed is still valid.

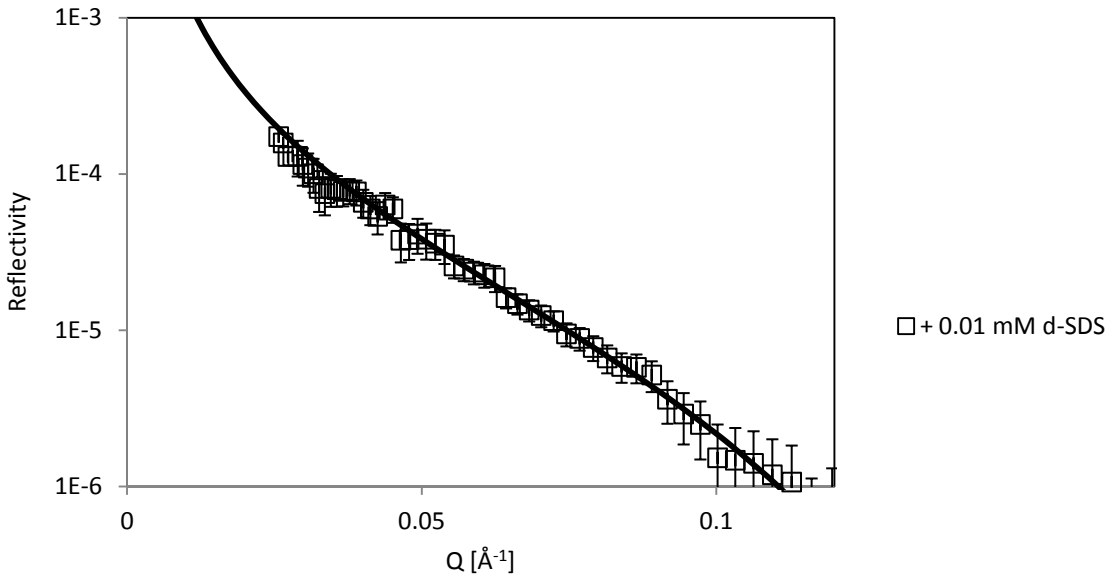

Fig. 5.5.1. Neutron reflection data for 1 mg/ml 40K + 0.01 mM d-SDS in NRW.

SDS/mM	τ/ Å	P_h/ x10^{-6} Å^{-2}	τ·P_h/ x10^{-6} Å^{-1}	P_d/ x10^{-6} Å^{-2}	τ·P_d/ x10^{-6} Å^{-1}
0.01	41	0.70	28.70	0.75	30.75

Table 5.5.1. Fitting parameters used for the 1-layer model of 1 mg/ml 40K + 0.01 mM SDS in NRW. The error in thickness is ± 3 Å and the error in scattering length density is ± 0.05 x10^{-6} Å^{-2}.

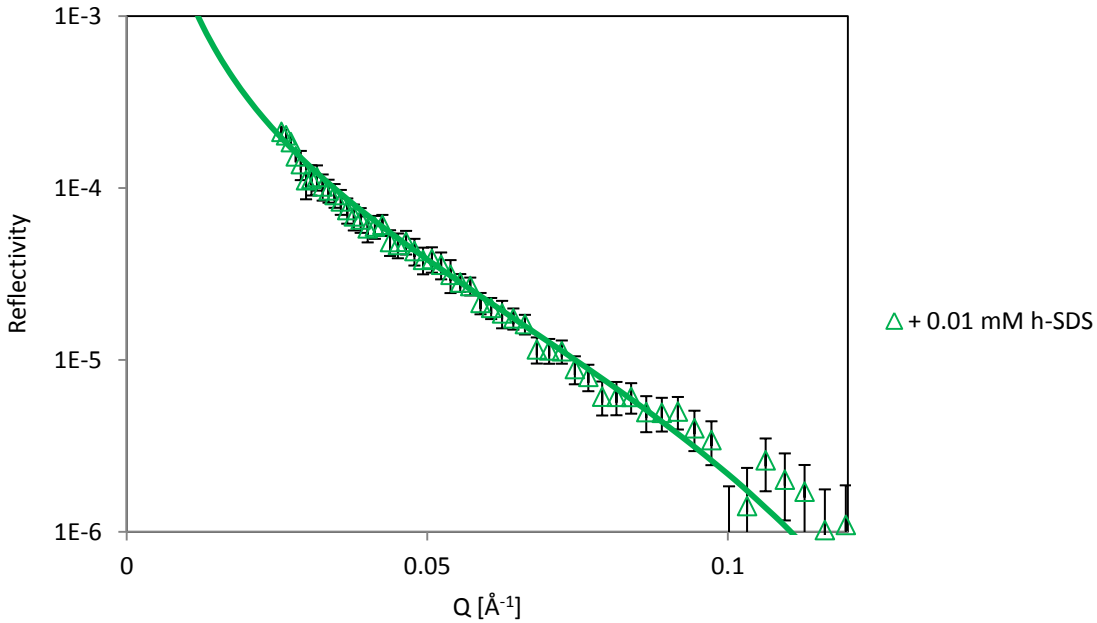

Fig. 5.5.2. Neutron reflection data for 1 mg/ml 40K + 0.01 mM h-SDS in NRW.

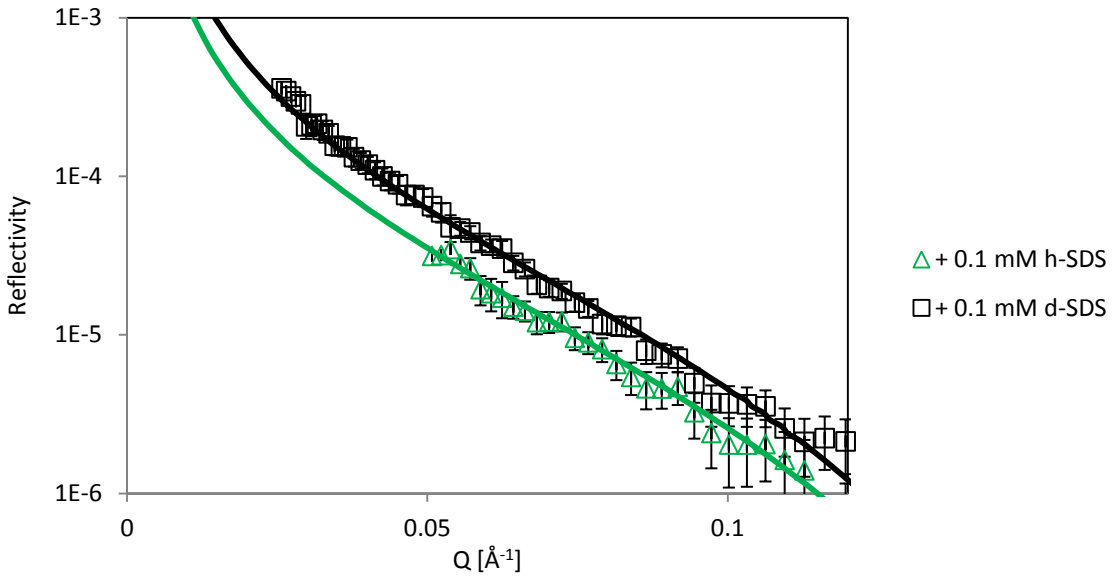

Fig 5.5.3. Neutron reflection data for 1 mg/ml 40K + 0.1 mM (d- or h-) SDS in NRW.

SDS/mM	τ/ Å	P_h/ x10^{-6} Å^{-2}	τ·P_h/ x10^{-6} Å^{-1}	P_d/ x10^{-6} Å^{-2}	τ·P_d/ x10^{-6} Å^{-1}
0.1	40	0.70	28.00	0.93	37.20
1	30	0.60	18.00	1.20	36.00

Table 5.5.2. Fitting parameters used for the 1-layer model of 1 mg/ml 40K + 0.1 and 1 mM SDS in NRW. The error in thickness is ± 3 Å and the error in scattering length density is ± 0.05 x10^{-6} Å^{-2}.

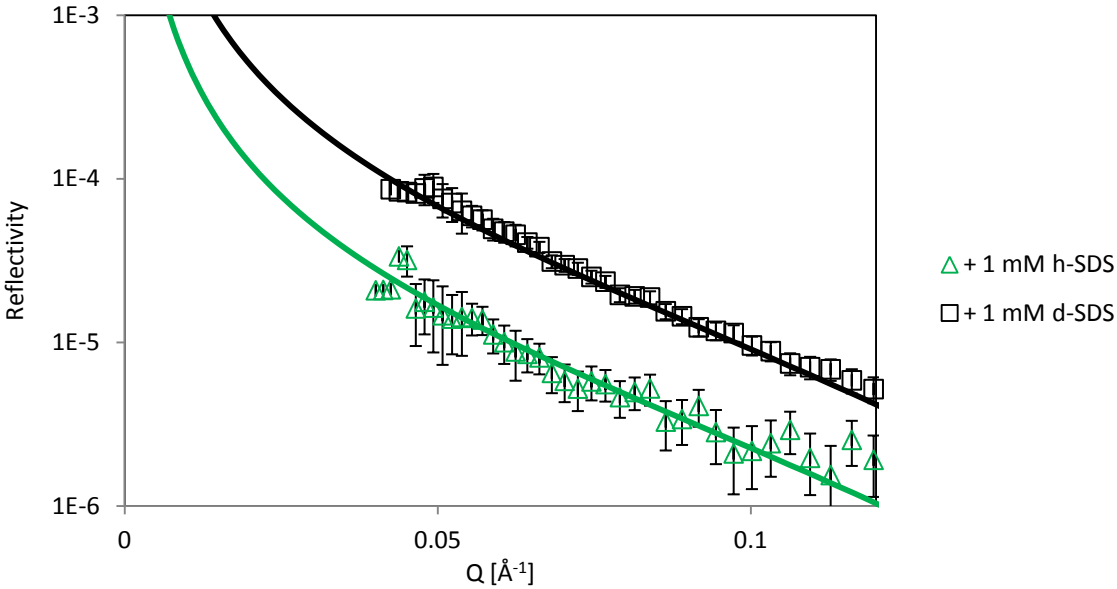

Fig 5.5.4. Neutron reflection data for 1 mg/ml 40K + 1 mM (d- or h-) SDS in NRW.

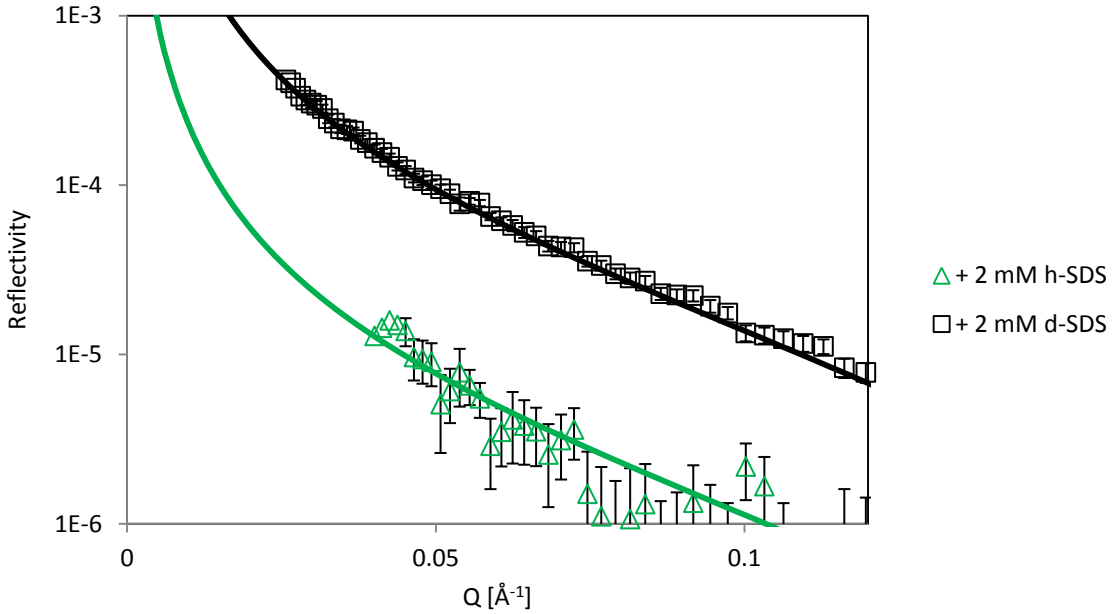

Fig 5.5.5. Neutron reflection data for 1 mg/ml 40K + 2 mM (d- or h-) SDS in NRW.

SDS/mM	τ/ Å	P_h/ x10^{-6} Å^{-2}	τ·P_h/ x10^{-6} Å^{-1}	P_d/ x10^{-6} Å^{-2}	τ·P_d/ x10^{-6} Å^{-1}
2	28	0.45	12.60	1.50	42.00
3	27	0.40	10.80	1.50	40.50

Table 5.5.3. Fitting parameters used for the 1-layer model of 1 mg/ml 40K + 2 and 3 mM SDS in NRW. The error in thickness is ± 3 Å and the error in scattering length density is ± 0.05 x10^{-6} Å^{-2}.

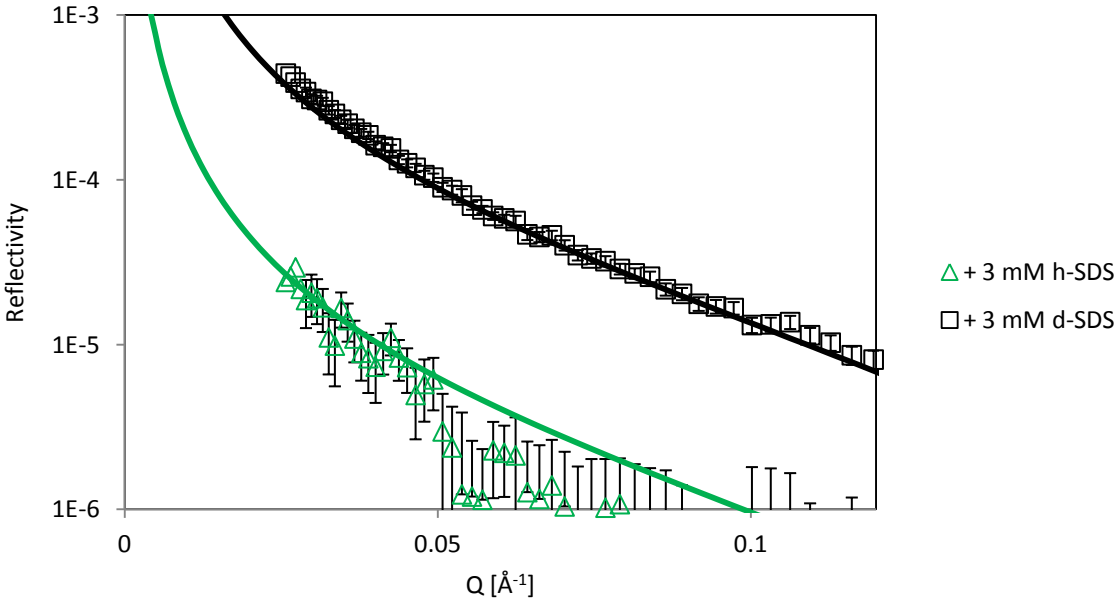

Fig 5.5.6. Neutron reflection data for 1 mg/ml 40K + 3 mM (d- or h-) SDS in NRW

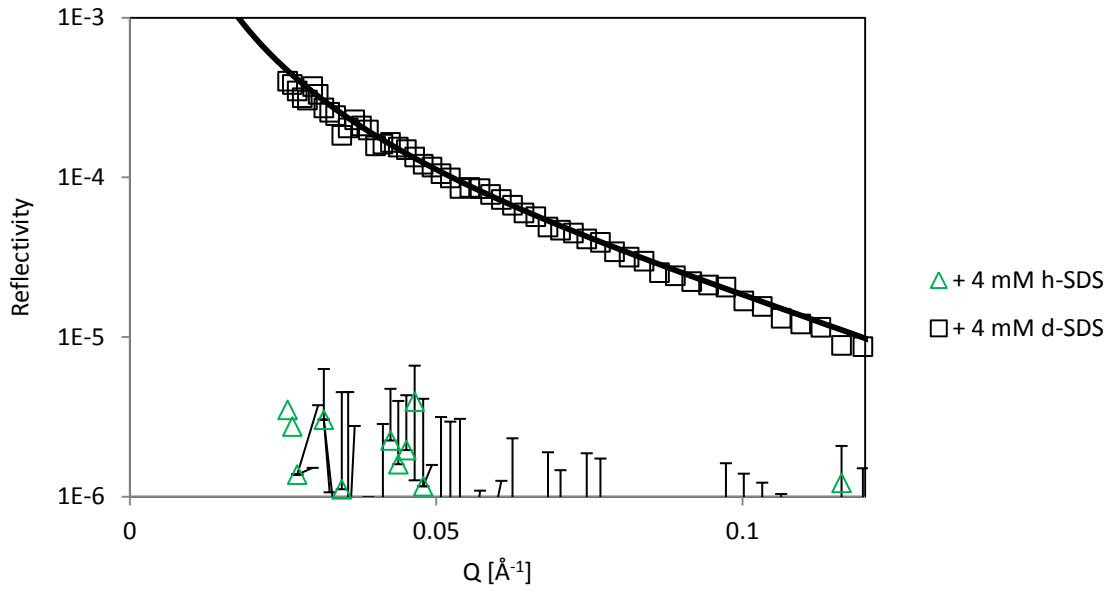

Fig 5.5.7. Neutron reflection data for 1 mg/ml 40K + 4 mM (d- or h-) SDS in NRW

SDS/mM	τ/ Å	P_h/ x10^{-6} Å^{-2}	τ·P_h/ x10^{-6} Å^{-1}	P_d/ x10^{-6} Å^{-2}	τ·P_d/ x10^{-6} Å^{-1}
4	24	*0.35*	8.40	1.80	43.20

Table 5.5.4. Fitting parameters used for the 1-layer model of 1 mg/ml 40K + 4 mM SDS in NRW. The error in thickness is ± 3 Å and the error in scattering length density is ± 0.05 x10^{-6} Å^{-2}. N.B. ρ_h cannot be adequately fitted as the signal merges into the background at low-Q values. Hence, the value given to this parameter is an assumption based on the results obtained for other concentrations.

SDS mM	Φpep	Φsds	Apep ± 6 %/ Å²	Asds ± 6 %/ Å²	Γpep ± 6 %/ mg·m^{-2}	Γsds ± 6 %/ mg·m^{-2}	n ± 5 %
0.01	0.35	0.01	5178	1259	2.12	0.04	4
0.1	0.35	0.04	5307	285	2.07	0.18	19
1	0.30	0.09	8256	152	1.33	0.34	58
2	0.22	0.15	11794	100	0.93	0.52	135
3	0.20	0.15	13759	101	0.80	0.51	159
4	0.17	0.19	17690	93	0.62	0.56	240

Table 5.5.5. Neutron reflection results obtained with 1 mg/ml of 40 KDa polypeptide at different SDS concentrations.

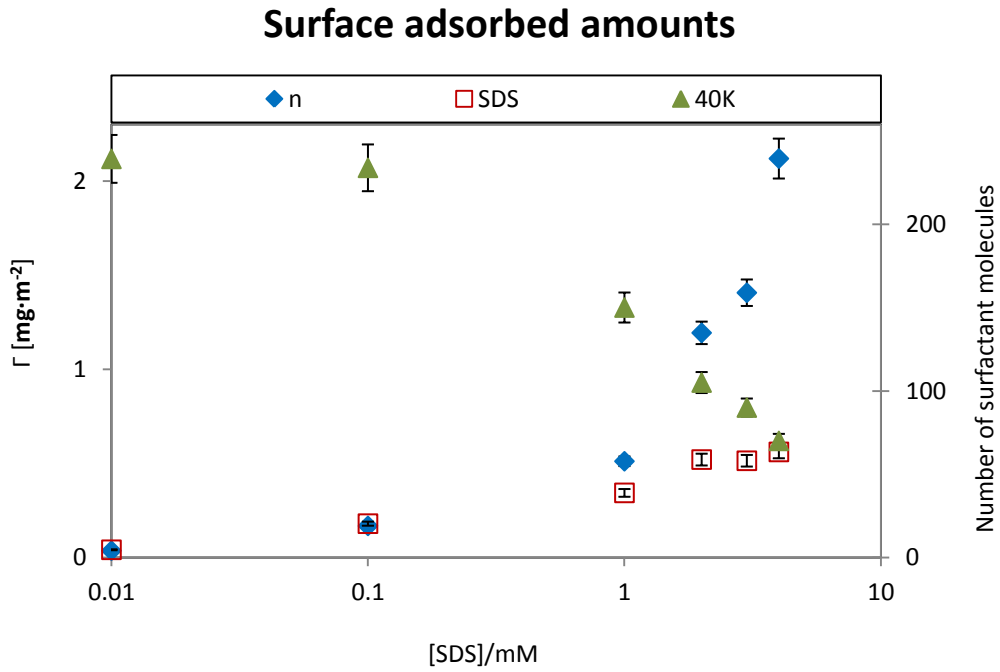

Fig. 5.5.8(a). Surfaces adsorbed amounts of polypeptide and surfactant when mixed in solution. The number of surfactant molecules per polypeptide molecule is represented by n.

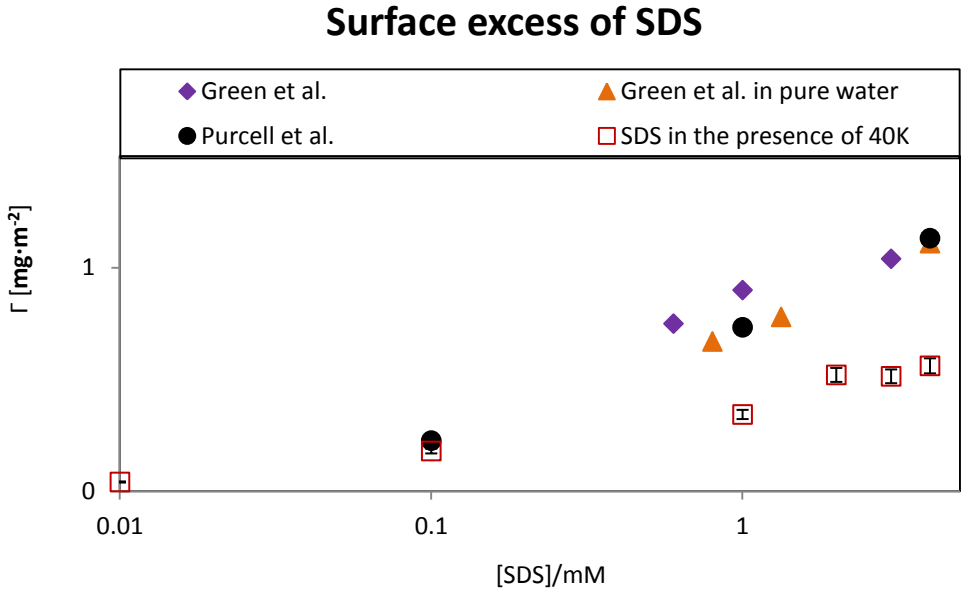

Fig. 5.5.8(b). A comparison of the SDS adsorbed amounts in the presence of 40 KDa polypeptide with the surface excess of SDS as calculated from neutron reflection experiments by Purcell et al. [18] in pure water and Green et al. [2] in pure water and in phosphate buffer at pH 7.

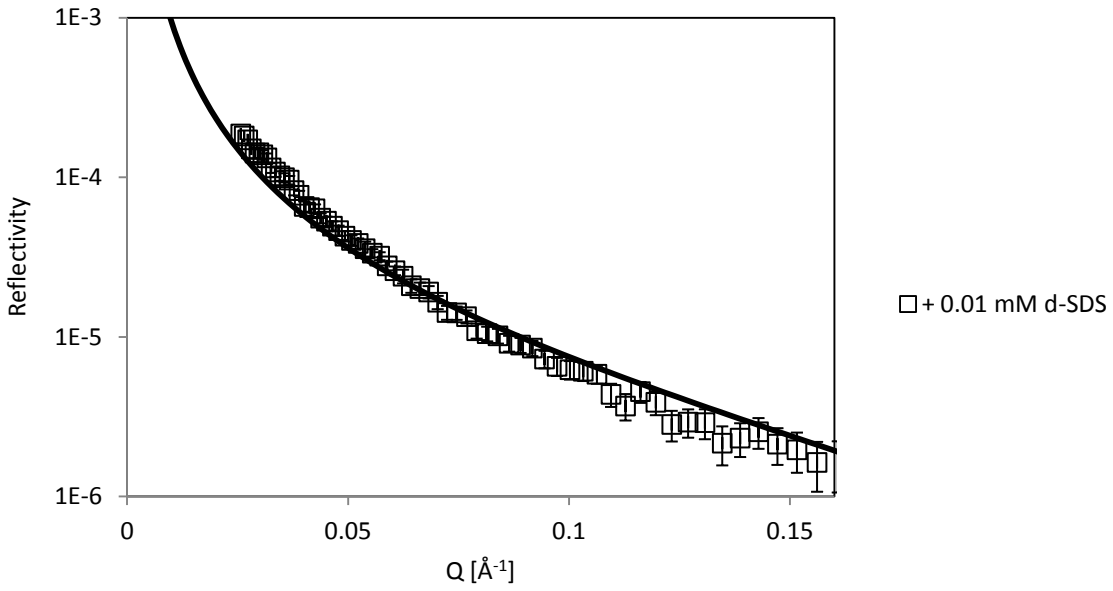

Fig 5.5.9. Neutron reflection data for 0.1 mg/ml 40K + 0.01 mM d-SDS in NRW.

SDS/mM	τ/ Å	P_h/ x10^{-6} Å^{-2}	τ·P_h/ x10^{-6} Å^{-1}	P_d/ x10^{-6} Å^{-2}	τ·P_d/ x10^{-6} Å^{-1}
0.01	18	1.20	21.60	1.45	26.10

Table 5.5.6. Fitting parameters used for the 1-layer model of 0.1 mg/ml 40K + 0.01 mM SDS in NRW. The error in thickness is ± 3 Å and the error in scattering length density is ± 0.05 x10^{-6} Å^{-2}.

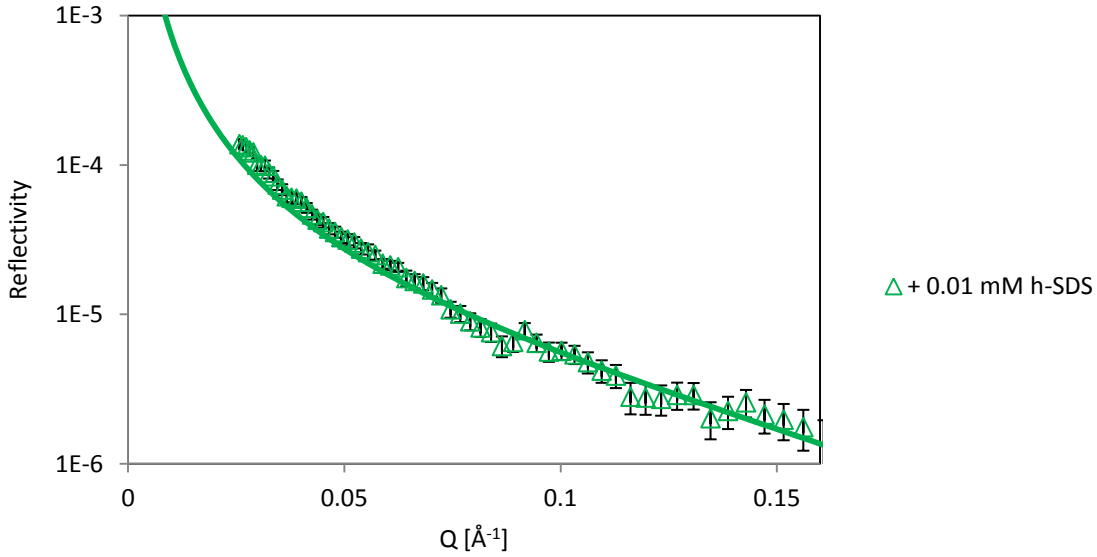

Fig 5.5.10. Neutron reflection data for 0.1 mg/ml 40K + 0.01 mM h-SDS in NRW.

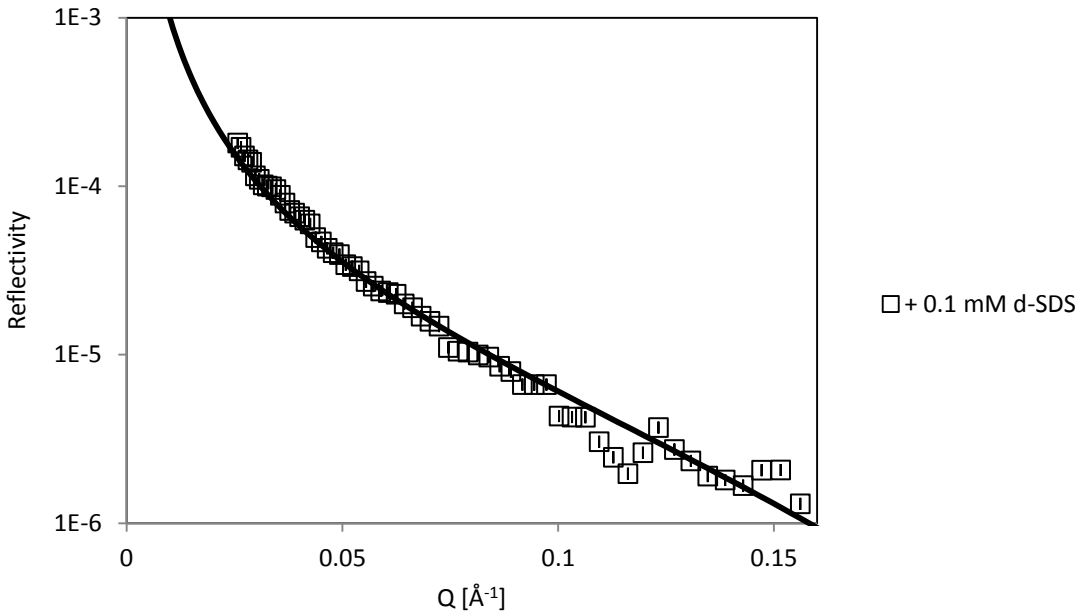

Fig 5.5.11. Neutron reflection data for 0.1 mg/ml 40K + 0.1 mM d-SDS in NRW.

SDS/mM	τ/ Å	P_h/ x10^{-6} Å^{-2}	τ·P_h/ x10^{-6} Å^{-1}	P_d/ x10^{-6} Å^{-2}	τ·P_d/ x10^{-6} Å^{-1}
0.1	23	0.95	21.85	1.05	24.15

Table 5.5.7. Fitting parameters used for the 1-layer model of 0.1 mg/ml 40K + 0.1 mM SDS in NRW. The error in thickness is ± 3 Å and the error in scattering length density is ± 0.05 x10^{-6} Å^{-2}.

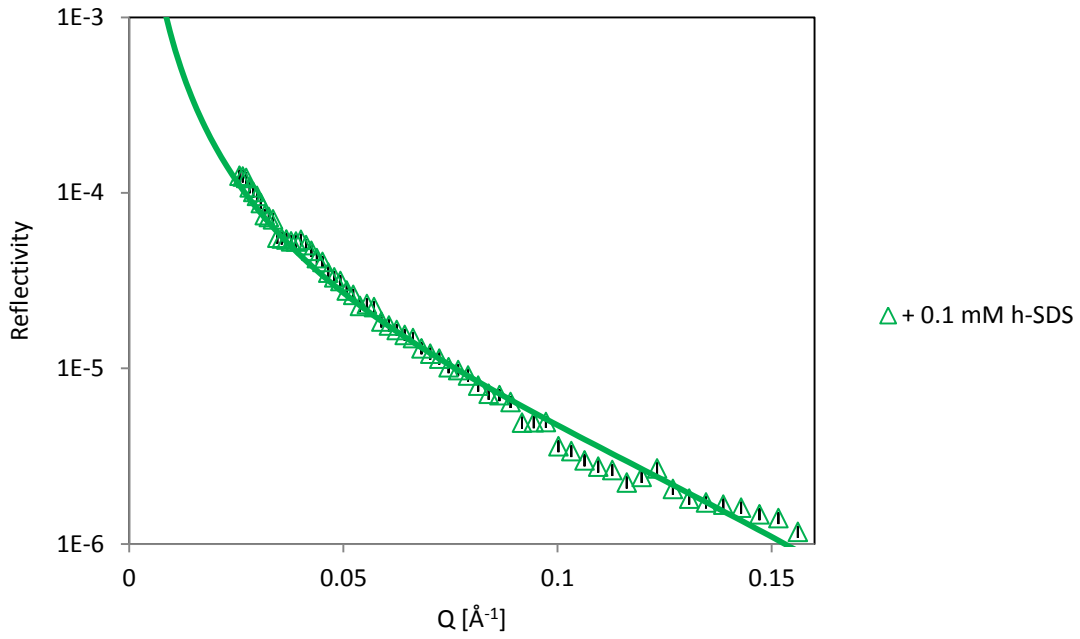

Fig 5.5.12. Neutron reflection data for 0.1 mg/ml 40K + 0.1 mM h-SDS in NRW.

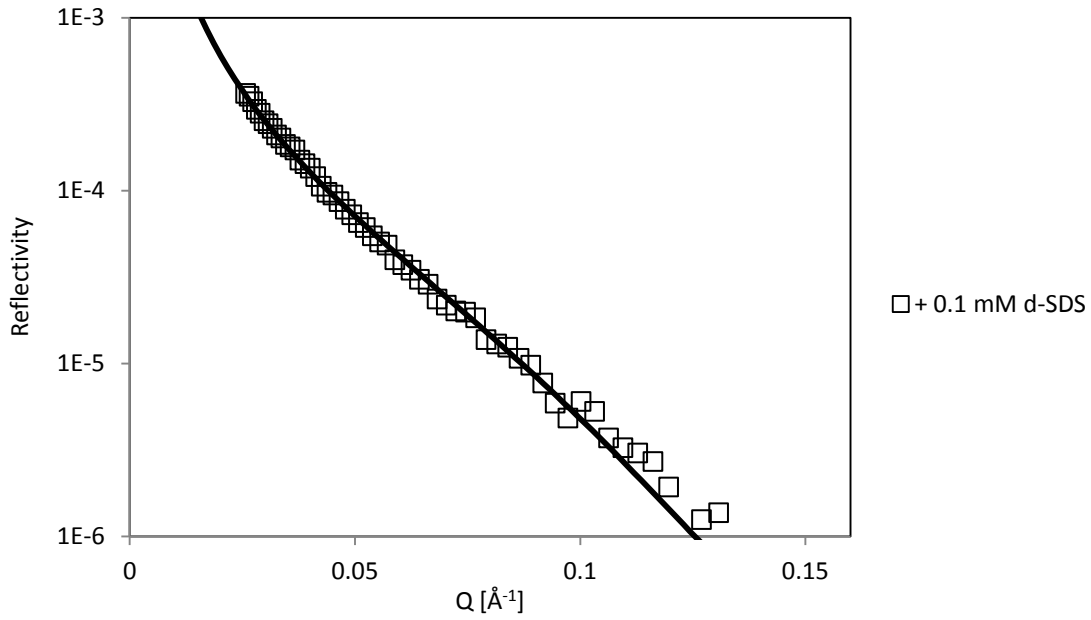

Fig 5.5.13. Neutron reflection data for 2 mg/ml 40K + 0.1 mM d-SDS in NRW.

layer	τ/ Å	P_h/ x10^{-6} Å^{-2}	τ·P_h/ x10^{-6} Å^{-1}	P_d/ x10^{-6} Å^{-2}	τ·P_d/ x10^{-6} Å^{-1}
air	20	1.10	22.00	1.30	26.00
D_2O	23	0.37	8.51	0.70	16.10

Table 5.5.8. Fitting parameters used for the 2-layer model of 2 mg/ml 40K + 0.1 mM SDS in NRW. The error in thickness is ± 3 Å and the error in scattering length density is ± 0.05 x10^{-6} Å^{-2}.

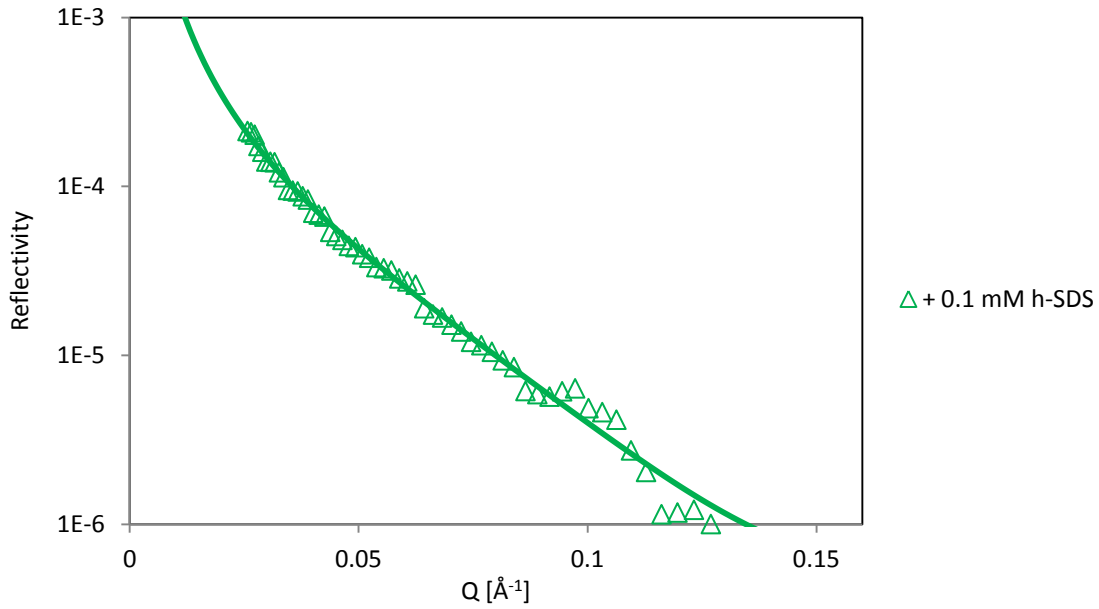

Fig 5.5.14. Neutron reflection data for 2 mg/ml 40K + 0.1 mM h-SDS in NRW.

SDS/ mM	Φ_{pep}	Φ_{sds}	A_{pep} ± 6 %/ Å²	A_{sds} ± 6 %/ Å²	Γ_{pep} ± 6 %/ mg·m^{-2}	Γ_{sds} ± 6 %/ mg·m^{-2}	n ± 5 %
0.01	0.60	0.04	6880	578	1.59	0.09	12
0.1	0.47	0.02	6801	1125	1.61	0.05	6

Table 5.5.9. Neutron reflection results obtained with 0.1 mg/ml of 40 KDa polypeptide at different SDS concentrations.

layer	Φ_{pep}	Φ_{sds}	A_{pep} ± 6 %/ Å²	A_{sds} ± 6 %/ Å²	Γ_{pep} ± 6 %/ mg·m^{-2}	Γ_{sds} ± 6 %/ mg·m^{-2}	n ± 5 %
air	0.55	0.03	6755	650	1.62	0.08	11
D_2O	0.18	0.05	17462	357	0.63	0.15	52

Table 5.5.10. Neutron reflection results obtained with 2 mg/ml of 40 KDa polypeptide and 0.1 mM of SDS with a 2-layer model.

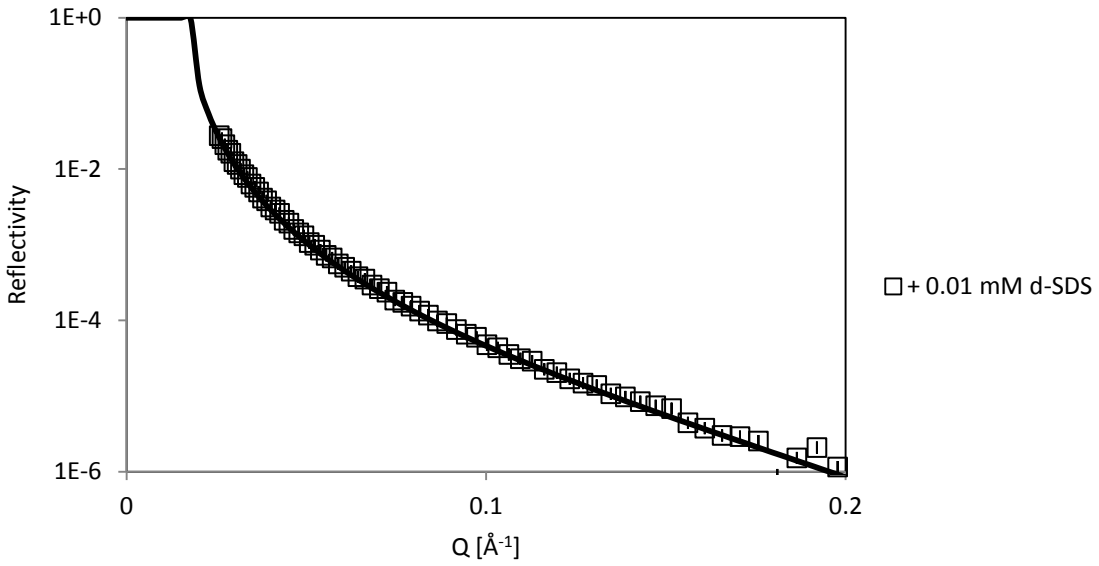

Fig 5.5.15. Neutron reflection data for 0.1 mg/ml 40K + 0.01 mM d-SDS in D_2O.

	h-SDS			d-SDS		
Layer	**τ/Å**	**P_{exp}/ x10^{-6} Å^{-2}**	**P_{calc}/ x10^{-6} Å^{-2}**	**τ/Å**	**P_{exp}/ x10^{-6} Å^{-2}**	**P_{calc}/ x10^{-6} Å^{-2}**
1	6	2.20	2.20	6	2.46	2.46
2	9	4.50	4.50	9	4.76	4.76

Table 5.5.11. Fitting parameters used for the 2-layer model of 0.1 mg/ml 40K + 0.01 mM SDS in D_2O. The error in thickness is ± 3 Å and the error in scattering length density is ± 0.05 x10^{-6} Å^{-2}.

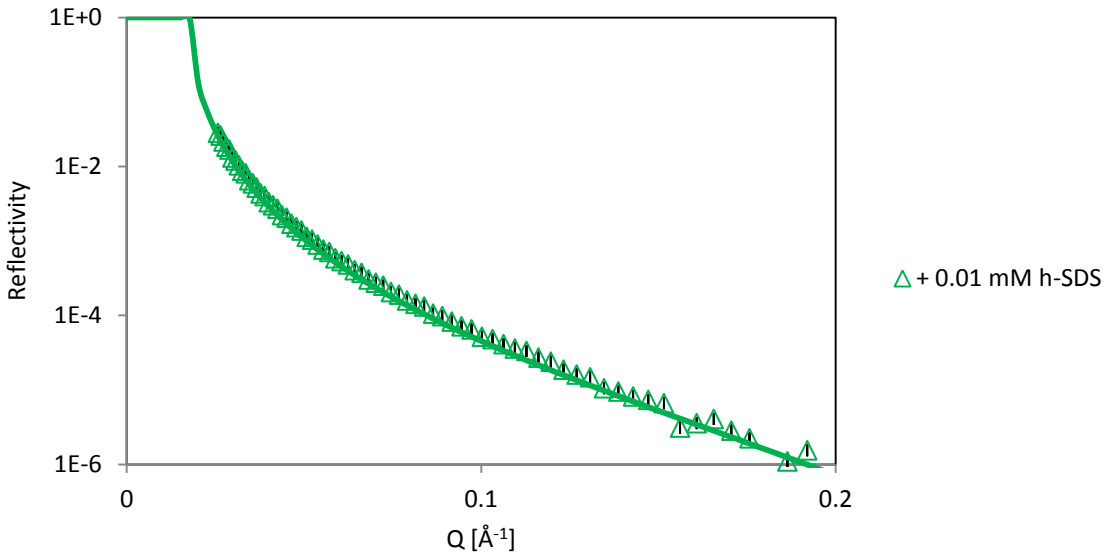

Fig 5.5.16. Neutron reflection data for 0.1 mg/ml 40K + 0.01 mM h-SDS in D_2O.

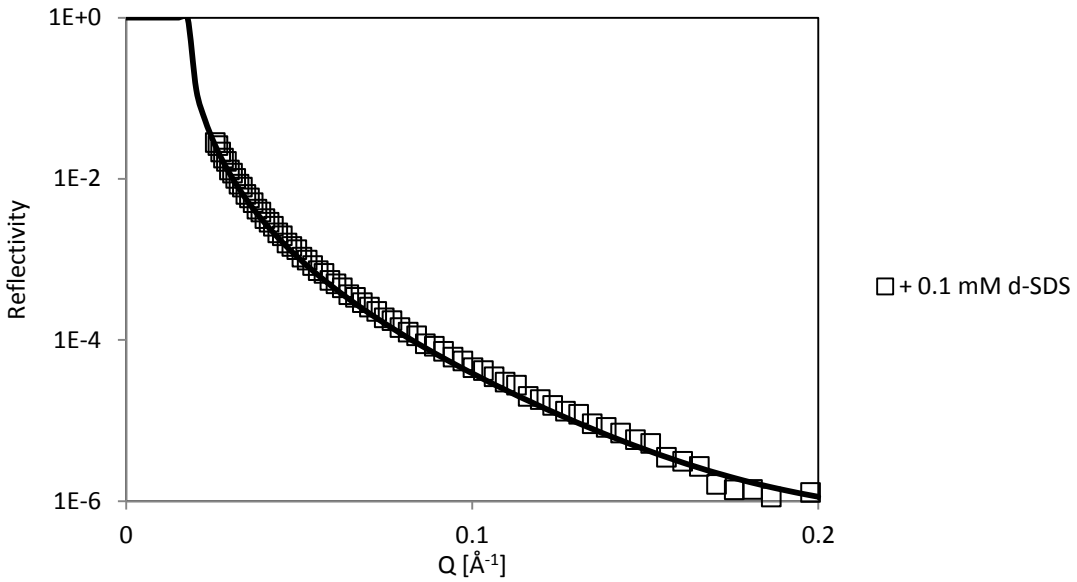

Fig. 5.5.17. Neutron reflection data for 0.1 mg/ml 40K + 0.1 mM d-SDS in D_2O.

	h-SDS			d-SDS		
Layer	**τ/Å**	**P_{exp}/ x10^{-6} Å^{-2}**	**P_{calc}/ x10^{-6} Å^{-2}**	**τ/Å**	**P_{exp}/ x10^{-6} Å^{-2}**	**P_{calc}/ x10^{-6} Å^{-2}**
1	6	1.74	1.74	6	1.84	1.84
2	16	5.70	4.98	16	5.50	5.09

Table 5.5.12. Fitting parameters used for the 2-layer model of 0.1 mg/ml 40K + 0.1 mM SDS in D_2O. The error in thickness is ± 3 Å and the error in scattering length density is ± 0.05 x10^{-6} Å^{-2}.

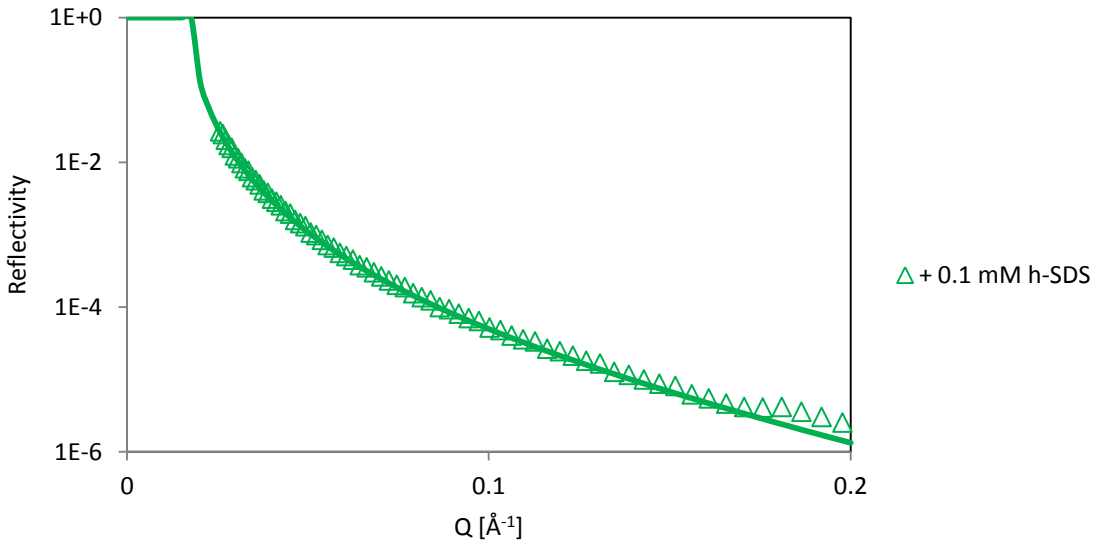

Fig 5.5.18. Neutron reflection data for 0.1 mg/ml 40K + 0.1 mM h-SDS in D_2O.

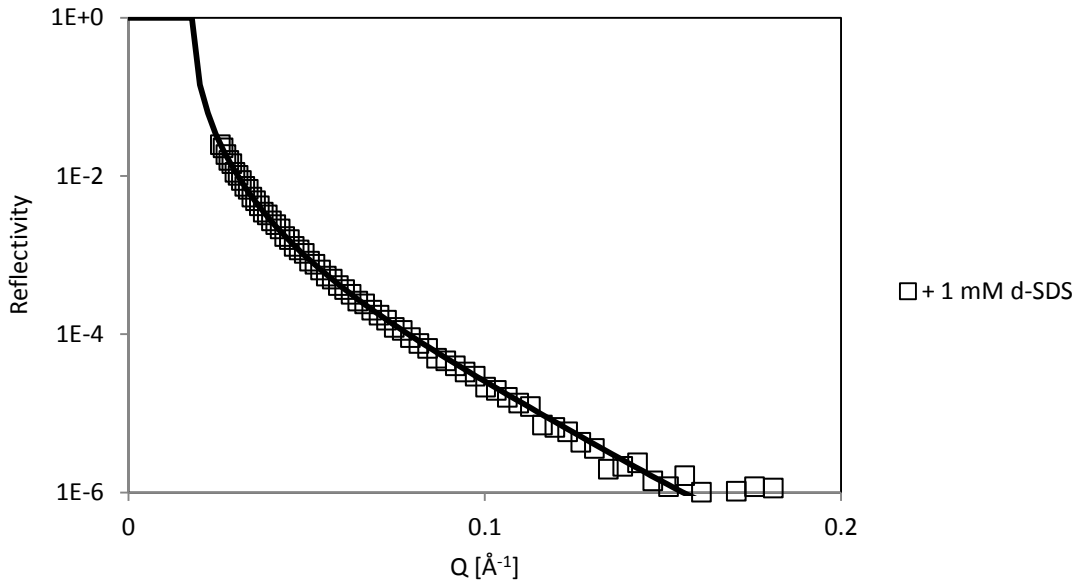

Fig 5.5.19. Neutron reflection data for 1 mg/ml 40K + 1 mM d-SDS in D_2O.

	h-SDS			d-SDS		
Layer	**τ/Å**	**P_{exp}/ x10^{-6} Å^{-2}**	**P_{calc}/ x10^{-6} Å^{-2}**	**τ/Å**	**P_{exp}/ x10^{-6} Å^{-2}**	**P_{calc}/ x10^{-6} Å^{-2}**
1	15	0.80	1.12	17	1.80	1.71
2	12	5.10	5.00	13	5.60	5.59

Table 5.5.13. Fitting parameters used for the 2-layer model of 1 mg/ml 40K + 1 mM SDS in D_2O. The error in thickness is ± 3 Å and the error in scattering length density is ± 0.05 x10^{-6} Å^{-2}.

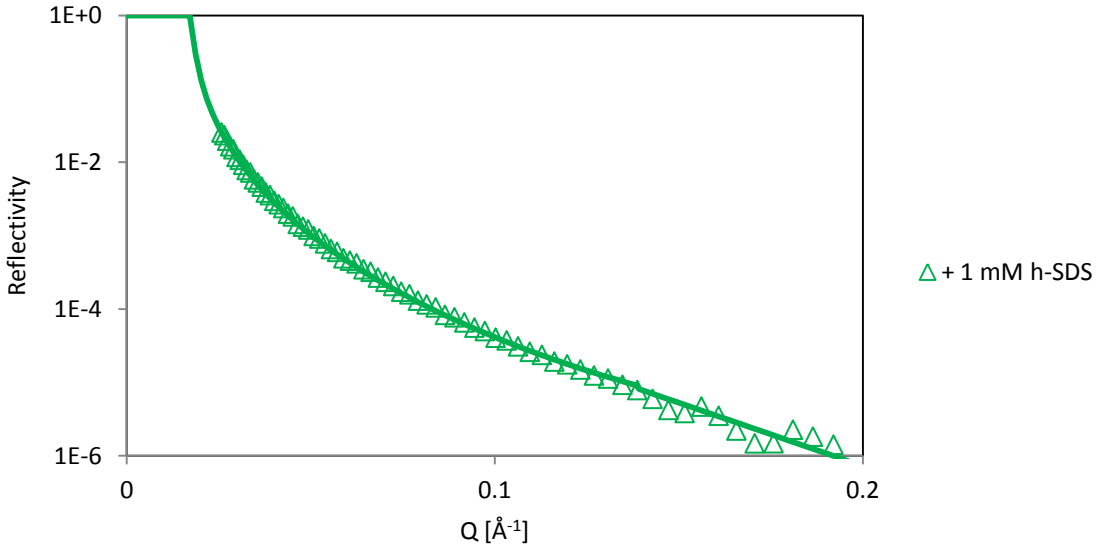

Fig 5.5.20. Neutron reflection data for 1 mg/ml 40K + 1 mM h-SDS in D_2O.

Looking at the surface amounts of the mixtures with a concentration of the 40 KDa polypeptide fixed at the CAC (Table 5.5.5), there are noticeable differences when compared with the components on their own. The first thing to notice is that, in the case of the polypeptide, at the lowest SDS concentration, i.e. 0.01 mM, the amount of 40 KDa polypeptide adsorbed at the interface was 2.12 $mg \cdot m^{-2}$, which was lower than the value for the polypeptide alone (without SDS), i.e. 2.32 $mg \cdot m^{-2}$. Although these values are close within experimental error, the fact that SDS is found to adsorb at the surface reflects the difference between the two systems.

As SDS concentration increases, the polypeptide surface adsorbed amount continues decreasing, till it reaches an adsorbed amount close to that of SDS. This is visibly clear in the 2-3 mM of SDS vicinity in Figure 5.5.8(a). Note that neutron reflection measurements of the adsorption of pure SDS in pure water and buffered solution have been well studied by Purcell et al. [18] and Green et al. [2]. These data are directly compared to our results in the presence of 40 KDa polypeptide in Figure 5.5.8(b). If we follow the SDS surface amount in the same Figure, only at low concentrations does it seem to follow a similar trend to that obtained in the absence of polypeptide.

For concentrations just below its CMC, the curve approaches a plateau. When comparing the amounts adsorbed with the number of SDS molecules per polypeptide molecule, n, as functions of surfactant concentration, three different regions appear. As already explained, we treated the polypeptide the same as BSA because we do not know the sequence of the polypeptide and yet it is an unknown polypeptide mixture.

The first one corresponds to a low level of SDS adsorption that increases with concentration of SDS in solution. This is in marked contrast with a high 40K adsorption that decreases with addition of SDS.

These results highlight the existence of polypeptide/surfactant monomers complexes at the interface in agreement with equilibrium surface tension results in region A.
The SDS surface excess departs from the curves obtained in the absence of polypeptide at 1 mM, where the plateau region starts. This region constitutes the second distinctly

patterned increase in number of molecules of SDS per polypeptide molecule and corresponds to regions B and C in equilibrium surface tension profile.
When discussing the equilibrium surface tension results, it was argued that in this region the increasing presence of surfactant monomers saturated the polypeptide. This is consistent with the neutron reflection data observed here. The surface excess of polypeptide continues decreasing whereas the surface excess of SDS is practically stable. However, the number of SDS molecules increases. This could be due to the sublayer of surfactant forming below the polypeptide/monomers complexes. Although theoretically this sublayer is below the interfacial layer, the neutron reflection results account for it as part of the interface.

Finally, at the CMC, a further step in the number of surfactant molecules per polypeptide indicates that SDS is dominating the interface. This is region D in the equilibrium surface tension curve. Figure 5.5.8(b) highlights the difference between the adsorbed SDS with and without polypeptide present in the solution. At 4 mM, the adsorbed amount is half of that found by Purcell et al. [18] and Green et al. [2]. This is due to remaining polypeptide molecules adsorbed at the surface as indicated by its non-zero adsorption at this concentration of SDS, i.e. the CMC.

Thus, neutron reflection data suggests that at low SDS concentrations complexes of mixed 40K/SDS form in solution and are able to adsorb at the interface more efficiently than the peptide or the surfactant alone. This is reflected in the fact that 40K adsorbed amounts are less than the adsorbed amount at the CAC in the absence of surfactant. On the other hand, SDS adsorption is slowed down in comparison to adsorption of SDS only. Because the polypeptide concentration is fixed at the CAC, it is reasonable to initially think that some sort of aggregate is formed at very low SDS concentration.

The fact that just below the CMC of SDS, both components adsorbed in nearly equal amounts indicates that SDS is replacing the polypeptide from the surface, what in turn indicates that the complexes are becoming SDS-rich. At the CMC, the number of SDS molecules per polypeptide increases sharply. This is explained by a further increase in the amount of SDS due to SDS-only micelles reaching the interface.

Although adsorption of free SDS molecules and free polypeptides could be considered throughout the entire range of SDS concentrations, it is disregarded due to the lower (than individual components) surface tension results obtained below the CMC of the surfactant meaning that reaching the interface is more favourable for the complexes.
So far, the mixtures with 1 mg/ml of 40K have been studied in detail assuming complexes are formed. Hence, looking at the details of the interactions at different polypeptide concentrations is an obvious step to follow.

Below its CAC, the 40 KDa polypeptide has been mixed at a fixed concentration of 0.1 mg/ml with 0.1 mM and 0.01 mM SDS. The results are presented in Table 5.5.9. As expected, reducing the polypeptide concentration allows more space at the interface per molecule, thus reducing the adsorbed amounts. As in the mixtures with 1 mg/ml of polypeptide, the adsorbed amount of 40 KDa polypeptide is lower in the presence of surfactant. When plotted together it is clear that both mixtures are very similar and both result in similar values of adsorbed amounts.

Above the CAC, only one concentration of SDS has been studied, 0.1 mM. The results (Table 5.5.10) are slightly higher SDS and 40K adsorption than seen with 1 mg/ml at the same SDS concentration. Despite surface adsorbed amounts being similar, neutron reflection imposes the use of a two layer model to fit the mixed layer adsorbed at the interface: an upper thicker layer composed of surfactant alkyl chains and polypeptide hydrophobic segments tending towards the air side of the system, and a lower less dense layer (explained by the repulsion between surfactant polar heads) that tends towards the liquid phase.

5.6. Small angle neutron scattering

SANS was used to investigate the possible formation of mixed complexes of polypeptide and surfactant micelles in the bulk phase. Far from being an exhaustive study on the bulk properties of the mixed solutions, this experiment was intended as a first approximation to understand the relation between the structures found in the bulk phase and those at the air/liquid interface.

It is well known that a common complex formed by many surfactant/polymer mixtures is a spherical core/shell shape in which the core is a surfactant micelle (or rather the surfactant tails) and the shell is the polymer wrapped around the micelle [5, 20, 21]. The interaction between the spherical complexes is often modelled with a Hayter-Penfold structure factor (Equation 2.4.50).

Four different concentrations of SDS mixed with a fixed concentration of 10 mg/ml of 40 KDa polypeptide were tested in D_2O solutions containing 10 mM of NaCl and adjusted to pH 5. Two contrasts were measured per each surfactant concentration, polypeptide mixed with h-SDS and polypeptide mixed with d-SDS. The lowest surfactant concentration tested was 0.6 mM. This was followed by 1 and 2 mM; all of them below the CMC of the surfactant. Finally, a concentration over the CMC was also tested, i.e. 5 mM.

All mixtures except those with 0.6 mM of SDS seem to be modelled rather well using the core/shell described by Equation 2.4.42 in conjunction with a Hayter-Penfold structure factor. The remaining mixed solutions were modelled to a cylinder shape (almost like a sheet) with the same length as the cylinder modelled for the polypeptide alone but with a smaller radius and less polydispersity. We can assume that the SDS is responsible for these changes and that increases in SDS concentration lead to the formation of the core/shell structures at concentrations were the surfactant aggregation number increases, i.e. surface adsorbed material is solubilising and returning to the bulk phase to form these less surface active structures.

Thus, contrary to the explanation offered by Campbell et al. [11] but in agreement with Bell's model [9], at SDS concentrations leading to an increase in the surface tension, there is polypeptide present in the bulk solution in the form of core/shell complexes. This also proves that the arguments exposed by Penfold [8] in relation to polyamines/SDS mixtures, where the no existence of the cliff edge peak was attributed to the lack of formation of bulk polymer/surfactant micelle complexes, do not apply to the present system.

The scattering data obtained for the h-SDS and d-SDS mixtures and their model fits are presented in Figures 5.6.1 and 5.6.2, respectively. The fitting parameters are presented in Table 5.6.1. The scattering length density of the polypeptide has been fixed to $\rho_s = 3.6 \cdot 10^{-6}$ Å^{-2} in both models used. A similar method was used by Griffiths et al. [21] in their studies of endosomolytic polyamidoamine.

In the core/shell model, the scattering length densities of the protonated and deuterated cores have been fixed to the values $-0.4 \cdot 10^{-6}$ Å^{-2} and $2.2 \cdot 10^{-6}$ Å^{-2}, respectively. In the core/shell model application to the deuterated SDS samples, the surfactant tails become 'invisible'. Thus, it was expected to find a core with the scattering length density of D_2O or close to it so only a polypeptide ring was observed. However, it was found that a much lower scattering length density fits the model better and that much higher scattering length densities are not suitable. This may suggest that the polypeptide hydrophobic moieties are also found in the core.

The polypeptide aggregate in the absence of surfactant can be pictured as a disk-like sheet with a thickness (i.e. the cylinder length) approximately equal to a sequence of two amino acid residues and a radius similar to that of the BSA protein modelled as a random coil in a good solvent, i.e. 94 Å [22-24].

There is no evidence of triple collagen helix remnants. As a guidance, collagen I is typically 14 Å wide and 3000 Å long [24] what could be thought of as a thin long rod. Thus, the possession of the primary structure is not sufficient condition to achieve the original collagen folding.

Thus, the polypeptide adopts a sheet shape at concentrations beyond the critical aggregation concentration which turns into a spherical complex with addition of SDS. The core radius in the core/shell complex is approximately equal to the maximum extended length of the surfactant tail. If the volume of a sphere formed of surfactant tails is calculated using this length and divided by the volume of an individual tail (according to Tanford), the resultant aggregation number or surfactant units needed to form a micelle is 59.

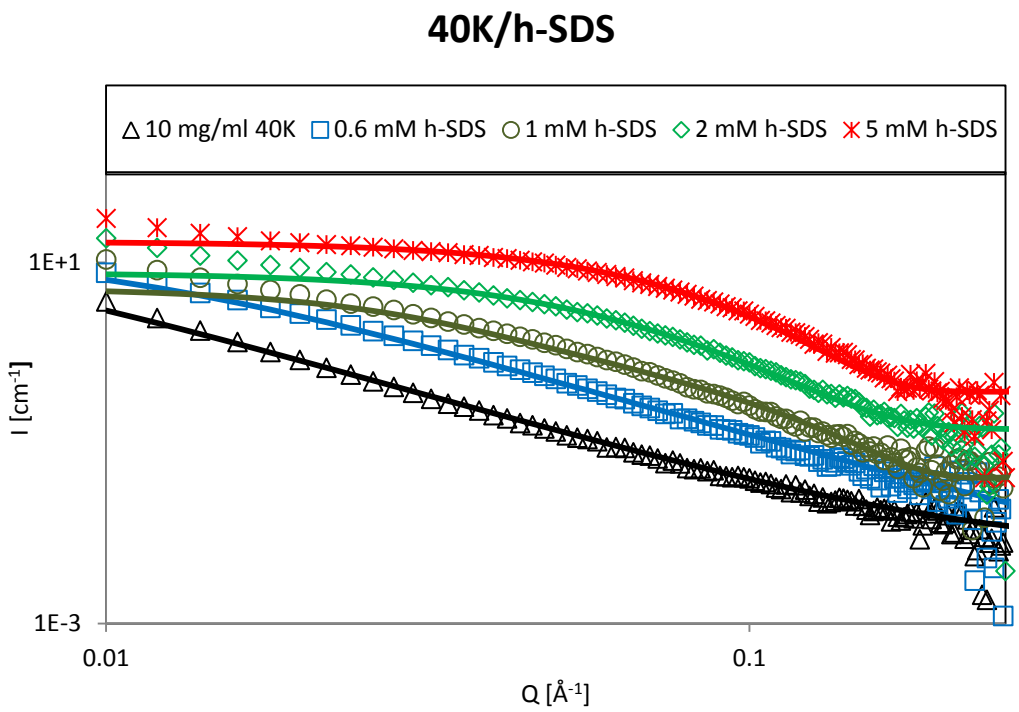

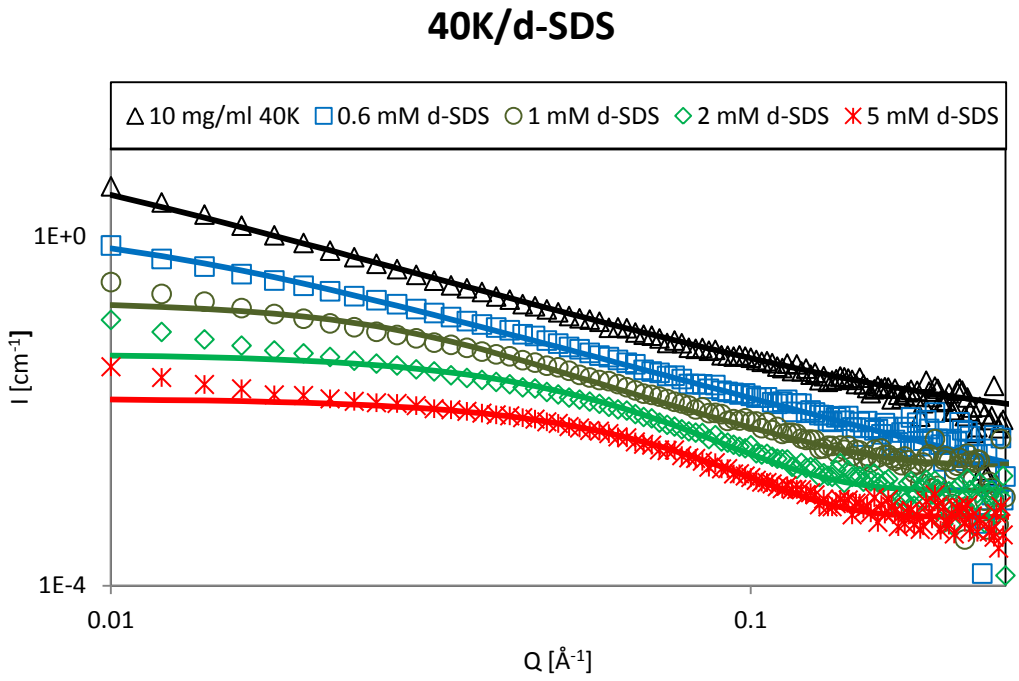

Figs. 5.6.1 (top) and 5.6.2 (bottom) SANS results for 40K/SDS mixtures. The straight lines correspond to the model fits. For clarity, mixtures with SDS have been scaled with multiples of 2.5 with respect to the scattering data of the polypeptide in the absence of surfactant and error bars are not included.

sample	model	l/± 1 Å	R/Å		p/± 0.2
10 mg/ml 40 KDa	cylinder	7	90 ± 20		1
0.6 mM h-SDS	cylinder	7	70 ± 10		0.5
0.6 mM d-SDS	cylinder	7	70 ± 10		0.7
sample	**model**	**R_c/± 2 Å**	**τ_s/± 2 Å**	**Φ/± 0.0005**	**p/± 0.2**
1 mM h-SDS	core/shell	19	5	0.0021	1.7
2 mM h-SDS	core/shell	15	11	0.0058	0.55
5 mM h-SDS	core/shell	18	10	0.0045	0.6
1 mM d-SDS	core/shell	18	5	0.002	1.7
2 mM d-SDS	core/shell	18	11	0.002	0.7
5 mM d-SDS	core/shell	18	10	0.018	0.6

Table 5.6.1. Fitting parameters for the scattering data obtained with 40K/SDS mixtures. Samples are identified by their SDS concentration. The cylinder model for 10 mg/ml of 40 KDa polypeptide is included as a reference. The parameters R and l are the radius and length of the cylinder, R_c and τ_s are the core radius and shell thickness, respectively. Φ is the volume fraction of scatterers and p is the polydispersity index.

At the air/liquid interface, the mixed samples with 10 mg/ml of 40 KDa polypeptide show negligible differences in their surface tension profile. However, neutron reflection showed us how for mixtures of SDS with 1 mg/ml of polypeptide there is a change in behaviour at around 1 mM of SDS where the number of SDS units associated per polypeptide molecule, i.e. 58, is approximately the number required to form a free surfactant micelle. With 0.6 mM SDS, the polypeptide is not hugely affected by the added component; there are not enough surfactant monomers to form micelles.

However, with the addition of 1 mM or more of SDS, the surfactant easily aggregates even below its CMC aided by the polypeptide wrapping around it. Thus, the number of surfactant molecules at the interface increases when the polypeptide returns to the bulk wrapping surfactant micelles.

The total volume of the different aggregates is at its maximum when no SDS is present, and decreases with added surfactant until the polypeptide is saturated at around 1 mM. At this point, the volume of the complex increases again when more SDS becomes available and associates with the existing aggregates.

The polydispersity in the shell thickness may be thought of as a parameter where small degrees of ellipticity and hydration effects are also accounted for. The high polydispersity values found at 1 mM SDS correspond to the transition between a short cylinder (sheet) shape and a sphere (see Figure 5.6.3). Therefore, we can assume that the flat sides of the cylinder shape are adopting a curved conformation while pulling from the edges thus reducing the radius to about a third of that for the polypeptide shape.

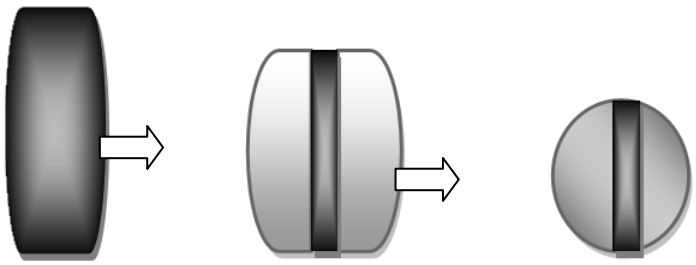

Fig. 5.6.3. 40 KDa polypeptide disk shape transition to a spherical complex upon addition of SDS. The darker areas symbolize the original short cylinder shape.

Summary

The mixtures of the 40 KDa polypeptide with SDS at pH 5, i.e. close to the isoelectric point of the polypeptide, result in a combination of a strong interaction between the components enhanced by the cooperative effect of the interaction between the surfactant alkyl chains, and an electrostatic interaction between the charges present in the polymer and the surfactant head group.

These interactions are responsible for the formation of complexes of different surface activities in the solution. With small amounts of surfactant added to the solution, the interfacial adsorption process is greatly enhanced, especially at polypeptide concentrations below the CAC, as proven by the equilibrium surface tension profiles and the foams obtained with these samples. Dynamic surface tension measurements confirmed that the association of both components at low concentrations of both components (below the CMC and CAC, respectively) slows down the rate of adsorption of the surfactant and reduces the lag time of the polypeptide.

Although no phase separation (characteristic of strongly interacting systems near the neutralization point) was observed, the electrostatic origins of the interaction have been proven trough ζ-potential.

Neutron reflection confirmed that the greatest amounts of interfacial adsorbed material are produced at low surfactant concentrations corresponding to region A of an 'S'-labelled curve, as explained in Chapter 2, in relation to the model described by Bell et al. [9].

SANS confirmed the existence of bulk aggregates which resemble the well-known core/shell shape at concentrations that fall in regions B and C in the model above mentioned. Thus, Campbell's suggestions [11] that no polymer exist in solution at these surfactant concentrations are not applicable in this case.

References

[1] V.B. Fainerman, S.V. Lylyk, E.V. Aksenenko, J.T. Petkov, J. Yorke, R. Miller (2010) "Surface tension isotherms, adsorption dynamics and dilational visco-elasticity of sodium dodecyl sulphate solutions", Colloids and Surfaces A: Physicochem. Eng. Aspects, 354, pp. 8–15.

[2] R.J. Green, T.J. Su, H. Joy, J.R. Lu (2000) "Interaction of lysozyme and sodium dodecyl sulphate at the air/liquid interface", Langmuir, 16, pp. 5797-5805.

[3] D.J. Cooke, C.C. Dong, J.R. Lu, R.K. Thomas, E.A. Simister, J. Penfold (1998) "Interaction between Poly(ethylene oxide) and Sodium Dodecyl Sulfate Studied by Neutron Reflection", J. Phys. Chem. B, 102, pp. 4912-4917.

[4] A.G. Bykov, S.Y. Lin, G. Loglio, R. Miller, B.A. Noskov (2010) "Dynamic surface properties of polyethylenimine and sodium dodecylsulfate complex solutions", Colloids and Surfaces A: Physicochem. Eng. Aspects, 367, pp. 129–132.

[5] X.L. Zhang, J. Penfold, R.K. Thomas, I.M. Tucker, J.T. Petkov, J. Bent, A. Cox, R.A. Campbell (2011) "Adsorption behaviour of hydrophobin and hydrophobin/surfactant mixtures at the air/water interface", Langmuir, 27, pp. 11316-11323.

[6] H. Comas-Rojas, E. Aluicio-Sarduy, S. Rodriguez-Calvo, A. Perez-Gramatges, S.J. Roser and K.J. Edler (2007) "Interactions and film formation in polyethylenimine–

cetyltrimethylammonium bromide aqueous mixtures at low surfactant concentration", Soft Matter, 3, pp. 747–753.

[7] J. Penfold, I. Tucker, R.K. Thomas, J. Zhang (2005) "Adsorption of polyelectrolyte/surfactant mixtures at the air-solution interface: poly(ethylenimine)/sodium dodecyl sulphate", Langmuir, 21, pp. 10061-10073.

[8] J. Penfold, R.K. Thomas, X.L. Zhang, D.J.F. Taylor (2009) "Nature of amine-surfactant interactions at the air-solution interface", Langmuir, 25, pp. 3972-3980.

[9] C.G. Bell, C.J.W. Breward, P.D. Howell, J. Penfold, R.K. Thomas (2010) "A theoretical analysis of the surface tension profiles of strongly interacting polymer–surfactant systems", J. Colloid Interface Sci., 350, pp. 486–493.

[10] E.D. Goddard (2002) "Polymer/surfactant interaction interfacial aspects", J. Colloid Interface Sci., 256, pp. 228–235.

[11] R.A. Campbell, A. Angus-Smyth, M. Yanez Arteta, K. Tonigold, T. Nylander, I. Varga (2010) "New perspective on the cliff edge peak in the surface tension of oppositely charged polyelectrolyte/surfactant mixtures", J. Phys. Chem. Lett., 1, pp. 3021–3026.

[12] B.M.D. O'Driscoll, E. Milsom, C. Fernandez-Martin, L. White, S.J. Roser, K.J. Edler (2005) "Thin films of polyethylenimine and alkyltrimethylammonium bromides at the air/water interface", Macromolecules, 38, pp. 8785-8794.

[13] J. Penfold, I. Tucker, R.K. Thomas, D.J.F. Taylor, X.L. Zhang, C. Bell, C. Breward, P. Howell (2007) "The interaction between sodium alkyl sulfate surfactants and the oppositely charged polyelectrolyte, polyDMDAAC, at the air-water interface the role of alkyl chain length and electrolyte and comparison with theoretical predictions", Langmuir, 23 (6), pp. 3128-3136.

[14] V.S. Alahverdjieva, V.B. Fainerman, E.V. Aksenenko, M.E. Leser, R. Miller (2008) "Adsorption of hen egg-white lysozyme at the air-water interface in presence of sodium dodecyl sulphate", Colloids and Surfaces A: Physicochem. Aspects 317, pp. 610-617.

[15] A.R. Mackie, A.P. Gunning, P.J. Wilde, V.J. Morris (1999) "Orogenic displacement of protein from the air/water interface by competitive adsorption", J. Colloid Interface Sci., 210, pp. 157–166.

[16] B.A.Noskov, G. Loglio, R. Miller (2011) "Dilational surface visco-elasticity of polyelectrolyte/surfactant solutions: formation of heterogeneous adsorption layers", Adv. Colloid Interface Sci., 168 (1-2), pp. 179-197.

[17] Malhotra, J.N. Coupland (2004) "The effect of surfactants on the solubility, zeta potential, and viscosity of soy protein isolates", Food Hydrocolloids, 18, pp. 101–108.

[18] I.P. Purcell, J.R. Lu, R.K. Thomas (1998) “Adsorption of sodium dodecyl sulfate at the surface of aqueous solutions of poly(vynilpyrrolidone) studied by neutron reflection”, Langmuir, 14, pp. 1637-1645.

[19] C. Tanford (1972) “Micelle shape and size”, J. Phys. Chem., 76 (21), pp. 3020-3023.

[20] P.C. Griffiths, A.Y.F. Cheung, G.J. Finney, C. Farley, A.R. Pitt, A.M. Howe, S.M. King, R.K. Heenan, B.L. Bales (2002) “Electron paramagnetic resonance and small angle neutron scattering studies of mixed sodium dodecyl sulfate and tetradecyl(malono)bis(N-methylglucamide) surfactant micelles”, Langmuir, 18 (4), pp. 1065-1072.

[21] P.C. Griffiths, Z. Khayat, S. Tse, R.K. Heenan, S.M. King, R. Duncan (2007) “Studies on the mechanism of interaction of a bioresponsive endosomolytic polyamidoamine with interfaces.1. Micelles as model surfaces”, Biomacromolecules, 8, pp. 1004-1012

[22] R.L. Baldwin, B.H. Zimm (2000) “Are denatured proteins ever random coils?”, PNAS, 97 (23), pp. 12391-12392.

[23] C.D. Geierhass, A.A. Nickson, K. Lindorff-Larsen, J. Clarke, M. Vendruscolo (2007) “BPPred: a web-based computational tool for predicting biophysical parameters of proteins”, Protein Science 16, pp. 125-134.

[24] D. Voet, J.G. Voet, C.W. Pratt (2006) “Fundamentals of biochemistry. Life at the molecular level”, 2nd ed., John Wiley and Sons.

Chapter 6. Mixtures with ionic surfactants II: DTAB/40K mixtures

This Chapter reports the studies of the mixtures of the 40 KDa polypeptide with the cationic surfactant DTAB. Equilibrium surface tension data were obtained through the plate method and dynamic surface tension changes were measured with the maximum bubble pressure method. The surface charge properties of the solution complexes were characterised through ζ-potential measurements. These studies are together used to guide the understanding of varying foam stability from different combinations of mixing between the polypeptide and DTAB. The results from foam studies of the mixtures are highly illustrative at highlighting the synergistic effects between the polypeptide and the surfactant and the relation between bulk phase and interfacial properties. This part of the study represents a good demonstration of aiming to link interfacial adsorption to foam stability and instability. Data from neutron reflection experiments are then presented to corroborate the interfacial adsorption from surface tension studies with the structure and composition, with particular emphasis to the changes in the relative adsorption and the two surface active components. Finally, SANS results help to establish a relation between the size and shape of the complexes formed in the bulk solution phase with respect to their interfacial properties with useful indications of changes in their size and shape.

6.1 Surface tension

The adsorption of the cationic surfactant DTAB was investigated with the plate method (Figure 6.1.1). At pH 5 and in a 10 mM NaCl solution at 25°C, the CMC was found to be at approximately 10.5 mM with a surface tension value of 43 ± 1 mN/m. The surface excess obtained via the Gibbs Equation is $(3.7 \pm 0.3) \cdot 10^{-6}$ mol·m^{-2} (Figure 6.1.2) which corresponds to an area per molecule of 45 ± 3 Å^2.

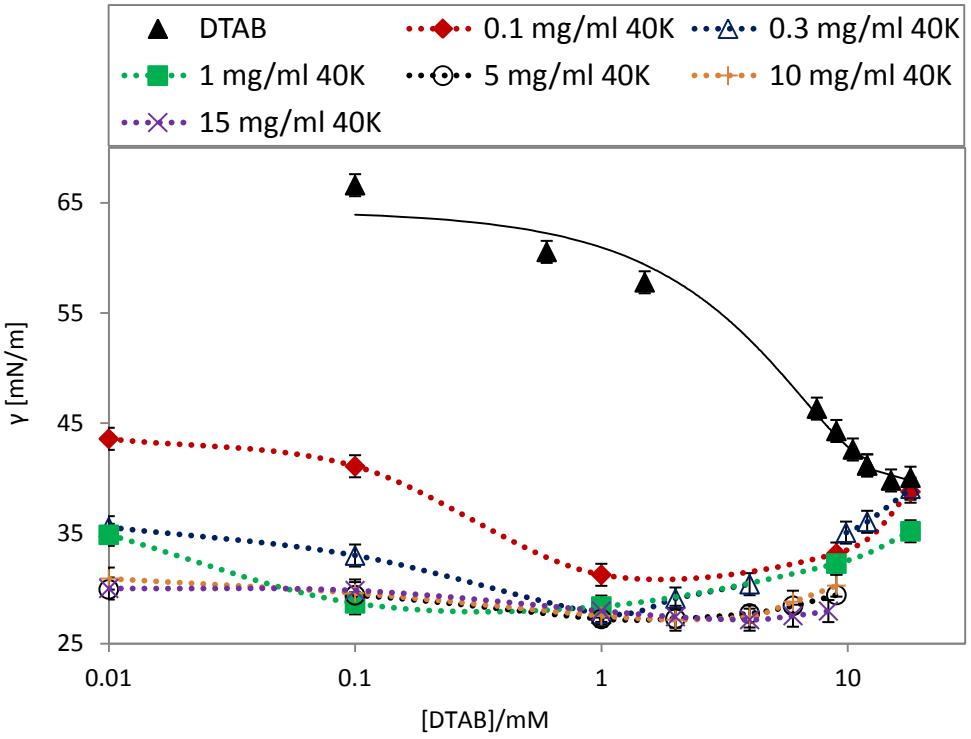

Fig. 6.1.1. Equilibrium surface tension profiles for 40K/DTAB mixtures. Lines are only a visual aid.

Literature values for the CMC of DTAB vary greatly. Lu et al. [1] reported the CMC at 14 mM and Ritacco et al. [2], at 15 mM at 25ºC and $\gamma_{cmc} \approx 39$ mN/m, both being measured in the absence of salt or buffer. Bell et al. [3] and Taylor et al. [4] reported similar values. In the absence of electrolyte, their reported CMC is at 13 mM and the maximum surface excess possible is $4.0 \cdot 10^{-6}$ mol·m^{-2}. Given that salt addition tends to lower the CMC, the results obtained from this work were broadly consistent with the values reported from pure water. In any case, the limiting area per molecule at the CMC or the maximum surface excess is within experimental error the same and appears to be independent of salt addition.

The surface tension from the mixtures of DTAB with 40 KDa polypeptide was subsequently investigated with the plate method and the results are also presented in Figure 6.1.1.

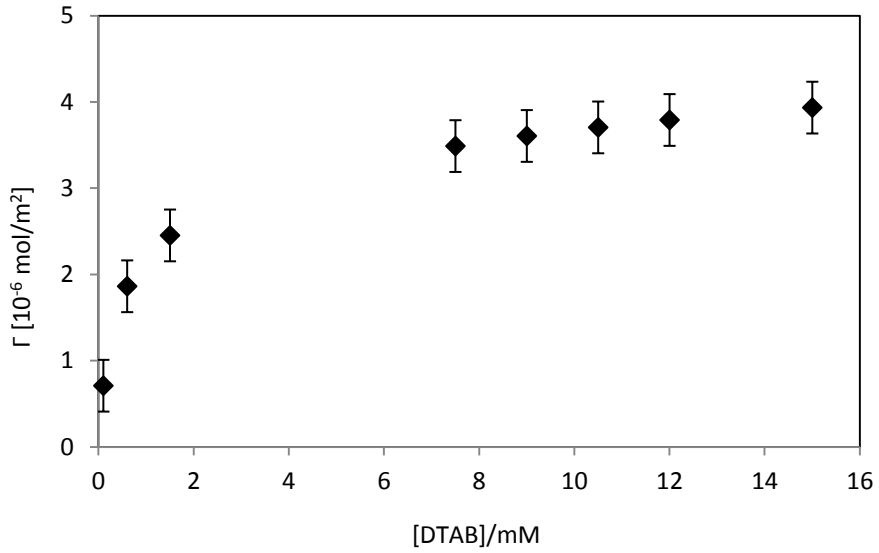

Fig. 6.1.2. Surface adsorbed amounts of DTAB.

It is possible to see immediately that even at the lowest concentration of the polypeptide, i.e. 0.1 mg/ml, the curves show a depression reaching a plateau at approximately 1 mM DTAB with surface tension values lower than those observed for DTAB alone. The plateau is followed by a raise in surface tension up to values equal to or close to the CMC of DTAB depending on the amount of polypeptide present. This shape follows the arguments proposed by Bell et al. [3] and it is similar to the PEI/SDS systems mentioned earlier in relation to mixtures of polypeptide with the anionic surfactant SDS. At first, the behaviour of PEI with ionic surfactants seems to be independent from the type of charge present in the surfactant. The 750 KDa branched PEI/C_{16}TAB system [5] also shows the same trend, i.e. lower surface tension values at low surfactant concentration compared with individual components followed by a plateau region of low surface tension values and an increase in surface tension leading towards CMC values. It is worth noticing that the group investigating the PEI/C_{16}TAB system identified the S1 point as the CAC as did Bykov et al. [6] for the 25 KDa branched PEI/SDS system.

Nevertheless, the comparison with the model proposed by Bell et al. [3, 7] still seems plausible in the alkyltrimethylammonium bromide mixtures with PEI and the 40 KDa polypeptide and therefore following their model, the CAC cannot be observed in the adsorption curve due to the strong interactions taking place at the surface.

As in the case of the PEI/C_{16}TAB system, the formation of surface active complexes at very low DTAB concentrations explains the low surface tension values in this region. Whilst the surfactant monomers find places to bind to in the polymer, the curve falls in the plateau region. Finally, when the polymer is saturated and the formation of DTAB micelles is energetically favoured, the material adsorbed at the surface is slowly redistributed following partial solubilisation. The latter is responsible for the formation of bulk polymer/DTAB micelle complexes that possess lesser surface activities than the polymer/monomer complexes already adsorbed at the interface. With further addition of surfactant, the surfactant starts forming free micelles that replace the complexes from the surface. At concentrations above the CMC, the surface is occupied mostly by DTAB-only micelles.

The mixtures of SDS and DTAB with the polypeptide exhibit very different phase behaviour albeit the similarities found in the adsorption curves. Whereas the 40K/SDS system did not show any turbidity in any of the experiments at SDS concentrations below the CMC including salt addition, the 40K/DTAB system changes from a clear appearance in region A to a highly turbid solution towards the end of the plateau region and a decreasing milky appearance with even further addition of surfactant (Figure 6.1.3). This effect may or may not be seen depending on the amount of polypeptide present. Thus, if we are to believe that the 'degree of milkiness' of the solutions leads to a description of the state of the colloidal system, then it is possible to argue that in the initial stages of polymer/monomer complexes formation the system is stable. At the plateau region, even though no apparent changes are observable in the surface tension profile, it is assumed that the increasing amount of surfactant is saturating the polypeptide. The 'milkiness' is at its highest in this region possibly indicating that this is a very unstable state (see Figure 6.1.3) due to charge neutralisation.

With increasing amount of surfactant, the solution starts regaining stability as observed by the decreasing 'milkiness'. This coincides with the formation of polymer/micelle complexes and an increase in surface tension. Thus, it is clear that a solution with polymer/micelle complexes is more stable than a solution with polymer/monomer complexes, i.e. the plateau region is not a real equilibrium phase.

Noskov et al. [8] found that in the PSS/DTAB system, the precipitation region starts at the neutralization point, i.e. ~ 0.5 mM of DTAB, and that it coincides with the presence of kinetically trapped aggregates at the interface. Hence, they believe this region is not in thermodynamic equilibrium.

Fig. 6.1.3. Solutions of different concentrations of 40 KDa polypeptide with DTAB at concentrations as marked at the top of each bottle (in mM). (Top) 10 mg/ml of polypeptide. (Middle) 1 mg/ml of polypeptide. (Bottom) 0.3 mg/ml of polypeptide. All solutions were prepared at pH 5 and in 10 mM NaCl.

According to Campbell et al. [9, 10] the plateau region occurring before the cliff edge peak in strongly interacting systems such as PDMDAAC/SDS and PEI/SDS, is not a thermodynamically stable state. However, they do not attribute this to the formation of more stable complexes. Instead, they believe that the precipitation region (which does not occur in the plateau region but rather in region C) lacks polymer in the bulk solution so no polymer-containing complexes could possibly be formed and therefore no competition between different complexes is possible. Thus, the true equilibrium is

reached when the precipitation has finished. This results in depletion of surface active material from the bulk phase which leads to depletion of surface active material at the interface and therefore an increase in surface tension which this group believes is the true equilibrium state. The low plateau values, they observed, are achieved again after redispersion of the surface active precipitated material by means of applying a mechanical stress.

From their studies of strongly interacting systems this group concluded that every strongly interacting system is dependent on the mixing protocol followed in the sample preparation and that the difference in surface tension results obtained with samples prepared with different procedures attests the fact that the lower values are not due to the system reaching thermodynamic equilibrium which is not accessible in real experimental times.

The mixing protocol used in the preparation of the 40 KDa polypeptide/surfactant samples tested with the plate method is roughly the same as the standard protocol according to Campbell's group [11], i.e. samples at different surfactant concentrations were prepared with a 10 mM NaCl solution. Separately, a solution of polypeptide was prepared with a 10 mM NaCl solution; the pH of which, was adjusted adding small concentrated volumes of HCl. The polypeptide was poured onto the surfactant solutions and the bottle was slightly agitated. However, they used solutions of 100 mM NaCl instead of 10 mM.

The turbid samples did indeed separate into a clear solution and a layer of precipitated material at the bottom of the vessel after some time. Nevertheless, they did not observe the formation of the peak when the samples were freshly prepared. In this case, they found that the highest dispersion of newly prepared samples produced clear solutions and only after a few days did the peak appear. In the mixed 40 KDa polypeptide/DTAB system, this was not observed. The turbidity occurred immediately after mixing and the surface tension values were recorded at times for up to ~16 hours yet no indication of high surface tension values in the form of the cliff edge peak were obtained.

It is also worth recalling that a strong interaction of similar characteristics resulted from the mixtures of the 40 KDa polypeptide with SDS and that no precipitation or phase

separation was observed at any polypeptide concentration at SDS concentrations below the CMC.

Finally, at surfactant concentrations high above the CMC, the mixed solution with DTAB becomes clear again and the system returns to equilibrium. Furthermore, the formation of a film of oily appearance at the interface at concentrations just below the plateau region is observable by naked eye in both, the 40K/DTAB and PEI/C_{16}TAB systems [5, 12]. The fact that it appears around the S1 point can be considered as proof of formation of complexes at this point. This film was reported to grow in thickness with increasing surfactant concentration in the PEI/C_{16}TAB system and it was still present at C_{16}TAB concentrations above the CMC [5]. The conclusion to this observation was that free C_{16}TAB micelles coexist at the interface with saturated polymer/surfactant aggregates. In principle, similar conclusions could be drawn for the polypeptide system. However, the thickness of the layer decreases with increasing surfactant concentration in our system as will be explained in the neutron reflection section.

Driscoll et al. [12] assessed the formation of the films in PEI/C_nTAB (n=12, 14, 16) in greater detail. They reported that the films seen by naked eye refracted light in a rainbow style that allowed them to measure the islands of material found at the surface through the film fault lines. In our system, the existence of these 'rainbow'-films was also observed but not used as a measured of the pockets of material formed.
These authors also described the appearance of films in the DTAB/NaPSS and the PDMDAAC/SDS systems.

Several methods were employed in the study of these systems and several conclusions were drawn. They noticed that the mobility of the film decreased with time possibly indicating increased ordering of the film; the surface pressure decreased with polymer concentration and the surface pressure curves suggested the existence of at least two or more processes occurring in the films; and the films were only formed when exposed to air. The later fact, also observed in the 40K/DTAB system, was explained by considering the system is in kinetic equilibrium as opposed to thermodynamic equilibrium. When the sample is set in a closed vial, the film disappears dissolving in the bulk phase.

As already mentioned, the results for the mixtures of 40K/DTAB closely resemble the 40K/SDS system featured in the previous Chapter. In fact, if the concentrations at which the different regions A-D are expressed in terms of CMC of the corresponding surfactant, it is possible to see that the different break points in both systems fall in the same range. That is for region A, both surfactants are at concentrations in the ranges 10^{-3}·CMC to 10^{-2}·CMC; the plateau region (region B) roughly coincides with the interval contained within 0.2·CMC and 0.6·CMC; region C, spans from 0.6·CMC to the CMC; and finally, region D covers the higher surfactant concentrations above the CMC.

It is noticeable that in both systems the adsorption profile corresponding to the CAC of the polypeptide, i.e. 1 mg/ml, presents a value of surface tension higher than for the polypeptide alone (32 ± 1 mN/m) at around 0.01 mM of SDS or DTAB, respectively. However, at lower or higher polypeptide concentrations, the surface tension values are never higher than for the individual polypeptide.

The hydrophobic parts present in the polypeptide are protected from entering in contact with water molecules during the micellization process. This could lead to an increasing separation between these hydrophobic parts and the surfactant chains thus interrupting the short ranged strong cooperative interaction. At higher polymer concentrations, aggregates are easily formed, thus the strong interaction is not capable to overcome the electrostatics that dominate when aggregate formation occurs as in the case of the 'T'-labelled curves. At the CAC, the system is highly unstable but regains stability with the addition of further surfactant. The strong hydrophobic interaction between surfactant tails and hydrophobic domains in the polypeptide is facilitated by the increased availability of surfactant tails, and coupled with the ion-dipole interaction it becomes stronger than the electrostatic interaction.

6.1.1. Addition of NaCl

In relation to addition of electrolytes, it was found that it prevents the film formation, as found by Edler et al. [13] for PEI/C_nTAB systems too. Driscoll et al. [12] also noticed that addition of salt prevents film formation in marked contrast to the enhanced formation of complexes encountered in the PDMDAAC/SDS system. This led them to

believe that interactions occurring in oppositely charged polymer/surfactant mixtures were different from those responsible of the behaviour of a like-charged polymer/surfactant system such as PEI/C_nTAB. Similarly, even though the 40K/ionic surfactant curves are very similar in appearance, the underlying mechanisms driving the interactions responsible for these curves depend to some extent on the charge in the head groups of the surfactants.

In Driscoll's work [12] the change in film properties produced with changes in pH were discussed in terms of the dipole interaction between the polymer amine groups and the TAB ammonium groups and was noticed that since the measurements were effected in alkaline conditions this was essentially a neutral/cationic interaction (recall that neutrality for PEI occurs at pH ~10). Thus, it seems reasonable to think that the 40K/DTAB system studied at a pH close to the isoelectric point (neutral conditions for the polypeptide) follows the same example.

As in the case of SDS mixed with the 40 KDa polypeptide, some mixtures of DTAB and polypeptide were initially measured using the ring method. However, due to the difficulties encountered during measurement of this system particularly at low polypeptide concentrations, the plate method also became the preferred choice for evaluating them. Nonetheless, the study of variations in surface tension with addition of NaCl was obtained with the ring method.

It is necessary to clarify at this point that both compounds, the polypeptide and the DTAB, belong to different batches from those used in the analysis with plate method. Despite this fact and the fact that the volumes used for the correct functioning of both methods differ by a factor of 2 to 3, the comparison between solutions of the same concentrations from different sources results in similar values overall.

In Figure 6.1.4, the results of adding different amounts of NaCl to a 1 mg/ml of polypeptide mixed with DTAB in a solution at pH 5 are shown together with the surface tension curve for DTAB to provide a reference point with respect to its CMC. At 10 mM NaCl, the results obtained with the plate method are replicated with the exception that the plateau region and region C occur at earlier DTAB concentrations; this could be attributed to differences in volume used in the experiments and differences in geometry

of the liquid-containing vessels. Once the validity of this data has been demonstrated it is possible to proceed with the analysis of the system under different NaCl concentrations.

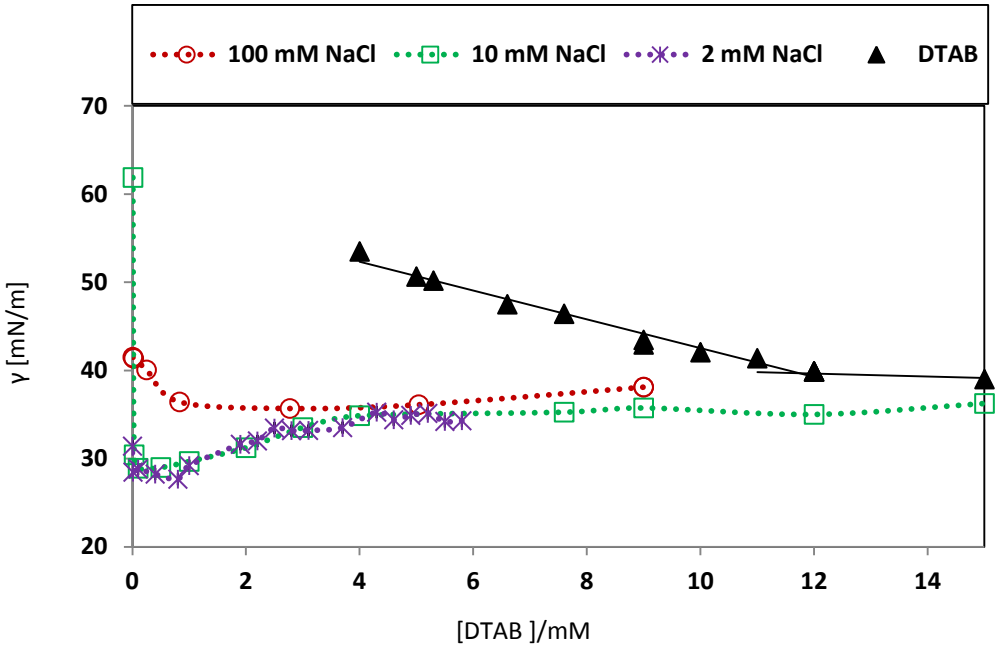

Fig. 6.1.4. Equilibrium surface tension profiles for 40K/DTAB mixtures at different NaCl concentrations. The polypeptide concentration was fixed at 1 mg/ml.

Thus, from Figure 6.1.4, it is possible to conclude that addition of 100 mM of NaCl does contribute to the disappearance of the depression region and the differences between 2 mM and 10 mM are essentially non-existent or negligible.

This has two main consequences. On the one hand, the fact that the biggest changes produced with addition of salt occur at DTAB concentrations ranging from regions A to C, indicates that the driving interaction at low surfactant concentrations (i.e. formation of polymer/monomer complexes), during the metastable plateau region and during the formation of polymer/surfactant micelles, is indeed electrostatic in nature; on the other hand, the very fact that this interaction has an electrostatic component that can be modulated at our will has been demonstrated. Furthermore, visual observation (Figure 6.1.5) of the different samples at different salt concentrations also leads us to the conclusion that an electrostatic interaction is in charge (at least partially) of the

behaviour at this range of DTAB concentrations, i.e. the ‘milkiness’ described earlier disappears with the addition of salt indicating an increase in colloidal stability in the bulk phase.

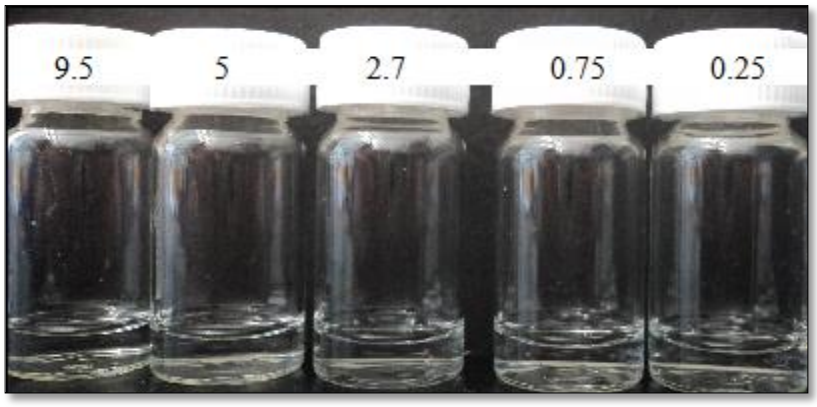

Fig. 6.1.5. Solutions of 1 mg/ml of polypeptide mixed with DTAB at pH 5 in 100 mM NaCl. DTAB concentrations (in mM) are shown at the top of each bottle.

This is in contrast with the 40K/SDS system, where no appreciable phase changes were observed below the CMC of the surfactant. A comparison between both systems leads to different interpretations of the adsorption curves. Although the general features are shared by both, the dominating interaction underlying the adsorption process seems to be different.

This could be due to the difference in ion species in the surfactant head group which gives raise to different orientations in the ion-dipole interaction due to the different locations of the charges present in the polymer which in turn, affects the cooperation with the surfactant chains. Another possibility arises from the different behaviour of the alkyl chains in SDS and DTAB. The C_{12} alkyl chain has been reported to behave as such in the case of SDS whereas for DTAB, one of the chain links behaves as an integral part of the polar head rather than the chain, thus effectively behaving as a shorter C_{11} alkyl chain [14]. However, the similarities found in the surfactant concentrations at which each adsorption step previously described takes place implies that this is not the case and that the cooperative interaction between the ion-dipole (formed by the surfactant and the polymer) and the surfactant alkyl chains is as strong with SDS as it is with DTAB.

Furthermore, Bell et al. [3] investigated the effect of alkyl chain length in the C_nTAB/NaPSS systems at n=12, 14 and 16, and concluded that the longer the chain, the more hydrophobic the surfactant and the stronger the interaction. This was associated with greater stability of polymer/surfactant micelle complexes with longer alkyl chains and a reduction in the length of the plateau region.
The surface tension is lower for mixed polypeptide with DTAB than with SDS so the argument of a DTAB effective shorter alkyl chain is disregarded.

As mentioned earlier, the standard mixing protocol uses 100 mM of NaCl to prepare the independent polymer and surfactant samples. At this concentration of salt, precipitation occurred in the PEI/SDS and PDMDAAC/SDS systems and enhancement of the adsorption at the interface was recorded [9-11]. In our system, no precipitation is observed with this amount of NaCl present in solution and the adsorption process is hindered.

Nevertheless, it is worth mentioning that the mixing protocol for the samples tested with the ring method was not the standard. On this occasion, the samples at different surfactant concentrations were prepared with a 10 mM NaCl solution. The polypeptide was poured onto the surfactant solutions in powder form and the pH was adjusted adding small concentrated volumes of HCl. The bottle was then shaken to mix the components.

6.2. Maximum bubble pressure

The dynamic adsorption of mixed polypeptide with DTAB was studied using the maximum bubble pressure method. Three concentrations of surfactant corresponding to values below, at and above the CMC were investigated, i.e. 1, 9 and 18 mM DTAB. For each surfactant concentration, five polypeptide concentrations were studied. These are 0.1, 0.3, 5, 10 and 15 mg/ml. The choice of polypeptide concentrations was made based on the position of the CAC and to investigate any differences occurring at several times the CAC.

The first observed phenomenon is the difference in the dynamic profile of the mixtures at different surfactant concentrations. For 1 mM (below the CMC), the mixed sample

departs from the curves of the individual components at every polypeptide concentration (Figures 6.2.1 to 6.2.5).

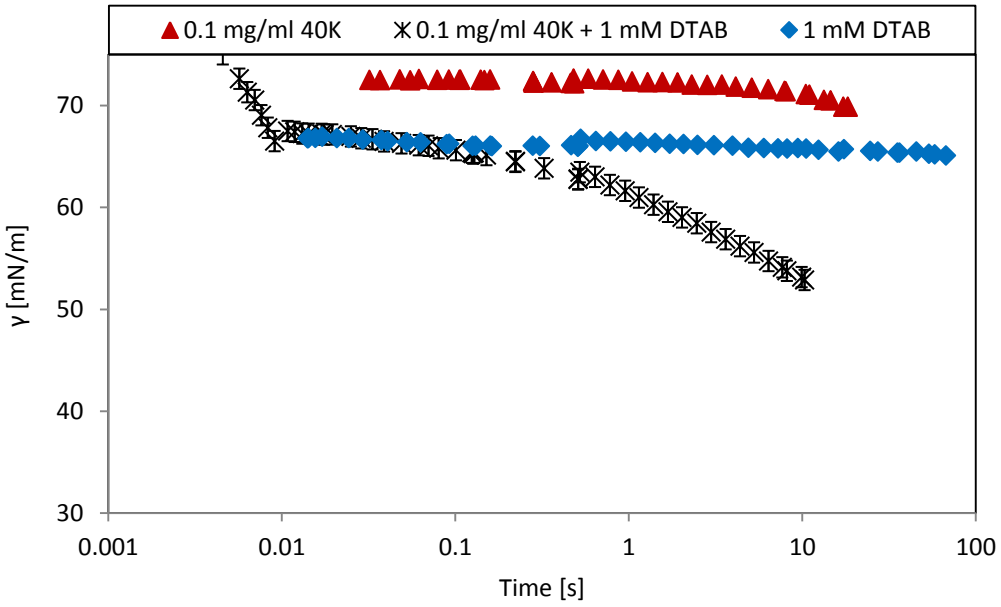

Fig. 6.2.1. Dynamic surface tension for 0.1 mg/ml 40K + 1 mM DTAB.

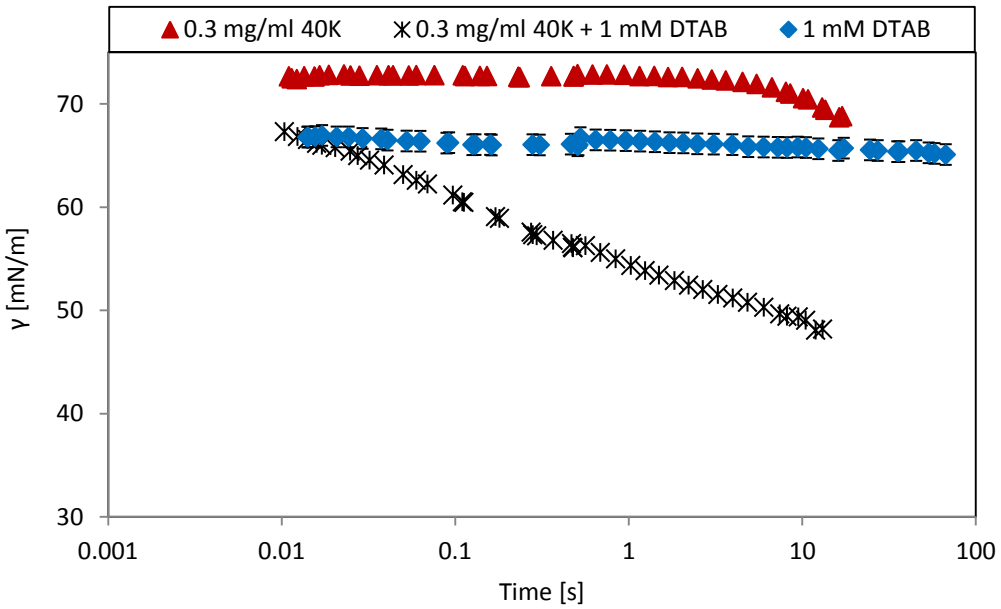

Fig. 6.2.2. Dynamic surface tension for 0.3 mg/ml 40K + 1 mM DTAB.

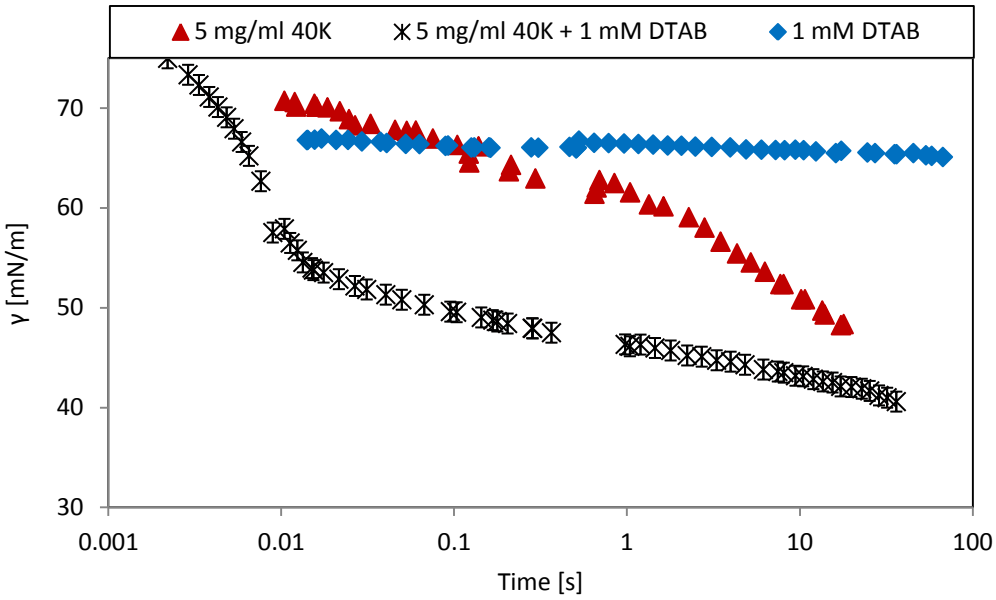

Fig. 6.2.3. Dynamic surface tension for 5 mg/ml 40K + 1 mM DTAB.

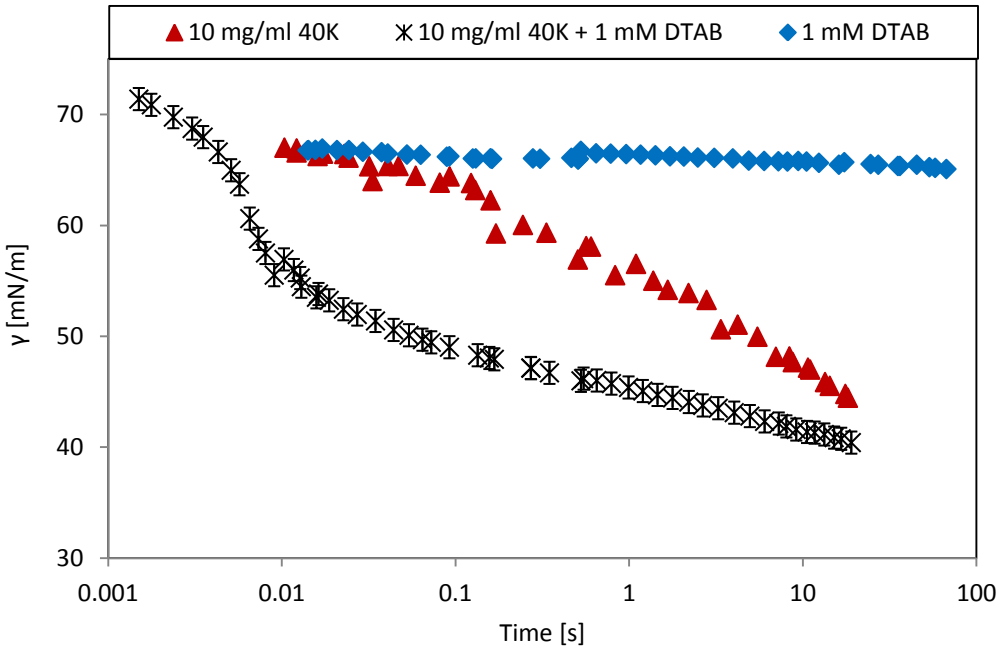

Fig. 6.2.4. Dynamic surface tension for 10 mg/ml 40K + 1 mM DTAB.

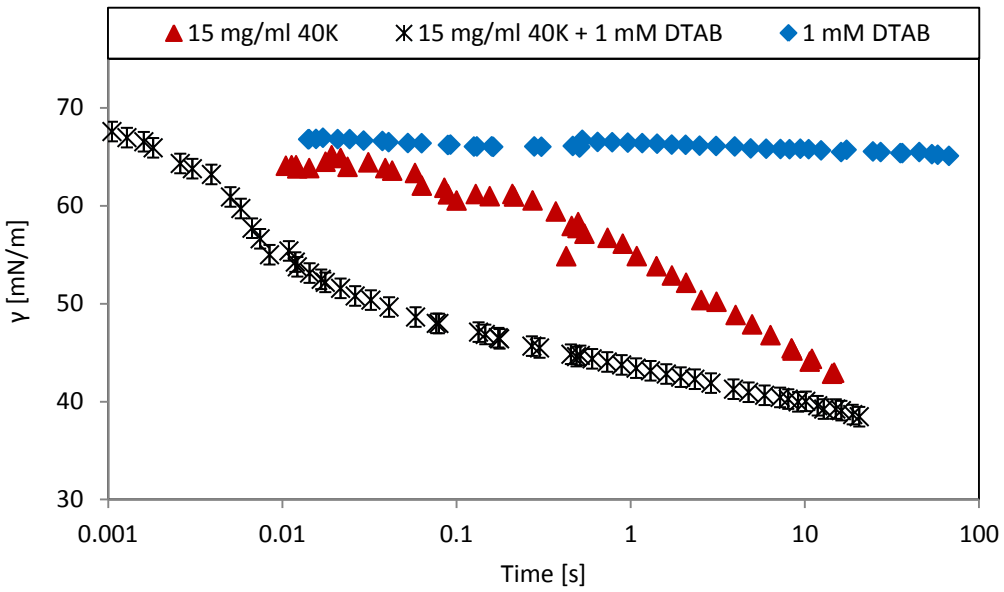

Fig. 6.2.5. Dynamic surface tension for 15 mg/ml 40K + 1 mM DTAB.

For 9 mM (close to the CMC), the mixed profile is initially influenced by the surfactant which it follows closely (Figures 6.2.6 to 6.2.10).

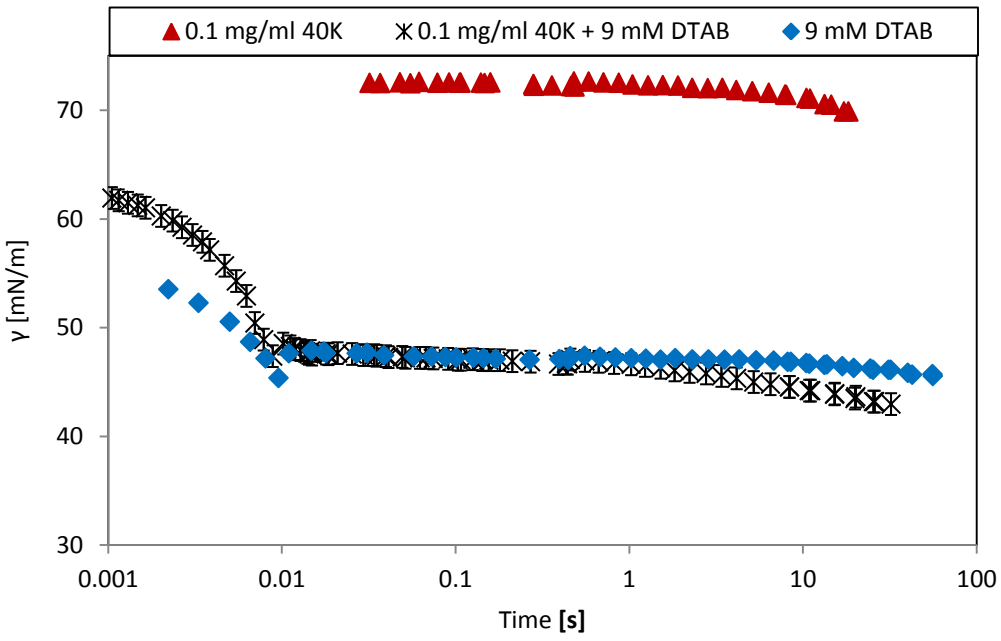

Fig. 6.2.6. Dynamic surface tension for 0.1 mg/ml 40K + 9 mM DTAB.

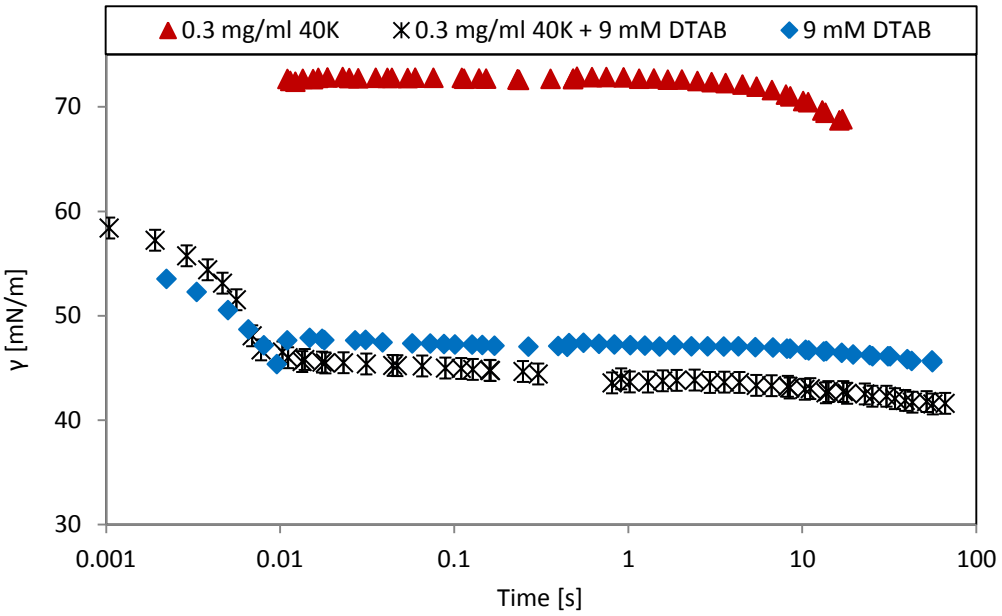

Fig. 6.2.7. Dynamic surface tension for 0.3 mg/ml 40K + 9 mM DTAB.

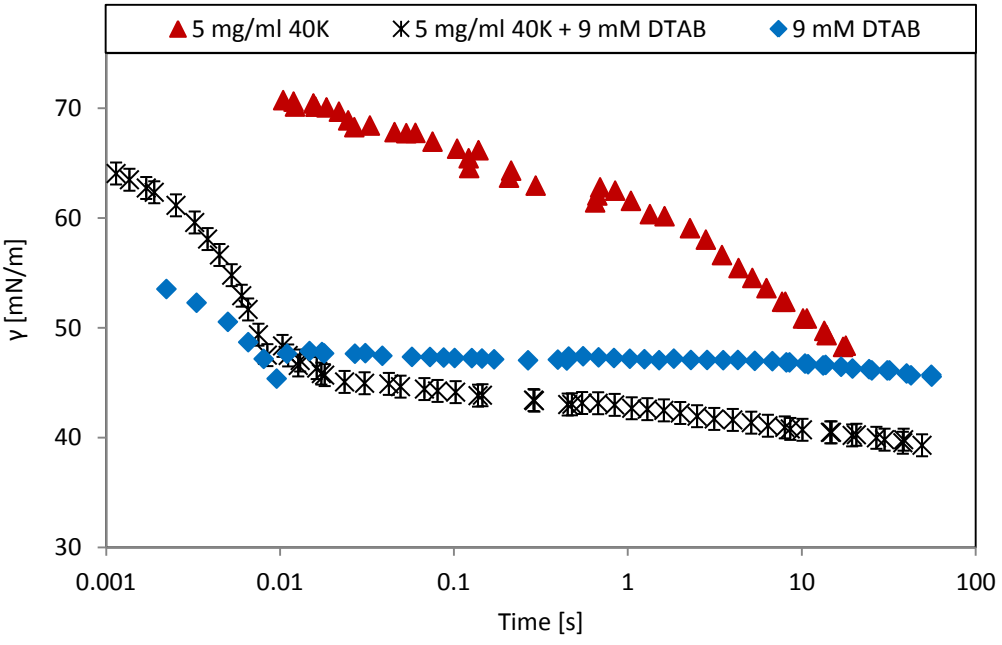

Fig. 6.2.8. Dynamic surface tension for 5 mg/ml 40K + 9 mM DTAB.

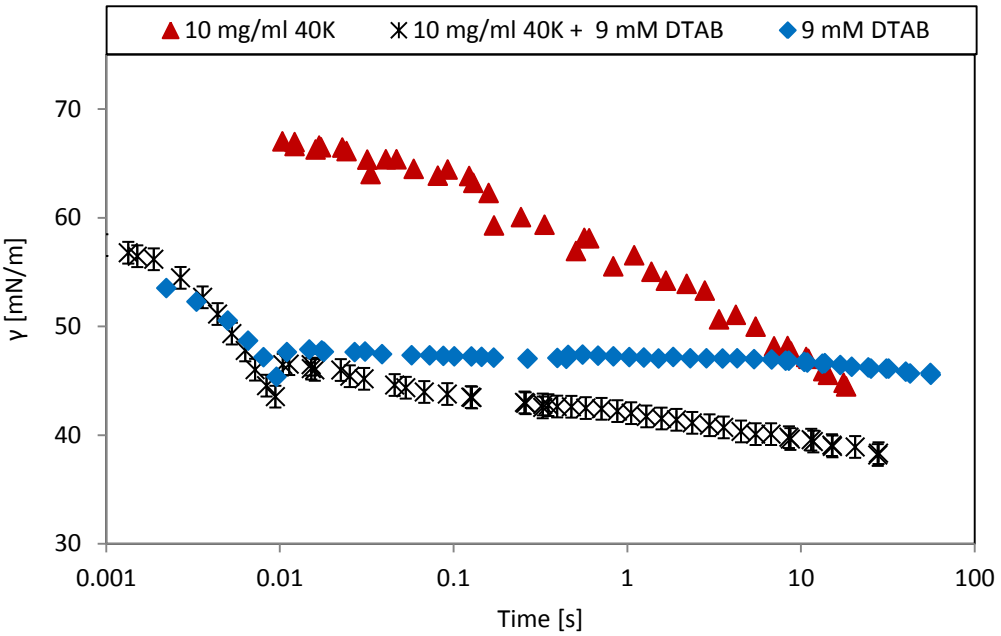

Fig. 6.2.9. Dynamic surface tension for 10 mg/ml 40K + 9 mM DTAB.

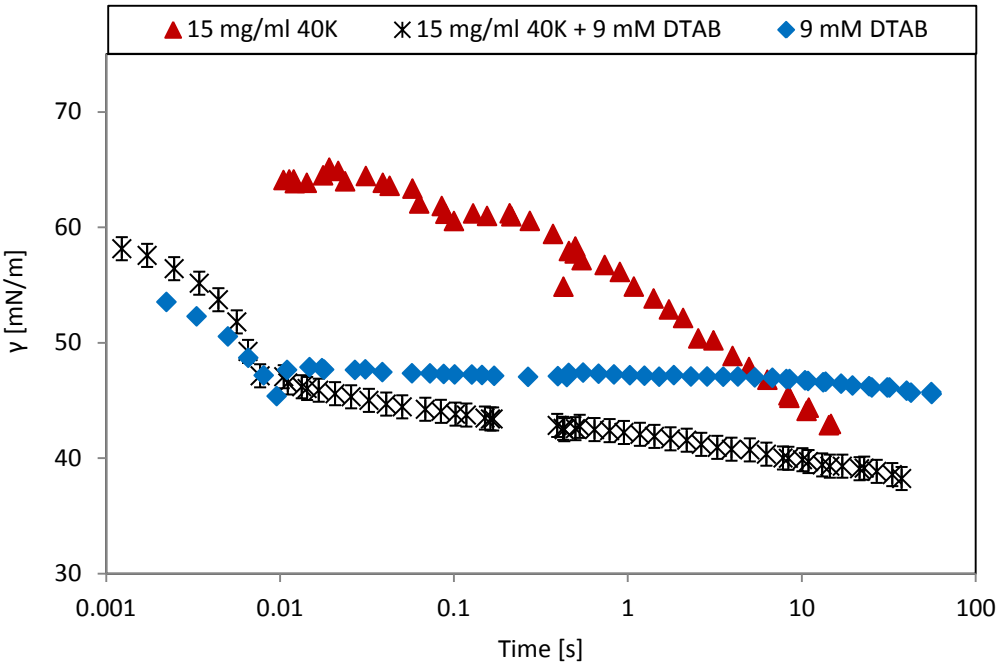

Fig. 6.2.10. Dynamic surface tension for 15 mg/ml 40K + 9 mM DTAB.

This behaviour differs from the surfactant-only curve after the induction of the polypeptide can be considered past, i.e. the surface tension starts decaying.

For 18 mM (above the CMC), the adsorption of the mixed sample is dominated by the surfactant (Figures 6.2.11 to 6.2.15).

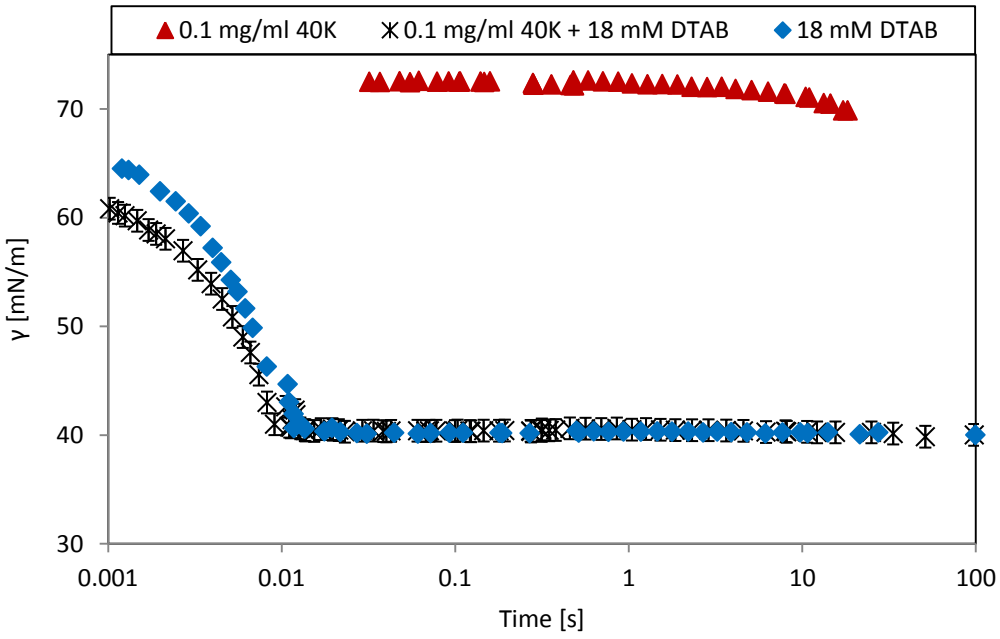

Fig. 6.2.11. Dynamic surface tension for 0.1 mg/ml 40K + 18 mM DTAB.

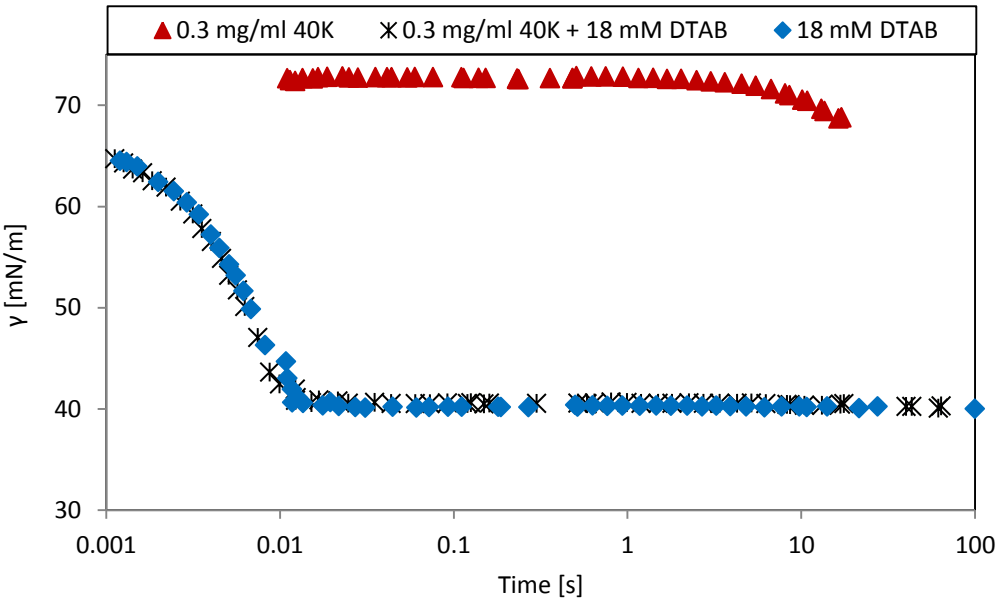

Fig. 6.2.12. Dynamic surface tension for 0.3 mg/ml 40K + 18 mM DTAB.

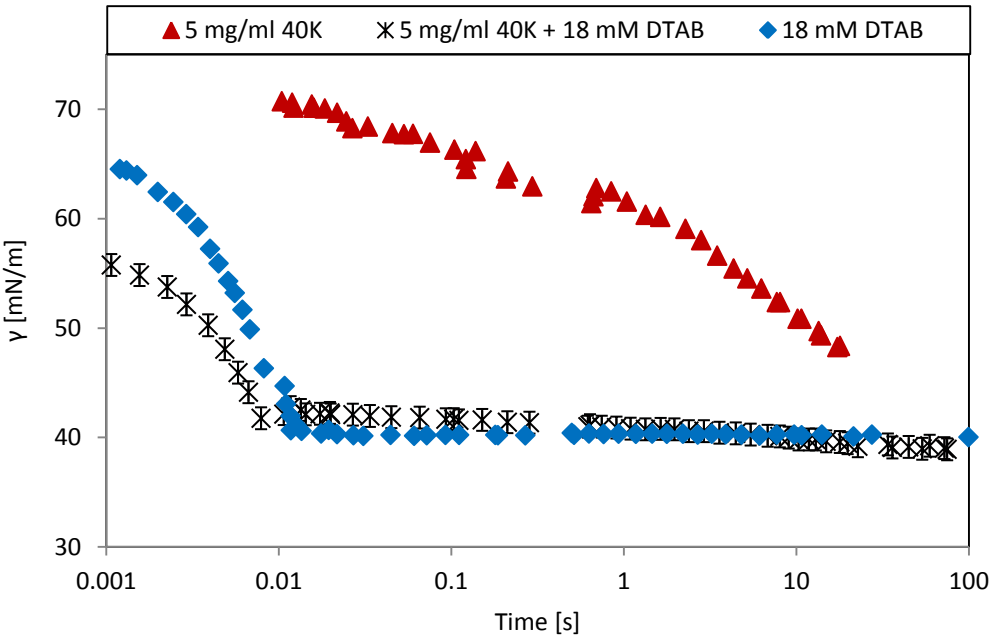

Fig. 6.2.13. Dynamic surface tension for 5 mg/ml 40K + 18 mM DTAB.

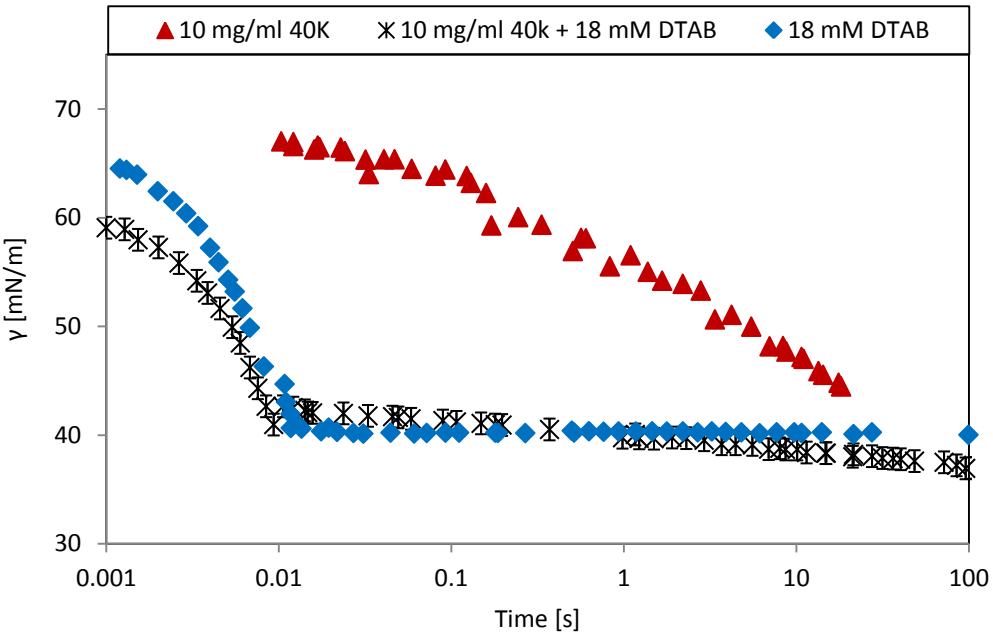

Fig. 6.2.14. Dynamic surface tension for 10 mg/ml 40K + 18 mM DTAB.

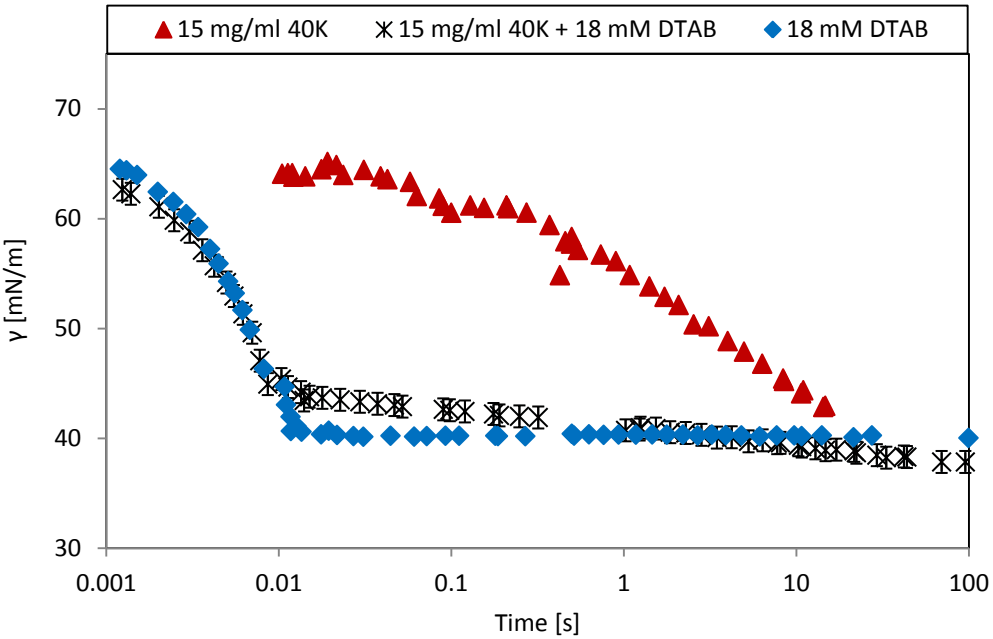

Fig. 6.2.15. Dynamic surface tension for 15 mg/ml 40K + 18 mM DTAB.

Within each surfactant concentration, the differences observed with addition of polypeptide are similar. For 1 mM DTAB, the mixed curve below the CAC after 0.01 s is concave and above the CAC, it is convex. It starts decaying after the polypeptide starts adsorbing at the interface.

The typical shape of a dynamic surface tension curve can be divided into four parts: an induction period, a rapid fall, a mesoequilibrium state and equilibrium [15]. If a curve is observed to adopt only a concave form, the mesoequilibrium region has not yet been reached.

For 9 mM DTAB, the profile of the mixture after 0.01 s decays almost linearly with time. For 18 mM DTAB and after 0.01 s, the mixture exhibits a nearly flat line for 0.1, 0.3, 5 and 10 mg/ml of polypeptide. With 15 mg/ml, there is an initial increase in surface tension values compared to the other polypeptide concentrations led by the increase in polypeptide in the bulk phase.

According to Alahverdjieva et al. [16], the dynamic adsorption process can be said to be controlled by a diffusion-only mechanism when the dynamic surface tension profile exhibits a concave shape. If the resultant shape is convex, a mixed diffusion-kinetic mechanism is responsible for the profile, i.e. for the protein to desorb, an energy barrier must be overcome. The concentration of protein determines the outcome. With 18 mM, the mixture follows a flat horizontal line at ~40 mN/m, i.e. it has undergone the induction period and the rapid fall and it has now reached the mesoequilibrium state. This position is shared by the surfactant-only curve demonstrating its dominance at high concentrations.

When 9 mM of DTAB is added to the polypeptide solutions, the mixed curves initially follow very closely the behaviour of the surfactant, especially at low polypeptide concentrations. However, when the lag time for the individual polypeptide has ended, the mixed curves suffer a further decrease in surface tension positioning them at lower values that those of the individual components. This is consistent with the lower equilibrium surface tension values obtained at this concentration.

With addition of 1 mM of DTAB, the rate of adsorption is greatly enhanced. The lag time of the mixed curve is shorter than that for the surfactant or the polypeptide. After approximately 10 s and for polypeptide concentrations over the CAC, the mixed profile and the curve for the individual polypeptide reach similar values. Thus, even though the values of surface tension are almost equal after 10 s, the rate of adsorption has been accelerated in the case of the mixed solutions in comparison with the polypeptide alone before this time. Nevertheless, the dynamic measurements suggest that this trend is reversed after this time. Thus, it can be concluded that the mixed samples differ in their adsorption behaviour from the individual components.

Furthermore, comparing the profiles of the mixtures with 1 and 9 mM of DTAB, it is possible to see that for the higher DTAB concentration, the surfactant is greatly influencing the interfacial adsorption process, whereas for the lowest DTAB concentration, there is clearly a synergistic effect that results in improved adsorption. This picture is consistent with the model described in relation to the equilibrium surface tension values, i.e. there are different kinds of complexes adsorbing at the interface at 1, 9 and 18 mM of DTAB. They are increasingly DTAB-rich with increasing concentration of surfactant and behave differently in regards to interfacial adsorption with the highest synergistic effect seen at the lowest DTAB concentration which falls within the plateau region in Figure 6.1.1.

Similar to the 40 KDa polypeptide mixed with SDS, there is a switch point in the dynamic behaviour which is located between 1 and 9 mM of DTAB for a polypeptide concentration of 0.1 mg/ml. For higher polypeptide concentrations, although no dynamic data is available at DTAB concentrations below 1 mM, i.e. in region A according to the description of the ‘S’-labelled curve, it is possible to assume that the switch point occurred at DTAB concentrations below 1 mM since all the dynamic profiles for the mixtures exhibit a double relaxation mode. In other words, the mixed profiles at these concentrations have followed the initial concave shape (lag time and rapid fall) at short times and the convex shape (mesoequilibrium leading to equilibrium) at higher times [2, 15].

For high polypeptide concentrations, all curves are concave up to approximately 0.01 s. Beyond this point in time, their shapes are either convex or nearly flat. Thus, following

Ritacco's arguments [2], an energy barrier comes into play at these concentrations that exhibit an intermediate plateau starting at ~0.01 s and the adsorption process switches from a diffusion-only to a mixed diffusion-kinetic model.

Evidence of this adsorption barrier in DTAB-only curves has been already presented by Ritacco et al. [2] who found that the diffusion coefficient at short times fits the diffusion only model with a value of $\sim 10^{-6}$ $cm^2 \cdot s^{-1}$. For longer times, the diffusion follows an exponential model that they failed to explain in terms of electrostatic interactions by applying a Poisson-Boltzmann based model.

They also observed a change in behaviour for DTAB solutions at concentrations in the range 2 to 3 mM. Furthermore, they related the intermediate plateau region in the dynamic profiles with a possible surface phase transition that takes place at constant surface pressure.

This change in behaviour for DTAB-only solutions is also supported by the adsorption studies conducted by Gilanyi et al. [14] in which the surface adsorbed amounts could be separated in two distinct regions, i.e. below and above $2 \cdot 10^{-6}$ $mol \cdot m^{-2}$. Below this adsorbed amount, the adsorbed layer is gas-like. Above this amount, the layer adsorbed is a liquid-like alkane layer.

This is also consistent with the existence of an adsorption barrier after a certain amount of material has been adsorbed at the interface. The mixed solutions seem to replicate this behaviour, exhibiting formation of a surface film in the presence of polypeptide at DTAB concentrations below 1 mM. The existence of the energy barrier and the presence of a surface film at concentrations in region A according to Bell's model [3, 7], point towards the formation of polymer/surfactant monomer complexes.

Noskov et al. [8] reviewed the literature for the DTAB/PSS system at DTAB concentrations below the CMC. In summary, a drop in surface elasticity was found at concentrations close to the CMC. The time to reach equilibrium adsorption values varied from several hours at low DTAB concentrations to less than an hour close to the CMC and the viscoelastic properties of the surface formed at low surfactant

concentrations resembles that of the pure surfactant indicating strong hydrophobic interactions. Although electrostatic interactions do exist between DTAB and PSS, it is the hydrophobic interaction that leads the adsorption process which is not purely diffusion controlled even at low DTAB concentrations much less than the CMC. Noskov et al. [8] associated the non-monotonous changes in the dynamic surface tension profiles to the formation of aggregates.

Similarly, in the 40K/DTAB system, equilibrium adsorption is reached at different times depending on the different surface structures present. Thus, at low surfactant concentrations mixed with 0.1 mg/ml of 40 KDa, the polypeptide co-adsorption never reached the equilibrium within 5 hours. For DTAB concentrations 0.1 and 1 mM (region A in the equilibrium surface adsorption isotherm) it took approximately 10 hours on the basis of surface tension changes. At higher polypeptide concentrations, equilibrium surface tension was reached at shorter times due to the high surface activity of the polypeptide. The existence of an energy barrier causes the solute to back diffuse to the bulk phase from the subsurface instead of adsorbing to the interface, thus prolonging the dynamic surface tension decay. According to Noskov et al., this time effect reflects the formation of different structures with different adsorption and interfacial elasticity.

Since we expect to find different complexes at different concentrations which reach equilibrium at different times, it is intuitive to also expect changes in the interfacial elasticity. Addition of salt proved the existence of electrostatic interactions yet dynamic surface tension shows that the adsorption profiles are in agreement with the existence of an energetic barrier which according to Ritacco et al. does not necessarily follow a model based solely on electrostatic interactions. Moreover, at low DTAB concentrations, Noskov et al. believe hydrophobic interactions dominate the adsorption process in the DTAB/PSS system. Thus, once again, it is necessary to contemplate the lead of hydrophobic interactions in relation to the present system.

Figures 6.2.16 to 6.2.19 clearly show that for mixtures of DTAB with polypeptide, the adsorption dependence with time is very similar to that of the surfactant at concentrations close to or above the CMC. Below the CMC, the reduction of surface tension at all times presented in these Figures is more effective for the mixtures than for the surfactant. At 0.1 mg/ml of 40 KDa polypeptide however, surface tension is noticeably reduced after 1 s in comparison with the behaviour exhibited by the surfactant only. Before this time, the surfactant dominates the adsorption process.

At 10 s, all mixtures with polypeptide concentrations above the CAC have already reached surfactant only levels of reduction in surface tension.

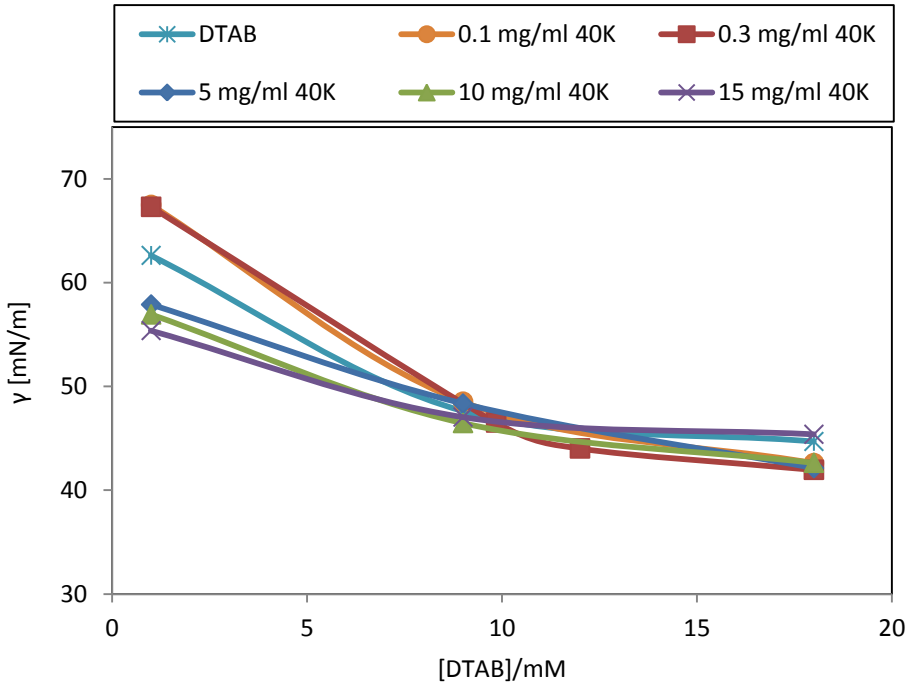

Fig. 6.2.16. Dynamic surface tension for the 40K/DTAB system at 0.01 s.

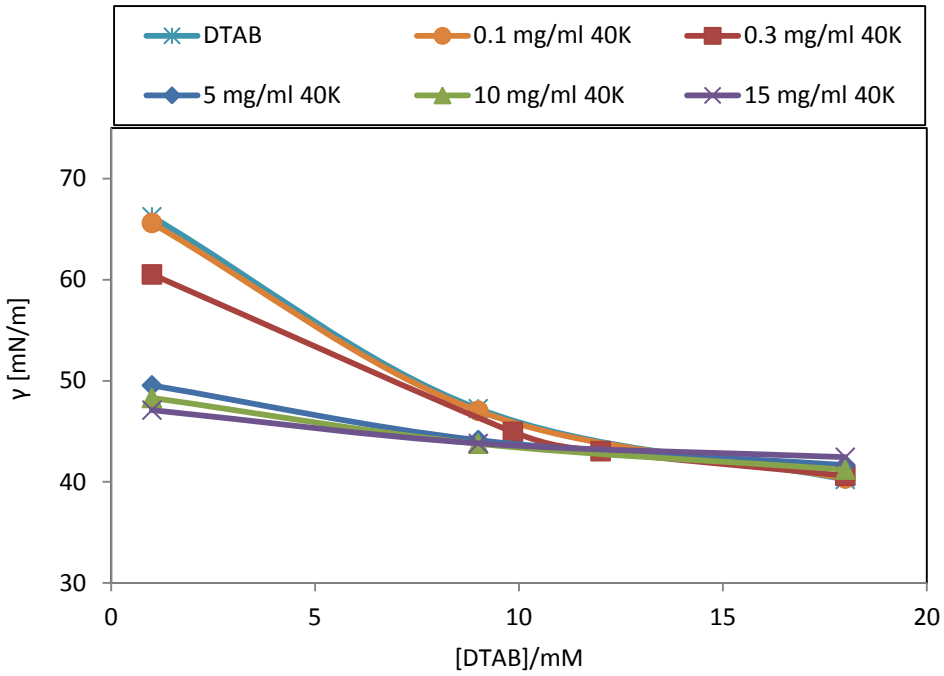

Fig. 6.2.17. Dynamic surface tension for the 40K/DTAB system at 0.1 s.

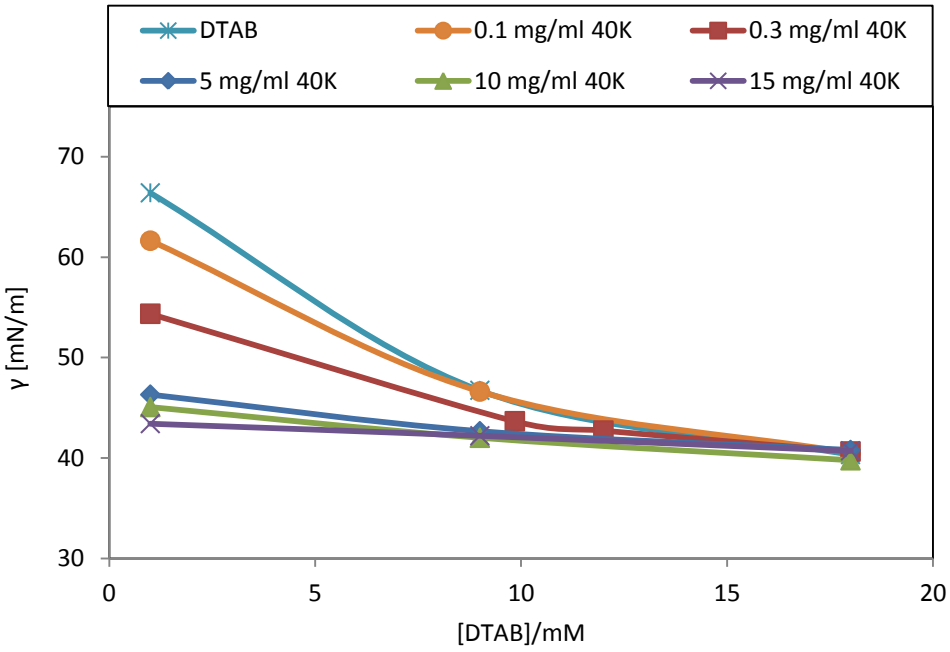

Fig. 6.2.18. Dynamic surface tension for the 40K/DTAB system at 1 s.

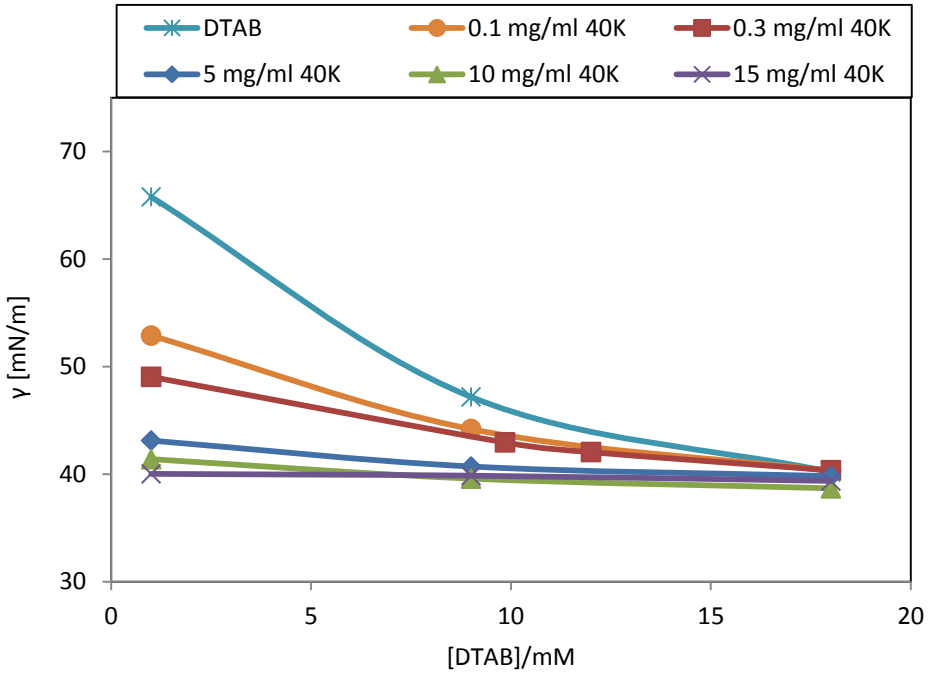

Fig. 6.2.19. Dynamic surface tension for the 40K/DTAB system at 10 s.

6.3. ζ-potential

The ζ-potential of polypeptide mixtures with DTAB was investigated at the CAC of the polypeptide and below and above the CMC of the surfactant. The results are shown in Figure 6.3.1.

The addition of DTAB to the polypeptide reduces the ζ-potential at pH 2.2 and pH 3 to similar values almost irrespective of the amount of DTAB added. At pH 5 and above, the addition of DTAB also lessens the charges present in the polypeptide. However, there is a clear relation between the amount of surfactant added and the resultant differences in ζ-potential with respect to the polypeptide. From pH 5 to pH 7.8, the curves are approximately linear for every fixed amount of DTAB added. Neutrality points are displaced towards slightly higher pH values with the ζ-potential profile for the mixture with 12 mM DTAB crossing the 0 ζ-potential at pH 5 followed very closely by the mixtures with 9 mM DTAB, i.e. close to the CMC of the surfactant.

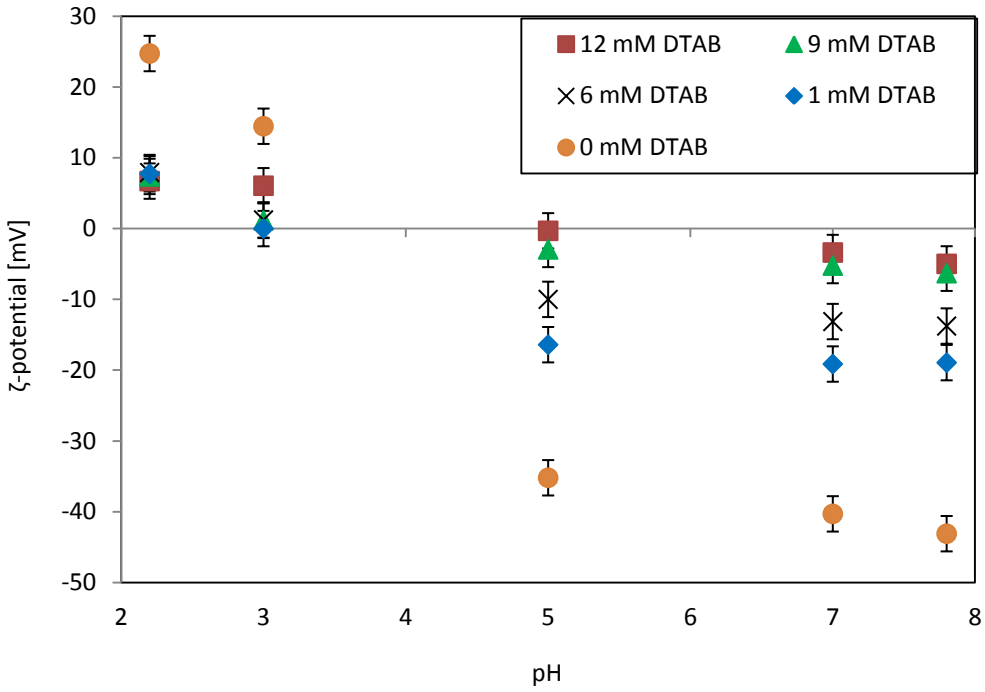

Fig. 6.3.1. ζ-potential for mixtures of 1 mg/ml of the 40 KDa polypeptide and DTAB at different DTAB concentrations.

As in the case of mixed polypeptide with SDS, the results show the effects of the polypeptide encapsulating the surfactant. With increasing surfactant present in the solution, the effect is diminished and the negatively charged polypeptide, i.e. pHs ≥ 5, becomes less negative. This gradually brings the mixed solutions deeper into the unstable region, see Figure 6.3.2.

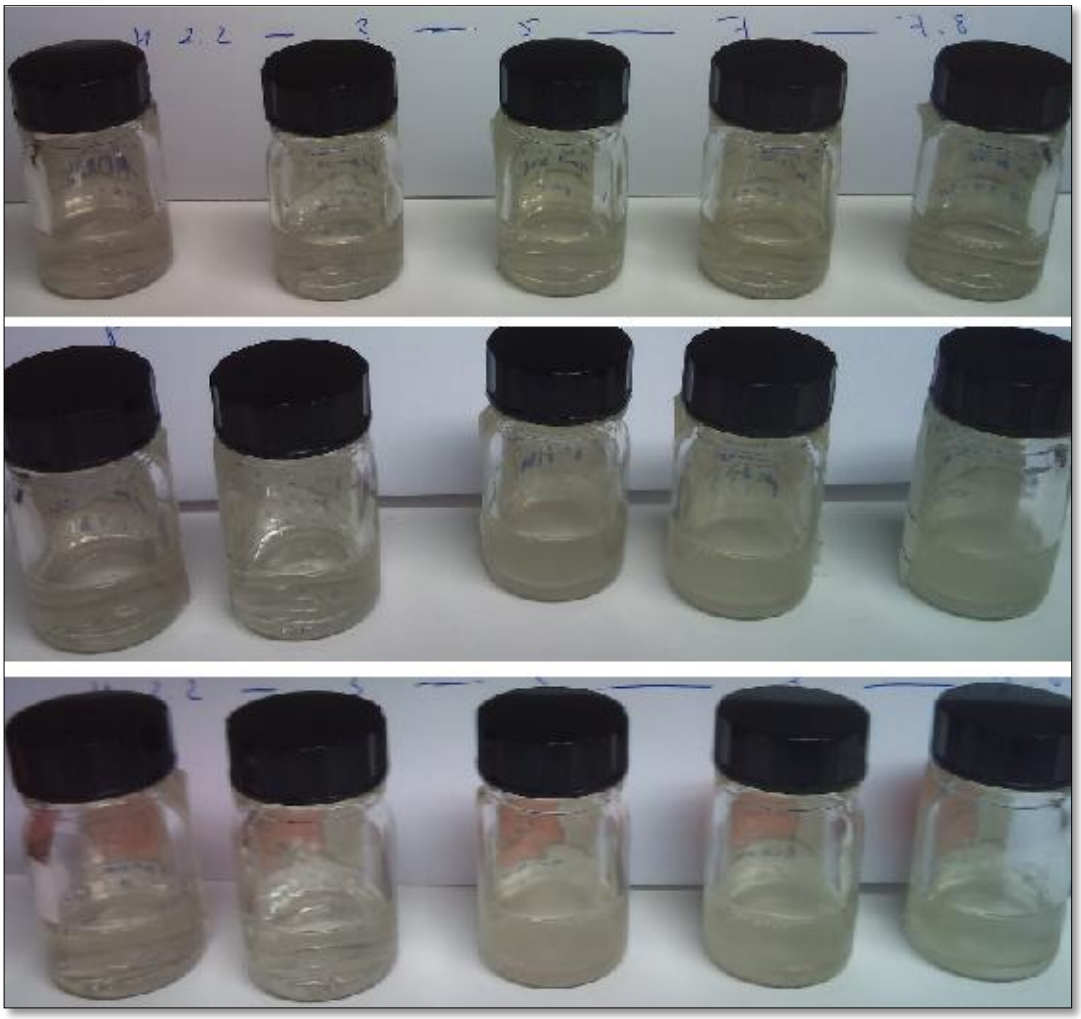

Fig. 6.3.2. Mixed solutions of 1 mg/ml of 40 KDa polypeptide with (top) 1 mM DTAB, (middle) 6 mM DTAB and (bottom) 9 mM DTAB, at pH (from left to right) 2.2, 3, 5, 7 and 7.8, respectively. Colloidal aggregates can be visually observed at pH 5, 7 and 7.8 at DTAB concentrations 6 and 9 mM.

Contrary to the observations with SDS, the ζ-potential depends on surfactant concentration at a pH close to the isoelectric point of the polypeptide (Figure 6.3.3). Thus, the different type of charges added to the solution by DTAB and SDS results in different effects on the colloidal stability of the solutions. Whilst addition of SDS reinforces the stability at pHs above the isoelectric point of the polypeptide, the addition of DTAB leads to the formation of aggregates at every pH probed according to the ζ-potential results. Salt addition inhibits their formation as observed by naked eye and proved via the ring method.

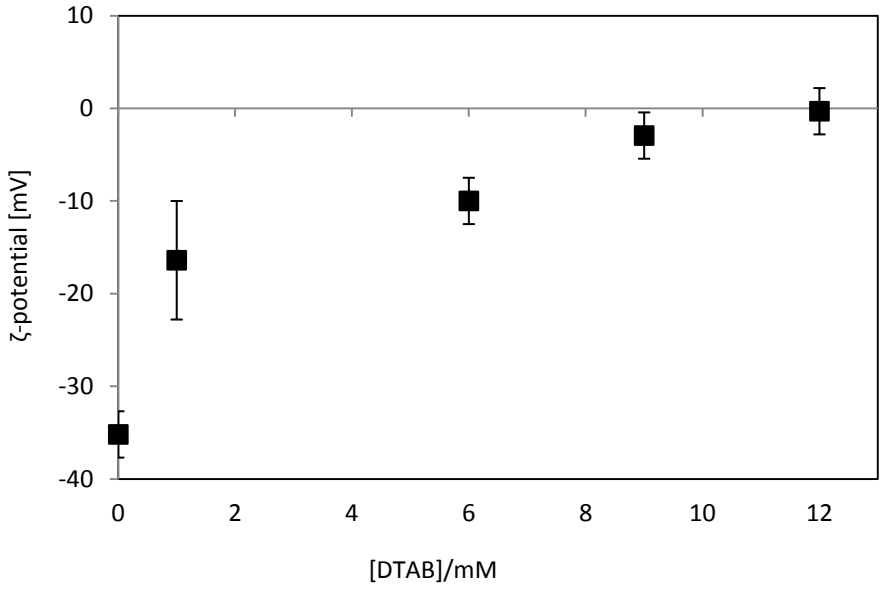

Fig. 6.3.3. ζ-potential for 1 mg/ml of the 40 KDa polypeptide as a function of DTAB concentration at pH 5.

For systems composed of lysozyme and DTAB, Mosquera et al. [17] found that at pH 3.2 the lysozyme is protonized and thus no electrostatic interaction takes place. This was demonstrated by the fact that the ζ-potential remained constant with increasing DTAB concentration. At pH 2.2 and pH 3, similar conclusions can be drawn for the 40K/DTAB system.

The point of zero charge is shifted from pH 3 with 1 or 6 mM DTAB to pH 5 with 12 mM DTAB. Hence, an increase in amount of DTAB in solution is reflected by the fact that charge reversal occurs at a higher pH, i.e. there is an increase in positive charges.
For a DTAB concentration of 5.5 mM, Mosquera et al. [17] concluded that the point of zero charge for the mixture with 1.25 mg/ml of lysozyme (pre-dialysis [17]) is at pH 10. The variation in the point of zero charge (pzc) with respect to 6 mM DTAB mixed with 1 mg/ml of the 40 KDa polypeptide, agrees with the initial difference in neutrality encountered in both biopolymers, i.e. the pI of lysozyme is at pH ~ 10 (see section 7.3).

6.4. Foam studies

The volumes of foam produced by 0.1, 1, 9 and 18 mM of DTAB were investigated in the absence and presence of 0.1 and 1 mg/ml of 40 KDa polypeptide. Some of the pictures recorded at different times for the different solutions tested are shown next.
Figure 6.4.1 clearly demonstrates the lack of ability to foam for DTAB concentrations 0.1 and 1 mM, i.e. below the CMC. In contrast, at 9 (close to the CMC) and 18 mM (above the CMC), DTAB produces high volumes of foam that although decaying with time, remain high after 15 minutes.

Rapid adsorption is required for the production of foams. The dynamic surface tension measurements of 1 mM of DTAB demonstrated its lack of ability for this purpose whereas 9 and 18 mM do show considerable adsorption within a few seconds.

When DTAB is mixed with the 40 KDa polypeptide at the CAC, i.e. 1 mg/ml, Figure 6.4.2 shows the generation of high volumes of foam (~5 ml) at the lowest DTAB concentrations relative to the volumes produced by the individual components (~0 ml for DTAB and 1.2 ml for 1 mg/ml of polypeptide) (see Figures 6.4.4 and 6.4.5). The dynamic surface adsorption measurements showed an almost constant DTAB adsorption at 1 mM reaching values at ~65 mN/m at 10 seconds. In Figure 4.2.1, the dynamic adsorption 1 mg/ml of 40 KDa polypeptide remains at high surface tension values (~71 mN/m) up to about 1 s when it starts decaying rapidly. In contrast, the mixed solution adsorbs rapidly within this time range and lowers the surface tension to ~61 mN/m at 1 s and ~49 mN/m at 10 s.

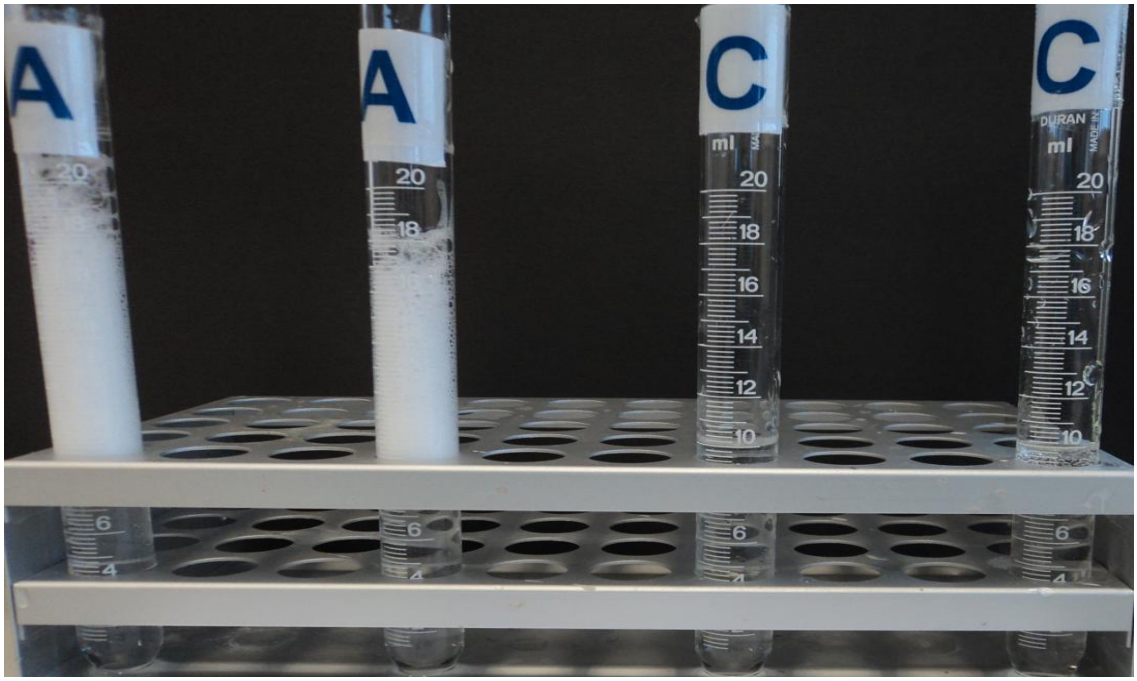

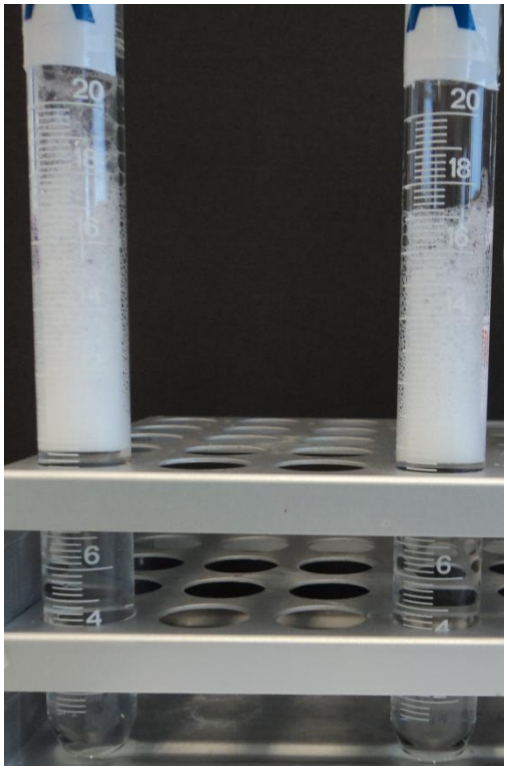

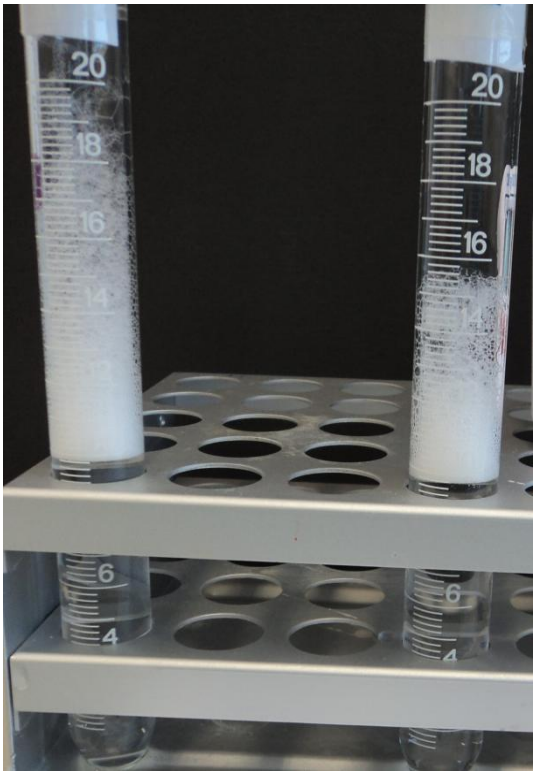

Fig. 6.4.1. Top: (left to right) 18, 9, 1, 0.1 mM DTAB at 10 seconds after shaking.
Bottom left: (left to right) 18,9 mM DTAB after 5 minutes.
Bottom right: (left to right) 18, 9 mM DTAB after 15 minutes.

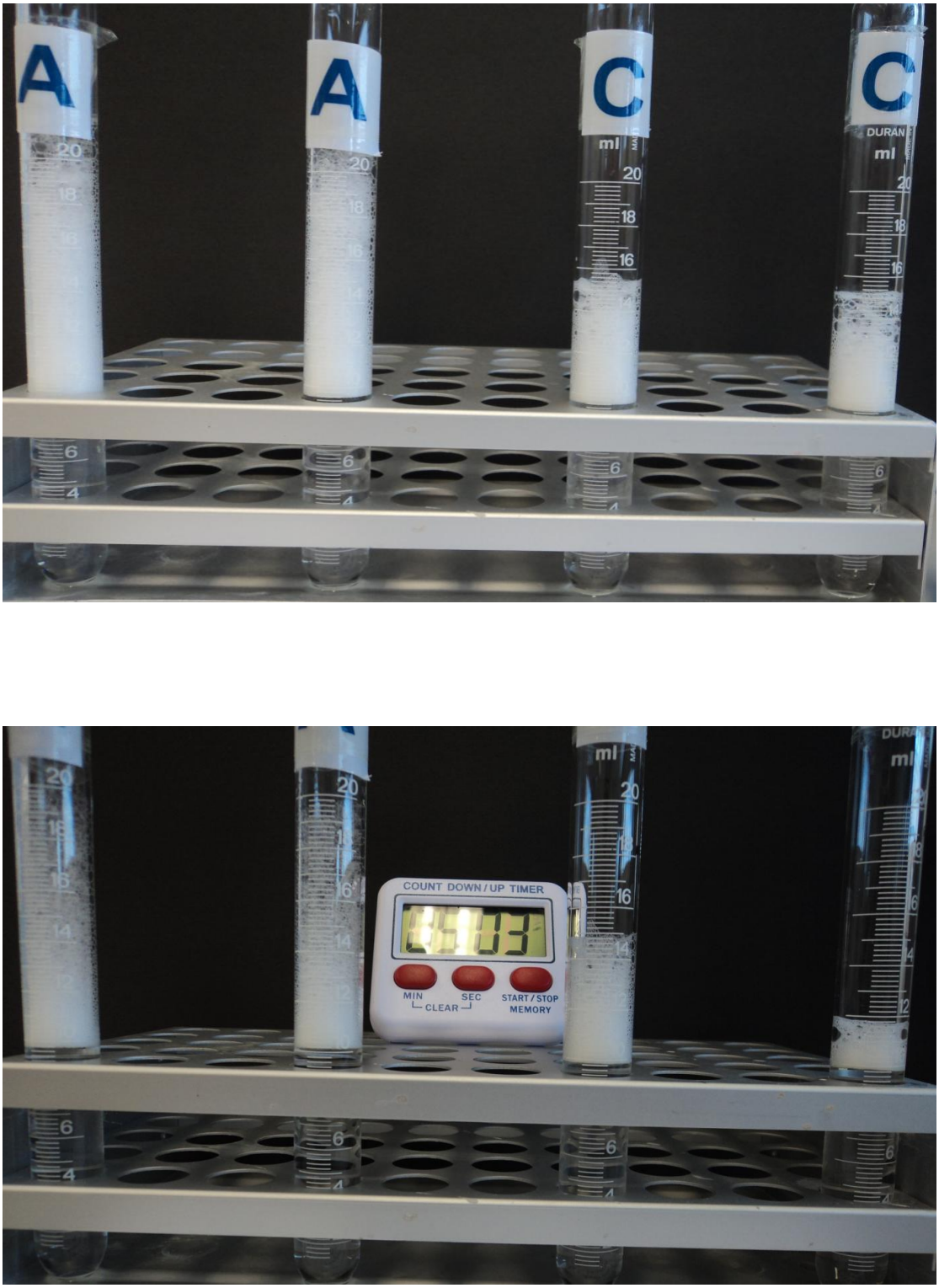

Fig. 6.4.2. Top: 1 mg/ml 40K + (left to right) 18, 9, 1, 0.1 mM DTAB at 10 seconds after shaking. Bottom: same samples after 5 minutes.

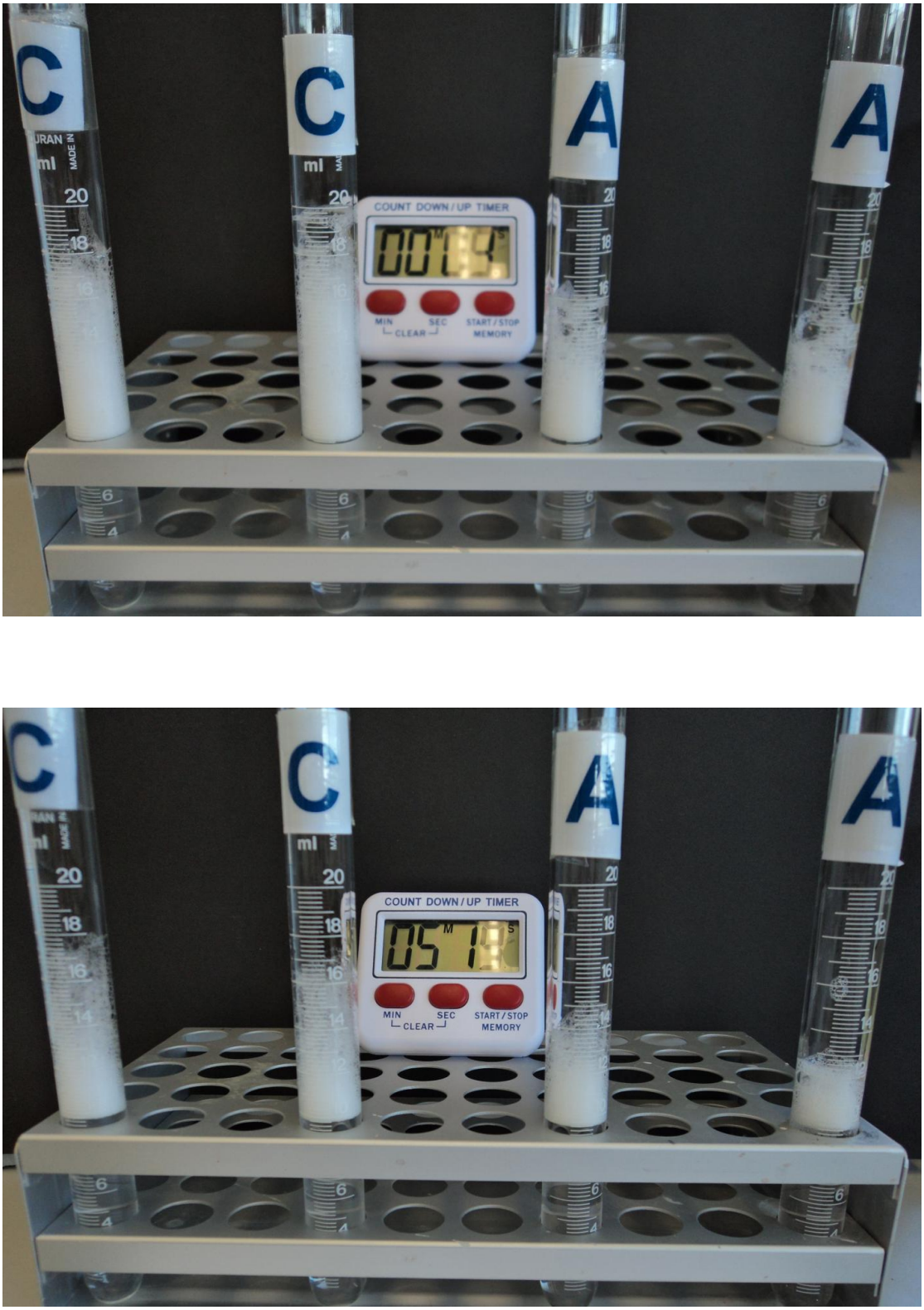

Fig. 6.4.3. Top: 0.1 mg/ml 40K + (left to right) 18, 9, 1, 0.1 mM DTAB at 9 seconds after shaking. Bottom: same samples after 5 minutes.

The volume of foams produced at the higher DTAB concentrations (Figures 6.4.6 and 6.4.7) are lower than those of the surfactant-only solutions immediately after shaking and become less dense after 5 minutes; although they still remain at high volumes. In the case of mixtures with 9 mM DTAB, the DTAB-only foam decays rapidly and the mixed foam remains stable and its volume is higher than that of DTAB alone after approximately 5 minutes from production. 18 mM DTAB also results in a high volume of foam (higher than for the mixture) and decays fast. At this concentration however, the volume remains at the same levels from approximately 5 to 15 minutes after shaking. The mixture behaves in a similar manner but the volumes it produces are lower than those obtained with DTAB in the absence of polypeptide.

For the mixtures with 0.1 mg/ml of 40 KDa polypeptide, i.e. Figure 6.4.3, similar behaviour to that shown by the mixtures with higher polypeptide concentration is observed. However, the volumes produced are lower in all cases (Figures 6.4.8 to 6.4.11). For 9 mM DTAB, the volume of the mixed foam surpasses that of the surfactant-only solution at around 2.5 minutes. For 18 mM DTAB, stability of both, pure surfactant and mixed solution, remain stable after ~7.5 minutes from production.

Thus, at low DTAB concentrations no foam is generated unless the solution is mixed with 40 KDa polypeptide. When this is the case, foam is generated due to a synergistic behaviour between both components. Although this behaviour exists at DTAB concentrations close to the CMC, its effect is not so noticeable in terms of ability to foam but remains strong in regards to foam stability.

The resulting foams from these mixtures, as in the case of mixtures with SDS, also seem to fit the model propose by Bykov et al. [6]. Hence, it is reasonable to assume that the transporting capabilities of the surfactant through the foam matrix and its rapid initial adsorption combined with the viscoelasticity of the polypeptide network lead to improved foam behaviour (ability to foam and stability) at low surfactant concentrations. The results are also in agreement with Mackie's interpretation of the situation [18]. At DTAB concentrations close to the CMC or higher, an excess of surfactant at the interface provokes the rupture of the protein network and the synergistic response observed at low concentrations is no longer observed due to the surfactant dominance of the interface. Considerable improvement in the ability to foam

is seen with respect to the polypeptide yet the overall results for generation of foams and their stability point towards a surfactant-only kind of behaviour with no obvious improvement over the ability to foam and stability of the latter; rather, a negative synergy.

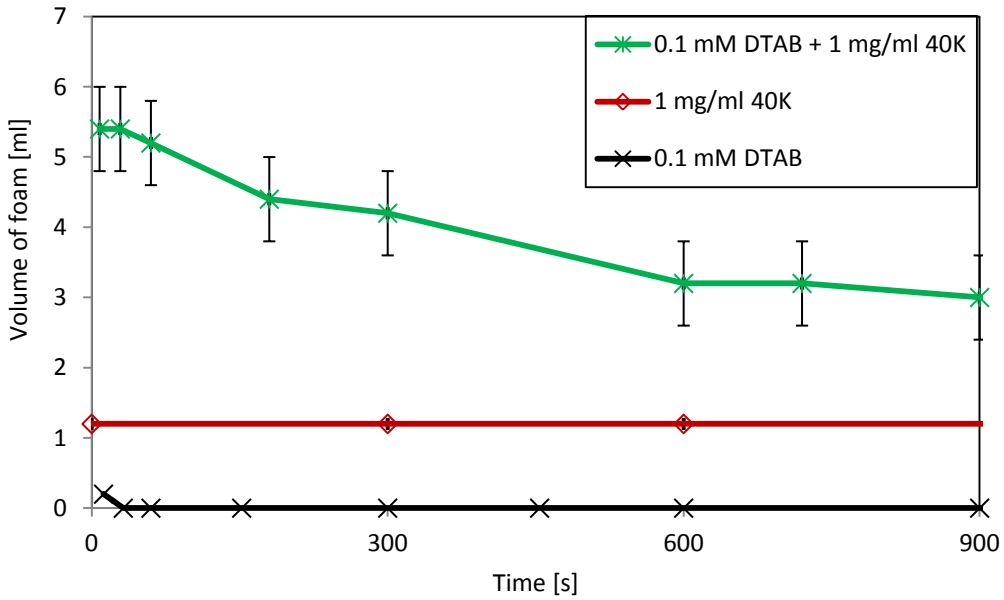

Fig. 6.4.4. Stability of foam produced by 0.1 mM of DTAB mixed with 1 mg/ml of polypeptide.

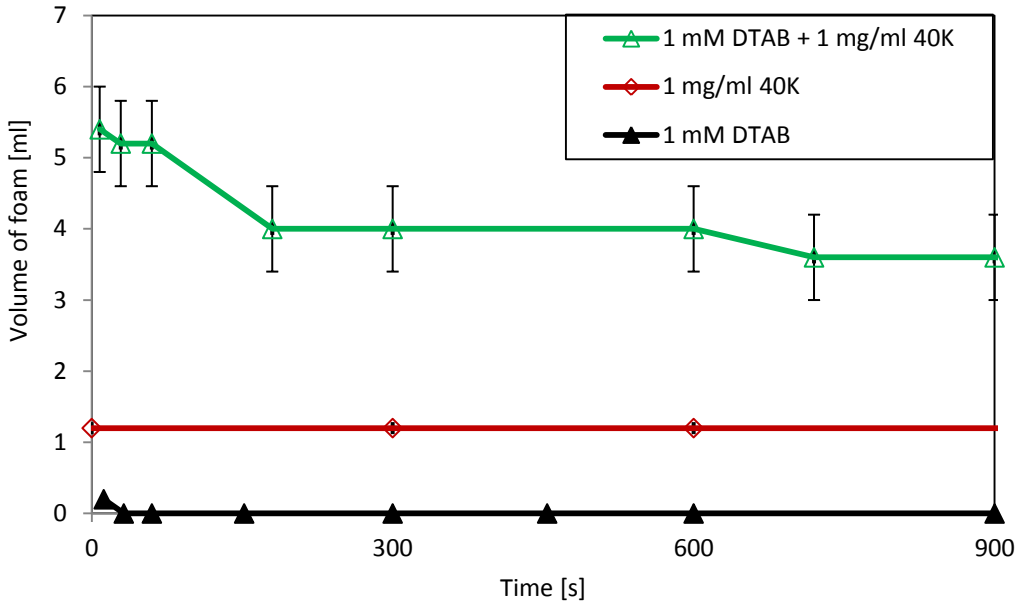

Fig. 6.4.5. Stability of foam produced by 1 mM of DTAB mixed with 1 mg/ml of polypeptide.

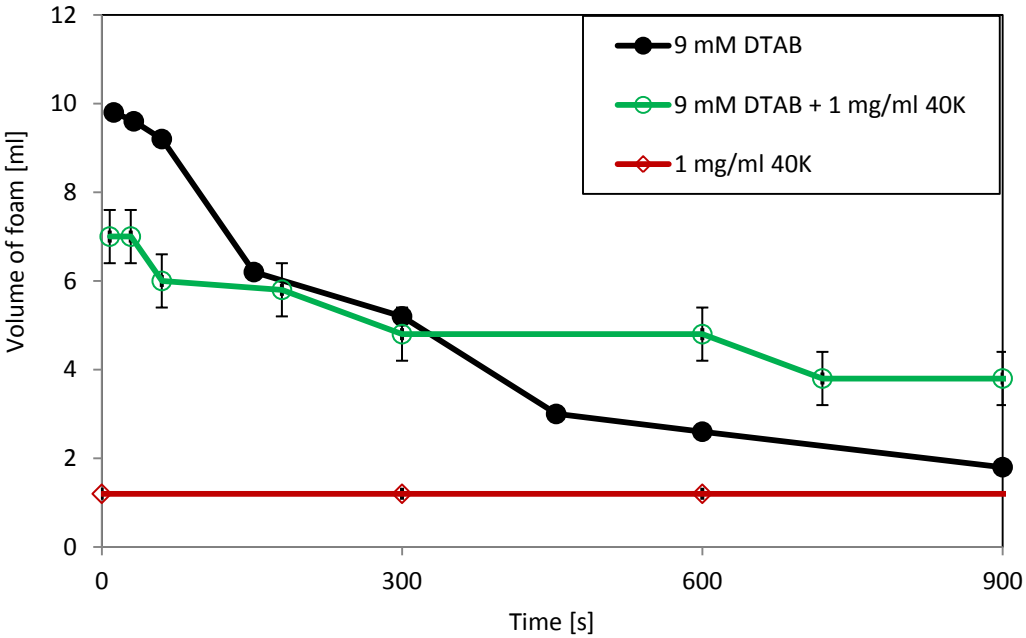

Fig. 6.4.6. Stability of foam produced by 9 mM of DTAB mixed with 1 mg/ml of polypeptide.

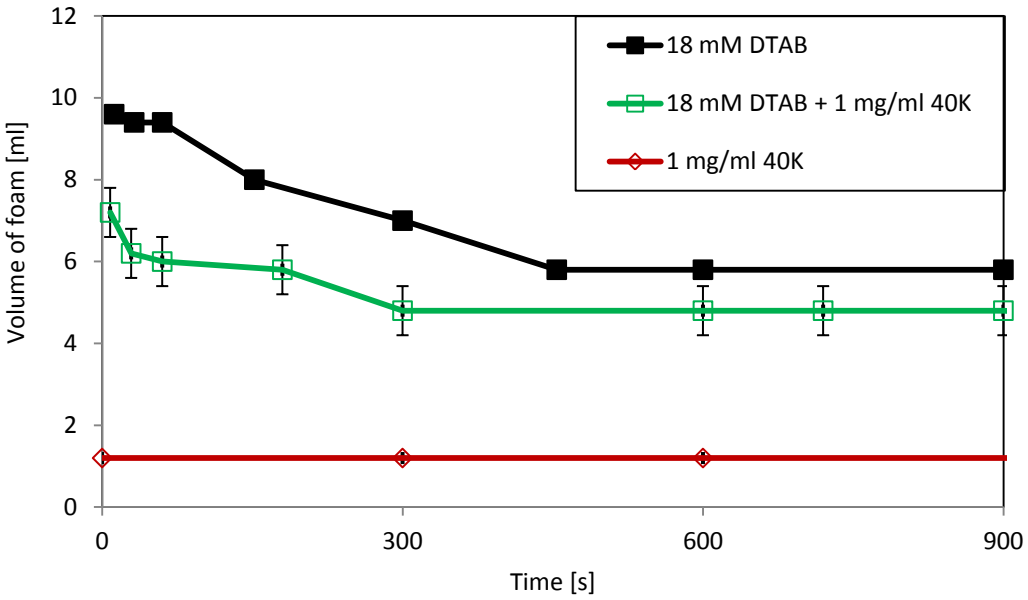

Fig. 6.4.7. Stability of foam produced by 18 mM of DTAB mixed with 1 mg/ml of polypeptide.

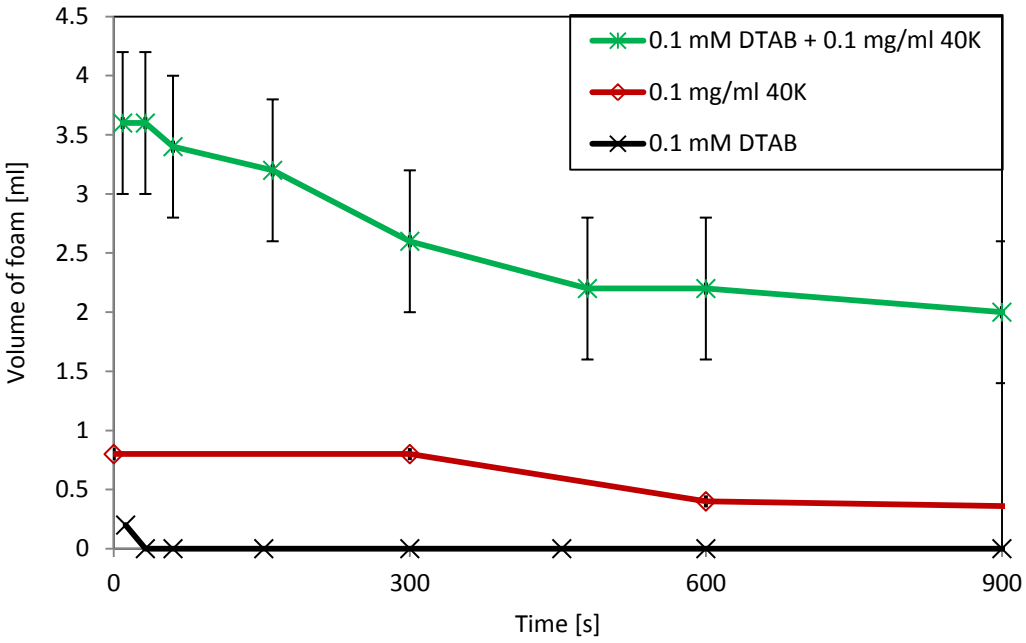

Fig. 6.4.8. Stability of foam produced by 0.1 mM of DTAB mixed with 0.1 mg/ml of polypeptide.

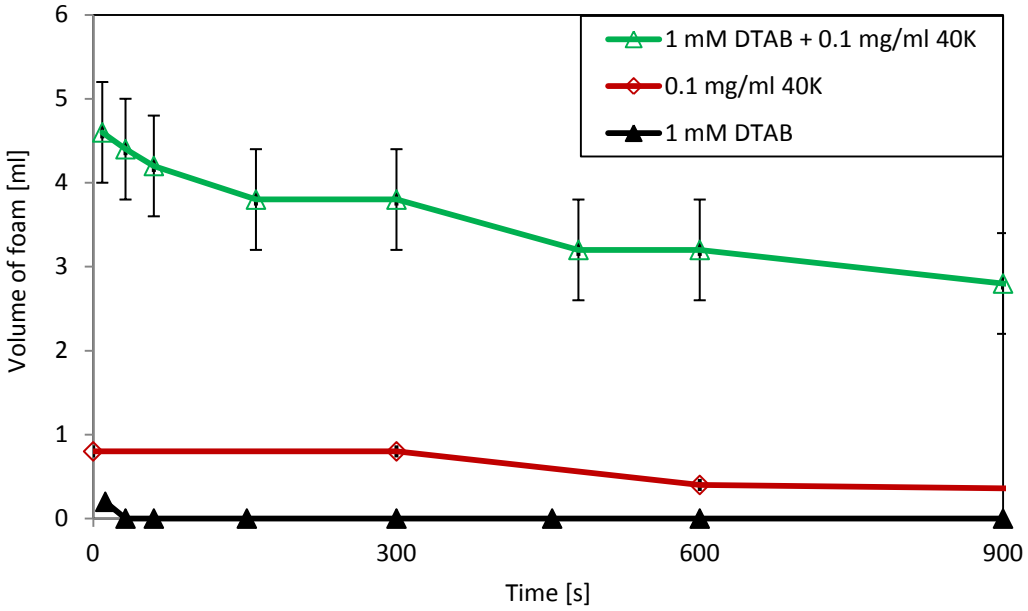

Fig. 6.4.9. Stability of foam produced by 1 mM of DTAB mixed with 0.1 mg/ml of polypeptide.

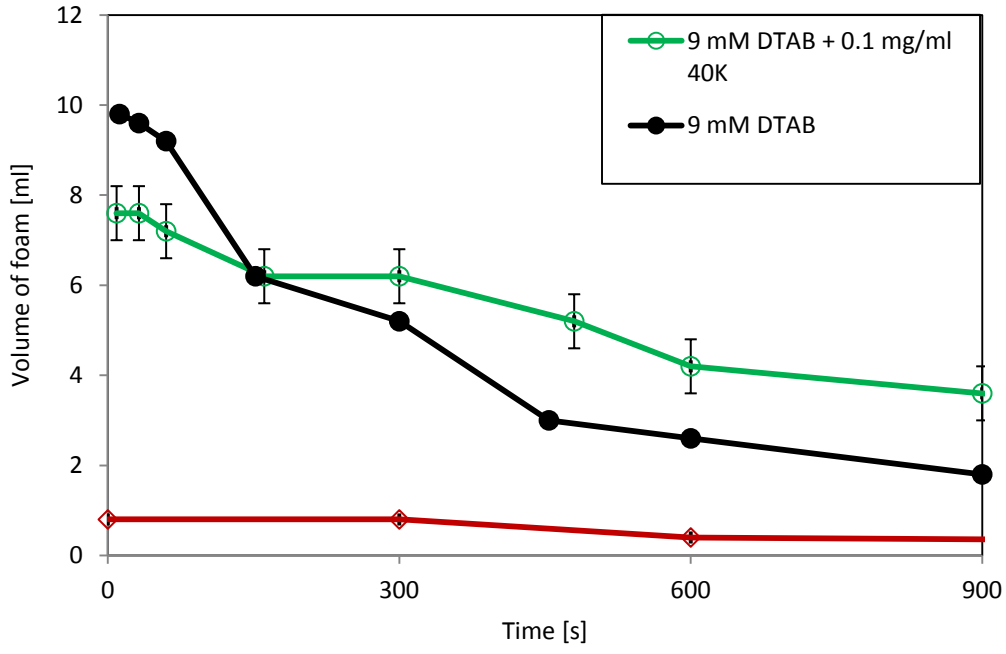

Fig. 6.4.10. Stability of foam produced by 9 mM of DTAB mixed with 0.1 mg/ml of polypeptide.

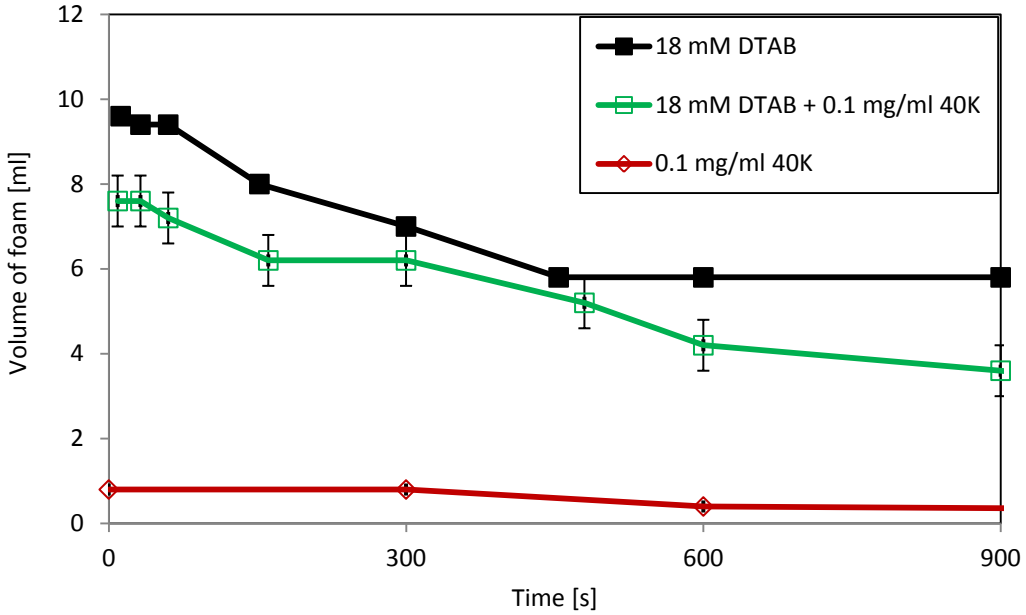

Fig. 6.4.11. Stability of foam produced by 18 mM of DTAB mixed with 0.1 mg/ml of polypeptide.

Figures 6.4.12 and 6.4.13 show how the volumes of foam produced by the mixtures do not improve in stability (within error) when doubling the surfactant concentration from 9 to 18 mM. After 5 minutes from generation, the volumes are approximately equal in the absence and presence of 0.1 and 1 mg/ml of polypeptide. With increasing time, the mixture with 9 mM of DTAB has a higher foam volume than DTAB alone. However, at a concentration above the CMC, the volume of DTAB-only foam is higher than the volume of the mixed foams.

At 0.1 and 1 mM of DTAB, since no foam was produced by the surfactant, the mixed foams represent a considerable improvement in the ability to foam. The fact that they remain almost at the same volumes after 5 and 15 minutes also highlights their stability and the strength of the interaction between both components.

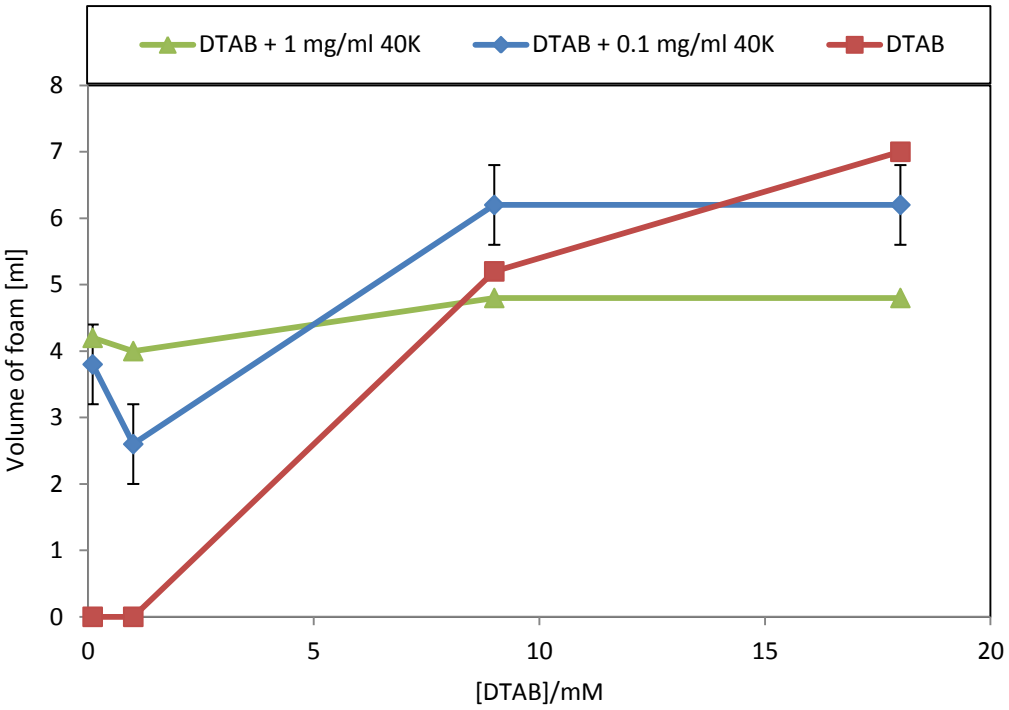

Fig. 6.4.12. Concentration dependence of foams as observed after 5 minutes.

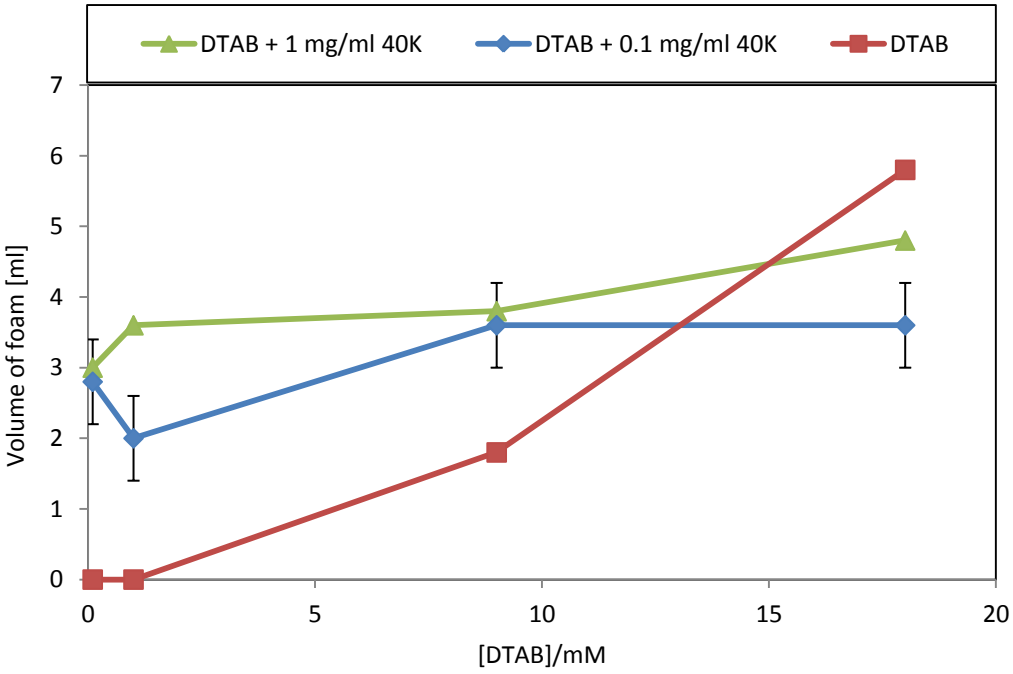

Fig. 6.4.13. Concentration dependence of foams as observed after 15 minutes.

6.5. Neutron reflection

The composition and structure of the interfacial layer formed by mixtures of 1 mg/ml of 40 KDa polypeptide and DTAB at different concentrations was studied with neutron reflection. The reflectivities obtained in Null Reflecting Water (NRW) are presented in Figures 6.5.1 to 6.5.10, i.e. protonated and deuterated surfactant mixed with polypeptide. All data shown in these Figures were modelled to a monolayer. The fitting parameters can be found in Tables 6.5.1 to 6.5.5. The calculated parameters obtained from these fittings are shown in Table 6.5.6.

For consistency of the model analysis, the thickness was fixed for each couple of protonated and deuterated samples. From the data mentioned above under NRW, it is possible to observe an overall decrease in the thickness of the polypeptide layer and scattering length density (for the protonated surfactant) with increasing surfactant concentration. The adsorbed amount of polypeptide at the interface also decreases accordingly. The adsorbed amounts of surfactant increase with increasing surfactant bulk concentration. The areas occupied per molecule of polypeptide and surfactant follow the inverse relation.

Figure 6.5.11(a) show the varying adsorbed amounts of the individual components and their relation with the number of surfactant molecules associated per polypeptide molecule, n. Three distinct regions can be distinguished. A first region covering low DTAB concentrations up to 1 mM; an intermediate region spanning from 1 mM to 10.5 mM, i.e. the CMC; and a final region starting at 10.5 mM where the DTAB concentrations above the CMC are found.

In comparison with equilibrium surface tension results, the first region is where the complexes of polymer/surfactant monomers are formed, i.e. region A. The second region corresponds to regions B and C where the increasing amount of surfactant molecules saturates the polypeptide and the amount of surfactant adsorbed at the interface surpasses that of polypeptide, i.e. the polypeptide is resolubilized and returns to the bulk solution. In the third region, there is not enough polypeptide present to inhibit the adsorption of surfactant-rich micelles at the surface as indicated by the increasing number of surfactant molecules per polypeptide molecule. This is region D in

the equilibrium surface tension profile matching to the formation of surfactant micelles in the bulk.

To compare the adsorption of DTAB in the presence and absence of polypeptide, Figure 6.5.11(b) has been plotted with data published by Lyttle et al. [19] of surface adsorbed amounts of DTAB in pure water as obtained with neutron reflection. At 4 mM, the layer thickness is 15 Å and the area occupied per DTAB molecule is 67 $Å^2$. At 14 mM, the layer thickness is 17.5 Å and the area occupied per DTAB molecule is 48 $Å^2$. These values result in a surface adsorbed amount of 0.83 $mg \cdot m^{-2}$ at 4 mM and 1.15 $mg \cdot m^{-2}$ at 14 mM. Lu et al. [1] reported a layer thickness for 14 mM DTAB in pure water of 19 ± 1 Å with an area occupied per molecule of 48 ± 2 $Å^2$.

At 14 mM DTAB, the area occupied per DTAB molecule in the presence of polypeptide is 42 Å and the layer thickness is 24 Å (higher than the value observed from DTAB alone in pure water). The differences arise from the presence of buffer and possible association of polypeptide, resulting in the net increase in surface excess. The change with respect to DTAB concentration however contrasts markedly with the data obtained for the mixed system with SDS where there is a clear difference in SDS adsorption from region B onwards. Given that the amounts of DTAB molecules remain almost intact, the structural changes must be a consequence of the polypeptide trying to adopt a more appropriate shape to reach the interface by infiltrating into the adsorbed surfactant molecules.

Moreover, the surface excess of 1 mg/ml of polypeptide alone is 2.32 $mg \cdot m^{-2}$. When adding 0.035 mM of DTAB to the solution, this amount is reduced to 1.70 $mg \cdot m^{-2}$ and the surfactant is already adsorbing at the interface with Γ = 0.21 $mg \cdot m^{-2}$. Figure 6.5.11(b) demonstrates that surface adsorption of DTAB is only slightly enhanced. However, the polypeptide adsorption into the interface is reduced with increasing surfactant amounts present in the bulk and at the interface.

The comparison with published data would not be complete without mentioning the existing differences with another DTAB/polymer system. Thus, when the polymer is a short PEI (~2 KDa) and it is kept at a fixed concentration of 60 mg/ml, the reflectivity

profiles at DTAB concentrations over 9 mM exhibit a Bragg peak as a consequence of the self-assembly of ordered structures that is displaced towards higher Q-values with increasing surfactant concentration [12]. For concentrations below 9 mM of DTAB, the mixed system with PEI does not show this feature or at least not clearly enough to be appreciable. If a PEI of higher molecular weight is employed (~750 KDa), the Bragg peak is observed even at ~2 mM of DTAB.

The 40 KDa polypeptide/DTAB system does not show any clear indications of Bragg peaks in the reflectivity profiles at the DTAB concentrations probed. However, it is worth noticing the difference in amount of polymer present in both studies. The appearance of three separate regions in Figure 6.5.11(a) demonstrates that some structural changes are taking place at certain surfactant concentrations. This was also observed with the plate method and clearly visualized with the foam studies. The thickness of the interfacial layer however, decreases with increasing surfactant concentration rather than increasing as in the PEI/DTAB system.

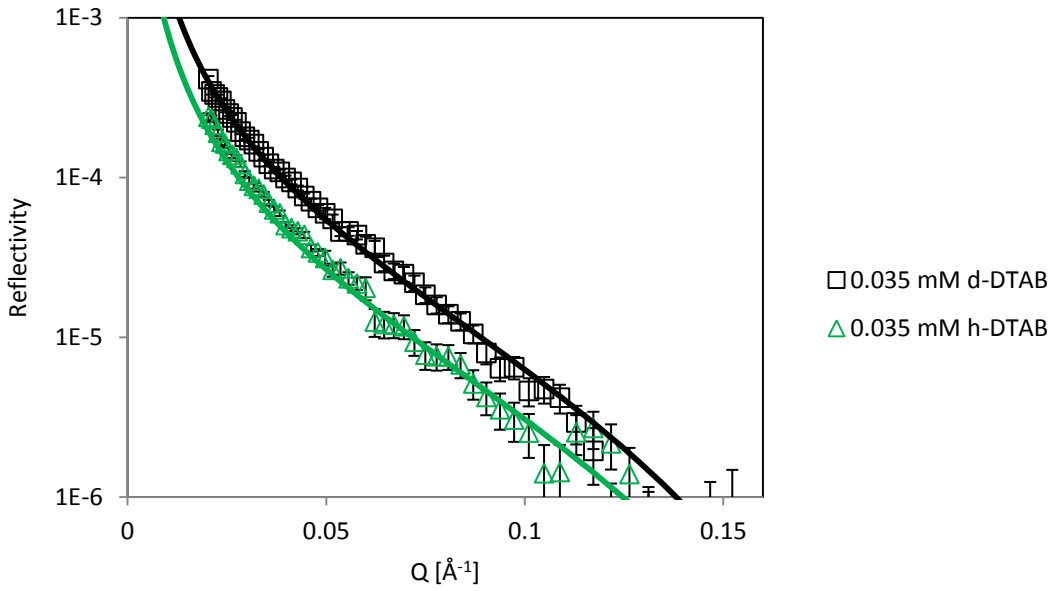

Fig 6.5.1. Neutron reflection data for 1 mg/ml 40K + 0.035 mM DTAB in NRW.

DTAB/mM	τ/ Å	P_h/ x10^{-6} Å^{-2}	τ·P_h/ x10^{-6} Å^{-1}	P_d/ x10^{-6} Å^{-2}	τ·P_d/ x10^{-6} Å^{-1}
0.035	33	0.70	23.10	1.0	33.00
0.35	32	0.55	17.60	1.2	38.40

Table 6.5.1. Fitting parameters used for the 1-layer model of 1 mg/ml 40K + 0.035 and 0.35 mM DTAB in NRW. The error in thickness is ± 3 Å and the error in scattering length density is ± 0.05 x10^{-6} Å^{-2}.

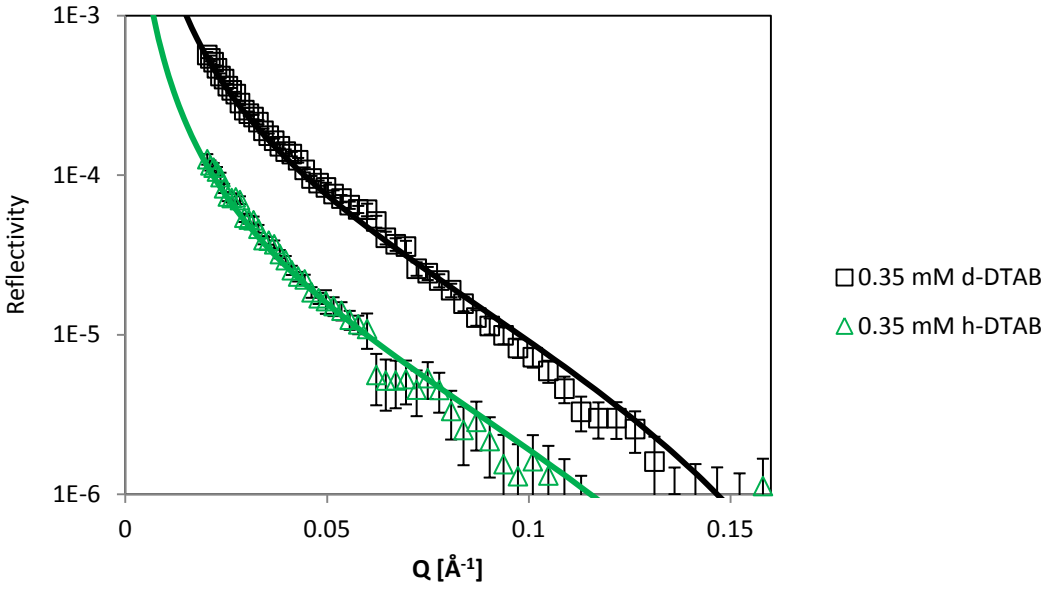

Fig. 6.5.2. Neutron reflection data for 1 mg/ml 40K + 0.35 mM DTAB in NRW.

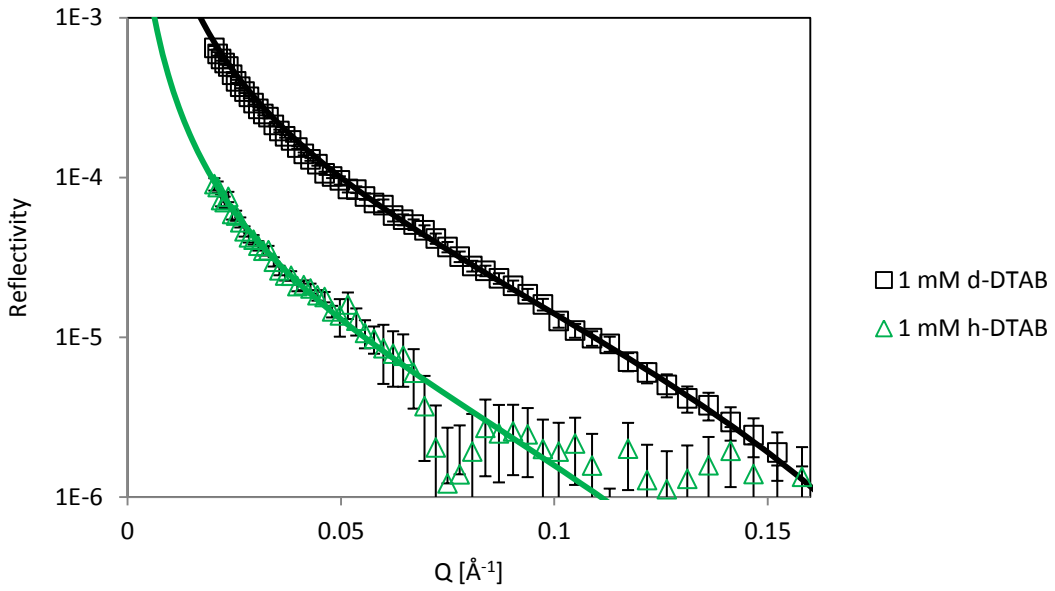

Fig 6.5.3. Neutron reflection data for 1 mg/ml 40K + 1 mM DTAB in NRW.

DTAB/mM	τ/ Å	P_h/ x10^{-6} Å^{-2}	τ·P_h/ x10^{-6} Å^{-1}	P_d/ x10^{-6} Å^{-2}	τ·P_d/ x10^{-6} Å^{-1}
1	32	0.50	16.00	1.50	43.50
3.5	32	0.30	9.60	1.40	44.80

Table 6.5.2. Fitting parameters used for the 1-layer model of 1 mg/ml 40K + 1 and 3.5 mM DTAB in NRW. The error in thickness is ± 3 Å and the error in scattering length density is ± 0.05 x10^{-6} Å^{-2}.

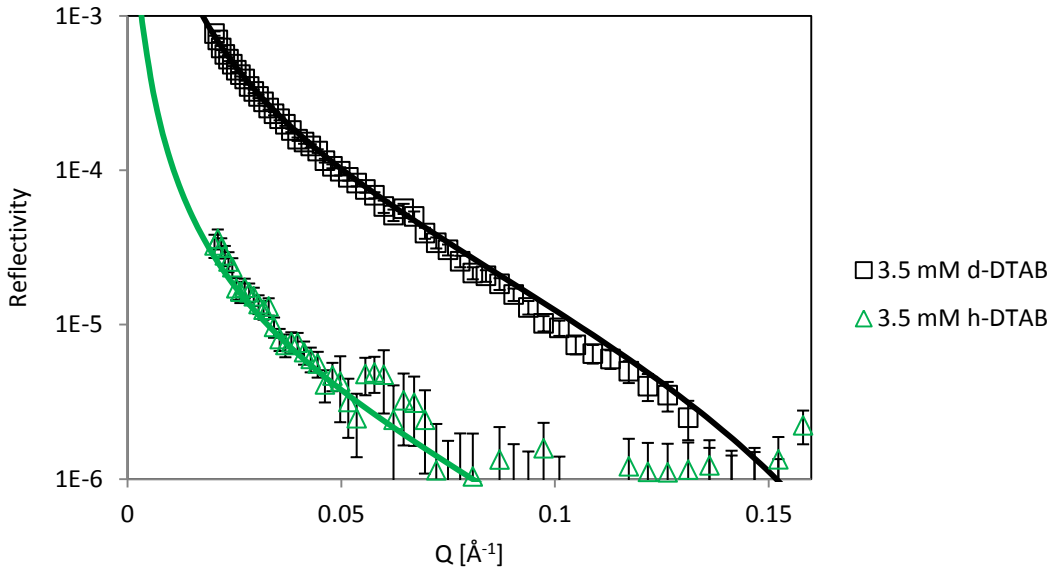

Fig 6.5.4. Neutron reflection data for 1 mg/ml 40K + 3.5 mM DTAB in NRW.

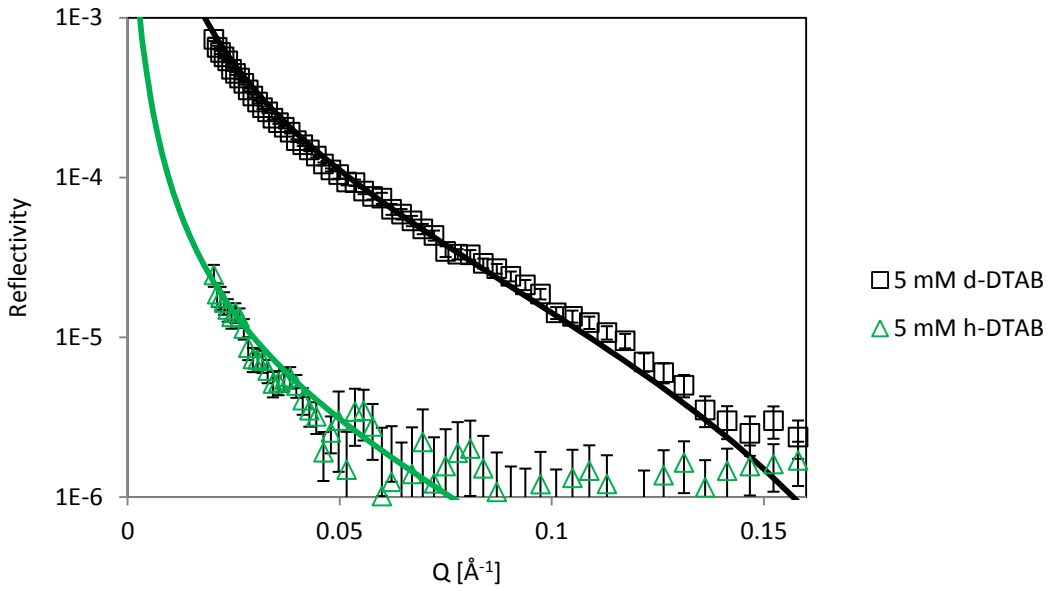

Fig 6.5.5. Neutron reflection data for 1 mg/ml 40K + 5 mM DTAB in NRW.

DTAB/mM	τ/ Å	P_h/ x10^{-6} Å^{-2}	τ·P_h/ x10^{-6} Å^{-1}	P_d/ x10^{-6} Å^{-2}	τ·P_d/ x10^{-6} Å^{-1}
5	31	0.25	7.75	1.50	46.50
7	28	0.23	6.44	1.60	44.80

Table 6.5.3. Fitting parameters used for the 1-layer model of 1 mg/ml 40K + 5 and 7 mM DTAB in NRW. The error in thickness is ± 3 Å and the error in scattering length density is ± 0.05 x10^{-6} Å^{-2}.

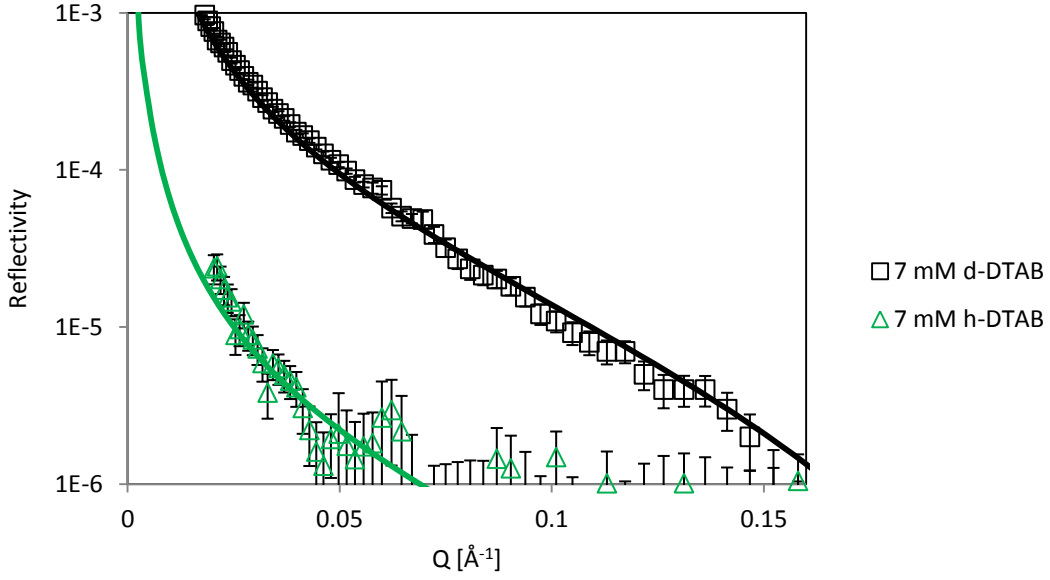

Fig 6.5.6. Neutron reflection data for 1 mg/ml 40K + 7 mM DTAB in NRW.

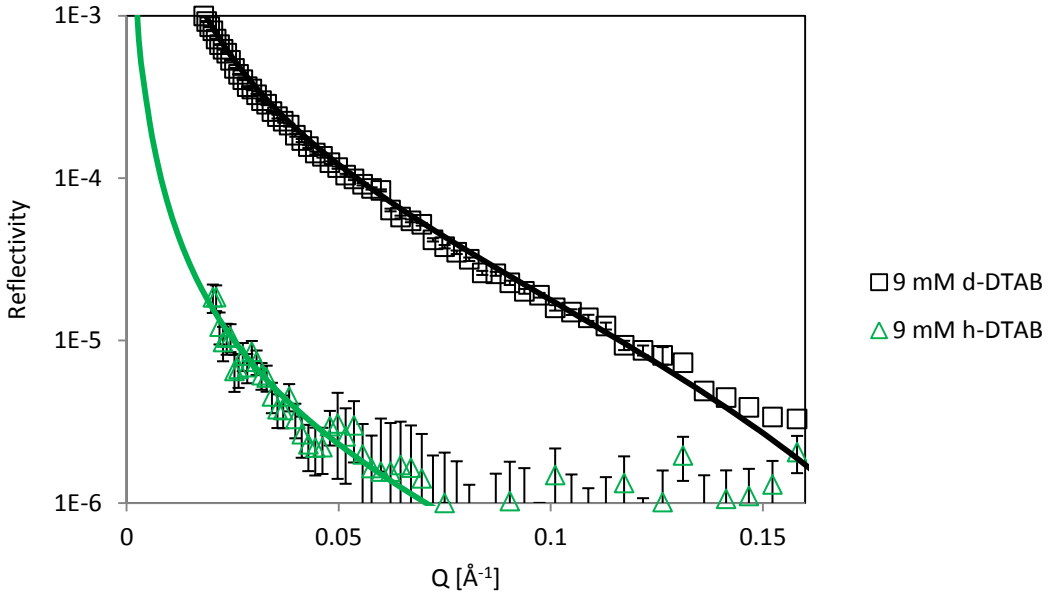

Fig 6.5.7. Neutron reflection data for 1 mg/ml 40K + 9 mM DTAB in NRW.

DTAB/mM	τ/ Å	P_h/ x10^{-6} Å^{-2}	τ·P_h/ x10^{-6} Å^{-1}	P_d/ x10^{-6} Å^{-2}	τ·P_d/ x10^{-6} Å^{-1}
9	26	0.25	6.50	1.70	47.60
10.5	28	0.25	7.00	1.70	47.60

Table 6.5.4. Fitting parameters used for the 1-layer model of 1 mg/ml 40K + 9 and 10.5 mM DTAB in NRW. The error in thickness is ± 3 Å and the error in scattering length density is ± 0.05 x10^{-6} Å^{-2}.

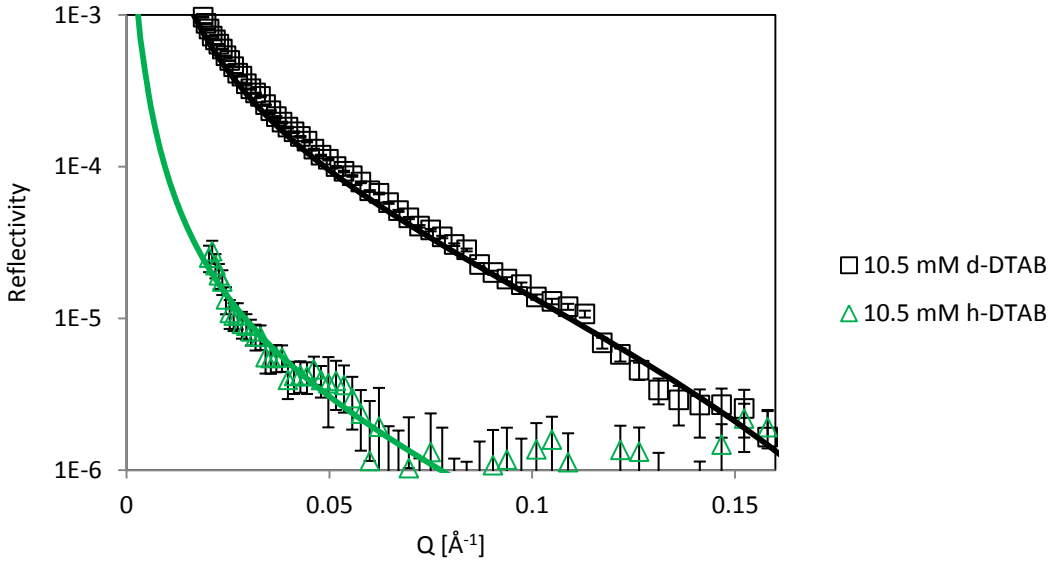

Fig 6.5.8. Neutron reflection data for 1 mg/ml 40K + 10.5 mM DTAB in NRW.

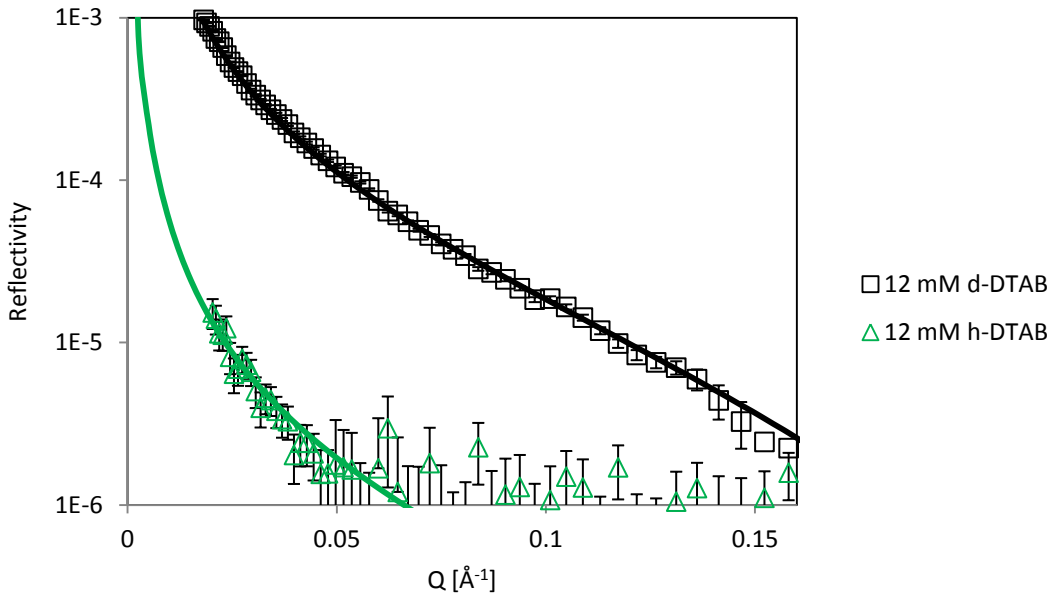

Fig 6.5.9. Neutron reflection data for 1 mg/ml 40K + 12 mM DTAB in NRW.

DTAB/mM	τ/ Å	P_h/ x10^{-6} Å^{-2}	τ·P_h/ x10^{-6} Å^{-1}	P_d/ x10^{-6} Å^{-2}	τ·P_d/ x10^{-6} Å^{-1}
12	26	0.23	5.98	1.80	44.50
14	24	0.20	4.80	1.85	44.40

Table 6.5.5. Fitting parameters used for the 1-layer model of 1 mg/ml 40K + 12 and 14 *mM DTAB in NRW. The error in thickness is ± 3 Å and the error in scattering length density is ± 0.05 x10^{-6} Å^{-2}.*

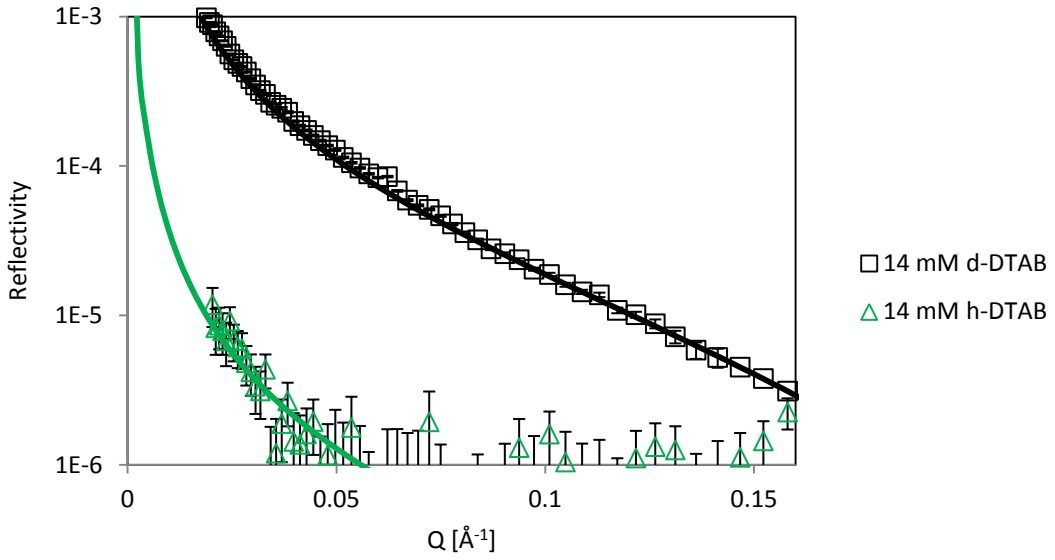

Fig 6.5.10. Neutron reflection data for 1 mg/ml 40K + 14 mM DTAB in NRW.

DTAB mM	Φ_{pep}	Φ_{dtab}	A_{pep} ± 6 %/ Å²	A_{dtab} ± 6 %/ Å²	Γ_{pep} ± 6 %/ mg·m^{-2}	Γ_{dtab} ± 6 %/ mg·m^{-2}	n ± 5 %
0.035	0.35	0.05	6432	258	1.70	0.21	25
0.35	0.27	0.11	8443	119	1.30	0.47	68
1	0.25	0.17	9287	74	1.18	0.75	114
3.5	0.15	0.21	15479	62	0.71	0.89	209
5	0.12	0.25	19174	53	0.57	1.05	285
7	0.11	0.30	23074	50	0.48	1.10	340
9	0.12	0.31	22861	52	0.48	1.07	331
10.5	0.12	0.31	21228	48	0.52	1.16	331
12	0.11	0.36	24849	45	0.44	1.24	390
14	0.10	0.41	30958	42	0.35	1.32	471

Table 6.5.6. Neutron reflection experimental results obtained for the 40K/DTAB system.

Some of the samples tested in Null Reflecting Water were also investigated in D_2O. The reflectivities and model fits can be seen in Figures 6.5.12 to 6.5.18.

As explained earlier, the interfacial layer thickness must remain constant for every contrast used thus making the use of different contrasts a useful tool to determine this parameter and verify the overall surface adsorbed amounts.

From the data obtained in Null Reflecting Water, it is possible to predict the scattering length densities of the air and water layers for the same sample in D_2O. The fitting parameters presented in Tables 6.5.7 to 6.5.10 are, within error, in overall agreement with the thicknesses of the layers at different surfactant concentrations.

The experimentally obtained scattering length densities also agree with the expected values. However, it was found that some of the samples presented slightly less dense layers at 0.035, 7 and 10.5 mM of DTAB. These differences are attributed to the problems encountered in measuring the samples due to the formation of film domains at the surface which can alter the overall structure as 'observed' by neutrons.

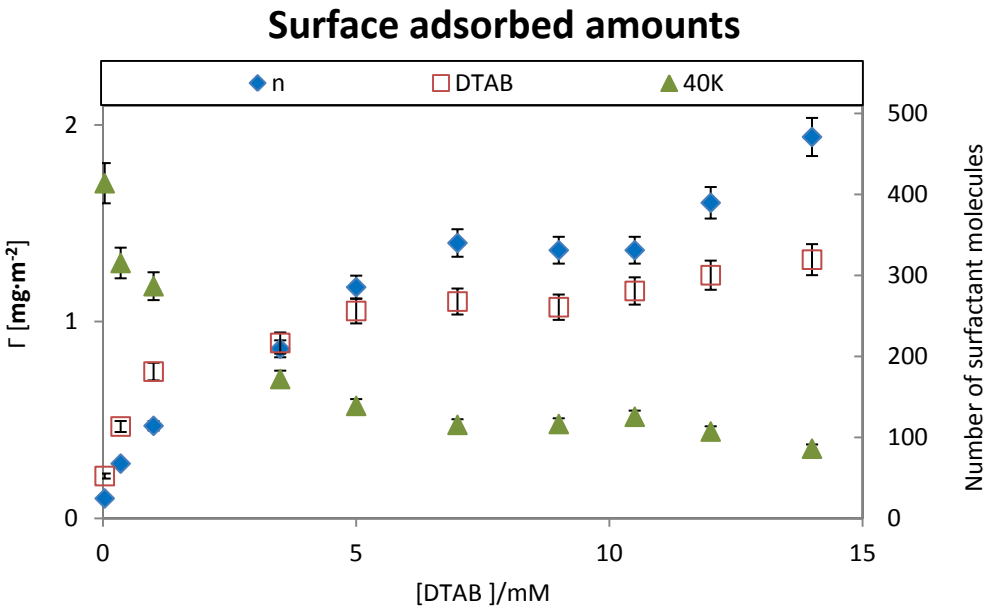

Fig. 6.5.11(a). Surfaces adsorbed amounts of polypeptide and surfactant when mixed in solution. The number of surfactant molecules per polypeptide molecule is represented by n.

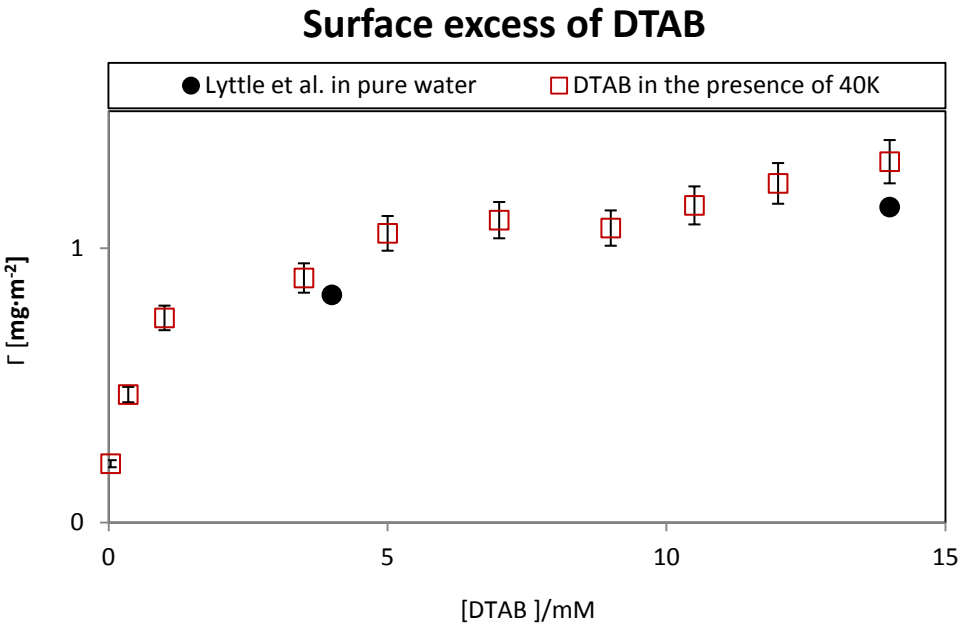

Fig. 6.5.11(b). A comparison of the DTAB adsorbed amounts in the presence of 40 KDa polypeptide with the surface excess of DTAB as calculated from neutron reflection experiments by Lyttle et al. [19] in pure water.

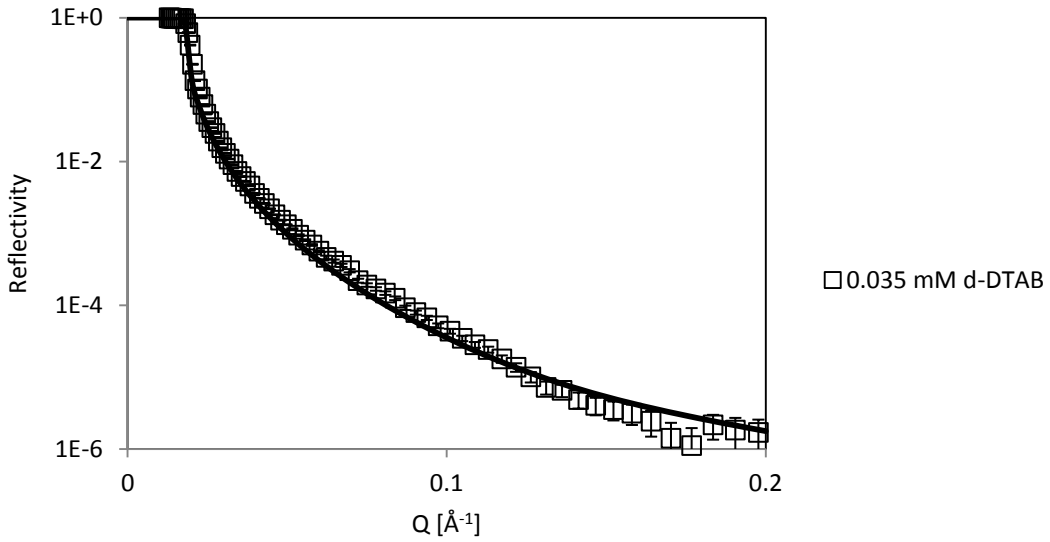

Fig. 6.5.12. Neutron reflection data for 1 mg/ml 40K + 0.035 mM d-DTAB in D_2O.

	h-DTAB			d-DTAB		
Layer	**τ/ Å**	**P_{exp}/ x10^{-6} Å^{-2}**	**P_{calc}/ x10^{-6} Å^{-2}**	**τ/ Å**	**P_{exp}/ x10^{-6} Å^{-2}**	**P_{calc}/ x10^{-6} Å^{-2}**
1	23	1.27	1.27	23	0.88	1.53
2	10	5.10	5.10	10	5.44	5.36

Table 6.5.7. Fitting parameters used for the 2-layer model of 1 mg/ml 40K + 0.035 mM DTAB in D_2O. The error in thickness is ± 3 Å and the error in scattering length density is ± 0.05 x10^{-6} Å^{-2}.

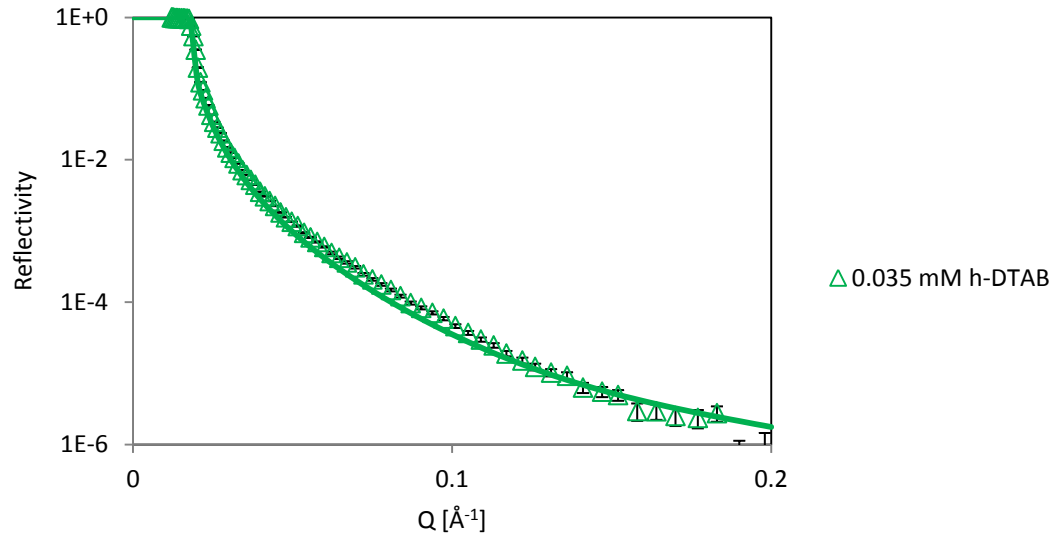

Fig. 6.5.13. Neutron reflection data for 1 mg/ml 40K + 0.035 mM h-DTAB in D_2O.

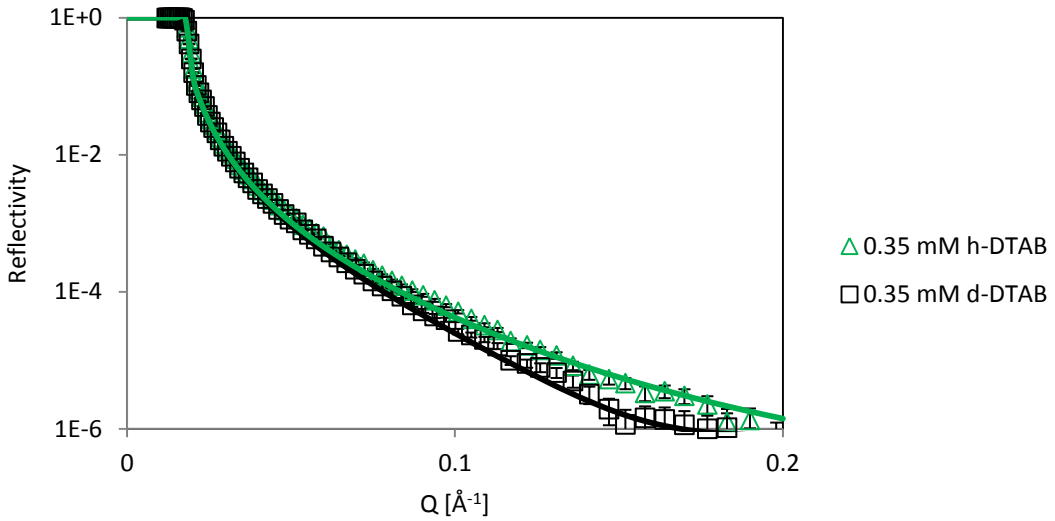

Fig. 6.5.14. Neutron reflection data for 1 mg/ml 40K + 0.35 mM DTAB in D_2O.

	h-DTAB			d-DTAB		
Layer	**τ/ Å**	**P_{exp}/ x10^{-6} Å^{-2}**	**P_{calc}/ x10^{-6} Å^{-2}**	**τ/ Å**	**P_{exp}/ x10^{-6} Å^{-2}**	**P_{calc}/ x10^{-6} Å^{-2}**
1(a)	23	0.98	0.98	19	1.57	1.57
2(a)	10	4.90	4.90	10	5.48	5.48
1(b)	19	0.51	0.51	19	1.62	1.62
2(b)	7	4.59	4.59	7	5.70	5.70

Table 6.5.8. Fitting parameters used for the 2-layer model of 1 mg/ml 40K + 0.35 (a) or 3.5 (b) mM DTAB in D_2O. The error in thickness is ± 3 Å and the error in scattering length density is ± 0.05 x10^{-6} Å^{-2}.

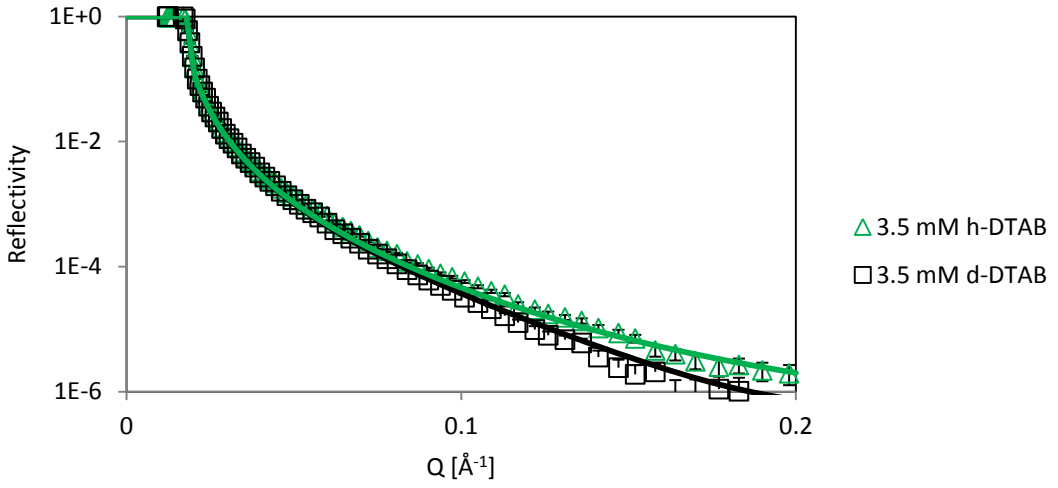

Fig. 6.5.15. Neutron reflection data for 1 mg/ml 40K + 3.5 mM DTAB in D_2O.

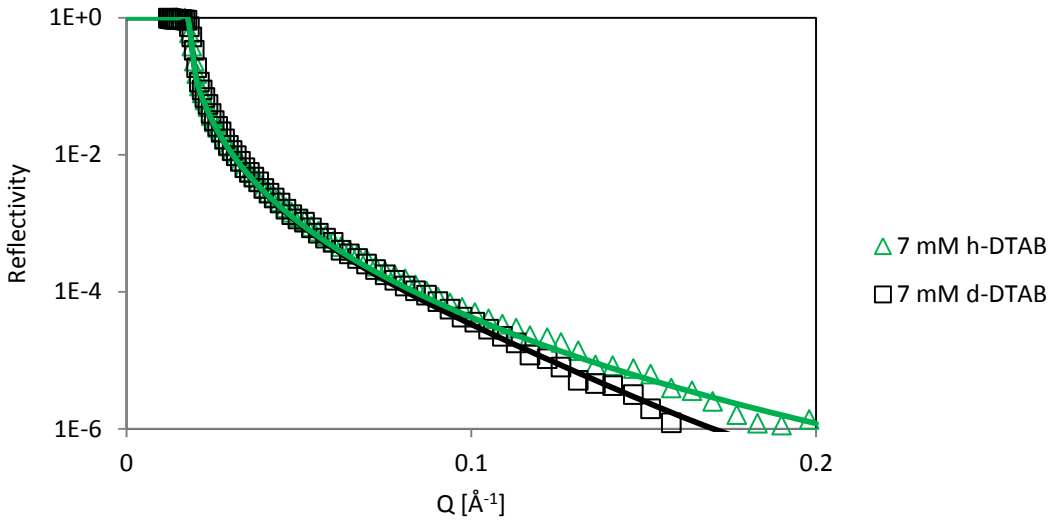

Fig. 6.5.16. Neutron reflection data for 1 mg/ml 40K + 7 mM DTAB in D_2O.

	h-DTAB			d-DTAB		
Layer	**τ/ Å**	**P_{exp}/ x10^{-6} Å^{-2}**	**P_{calc}/ x10^{-6} Å^{-2}**	**τ/ Å**	**P_{exp}/ x10^{-6} Å^{-2}**	**P_{calc}/ x10^{-6} Å^{-2}**
1(a)	19	0.37	0.37	17	1.94	1.94
2(a)	10	4.31	4.12	8	5.69	5.69
1(b)	20	0.45	0.44	20	1.70	2.05
2(b)	8	4.40	4.00	8	6.10	5.65

Table 6.5.9. Fitting parameters used for the 2-layer model of 1 mg/ml 40K + 7 (a) or 10.5 (b) mM DTAB in D_2O. The error in thickness is ± 3 Å and the error in scattering length density is ± 0.05 x10^{-6} Å^{-2}.

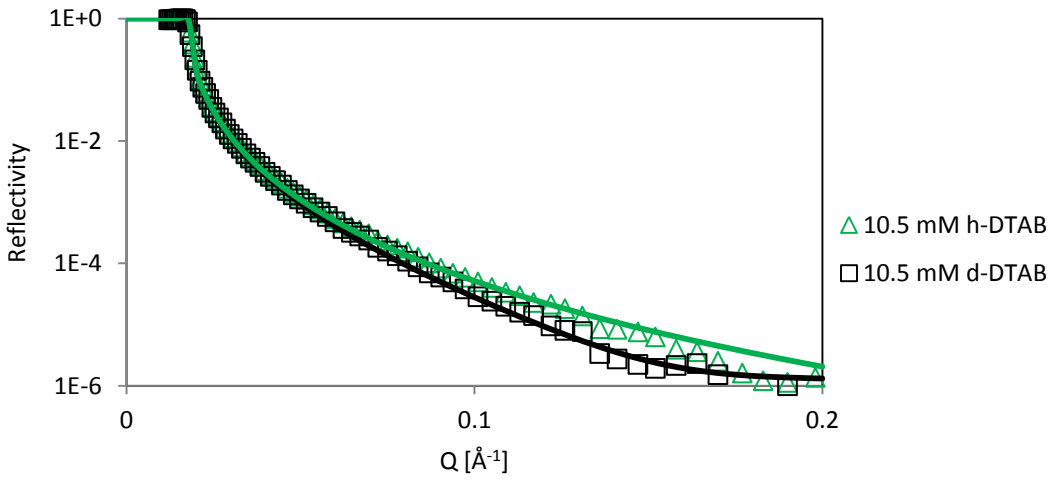

Fig. 6.5.17. Neutron reflection data for 1 mg/ml 40K + 10.5 mM DTAB in D_2O.

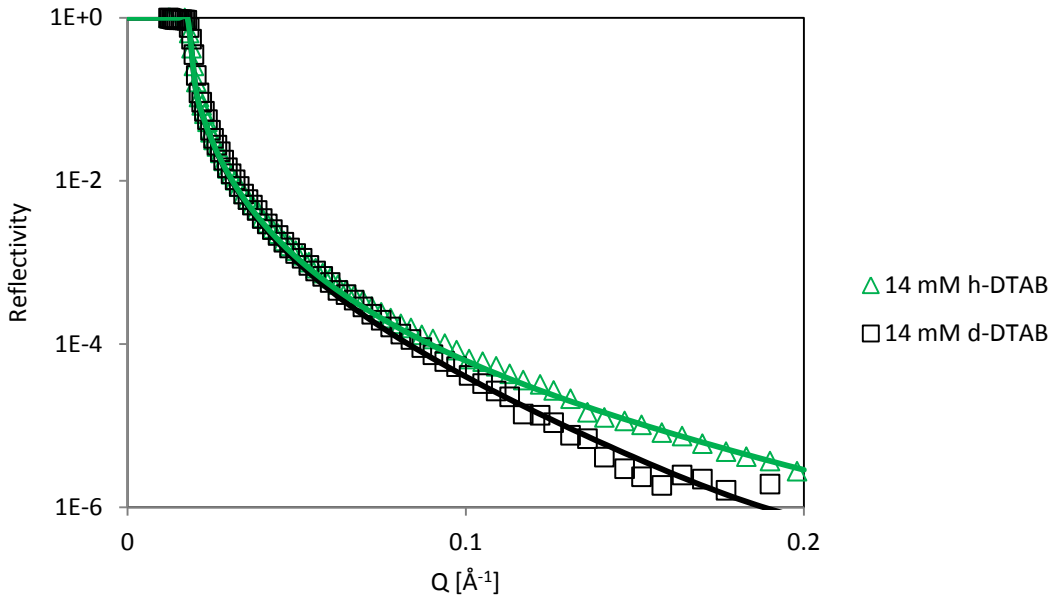

Fig. 6.5.18. Neutron reflection data for 1 mg/ml 40K + 14 mM DTAB in D_2O.

	h-DTAB			d-DTAB		
Layer	**τ/ Å**	**P_{exp}/ x10^{-6} Å^{-2}**	**P_{calc}/ x10^{-6} Å^{-2}**	**τ/ Å**	**P_{exp}/ x10^{-6} Å^{-2}**	**P_{calc}/ x10^{-6} Å^{-2}**
1	18	0.30	0.30	18	2.48	2.48
2	6	3.41	3.41	6	5.59	5.59

Table 6.5.10. Fitting parameters used for the 2-layer model of 1 mg/ml 40K + 14 mM DTAB in D_2O. The error in thickness is ± 3 Å and the error in scattering length density is ± 0.05 x10^{-6} Å^{-2}.

6.6. Small angle neutron scattering

The size and shape of the complexes formed in the bulk phase by the mixed solutions of 10 mg/ml of 40 KDa polypeptide and DTAB was studied using SANS in a similar manner to that already used with the polypeptide/SDS mixtures. The results were equally similar to the latter. That is, a short cylindrical polypeptide structure (or sheet) gradually converts into a spherical shape with addition of DTAB which can be explained with a core/shell model where electrostatic interactions between particles take place (as observed via ζ-potential) according to a Hayter-Penfold structure factor. The scattering data and model fits can be seen in Figures 6.6.1 and 6.6.2. The fitting parameters can be found in Table 6.6.1.

The core consists of an arrangement of surfactant monomer tails in micellar form and the composition of the shell is almost entirely due to the polypeptide wrapping around the surfactant micelle. The scattering length densities of the solvent and the polypeptide were fixed to $3.6 \cdot 10^{-6}$ Å^{-2} and $6.35 \cdot 10^{-6}$ Å^{-2}, respectively. The scattering length density of the core was fixed to $-0.4 \cdot 10^{-6}$ Å^{-2} and $2.2 \cdot 10^{-6}$ Å^{-2} for the protonated and deuterated samples, respectively. Similarly to the 40K/SDS system, the scattering length density of the core composed of d-DTAB is lower than initially expected probably due to the presence of polypeptide hydrophobic moieties intertwined with the surfactant tails and aided by the strong hydrophobic interaction acting upon them.

The C_nTAB surfactants are known to adopt elliptical shapes [20] so it is reasonable to believe that their mixtures with polyelectrolytes result in a deformation of the ellipsoid. This was already proved with the PEI/C_nTAB systems which resulted in an increasingly ellipsoidal form with increasing polymer concentration due to the strengthening of the interaction also with increasing polymer concentration [12]. These ellipsoidal shapes can vary from an oblate (disk-like) to a prolate ellipsoid and depend on the carbon length of the surfactant. Therefore, it is reasonable to assume that two different surfactants of equal carbon lengths result in similar structures.

The appearance of Bragg peaks in the neutron reflection data from the PEI/C_nTAB systems demonstrates the existence of self-assembled mesostructures. However, the Bragg diffraction peaks do not appear in the small angle scattering data. Hence, it can

be inferred that the ordered structures are found at the interface and not in the bulk phase. Furthermore, the spacing between these peaks is larger than the corresponding width or length of any of the ellipsoid forms adopted by the micelles [12]; a factor that further supports the above statement.

In the case of a long PEI molecule (750 KDa) at a concentration of 0.5 % in solution with cetyl trimethylammonium bromide (C_{16}TAB), the radius of gyration initially expands from 87.5 Å without surfactant to 100.5 Å with addition of surfactant [5]. However, with increasing surfactant concentration, it does decrease [5] to lower values than initially encountered for the polymer alone. This agrees with the data here presented and with the model of a sheet (short cylinder) being moulded into a more spherical shape due to the polypeptide wrapping around the surfactant forcing it to form micelles whilst reducing the radius of gyration, as already explained for the 40K/SDS system (recall Figure 5.6.3).

Since the core in the core/shell model usually takes the form of several surfactant tails associated together forming a micellar shape of radius approximately equal to their extended lengths; and the extended length depends on the number of carbon atoms in the tail, the aggregation number for SDS and DTAB (as obtained applying Tanford's Equation [21]) is approximately 60 molecules in both cases [22] if no other effects such as solvation are accounted for.

It is worth noticing that Cui et al. [23], proved by mixing HPG-borate and DTAB, that complexes were not formed with all mixtures of polyelectrolytes with DTAB. Although they did not offer a conclusive argument to explain this phenomenon, they suggested the need of high charge density sites in the polymer to initiate the nucleation of the surfactant and thus the complexation process.

In the system studied in the last Chapter, three distinct regions appeared in the neutron reflection and equilibrium surface tension data. These were related to the different type of structures found in the bulk phase. In particular, there exists an observed change in behaviour at the surface when the number of surfactant molecules per polypeptide is approximately equal to the number needed to form a micelle, i.e. ~60. The same argument is valid for the polypeptide mixtures with DTAB since the three interfacial

regions are also observed in these systems. At 0.1 and 1 mM of DTAB, the number of surfactant molecules per polypeptide as obtained from neutron reflection is 67 and 114, respectively. It is close to 1 mM that the first interfacial behavioural change takes place, i.e. region B. There is a hike in surface tension with increasing DTAB bulk concentration that has been explained in terms of resolubilisation of adsorbed polypeptide-based structures back to the bulk phase and proved by the growing number of surfactant molecules associated per polypeptide at the interface. In the bulk phase, the concentration at which this hike occurs in surface tension corresponds to the micellar complexes adopting the spherical core/shell form. This is consistent with a decrease in shell thickness and volume fraction of neutron scatterers found in the mixtures with chain-deuterated DTAB with an increase in surfactant present in the bulk. The relatively high polydispersity values account for the size distribution caused by the polydispersity of the polypeptide itself and possibly to other effects such as solvation.

sample	**model**	**l/± 1 Å**	**R/Å**		**p/± 0.2**
10 mg/ml 40 KDa	cylinder	7	90 ± 20		1
1 mM h-DTAB	cylinder	8	95 ± 10		0.5
1 mM d-DTAB	cylinder	8	95 ± 10		0.7
sample	**model**	**R_c/± 2 Å**	**τ_s/± 2 Å**	**Φ/± 0.0005**	**p/± 0.2**
5 mM h-DTAB	core/shell	17	8	0.002	0.6
10 mM h-DTAB	core/shell	17	6	0.002	0.8
20 mM h-DTAB	core/shell	17	6	0.004	0.8
5 mM d-DTAB	core/shell	17	8	0.001	0.6
10 mM d-DTAB	core/shell	17	7	0.0006	0.8
20 mM d-DTAB	core/shell	17	7	0.0004	0.8

Table 6.6.1. Fitting parameters for the scattering data obtained with 40K/DTAB mixtures. Samples are identified by their DTAB concentration. The cylinder model for 10 mg/ml of 40 KDa polypeptide is included as a reference. The parameters R and l are the radius and length of the cylinder, R_c and τ_s are the core radius and shell thickness, respectively. Φ is the volume fraction of scatterers, p is the polydispersity index.

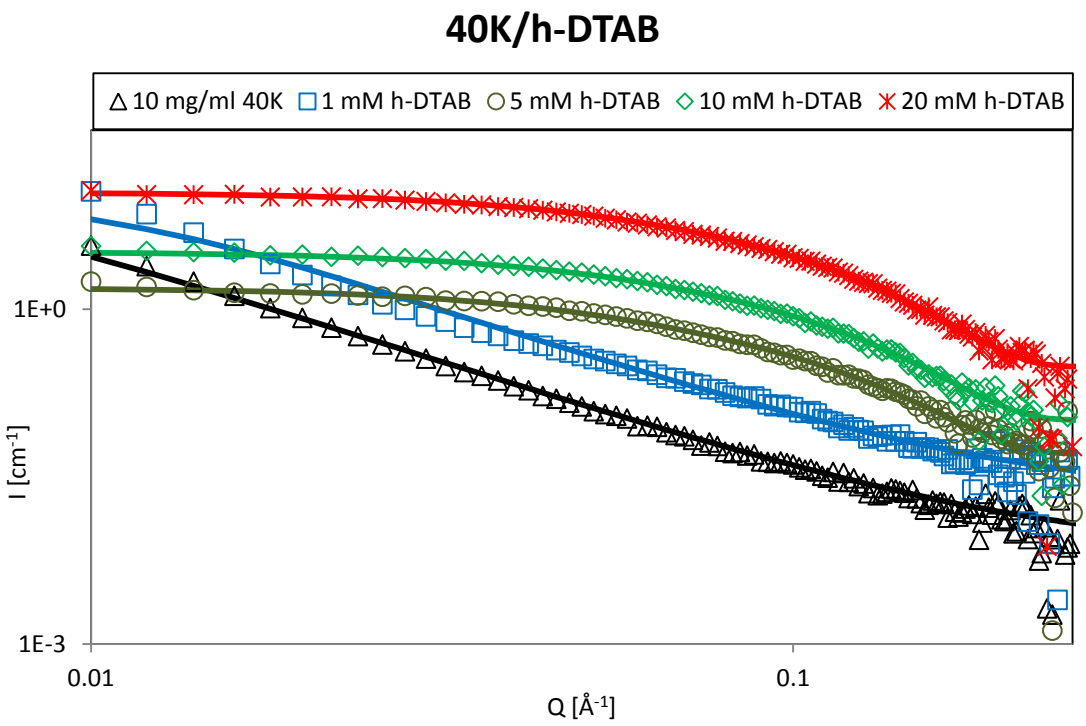

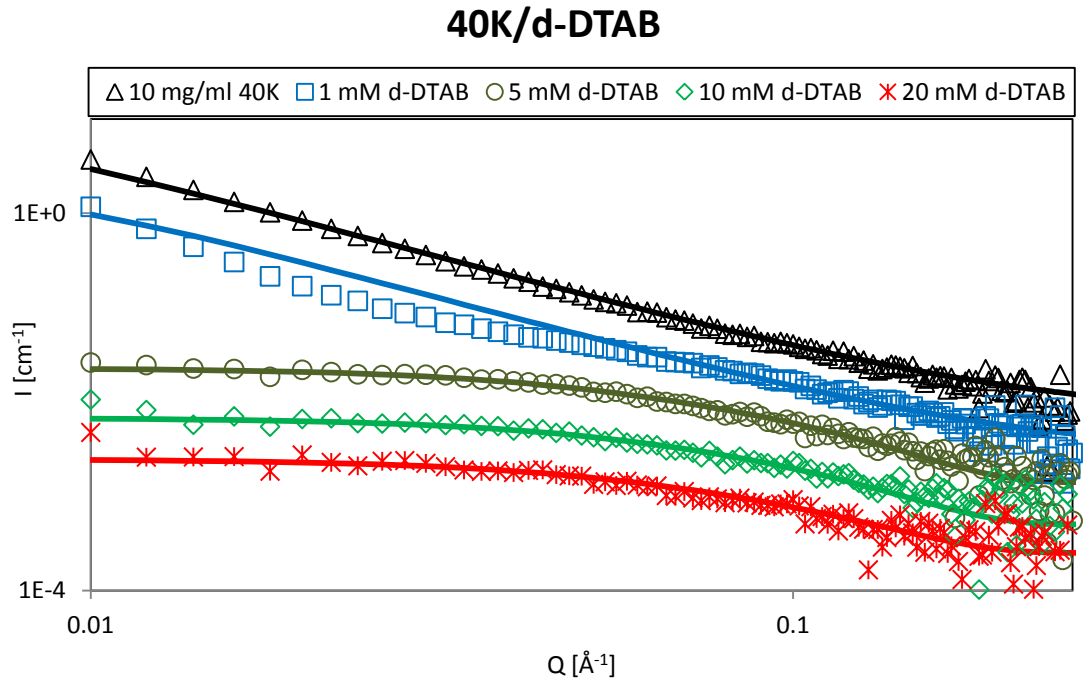

Figs. 6.6.1. (top) and 6.6.2. (bottom): SANS results for 40K/DTAB mixtures. The straight lines correspond to the model fits. For clarity, mixtures with DTAB have been scaled with multiples of 2.5 with respect to the scattering data of the polypeptide in the absence of surfactant and error bars are not included.

Summary

The mixtures of the 40 KDa polypeptide with DTAB at pH 5, i.e. close to the isoelectric point of the polypeptide, result in a synergistic behaviour that lowers the surface tension below the values obtained with the individual components at surfactant concentrations below the CMC and with small amounts of polypeptide. This synergy is clearly observable due to the appearance of stable high volumes of foams where no significant foams were obtained through the individual components. Dynamic surface tension measurements showed that at low concentrations of both components, the dynamic adsorption process of the complexes formed resembles that of a slowed down surfactant behaviour and enhanced polypeptide adsorption behaviour at short times.

Although addition of NaCl proved the existence of an electrostatic component at concentrations where the synergy is strong, the behaviour of these mixtures can be explained through Bell's model. Thus, hydrophobic association of polypeptide with the surfactant tails and between the tails, coupled with an ion-dipole interaction between the surfactant polar head and the polypeptide charges, is thought to be the cause of such strong synergy.

The electrostatic interactions in the bulk phase were demonstrated with ζ-potential. The unstable colloidal aggregates formed at pH 5 results in an observable phase separation at polypeptide concentrations at or above the CAC.
Neutron reflection proved that the adsorption of surfactant with addition of polypeptide remains mostly unaltered. However, the same cannot be said with respect to the polypeptide which decreases its adsorbed amounts with increasing surfactant concentration in the solution. The adsorbed layer thickness was found to decrease slightly with increasing surfactant concentration and the total adsorbed amounts are highest at low surfactant concentrations.

SANS helped to elucidate the shape of the aggregates formed in solution. A core/shell type of aggregate forms in the bulk phase at surfactant concentrations where the equilibrium surface tension profile falls in region C according to Bell's model. This demonstrates the presence of polypeptide in the bulk phase and thus disproves Campbell's explanation of the adsorption process.

References

[1] J.R. Lu, Z.X. Li, R.K. Thomas, J. Penfold, R.C. Ward (1996) “Structure of hydrocarbon chains in surfactant monolayers at the air/water interface: neutron reflection from dodecyl trimethylammonium bromide”, J. Chem. Soc., Faraday Trans., 92, pp. 403-408.

[2] H. Ritacco, D. Langevin, H. Diamant, D. Andelman (2011) “Dynamic surface tension of aqueous solutions of ionic surfactants: role of electrostatics”, Langmuir, 27 (3), pp. 1009–1014.

[3] C.G. Bell, C.J.W. Breward, P.D. Howell, J. Penfold, R.K. Thomas (2007) “Macroscopic modelling of the surface tension of polymer-surfactant systems”, Langmuir, 23, pp. 6042-6052.

[4] D.J.F. Taylor, R.K. Thomas, P.X. Li, J. Penfold (2003) “Adsorption of oppositely charged polyelectrolyte/surfactant mixtures. Neutron reflection from alkyl trimethylammonium bromides and sodium poly(styrenesulfonate) at the air/water interface: The effect of surfactant chain length”, Langmuir, 19, pp. 3712-3719.

[5] H. Comas-Rojas, E. Aluicio-Sarduy, S. Rodriguez-Calvo, A. Perez-Gramatges, S. J. Roser and K. J. Edler (2007) “Interactions and film formation in polyethylenimine–cetyltrimethylammonium bromide aqueous mixtures at low surfactant concentration”, Soft Matter, 3, pp. 747–753.

[6] A.G. Bykov, S.Y. Lin, G. Loglio, R. Miller, B.A. Noskov (2010) “Dynamic surface properties of polyethylenimine and sodium dodecylsulfate complex solutions”, Colloids and Surfaces A: Physicochem. Eng. Aspects, 367, pp. 129–132.

[7] C.G. Bell, C.J.W. Breward, P.D. Howell, J. Penfold, R.K. Thomas (2010) “A theoretical analysis of the surface tension profiles of strongly interacting polymer–surfactant systems”, J. Colloid Interface Sci., 350, pp. 486–493.

[8] B.A.Noskov, G. Loglio, R. Miller (2011) “Dilational surface visco-elasticity of polyelectrolyte/surfactant solutions: formation of heterogeneous adsorption layers”, Adv. Colloid Interface Sci., 168 (1-2), pp. 179-197.

[9] R.A. Campbell, M. Yanez Arteta, A. Angus-Smyth, T. Nylander, I. Varga (2011) “Effects of bulk colloidal stability on adsorption layers of poly(diallyldimethylammonium chloride)/sodium dodecyl sulfate at the air–water interface studied by neutron reflectometry”, J. Phys. Chem. B, 115 (51), pp 15202–15213.

[10] R.A. Campbell, A. Angus-Smyth, M. Yanez Arteta, K. Tonigold, T. Nylander, I. Varga (2010) "New perspective on the cliff edge peak in the surface tension of oppositely charged polyelectrolyte/surfactant mixtures", J. Phys. Chem. Lett., 1, pp. 3021–3026.

[11] K. Tonigold, I. Varga, T. Nylander, R.A. Campbell (2009) "Effect of aggregates on mixed adsorption layers of poly(ethyleneimine) and sodium dodecyl sulphate at the air/liquid interface", Langmuir, 25, pp. 4036-4046.

[12] B.M.D. O'Driscoll, E. Milsom, C. Fernandez-Martin, L. White, S.J. Roser, K.J. Edler (2005) "Thin films of polyethylenimine and alkyltrimethylammonium bromides at the air/water interface", Macromolecules, 38, pp. 8785-8794.

[13] K.J. Edler, A. Goldar, T. Brennan, S.J. Roser (2003) "Spontaneous free-standing nanostructured film growth in polyelectrolyte-surfactant systems", Chem. Commun., pp. 1724-1725.

[14] T. Gilanyi, I. Varga, C. Stubenrauch, R. Meszaros (2008) "Adsorption of alkyl trimethylammonium bromides at the air/water interface". J. Colloid Interface Sci., 317, pp. 395-401.

[15] J. Eastoe, J.S. Dalton (2000) "Dynamic surface tension and adsorption mechanisms of surfactants at the air-water interface", Adv. Colloid Interface Sci., 85, pp. 103-144.

[16] V.S. Alahverdjieva, V.B. Fainerman, E.V. Aksenenko, M.E. Leser, R. Miller (2008) "Adsorption of hen egg-white lysozyme at the air–water interface in presence of sodium dodecyl sulphate", Colloids and Surfaces A: Physicochem. Eng. Aspects, 317, pp. 610–617.

[17] V. Mosquera, J.M. Ruso, G. Prieto, F. Sarmiento, (1996) "Characterization of the interactions between lysozyme and n-alkyltrimethylammonium bromides by zeta potential measurements" J. Phys. Chem., 100, pp.16749-16753.

[18] A.R. Mackie, A.P. Gunning, P.J. Wilde, V.J. Morris (1999) "Orogenic displacement of protein from the air/water interface by competitive adsorption", J. Colloid Interface Sci., 210, pp. 157–166.

[19] D.J. Lyttle, J.R. Lu, T.J. Su, R.K. Thomas, J. Penfold (1996) "Structure of a dodecyltrimethylammonium bromide layer at the air/water interface determined by neutron reflection: comparison of the monolayer structure of cationic surfactants with different chain lengths", Langmuir, 11, pp. 1001-1008.

[20] S. S. Berr (1987) "Solvent isotope effects on alkyltrimethylammonium bromide micelles as a function of alkyl chain length", J. Phys. Chem., 91, pp. 4760-4765.

[21] C. Tanford (1972) "Micelle shape and size", J. Phys. Chem., 76 (21), pp. 3020-3023.

[22] J.F. Berret (2005) "Evidence of overcharging in the complexation between oppositely charged polymers and surfactants", J. Chem. Phys. 123 (16), pp. 164703-164712.

[23] Y. Cui, R. Pelton, T. Cosgrove, R. Richardson, S. Dai, S. Prescott, I. Grillo, H. Ketelson, D. Meadows (2009) "Not all anionic polyelectrolytes complex with DTAB", Langmuir, 25 (24), pp. 13172-13717.

Chapter 7. Mixtures with non-ionic surfactants: $C_{10}E_8$/40K mixtures

This Chapter presents the results obtained for the mixtures of the 40 KDa polypeptide with the non-ionic surfactant $C_{10}E_8$. Interfacial adsorption was investigated using the plate method and maximum bubble pressure. Since the synergy observed with the ionic surfactants SDS and DTAB was not replicated in this case and no improvement in the foaming properties was expected, no foam studies were performed.

The bulk solution properties in the presence of $C_{10}E_8$ were investigated through ζ-potential measurements. The behaviour from the 40 KDa polypeptide/$C_{10}E_8$ mixtures was compared with that of the non-ionics/lysozyme mixtures.

These studies serve as a useful basis to understand how the polypeptide interacts with ionic surfactants at the interface and in solution, with the results presented in the previous two Chapters.

7.1 Surface tension

The equilibrium surface tension of the non-ionic surfactant $C_{10}E_8$ in an aqueous solution (pH 5, 10 mM NaCl) was measured using the plate method. The adsorption isotherm obtained is shown in Figure 7.1.1.

The CMC under these conditions was found to be at 0.5 mM with a surface tension value of γ_{CMC} = 35 ± 1 mN/m. No reliable information was found in the literature for this compound in buffered solutions other than deionized water. Stanley et al. [1] using pressure-driven flow with capillary electrophoresis found the CMC of $C_{10}E_8$ (obtained from Sigma-Aldrich) at ~0.95 mM in deionized water at 25°C. Under similar conditions, Doulia et al. [2] reported using a decyl alcohol ethoxylate, or Neodol, obtained from Shell Chemicals [3] with a molecular weight of 512 g/mol and a CMC at 1 mM. Chang et al. [4] also reported CMC to be at ~ 1 mM and at a surface tension value of ~35 mN/m using the pendant drop method.

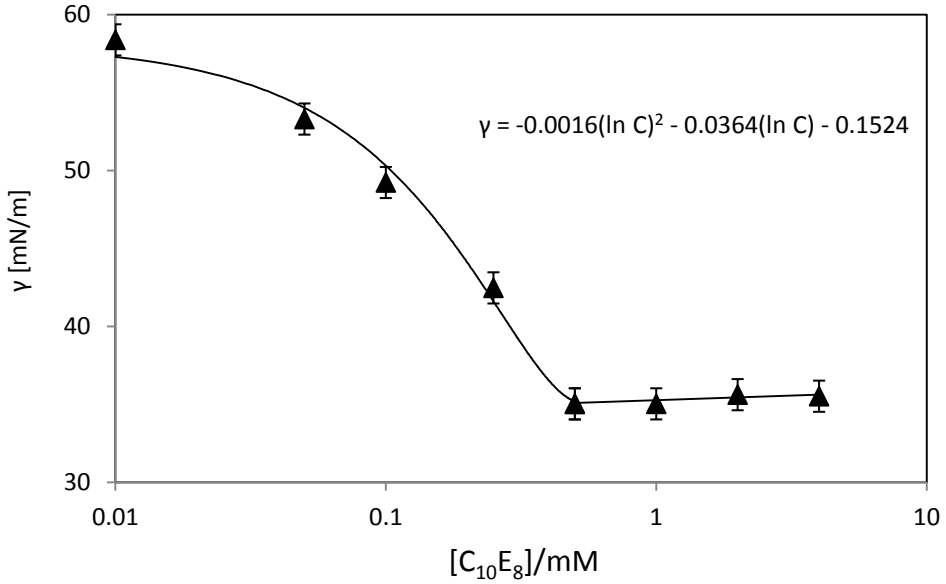

Fig. 7.1.1. Interfacial adsorption of $C_{10}E_8$ at the air/water interface (10 mM NaCl, pH 5). Continuous line is only a visual aid. The Equation corresponds to the second order polynomial fit applied to the values below the CMC.

A decrease in CMC with addition of electrolyte was already observed with SDS and DTAB. However, the response of non-ionic surfactants to addition of electrolytes may be expected to be somewhat different since no electrostatic interactions are possible with these. Several studies have shown that addition of electrolytes to non-ionic surfactants results in a lower CMC [5, 6]. This has been attributed to a 'salting out' effect whereby the work necessary to disrupt the water structure is increased by the addition of electrolyte [7] hindering the non-ionic surfactant capabilities to do so and reducing its solubility. This in turn, results in an increased surface adsorption and thus a reduced CMC.

The surface excesses obtained by applying Gibbs Equation are shown in Figure 7.1.2. At the CMC, the surface excess is $(4.86 \pm 0.3) \cdot 10^{-6}$ mol·m^{-2} and the area per molecule at this concentration is 34 ± 3 Å^2.

The equilibrium surface tension of mixed polypeptide with $C_{10}E_8$ was also measured by the plate method. The curves obtained with 0.1, 1 and 5 mg/ml of polypeptide are shown in Figure 7.1.3.

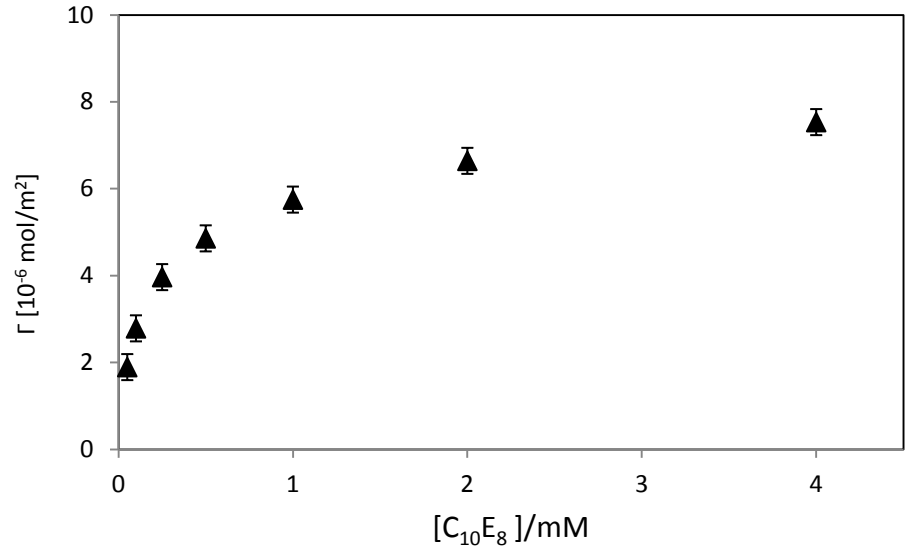

Fig. 7.1.2. Surface adsorbed amounts of $C_{10}E_8$ as calculated from equilibrium surface tension.

At low surfactant concentrations, surface tension values decrease with increasing polypeptide concentration as expected. All the curves give lower values than those obtained for the surfactant alone at these concentrations. At higher surfactant concentrations the three curves converge towards the CMC of the surfactant at approximately 0.5 mM. From this point onwards, all curves show negligible differences from the surfactant alone indicating a displacement of polypeptide from the surface which is now dominated by adsorbed surfactant. An interesting feature presented by these mixtures occurs at low surfactant concentrations; for 1 mg/ml of polypeptide (the CAC), the curve has an increase in surface tension values of ~ 5 mN/m when compared to the polypeptide alone which may suggest there is some kind of cooperative interaction such as in the lysozyme/$C_{12}E_5$ mixtures [8]. In the latter case, although no clear signs were visible in the surface tension profiles, the interaction was observed by neutron reflection and the results pointed towards some degree of denaturation of the protein by the addition of $C_{12}E_5$, implying some kind of cooperative interactions between the polypeptide and the non-ionic surfactant.

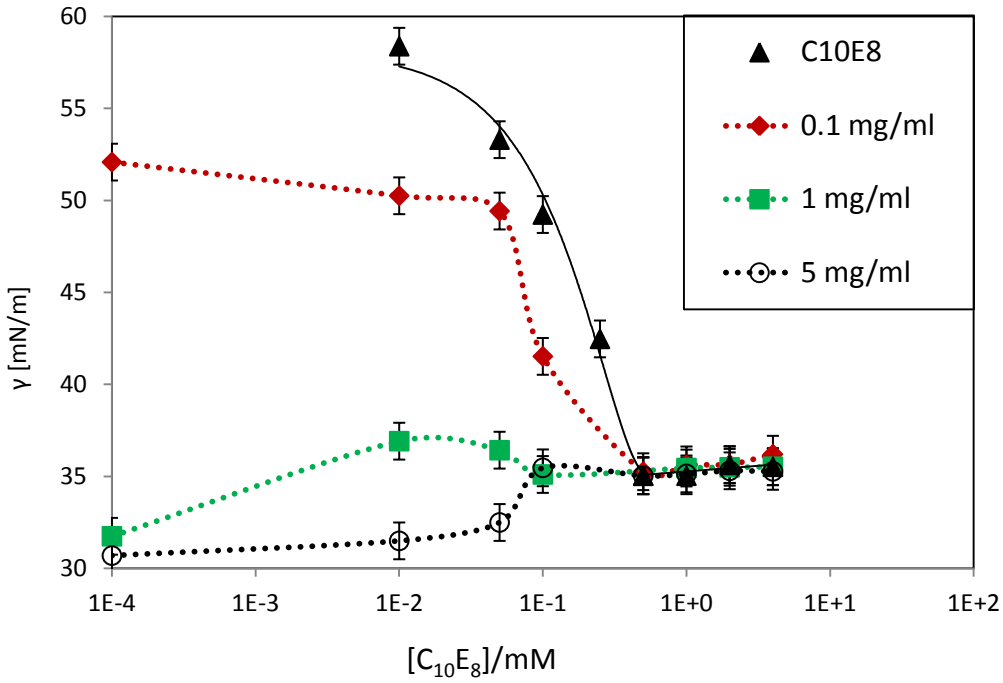

Fig. 7.1.3. Interfacial adsorption of 40K/$C_{10}E_8$ at the air/water interface. Continuous lines are only added as a visual aid. The concentrations of added polypeptide can be seen in the legend, i.e. 0.1, 1 and 5 mg/ml. The surface tension values of these polypeptide concentrations have been added as a reference at $1e^{-4}$.

When the polypeptide concentration is increased to 5 mg/ml, the curve behaviour at concentrations below the CMC of the surfactant reaches lower values than the latter and in the range of the polypeptide CAC, with the exception of the 0.1 mM point where both curves, 1 and 5 mg/ml, seem to have reached the micellar surfactant concentration already.

In comparison with the strongly interacting systems studied earlier, the mixtures of polypeptide and $C_{10}E_8$ present no depression below the CMC. Instead, the values of polypeptide equilibrium surface tension are reached (or nearly reached) with addition of small surfactant amounts and the curves progress into a surfactant-like behaviour with increasing amounts of added surfactant. The polypeptide is very surface active and it adsorbs at the surface preferentially when not much surfactant is present. However, with increasing surfactant, it gets replaced by surfactant micelles at the interface.

It is very likely that for surfactant concentrations below 0.5·CMC, the non-ionic surfactants and the polypeptide molecules were co-adsorbed. Given the hydrophobic fragments in both molecules, some degree of affinitive interactions was possible, leading to the formation of surface active aggregates.

This is consistent with observations from different polymer/non-ionic systems and can be explained with the orogenic model which explains how the surfactant disrupts the adsorbed interfacial protein network by adsorbing at defects and increasing the size of the domain where surfactant nucleation takes place with increasing concentration until eventually leading to the network collapse.

7.2. Maximum bubble pressure

The dynamic characteristics of the interfacial adsorption of the non-ionic surfactant $C_{10}E_8$ and its mixtures with different concentrations of the 40 KDa polypeptide were investigated using the maximum bubble pressure method. Figure 7.2.1 shows the concentration dependence of the surface tension of the surfactant. The variations induced by different concentrations in the curvatures are easily observable and at the CMC, 0.5 mM, there is a markedly clear change in behaviour (from concave to convex). Generally, the dynamic adsorption of non-ionic surfactants is well described by the Frumkin model and when mixed with a protein, there is a competition process at the interface [4].

As expected, higher surfactant concentrations produce a faster decay of surface tension with the highest concentration, 4 mM, reaching close-to-equilibrium values at 0.01 s. In comparison with previous studies in pure water [4], at 0.1 mM the equilibrium surface tension (as deduced from the asymptotes at long-time range) was found at 59.67 mN/m (i.e. at ~1000 s).

In the present case, the dynamic surface tension value at 13.6 s is 54.57 mN/m and at equilibrium (i.e. after ~11 hours) it is 49.23 mN/m. In pure water, there is a reported shift from diffusion controlled to a mixed controlled mechanism at 0.01 mM which is well characterized with the Frumkin model, indicating the existence of significant

intermolecular interactions. The overall adsorption process is anticooperative and thus adsorption is hindered with increasing amounts of adsorbed material at the interface [4].

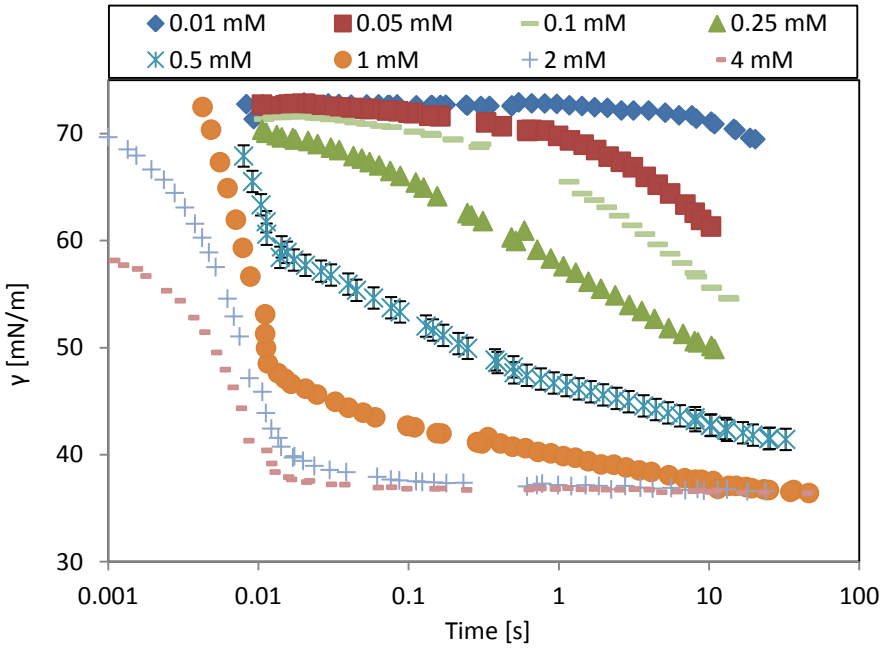

Fig. 7.2.1. Dynamic surface tension dependence on concentration of $C_{10}E_8$. Error bars are only shown in one curve for clarity.

To contrast the equilibrium surface tension curves obtained with the plate method with the dynamic values, four different surfactant concentrations have been tested with maximum bubble pressure for every polypeptide concentration, 0.01, 0.1, 1 and 4 mM, i.e. two concentrations below the surfactant's CMC, one at the CMC and one at 8·CMC. The results are presented in Figures 7.2.2 to 7.2.13. In order to facilitate the comparison of the results to the reader, the following series of graphs use the same scale values and error bars are only shown in one curve for clarity.

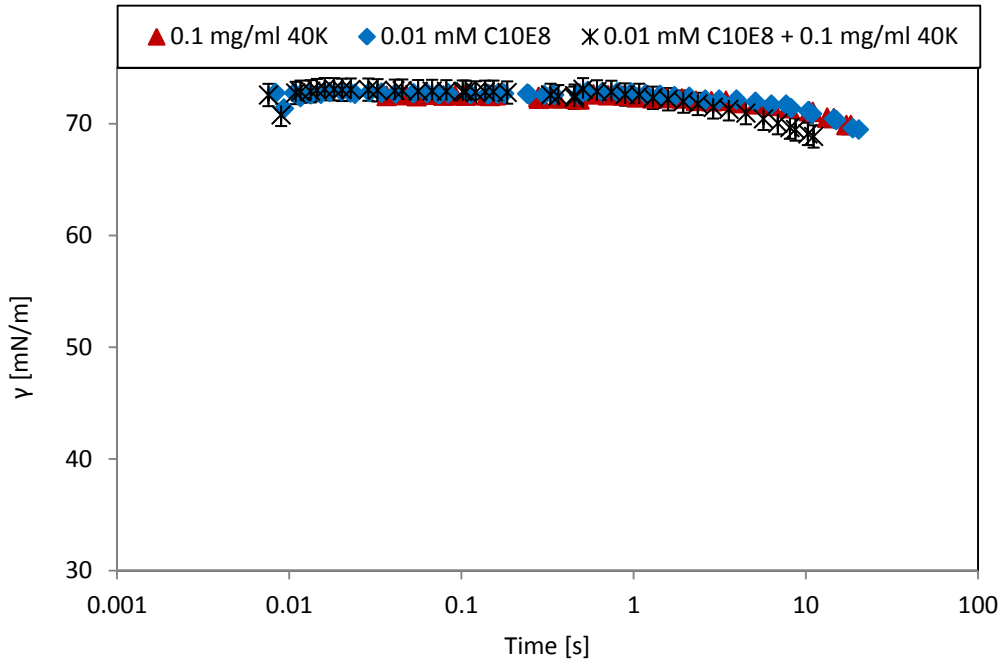

Fig. 7.2.2. Dynamic surface tension for 0.1 mg/ml of 40K + 0.01 mM $C_{10}E_8$.

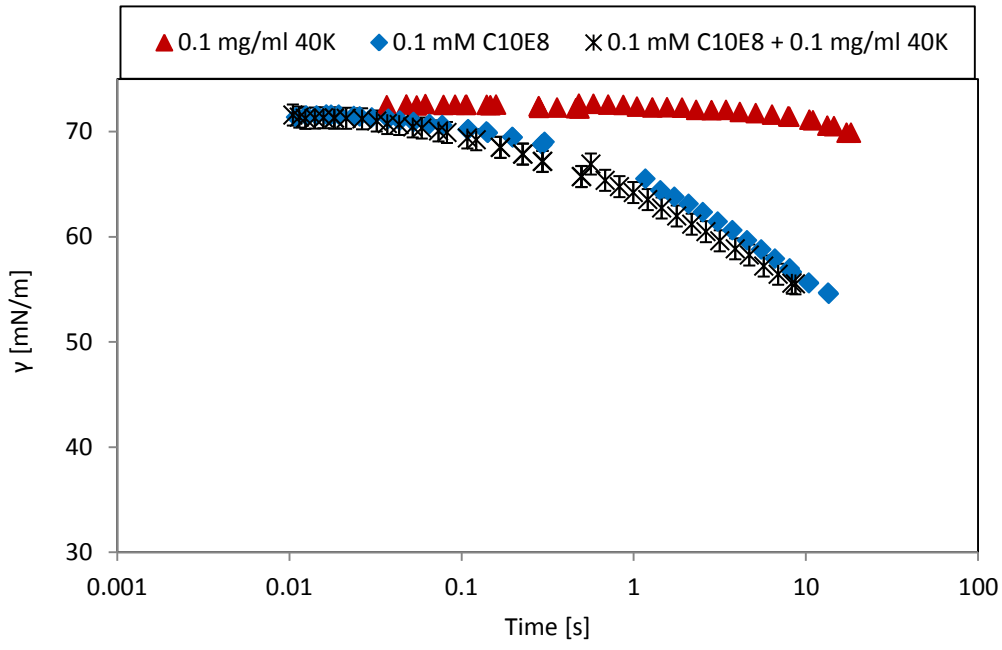

Fig. 7.2.3. Dynamic surface tension for 0.1 mg/ml of 40K + 0.1 mM $C_{10}E_8$.

For 0.1 mg/ml of polypeptide, the equilibrium surface tension shows that for surfactant concentrations below the CMC (see Figures 7.2.2 and 7.2.3), the surface tension of the mixture is close to that of the surfactant but with slightly lower values. In the dynamic measurements, the decay of surface tension of the mixture at these concentrations and at times below 10 s, follows the surfactant decay very closely. Thus, the lower equilibrium surface tension values are reached at longer times, once the polypeptide has passed the induction period.

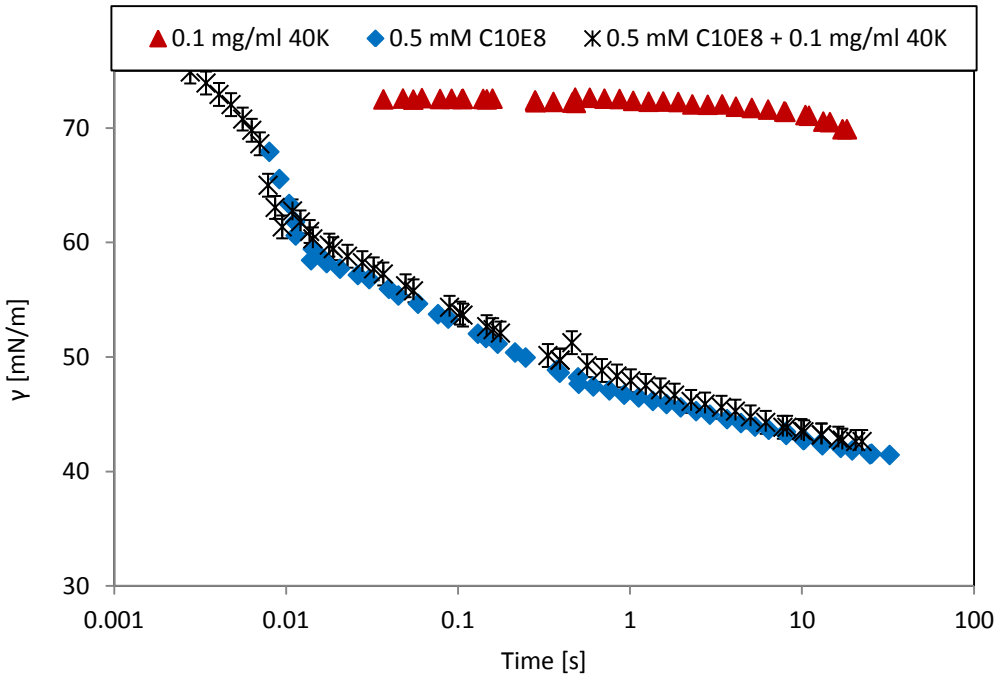

Fig. 7.2.4. Dynamic surface tension for 0.1 mg/ml of 40K + 0.5 mM $C_{10}E_8$.

At the CMC and above, Figures 7.2.4 and 7.2.5, the dynamic surface tension curves of the mixtures continue following the surfactant very closely and a faster decay is observed. At 4 mM, equilibrium is almost reached within 100 s. The results at 0.5 mM and 4 mM mixed with 1 mg/ml and 5 mg/ml of 40 KDa polypeptide also show the same trends (see Figures 7.2.8, 7.2.9, 7.2.12, 7.2.13).

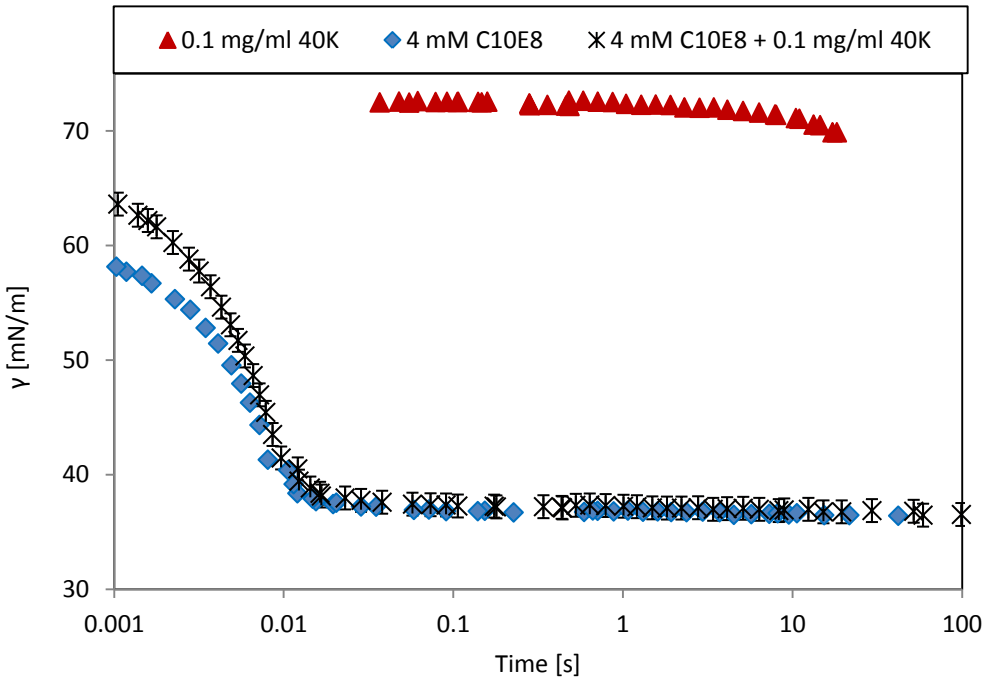

Fig. 7.2.5. Dynamic surface tension for 0.1 mg/ml of 40K + 4 mM $C_{10}E_8$.

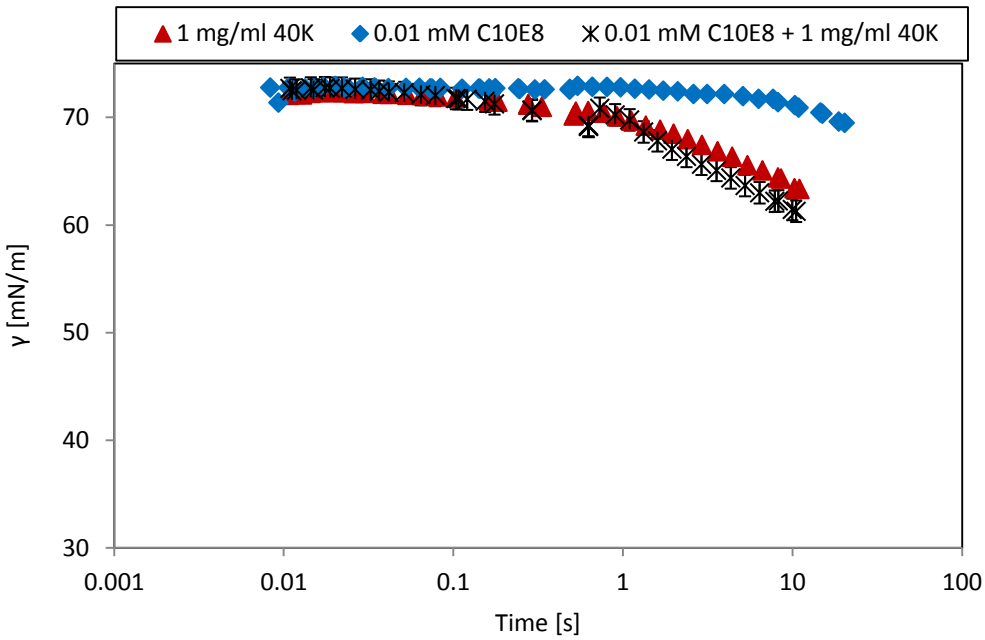

Fig. 7.2.6. Dynamic surface tension for 1 mg/ml of 40K + 0.01 mM $C_{10}E_8$.

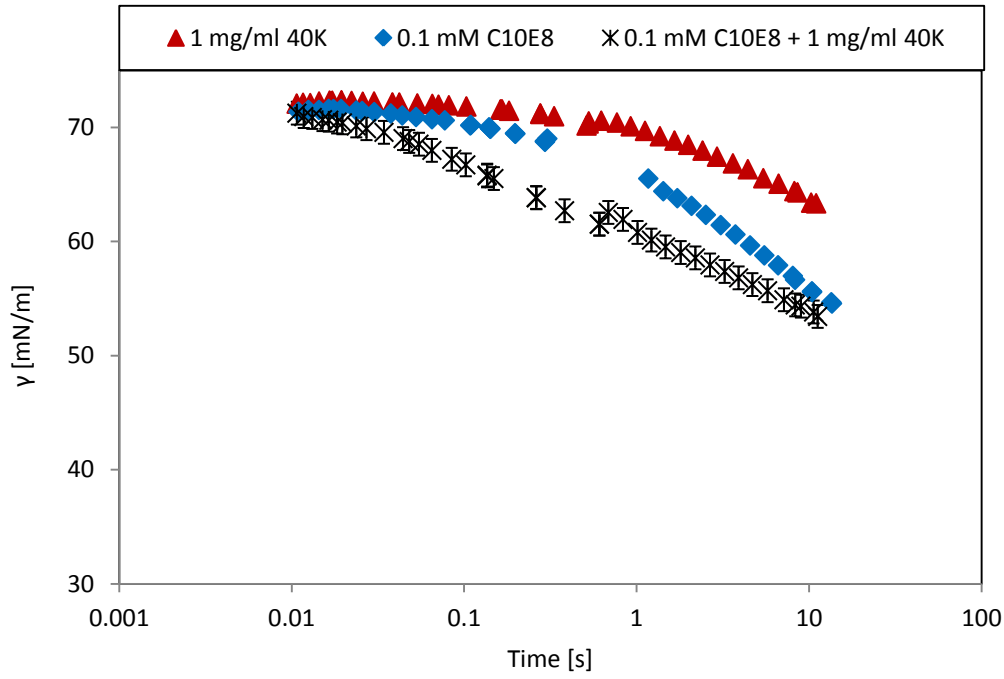

Fig. 7.2.7. Dynamic surface tension for 1 mg/ml of 40K + 0.1 mM $C_{10}E_8$.

At the lowest surfactant concentration, i.e. 0.01 mM, when mixed with 1 and 5 mg/ml of polypeptide (Figures 7.2.6, 7.2.10), the decay of surface tension with increasing time follows a close resemblance to the decay of the polypeptide. The surfactant at this low concentration does need a longer time to start showing visible signs of surface adsorption. This is consistent with the polypeptide dominated equilibrium surface tension curves at these surfactants concentrations, i.e. the mixture is also dependent on the induction period of the protein.

At 0.1 mM with 1 and 5 mg/ml of polypeptide, respectively, the dynamic curves fall faster than for any of the individual components. However, the plate method indicates that these two samples reach the same values of equilibrium surface tension and this value was higher than the corresponding polypeptide value. Thus, rapid adsorption at the interface occurred that resulted in the polypeptide adsorption being hindered and the process of surfactant adsorption being favoured. This can be seen in Figure 7.2.7 at 10 s when the adsorption curve for the mixture reached surfactant levels, i.e. the surfactant displaced the mixed components for the surface.

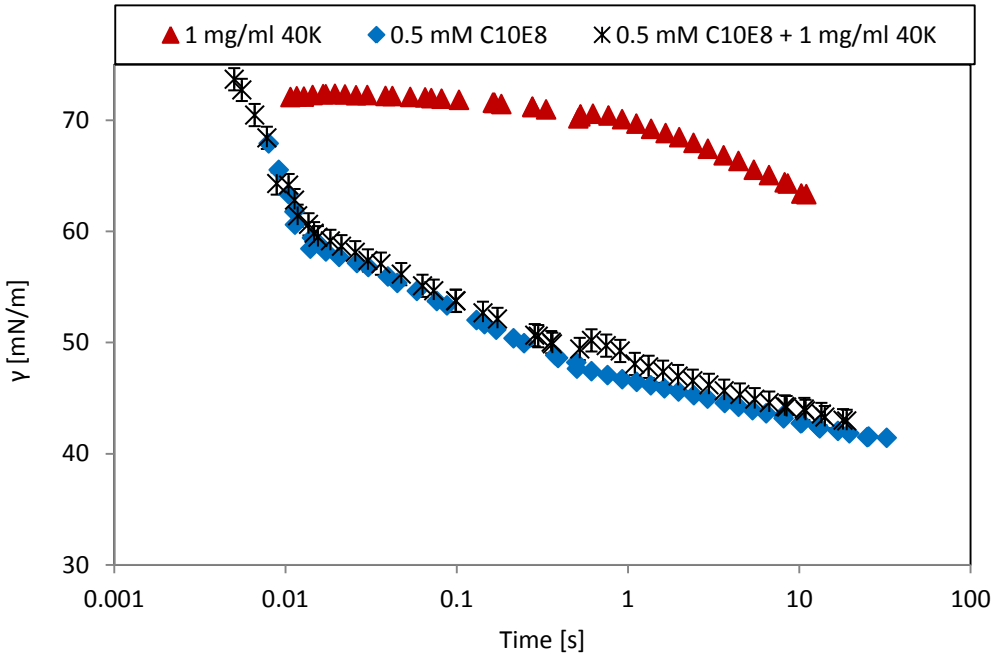

Fig. 7.2.8. Dynamic surface tension for 1 mg/ml of 40K + 0.5 mM $C_{10}E_8$.

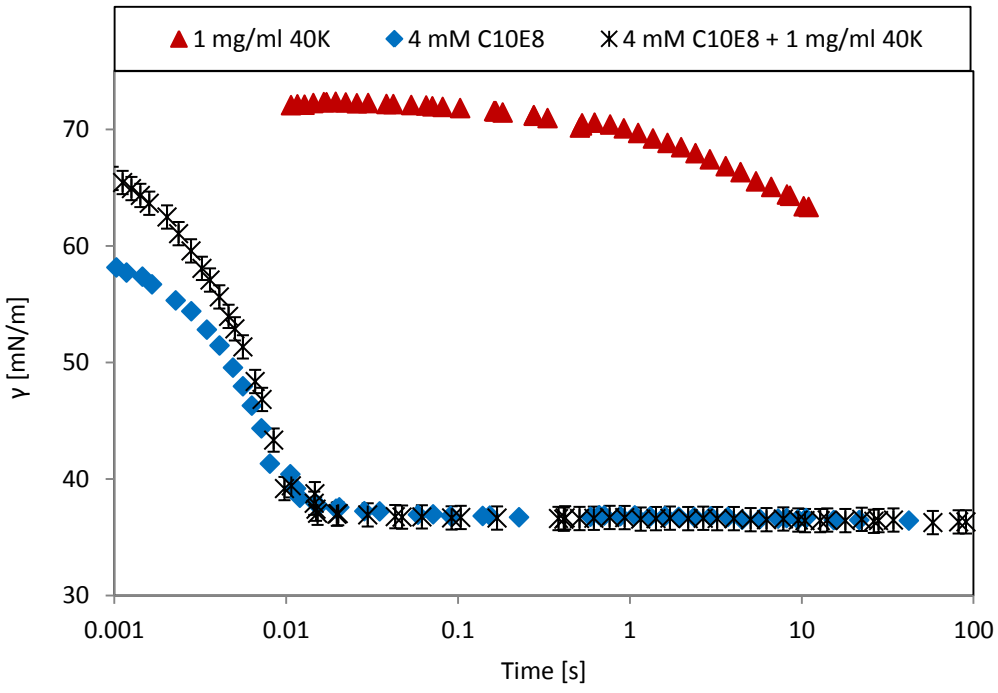

Fig. 7.2.9. Dynamic surface tension for 1 mg/ml of 40K + 4 mM $C_{10}E_8$.

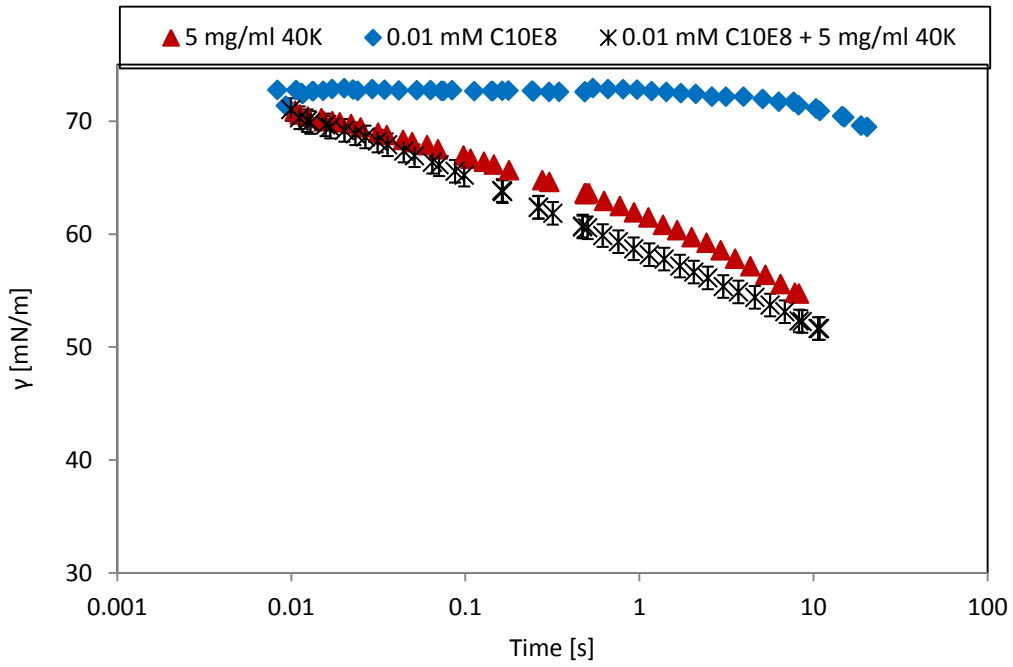

Fig. 7.2.10. Dynamic surface tension for 5 mg/ml of 40K + 0.01 mM $C_{10}E_8$.

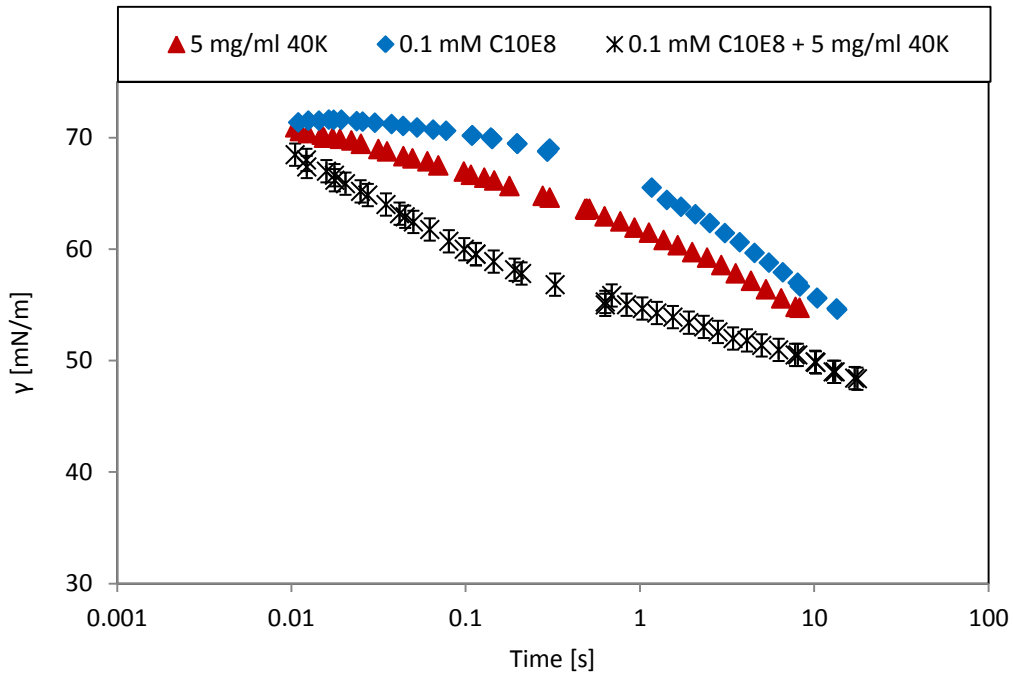

Fig. 7.2.11. Dynamic surface tension for 5 mg/ml of 40K + 0.1 mM $C_{10}E_8$.

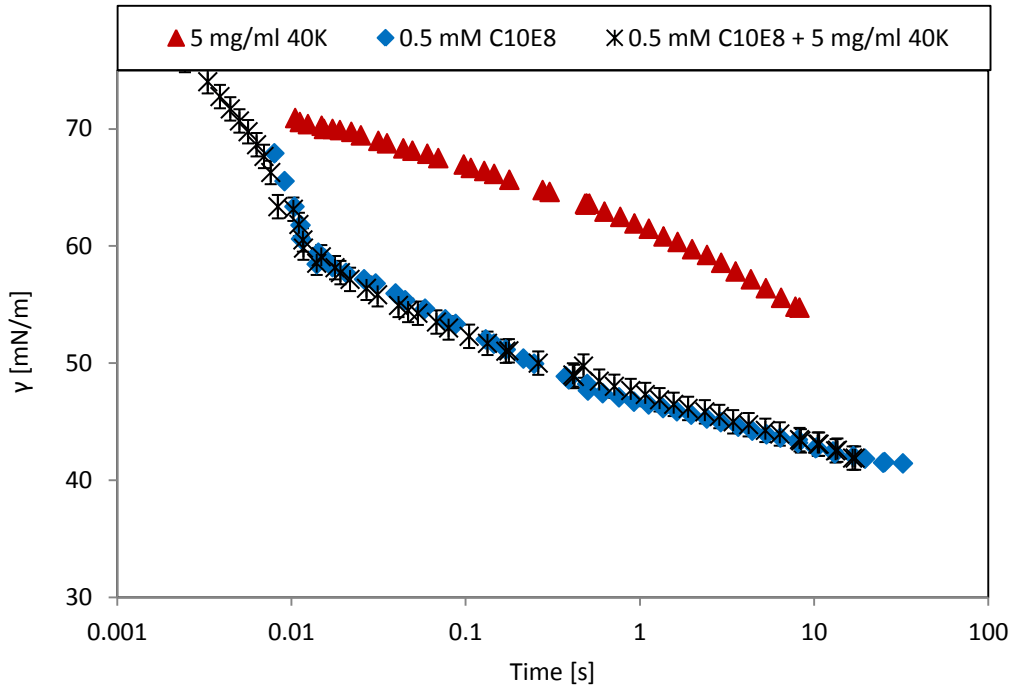

Fig. 7.2.12. Dynamic surface tension for 5 mg/ml of 40K + 0.5 mM $C_{10}E_8$.

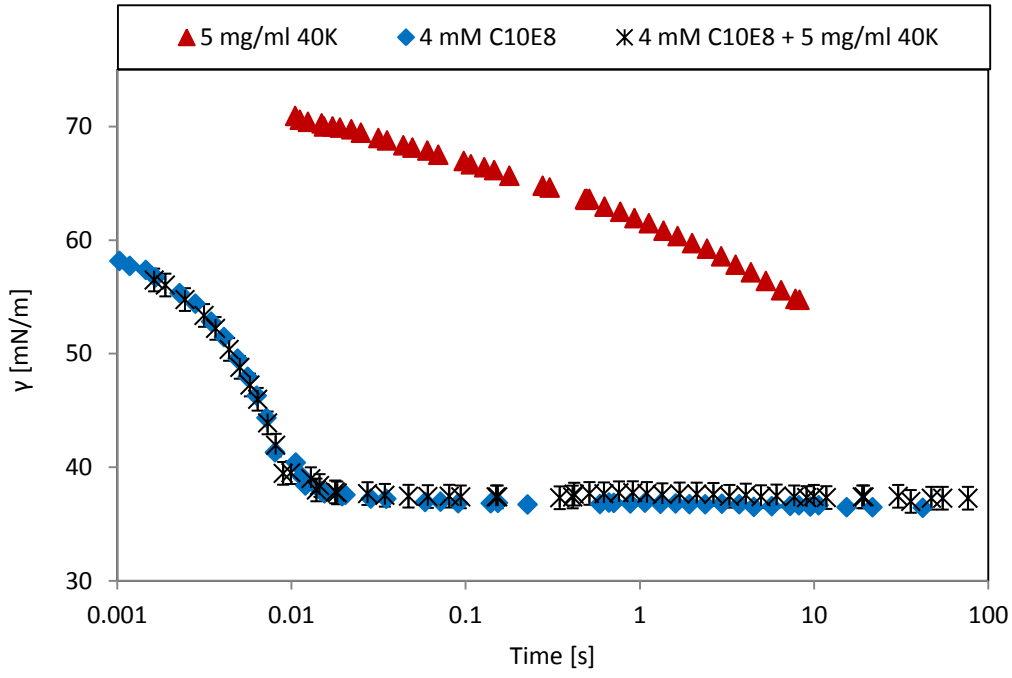

Fig. 7.2.13. Dynamic surface tension for 5 mg/ml of 40K + 4 mM $C_{10}E_8$.

As observed in previous Chapters dealing with ionic surfactants, the decay of surface tension with time exhibits different behaviour at different concentrations. In particular, at polypeptide concentrations above the CAC and after the induction period, the curves part further away from the surfactant behaviour at low surfactant concentration. This suggests that at the highest polypeptide concentrations, initial surface adsorption is dominated by the polypeptide. In contrast, Figure 7.2.14 shows the relevant curves for $C_{10}E_8$ and the effect of polypeptide concentration does not seem to affect the decay of surface tension. Rather, the curves follow the surfactant behaviour very closely at all times. Thus, adsorption at the surface is not aided by any polypeptide-surfactant interaction, at least in the first 10 seconds of decay.

At all times, the curves reach almost the same values of surface tension at a surfactant concentration of 4 mM.

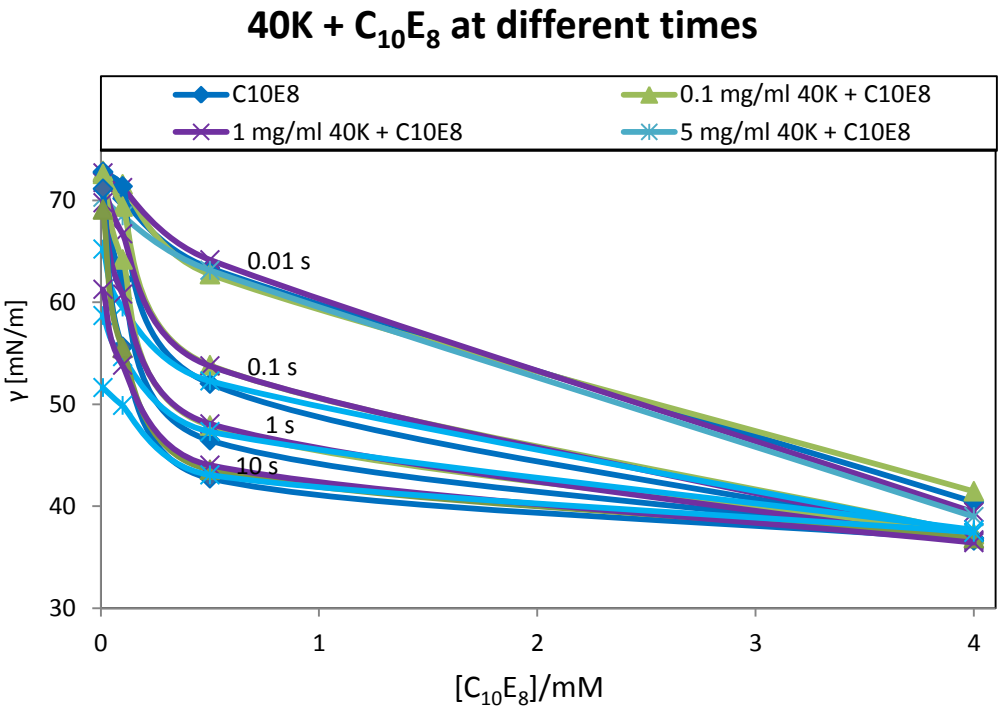

Fig. 7.2.14. Dynamic surface tension for different concentrations of $C_{10}E_8$ at different times.

7.3. ζ-potential

Since the ζ-potential of a solution is calculated (in this work) from the electrophoretic mobility of the particles in solution (see Equation 2.2.7) and therefore is dependent upon the charges present in the system, the results of the measured ζ-potential for a mixed system containing protein and a non-ionic surfactant are expected to be similar to that of the protein alone. With previous studies of such systems [6] this has been indeed the case. Nevertheless, electrophoretic mobility is also a function of the solution's viscosity and this parameter can be affected by the addition of neutral material to the protein solution [9] by thickening the solution. The addition of hydrophobic moieties increases the viscosity of the solution and they can become part of the electrical double layer by travelling with the charged particles. Therefore, they may hinder the electrophoretic velocity of the charged particles under measurement and produce a deviation from the value of ζ-potential of protein alone.

With this in mind, a test was conducted with a mixture of the non-ionic $C_{10}E_8$ and the polypeptide at a series of different pHs. Figure 7.3.1 shows the results obtained.

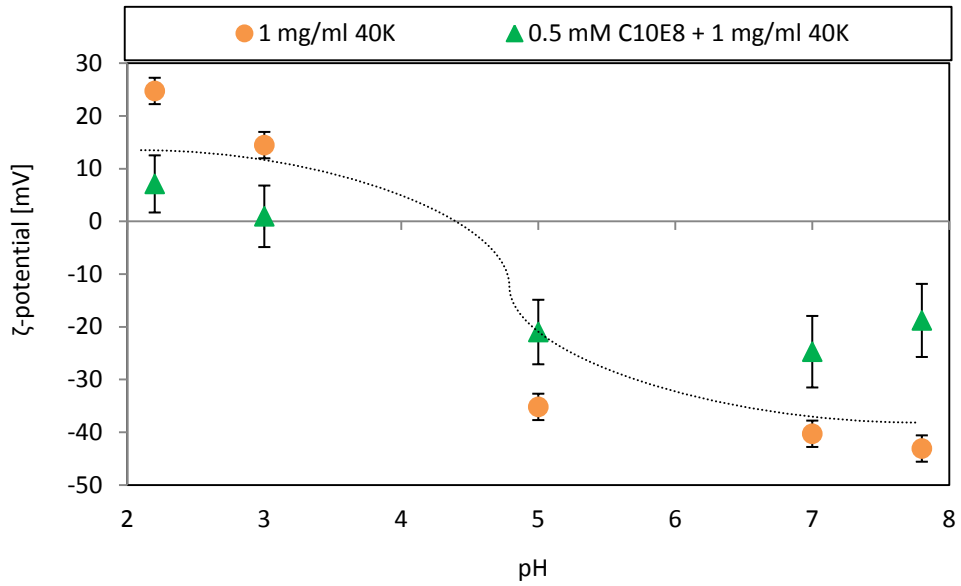

Fig. 7.3.1. ζ-potential of 1 mg/ml of polypeptide with and without added $C_{10}E_8$. Sigmoidal curve is only a visual aid.

The concentrations of both compounds were the CAC and the CMC, respectively, with the aim of achieving encapsulation of the polypeptide by the non-ionic (coating). The process of coating proteins with non-ionic surfactant is well-known within the pharmaceutical industry where non-ionic surfactants such as the polysorbates Tween 20 and Tween 80 are commonly used for drug encapsulation [10] and steric stabilization against protein aggregation [11]. Such interactions rely mainly on hydrophobic affinity.

The mixture gave consistent results close to those previously obtained for the polypeptide. Some steric hindrance can be seen at every pH tested which departs further from the polypeptide ζ-potential with increasing distance from the isoelectric point towards higher or lower pHs, i.e. some charged groups are encapsulated in non-ionic surfactant. At zero ζ-potential or isoelectric point, none of the samples possesses measurable surface charges and thus, the results should be identical since no electrophoretic mobility could occur. This is consistent with the idea that a higher charged particle coated in non-ionic surfactant travels more slowly than in the absence of the non-ionic and with decreasing charge the shielding effects should be reduced as there are less charges that can be screened. In order to corroborate that the difference in the obtained ζ-potential curves is entirely due to steric interactions and not any other kind of interaction, the non-ionic surfactant was also tested in a mixed solution with a well-known protein, i.e. lysozyme. The properties of lysozyme have been extensively studied and include the ζ-potential curve as a function of pH [12]. Thus, by measuring the mixed lysozyme/$C_{10}E_8$ system, it is possible to reproduce the values of ζ-potential previously reported for lysozyme and compare them to the new values for the mixture to check on the existence of any possible effects caused by the surfactant. The results of this experiment are presented in Figure 7.3.2.

The concentrations of lysozyme and surfactant were 5 mg/ml and 0.5 mM, respectively. The 5 mg/ml value was chosen to account for the difference in molecular weight with respect to the 40 KDa polypeptide and also to obtain a reduced signal/noise ratio. In addition, results available to the general public of a sample of 20 mg/ml of lysozyme (obtained from Sigma-Aldrich) in a solution of 0.6 mM NaCl at 25ºC [13] are shown together with the experimental data obtained in this project for comparison.

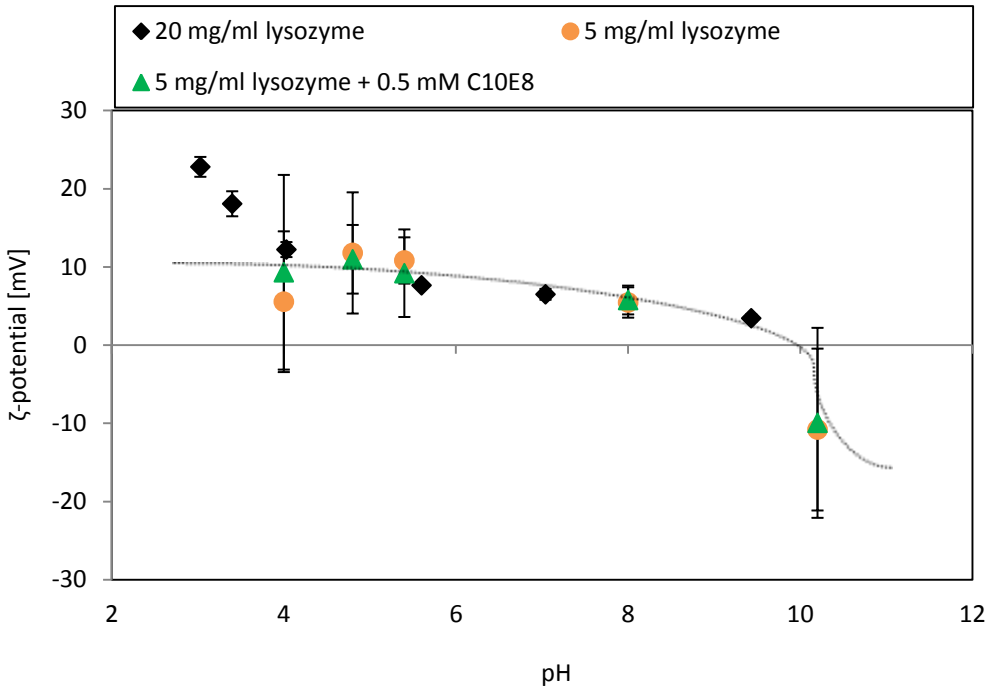

Fig. 7.3.2. ζ-potential of 5 mg/ml of lysozyme with and without added $C_{10}E_8$. Sigmoidal curve is only a visual aid.

As seen in the Figure, ζ-potential values for all three curves are in excellent agreement. The isoelectric point of lysozyme adopts a range of different values in the literature, from 9.3 [14] to 11.35 [15], as stated in the information leaflet accompanying the lysozyme obtained from the company Sigma-Aldrich which is based on the 1951's results from Wetter et al. [15]. Our experimental results lead to the interpretation that the pI is located approximately at pH 10, in agreement with more recent studies by Lee at al. [16] and Rothemund et al. [17].

A similar cationic biopolymer of molecular weight 6 to 16 KDa and pI at pH ~ 10 was extracted from Moringa oleifera seeds [18]. Its mixtures with the non-ionic surfactant Triton X-100 also resulted in little or no change in the ζ-potential of the polymer. It was reported [18] that addition of Triton X-100 to the cationic polymer resulted in increased solubility due to the shielding effect of the hydrophobic interaction between the components on the hydrophobic moieties of the polymer. As expected from the lack of electrostatic interactions, the solution remained clear with increasing addition of

surfactant. These conclusions also hold true for the 40K/$C_{10}E_8$ and the lysozyme/$C_{10}E_8$ systems.

Summary

Equilibrium and dynamic surface adsorption experiments show the displacement of the 40 KDa polypeptide from the air/water interface by the non-ionic surfactant $C_{10}E_8$ with increasing surfactant concentration as expected from previous studies of similar systems. The displacement is consistent with the orogenic model and shows no similarities with the surface adsorption processes seen with the mixed ionic surfactant systems.

The low surface tension values as observed from low non-ionic surfactant concentrations must arise from the co-adsorption of surfactant and polypeptide, likely to be synergised by hydrophobic interaction at the interface over this region.

The colloidal stability of the polypeptide/non-ionic mixtures shows only small albeit increasing deviations with increasing pH distance from the isoelectric point of the polypeptide. This can be attributed to steric interactions between both compounds associated with some structural changes as a result of surfactant binding driven mainly by hydrophobic interaction. Such structural changes were not expected from the lysozyme system because lysozyme is very robust and non-ionic association, if any, was not expected to cause any structural deformation of the globular and robust protein.

References

[1] F.E. Stanley, A.M. Warner, E. Schneiderman, A.M. Stalcup (2009) "Rapid determination of surfactant critical micelle concentrations using pressure-driven flow with capillary electrophoresis instrumentation", J. Chromatogr. A, 1216 (47), pp. 8431-8434.

[2] D. Doulia, I. Xiarchos (2007) "Ultrafiltration of micellar solutions of nonioni surfactants with or without alachlor pesticide", J. Membr. Sci., 296, pp. 58-64.

[3] Shell Chemicals (2005) "Neodol 91-8, Primary alcohol ethoxylate datasheet".

[4] C. Chang, C.T. Hsu, S.Y. Lin (1998) "Adsorption kinetics of $C_{10}E_8$ at the air-water interface*",* Langmuir, 14, pp. 2476.

[5] J.A. Molina Bolivar, J.M. Hierrezuelo, C. Carnero Ruiz (2006) “Effect of NaCl on the self-aggreagtion of n-octyl β-D-thioglucopyranoside in aqueous medium”, J. Phys. Chem., 110, pp. 12089-12095.

[6] H. Schott, S.K. Han (1976) “Effect of inorganic additives on solutions of non-ionic surfactants III: CMC's and surface properties”, J. Pharm. Sci., 65 (7), pp. 975-978.

[7] Y. Levin, J.E.Flores-Mena (2001) “Surface tension of strong electrolytes”, Europhys. Lett., 56 (2), pp. 187–192.

[8] R.J. Green, T.J. Su, J.R. Lu, J. Webster, J. Penfold (2000) “Competitive adsorption of lysozyme and $C_{12}E_5$ at the air/liquid interface”, Phys. Chem. Chem. Phys., 2, pp. 5222-5229.

[9] A. Malhotra, J.N. Coupland (2004) “The effect of surfactants on the solubility, zeta potential, and viscosity of soy protein isolates”, Food Hydrocolloids, 18, pp. 101–108.

[10] Z. Zhang, S. Feng (2006) “In Vitro investigation on poly(lactide)-Tween 80 copolymer nanoparticles fabricated by dialysis method for chemotherapy”, Biomacromolecules, 7, pp. 1139-1146.

[11] L. Shi, G. Sanyal, A. Ni, Z. Luo, S. Doshna, B. Wang, T.L. Graham, N. Wang, D.B. Volkin (2005) “Stabilization of Human Papillomavirus Virus-like particles by non-ionic surfactants”, J. Pharm. Sci., 94 (7), pp. 1538-1551.

[12] V. Mosquera, J.M. Ruso, G. Prieto, F. Sarmiento, (1996) “Characterization of the interactions between lysozyme and n-alkyltrimethylammonium bromides by zeta potential measurements” J. Phys. Chem., 100, pp.16749-16753.

[13] F. McNeil-Watson , M. Kaszuba (2010), “A Novel Method for Measuring Zeta Potential of High Concentration, Low Volume Protein Samples”, American Laboratory, 42 (10), pp. 15-16.

[14] R.L. Moritz, R.J. Simpson (2005) “Liquid-based free-flow electrophoresis-reversed-phase HPLC: a proteomic tool”, Nature Methods, 2 (11), pp. 863-873.

[15] L.R. Wetter, H.F. Deustch. (1951) “Inmunological studies on egg white proteins IV. Immunological and physical studies of lysozyme”, J. Biol. Chem., 192, pp. 237-242.

[16] B. Lee, S. Kim, J. Cho, (2011) “Notes: Multi-biocatalytic properties of layer- by-layer assembled lysozyme/catalase multilayers”, Macromol. Res., Vol. 19 (6), pp. 635-638.

[17] D.L. Rothemund, T.M. Thomas, D.B. Rylatt (2002) “Purification of the basic protein avidin using Gradiflow technology”, Protein Expression and Purification, 26, pp. 149-152.

[18] H.M. Kwaambwa, A.R. Rennie (2011) “Interactions of surfactants with a water treatment protein from Moringa oleifera seeds in solution studied by zeta-potential and light scattering measurements”, Biopolymers, 97 (4), pp. 209-218.

Chapter 8. Concluding discussion and future work

8.1. Discussion

A polydisperse biopolymer derived from chicken eggshell membranes has been characterized from surface adsorption and bulk solution properties. This biosurfactant is obtained from a waste product which is readily available in high quantities. Therefore, its use as a biosurfactant would help reduce food pollution issues.

The 40 KDa polypeptide, referred to as the biopolymer, has shown that it can act as a surface active agent. The equilibrium surface tension profiles obtained with this material produced typical surfactant adsorption that is indicative of the occurrence of critical aggregation concentration (CAC) in the bulk solution. The plateau is located at lower surface tension values (around 32 ± 1 mN/m) than those obtained from conventional LMW surfactants such as SDS and DTAB, or other biopolymers such as lysozyme and BSA. These values are however not as low as that achieved with the protein biosurfactant hydrophobin HFBII, i.e. 25 mN/m [1].

The maximum bubble pressure method was used to study the dynamic adsorption process from the 40 KDa polypeptide. The lag time can be interpreted as the time needed for the biopolymer to unfold to an extent that allows it to adsorb at the air/water interface [2]. Thus, the lag times observed at different concentrations suggest that the structure of this biopolymer is not as rigid as that of lysozyme or as flexible as that of BSA, since the rate of adsorption exhibits a rapid fall at intermediate lag times. This is further proved by the foams produced (after three handshakes) of ~10 ml of solutions containing this material. The volumes of foam produced are low compared to BSA [3] but also very stable.

Dynamic adsorption studies and the foams produced point towards a structure closer to that of lysozyme, yet the low equilibrium surface tension values attained at the CAC are considerably lower than those of BSA or lysozyme [4].

A ζ-potential investigation of the 40 KDa polypeptide under different pH conditions tells us that the isoelectric point in a 10 mM NaCl solution is close to pH 5.
Adsorption at a pH other than pH 5 results in either a lower total adsorbed amount (at higher pH) or a conformational change (at lower pH) manifested through a loss of solubility.

The CAC at pH 5 and 10 mM NaCl is reached at 1 mg/ml. At this concentration the surface adsorbed amount is 2.32 ± 0.14 $mg \cdot m^{-2}$ and the area per molecule is 4717 ± 283 $Å^2$, as determined by specular neutron reflection. The adsorbed amounts calculated by means of applying the Gibbs Equation to the equilibrium surface tension profile have proven to be physically unreasonable for this material. This can be a consequence of the various non-precise assumptions used in the application of the Gibbs Equation.

At 10 mg/ml, the aggregates of the 40 KDa polypeptide formed in the bulk solution adopt a short cylindrical shape (or disk-like sheet) of radius 90 Å and length 7 Å, approximately, as observed with SANS.

When SDS or DTAB are present in the solutions containing the 40 KDa polypeptide, a strong synergy is observed in the interfacial adsorption profiles obtained with the plate method especially at low concentrations of surfactant and polypeptide. Both systems seem to rely on an interaction between the surfactant head and a dipole formed by the polypeptide in a polar solvent solution aided by the cooperative effect of the hydrophobic effect between the surfactant alkyl chains and the hydrophobic moieties of the polypeptide. This mechanism of interaction has been already proposed for other polymer/surfactant systems that exhibit similar interfacial adsorption behaviour, such as PEI/C_{16}TAB [5] and PEI/SDS [6], and can be explained through the model developed by Bell et al. [6], in which different bulk aggregates are formed at different surfactant concentrations with different surface activities.

These bulk aggregates then compete to reach the interface and the difference in surface activities between them is thus held responsible for the type and amount of aggregates found at the interface. The adsorption at the interface of the different aggregates formed

with increasing surfactant concentration gives rise to distinctly separated regions in the adsorption profiles at long times.

Strongly interacting systems of oppositely charged components are commonly associated with a phase separation and precipitation at surfactant concentrations close to neutrality [7]. This effect is replicated by the 40K/DTAB system but not by the 40K/SDS system. Information on strongly interacting systems of likely charged components is not abundant. Nevertheless, they do exist and generally present this precipitation region too [5, 8].

Another model developed by Campbell et al. [7, 9] exists that interprets the distinctive surface tension profiles obtained through strongly interacting systems in the precipitation region as a consequence of the depletion of surface active material from the bulk solution that in turn causes its depletion from the interface. This model has proved unsuitable in the study of the 40 KDa polypeptide systems. The total depletion of polymer from this region as expected from this model is not reached in the present systems. Neutron reflection shows distinctly separated regions of interfacial adsorption of polypeptide and surfactant along the whole surfactant concentration range studied below the CMC of the surfactant in agreement with the regions observed in the adsorption profiles obtained with the plate method, and SANS proves the existence of complexes in the bulk solution that are composed of micellar surfactant aggregates wrapped in a polypeptide shell.

Both surfactants have a C_{12} alkyl chain which must result in similar (if not identical) hydrophobic interactions between the surfactant chains. However, although the interfacial adsorption behaviour imprinted in the surface tension profiles at long times are similar in appearance; the cationic DTAB lowers the surface tension more effectively than the anionic SDS.

This difference in strength of interactions could be attributed to the orientation adopted by the hydrophobic segments of the polypeptide in relation to the surfactant alkyl chains which we suspect is affected by the type of charges present in the surfactant heads and the spacing they need due to the Coulombic interactions acting upon them. A comparison with the anionic polyelectrolyte HPG-borate/DTAB system [10] suggests

that the charge distribution along the polypeptide is decisive for the surfactant nucleation that causes the typical strong interaction between surfactant and oppositely charged polymers. This is also consistent with the orogenic model proposed by Mackie et al [11].

Addition of NaCl to the mixed solutions with DTAB or SDS results in the disappearance of the strong synergy at low concentrations which can be explained if the surfactant polar head charges are screened by NaCl thus hindering the orientation that favours cooperative interaction of hydrophobic moieties between the polypeptide and the surfactant and between the surfactant tails. This could explain the similarities (surface adsorption profiles) and differences (formation of precipitates) in the strong synergy observed when mixing the 40 KDa polypeptide with two surfactants of opposite charges.

The solutions of polypeptide and surfactant concentrations at which the strong synergy is observed, exhibit a dynamic adsorption behaviour that clearly differs from that of the individual components within the first 100 s. These results demonstrate that the effect of the interactions at short times is the formation of complexes of different surface activity to that of the individual components. Whether the complexes are formed at the interface or in the bulk solution and then adsorbed at the interface remains unanswered although Noskov et al. [12] believe that these non-monotonous rates of adsorption are due to the formation of aggregates at the surface and can be proven through the study of the viscoelastic properties of the surface layer.

The ζ-potential studies of the mixtures with ionic surfactants under different pH conditions reveal some important differences between the 40KDa/SDS and the 40KDa/DTAB systems. At a fixed polypeptide concentration of 1 mg/ml and at pH 5, the mixed solutions with and without SDS remain stable and almost unaltered at $\zeta < -30$ mV, i.e. no precipitation or phase separation is observed. At a higher pH, the solutions become slightly more electronegative but invariant with respect to the amount of SDS present (at least below the CMC). At a lower pH, the polypeptide is protonized and addition of negative charges in the form of SDS lowers the effect of the electrostatic colloidal interaction.

For 1 mg/ml of the 40KDa polypeptide at pH 5, addition of DTAB turns the stable negatively charged colloids into an unstable colloidal solution at DTAB concentrations 1 and 6 mM, i.e. below the CMC. Close to the CMC this trend continues and the colloidal system is essentially neutral. Similar conclusions can be reached at a higher pH. When the pH is lower, addition of DTAB positive charges results in a milder electrostatic interaction between colloids that remain positively charged.

SANS measurements showed a decrease in the polypeptide shell thickness of the core/shell aggregates found in the bulk solution at DTAB concentrations 5, 10 and 20 mM. This is consistent with an increase of surfactant present in solution and a more neutral environment in which the colloids are closer to each other. Moreover, the concentrations at which the core/shell aggregates form coincide with the region where phase transition separation and precipitation is observed. Hence, the presence of the polypeptide in the bulk solution within the precipitation region is demonstrated.

The presence of a film on the surface of the 40KDa/DTAB system can be considered a further proof of the differences in the state of the bulk colloidal solution between the mixtures with the anionic and the cationic surfactants. In other words, the formation of the film close to the plateau region when the solution is unstable indicates that the aggregates either form or adsorb at the surface to avoid the non-equilibrium conditions of the bulk. However, the formation of these aggregates is not observable (by naked eye) in the case of the 40KDa/SDS system. This could be due to the more favourable and stable conditions of the bulk phase in this system.

When the 40 KDa polypeptide is mixed with the non-ionic surfactant $C_{10}E_8$, the synergism previously observed with the mixtures with ionic surfactants does not take place and the surface adsorption profiles obtained with the plate method do not present regions of surface tension lower than the surface tension of the individual components at small concentrations of them.

Furthermore, the ζ-potential study conducted on the non-ionic surfactant $C_{10}E_8$ in the presence of the 40 KDa polypeptide or another biopolymer, i.e. lysozyme, shows that there is no deviation (other than that due to steric effects) from the typical electrostatic behaviour of the biopolymers in the absence of the surfactant over the entire range of

pH studied. This further suggests that although the synergistic effect observed in mixtures with ionic surfactants cannot be explained solely based in an electrostatic interaction between the charges in the polypeptide and those of the surfactant head, this interaction plays an important role even in pH conditions close to the isoelectric point of the polypeptide when the latter is regarded as neutral. This has also been previously observed by Penfold et al. in their studies of interfacial adsorption of mixed SDS/amine solutions [13].

Thus, the presence of a charged surfactant, or rather the presence of a charged molecule, seems to be a necessary condition for the strong synergy to manifest. Nevertheless, since it is clear that the profiles obtained with the plate method alone do not provide enough information about the interactions occurring in the bulk solution in any of the mixed solutions investigated, the assumption that the 40KDa/$C_{10}E_8$ mixtures result in a competitive interaction and no binding takes place can only be proved by carrying out further investigations using different techniques such as neutron reflection. This was already demonstrated by Green et al. in their investigation of the mixed lysozyme/$C_{12}E_5$ system [14].

The fact that dynamic adsorption profiles at 0.1 mM of $C_{10}E_8$ with 1 and 5 mg/ml of the polypeptide exhibit a different behaviour from that of the individual components may be interpreted as an indication of the above.

8.2. Future work

The results presented in this work although promising are not yet complete. Different lines of work can be followed in order to improve our understanding of the behaviour exhibited by the 40 KDa polypeptide in the absence and presence of ionic surfactants and to develop products which exploit this behaviour and may prove of commercial interest.

At the air/liquid interface, these studies could be continued by extending the range of LMW surfactants investigated in order to gain a better understanding of the interactions that take place at different concentrations of solution components and the type of complexes formed. Atomic force microscopy and Fourier-transformed infrared

spectroscopy would provide complementary information about the complexes and the state of the surface.

Neutron reflection and SANS could be employed to compare the behaviour of the 40KDa/$C_{10}E_8$ mixtures to the lysozyme/$C_{12}E_5$ system and discern whether the interaction between these components is purely competitive or indeed there is a non-competitive interaction. Further studies by deploying non-ionics with longer alkyl chains or more hydrophobic moieties such as aromatic rings could strengthen the hydrophobic interaction, thereby increasing cooperative interactions. Furthermore, if a non-competitive interaction was found, the model developed by Bell et al. [6] should be further improved.

Surface viscoelasticity would offer an insight into the relation between the formation of different complexes and the viscoelasticity of the interface as suggested by Noskov et al [12, 15]. Since the orientation of the surfactant tails in relation to the polypeptide is one of the main causes of the synergy observed in this work, it seems logical to apply off-specular neutron reflection to search for this orientational pattern in the aggregates adsorbed at the surface.

If we turn our interest towards the ability to foams of the mixtures studied, Eastoe et al. [16] reported that using an overflowing cylinder in conjunction with neutron reflection proves useful in the dynamic study of the surface adsorption. Moreover, ζ-potential studies of the bubbles could reveal further information about the relation between the foams and the molecules present in the solution by investigating the charges at the bubble surfaces [17].

The polypeptide adsorption (with and without surfactants) on different interfaces such as silicon oxide/water may prove useful for products that are destined to be in contact with different types of living tissues and can be further investigated through techniques such as surface ζ-potential, spectroscopic ellipsometry, specular neutron reflection or SANS amongst others. Toxicity and biocompatibility studies should follow.

References

[1] A. Cooper, M.W. Kennedy (2010) “Biofoams and natural protein surfactants”, Biophys. Chem., 151(3), pp. 96-104.

[2] C. Ybert, J.M. di Meglio (1998) “Study of protein adsorption by dynamic surface tension measurements: diffusive regime”, Langmuir, 14, pp. 471-475.

[3] B.C. Tripp, J.J. Magda, J.D. Andrade (1995) “Adsorption of globular proteins at the air/water interface as measured via dynamic surface tension: concentration dependence, mass-transfer considerations, and adsorption kinetics”, J. Colloid Interface Sci., 173, pp. 16-27.

[4] A. Cooper, M.W. Kennedy, R.I. Fleming, E.H. Wilson, H. Videler, D.L. Wokosin, T. Su, R.J. Green, J.R. Lu (2005) “Adsorption of frog foam nest proteins at the air-water interface”, Biophys. J., 88, pp. 2114–2125.

[5] H. Comas-Rojas, E. Aluicio-Sarduy, S. Rodriguez-Calvo, A. Perez-Gramatges, S. J. Roser and K. J. Edler (2007) “Interactions and film formation in polyethylenimine–cetyltrimethylammonium bromide aqueous mixtures at low surfactant concentration”, Soft Matter, 3, pp. 747–753.

[6] C.G. Bell, C.J.W. Breward, P.D. Howell, J. Penfold, R.K. Thomas (2010) “A theoretical analysis of the surface tension profiles of strongly interacting polymer–surfactant systems”, J. Colloid Interface Sci., 350, pp. 486–493.

[7] R.A. Campbell, A. Angus-Smyth, M. Yanez Arteta, K. Tonigold, T. Nylander, I. Varga (2010) "New perspective on the cliff edge peak in the surface tension of oppositely charged polyelectrolyte/surfactant mixtures", J. Phys. Chem. Lett., 1, pp. 3021–3026.

[8] B.M.D. O’Driscoll, E. Milsom, C. Fernandez-Martin, L. White, S.J. Roser, K.J. Edler (2005) “Thin films of polyethylenimine and alkyltrimethylammonium bromides at the air/water interface”, Macromolecules, 38, pp. 8785-8794.

[9] R.A. Campbell, M. Yanez Arteta, A. Angus-Smyth, T. Nylander, I. Varga (2011) “Effects of bulk colloidal stability on adsorption layers of poly(diallyldimethylammonium chloride)/sodium dodecyl sulfate at the air–water interface studied by neutron reflectometry”, J. Phys. Chem. B, 115 (51), pp 15202–15213.

[10] Y. Cui, R. Pelton, T. Cosgrove, R. Richardson, S. Dai, S. Prescott, I. Grillo, H. Ketelson, D. Meadows (2009) “Not all anionic polyelectrolytes complex with DTAB”, Langmuir, 25 (24), pp. 13172-13717.

[11] A.R. Mackie, A.P. Gunning, P.J. Wilde, V.J. Morris (1999) “Orogenic displacement of protein from the air/water interface by competitive adsorption”, J. Colloid Interface Sci., 210, pp. 157–166.

[12] B.A.Noskov, G. Loglio, R. Miller (2011) “Dilational surface visco-elasticity of polyelectrolyte/surfactant solutions: formation of heterogeneous adsorption layers”, Adv. Colloid Interface Sci., 168 (1-2), pp. 179-197.

[13] J. Penfold, R.K. Thomas, X.L. Zhang, D.J.F. Taylor (2009) “Nature of amine-surfactant interactions at the air-solution interface”, Langmuir, 25, pp. 3972-3980.

[14] R.J. Green, T.J. Su, J.R. Lu, J. Webster, J. Penfold (2000) “Competitive adsorption of lysozyme and $C_{12}E_5$ at the air/liquid interface”, Phys. Chem. Chem. Phys., 2, pp. 5222-5229.

[15] A.G. Bykov, S.Y. Lin, G. Loglio, R. Miller, B.A. Noskov (2010) “Dynamic surface properties of polyethylenimine and sodium dodecylsulfate complex solutions”, Colloids and Surfaces A: Physicochem. Eng. Aspects, 367, pp. 129–132.

[16] J. Eastoe, J.S. Dalton (2000) “Dynamic surface tension and adsorption mechanisms of surfactants at the air-water interface”, Adv. Colloid Interface Sci., 85, pp. 103-144.

[17] A. Phianmongkhol, J. Varley (2003) “ζ-potential measurements for air bubbles in protein solutions”, J. Colloid Interface Sci., 260, pp. 332-338.